Preparation of biobased materials from nano-polysaccharides and lignin particles for food packaging applications

Eva Pasquier

THÈSE

Pour obtenir le grade de

DOCTEUR DE L'UNIVERSITE GRENOBLE ALPES

Spécialité : **Matériaux, Mécanique, Génie civil, Electrochimie**

Arrêté ministériel : 25 mai 2016

Présentée par

Eva PASQUIER

Thèse dirigée par **Julien Bras,** Maitre de Conférences, Grenoble INP-UGA, et codirigée par **Orlando J. Rojas,** Professeur, Université de Colombie Britannique

Préparée au sein du **Laboratoire de Génie des Procédés Papetiers** et du **Department of Bioproducts and Biosystems, Aalto University**

Dans l'École Doctorale IMEP-2, Ingénierie, Matériaux, Mécanique, Environnement, Energétique, Procédés, Production

Preparation of Biobased Materials from Nano-polysaccharides and Lignin Particles for Food Packaging Applications

Préparation de matériaux biosourcés à partir de nano-polysaccharides et de particules de lignine pour la fabrication d'emballage alimentaire

Thèse soutenue publiquement le **1er mars 2022**,
Devant le jury composé de :

Pr. Alain Dufresne
Professeur à Grenoble INP-UGA, Président
Pr. Aji Mathew
Professeur à l'Université de Stockholm, Rapportrice
Dr. Véronique Coma
Maitre de conférences à l'Université de Bordeaux, Rapportrice
Dr. Susana De Matos Fernandes
Maitre de conférences à l'Université de Pau et des Pays de l'Adour, Examinatrice
Dr. Julien Bras
Maitre de conférences à Grenoble INP-UGA, Directeur de thèse
Pr. Orlando J. Rojas
Professeur à l'Université de Colombie Britannique, Co-directeur de thèse
Dr. Bruno D. Mattos
Post-doc à l'Université d'Aalto, Co-encadrant de thèse, Invité
Pr. Naceur M. Belgacem
Professeur à Grenoble INP-UGA, Co-encadrant de thèse, Invité

Acknowledgments

First, I would like to thank the jury for accepting to review my work. A special thanks goes to Dr. Veronique Coma and Pr. Aji Mathew for the extensive reading of this manuscript as well as the constructive remarks in the reports and during the defense. Pr. Alain Dufresnes and Dr. Susana Fernandes, thank you for examining my work and for your presence during the defense. It was highly appreciated to discuss face to face. Moreover, I would like to thank you all for the relevant comments and the interesting discussion we had after my presentation.

A big thanks to my supervising "team" that supported me during these 3 years and without whom this project would not have been possible. I appreciated all the ideas you gave me to develop this thesis, and I learnt a lot from you all. Thanks for letting me attend all the conferences, as it made me discover the small community of nanocellulose fans. Thank you, Julien, for starting this project and collaboration with Orlando. You trusted me from the beginning to carry this project to the end. Orlando, although we were not physically together in Finland, you were always available for a zoom call to give great advice. Naceur, you joined the team in the middle of my PhD as a "replacement" but your knowledge was always relevant and warmly welcome, especially since I did not study at Pagora. Last but not least, Bruno, I am so glad I knocked on your door not long after arriving in Finland. You were always available for discussions and your guidance and advice were great assets throughout this long journey.

I would also like to thank the collaborators I had the chance to work with: Marco Beaumont, Caio Otoni, Alexey Khakalo and Anna Koivula. We had interesting discussions and it definitely improved the quality of my work.

La première partie de ma thèse s'est déroulée au LGP2 à Grenoble. Pour cela j'aimerais remercier Cécile pour sa précieuse aide dans les labos, Bertine Khelifi pour les nombreuses images MEB, Jean-Luc Puteaux pour les discussions et l'accès au TEM, mais aussi le service technique et l'administration qui répondent toujours présent en cas de besoin. Merci également aux nombreux doctorants et post-doc avec qui j'ai pu passer du temps au labo et à l'extérieur Maxime, Etienne, Claire, Manon, Lili, Etienne M., Andrea, Valentin, Gabriel, Fleur, Malek, Ahlem, Clémentine, Hugo, Khawla et tous les autres. Nos sorties au bar, au parc et même en montagne ont permis de me changer les idées et de profiter de la magnifique région de Grenoble. Un immense merci également à Bastien et Lorelei pour ces 3 ans passés

ensemble, même après mon départ en Finlande on a réussi à garder contact et vous avez toujours été là pour répondre à mes nombreuses questions.

In the middle of my PhD, I moved to Helsinki and had to adapt to a new country, a new lab, and a new way of working. But this also allowed me to meet a whole new team and I would like to thank the BicMat team for their warm welcome in Finland. Despite Covid, I managed to meet incredible people that made me enjoy Finland much more. A big thanks to Bruno, Tainise, Rubina, Joice, Bin, Mamata, Urs, Dmitry, Janika, Marcel, Blaise, Roozbeh, Guillermo, Luiz, Wenchao, Konrad, Ya and many others. I also want to acknowledge all the people working behind the scenes that made our work possible in the labs, from the administration to the technical staff. A special thanks to Tuyen Nguyen for all the microfluidization experiments.

Merci également à tous mes amis que j'ai rencontré à travers les années, du lycée à Grenoble en passant par Strasbourg et qui ont chacun à leur manière influencé mon parcours et m'ont permis d'en arriver là aujourd'hui. Notamment un grand merci à ma coloc Faustine, pour cette année et demie passée ensemble et sans qui je n'aurais jamais eu le courage d'aller à tous ces entrainements de volley.

Je voulais aussi remercier ma famille pour avoir essayé de comprendre mon sujet de thèse et pourquoi je faisais une thèse. J'espère que vous avez réussi à comprendre quelque chose et aussi qu'on ne fait pas que chercher mais que parfois on trouve.

Et le meilleur pour la fin, tusen takk Peder for at du er her for meg og deler livet med meg. Takk for at du ble med meg til Finland, jeg kunne ikke overlevd kulda uten deg. Jeg håper at vi fortsetter å være sammen i lang tid fremover.

General Table of Content

Scientific contributions (2018-2021) **7**

Abbreviations **9**

General Introduction **11**

Chapter I: Literature review **19**

I.1 Cellulose, chitin and lignin colloids: sources, processing and properties 24

I.2 Biobased colloids in packaging: developments and challenges 49

Chapter II: Preparation of colloids and first assembly into films **99**

II.1 Production of chitin nanofibers and films from insects (fly larvae and mealworm) ... 105

II.2 Preparation of lignin microparticles and their incorporation in CNF films 131

Chapter III: New method for preparation of lignin particles **151**

III.1 Effects of lignin particles size on cellulose nanofibers film structure and properties 157

III.2 *In-situ* preparation of lignin particles with different nanofiber supports 173

Chapter IV: Towards packaging applications **199**

IV Multilayered films with high barrier properties 205

General conclusion and perspectives **237**

Poster **244**

Extended French abstract **247**

Scientific contributions (2018-2021)

Publications in scientific journals

1. “Lignin nanoparticle nucleation and growth on cellulose and chitin nanofibers”, E. Pasquier, B. D. Mattos, N. Belgacem, J. Bras, O. J. Rojas, *Biomacromolecules*, **2021**, 22 (2), 880–889

2. “Upcycling Byproducts from Insect (Fly Larvae and Mealworm) Farming into Chitin Nanofibers and Films”, E. Pasquier, B. D. Mattos, C. G. Otoni, A. Winter, T. Rosenau, N. Belgacem, O. J. Rojas, J. Bras, *ACS Sustainable Chemistry*, **2021**, 9 (40), 13618–13629

3. “Biobased waste for the conception of cellulose, chitin and lignin colloids for the development of new packaging materials”, E. Pasquier, J. Bras, N. Belgacem, O. J. Rojas, B. D. Mattos, to be submitted in Industrial Crops and Products.

4. “Integration of lignin micro- and nano-particles in cellulose nanofiber films, size effect on film structure and properties”, E. Pasquier, B. D. Mattos, N. Belgacem, J. Bras, O. J. Rojas, to be submitted in Colloid and Polymer Science.

5. “High barrier multilayered film fabricated from bio-based polymers”, E. Pasquier, B. D. Mattos, H. Koivula, A. Khakalo, M. N. Belgacem, O. J. Rojas, J. Bras, to be submitted in ACS Applied Materials and Interfaces.

Oral presentations in international conferences

1. E. Pasquier, J. Bras, O. Rojas, Hybrid films of cellulose nanofibers and lignin particles for advanced applications, ACS National meeting, CELL division, Orlando, USA, 2019
2. E. Pasquier, J. Bras, N. Belgacem, O. Rojas, Hybrid films of cellulose nanofibers and lignin particles for packaging applications, NRC-Grenoble INP International Conference, Cairo, Egypt, 2019
3. E. Pasquier, M. Beaumont, B. D. Mattos, M. N. Belgacem, O. J. Rojas, J. Bras, Production of chitin nanofibers from insects and comparison with conventional sources, 4th International EPNOE Junior Scientist Meeting, online event, 2021
4. E. Pasquier, B. D. Mattos, N. Belgacem, J. Bras, O. Rojas, Biobased Multilayered Films based on Cellulose and Chitin Nanofibers for Food Packaging, Tappi Nano, online event, 2021

Poster presentation in scientific conference

1. E. Pasquier, J. Bras, N. Belgacem, O. Rojas, *In-situ* preparation of lignin nanoparticles on different types of cellulose nanofibers, 6th EPNOE International Polysaccharides Conference. Aveiro, Portugal, 2019
2. E. Pasquier, L. Charlet, J. Bras, Synthesis of zero valent iron nanoparticles on cellulose nanofibers for active food packaging applications, Global Science Week, Grenoble, France, 2019

Abbreviations

Materials and chemicals

ABTS	2,2'-azino-bis(3-ethylbenzothiazoline-6-sulfonic acid)
ChNC	Chitin nanocrystals
ChNF	Chitin nanofibers
CNC	Cellulose nanocrystals
CNF	Cellulose nanofibers
HCl	Hydrochloric acid
LP	Lignin particles
NaOH	Sodium hydroxide
NPs	Nanoparticles
TEMPO	2,2,6,6-Tetramethylpiperidine-1-oxyl
WP	Wax particles

Methods

AFM	Atomic force microscopy
DLS	Dynamic light scattering
DMA	Dynamic mechanical analysis
FTIR	Fourier-transform infrared spectroscopy
NMR	Nuclear magnetic resonance
OP	Oxygen permeability
OTR	Oxygen transmission rate
RH	Relative humidity
RT	Room temperature
SEM	Scanning electron microscopy
TEM	Transmission electron microscopy
TGA	Thermogravimetric analysis
UV	Ultra-violet
WCA	Water contact angle
WVP	Water vapor permeability
WVTR	Water vapor transmission rate
XRD	X-ray diffraction

General Introduction

General Introduction

About 8300 million ton of plastic were produced worldwide between 1950 and 2015. Among the total waste generation from these, it was calculated that 9% of the plastic wastes were recycled, while 12% were incinerated and 79% disposed in landfills or in nature (**Figure 1**).[1] In Europe, and on the basis of the total plastics that were sorted in 2018, 33% was recycled and 43% was used for energy recovery. No statistics were available for the total plastics used.[2] These figures indicate that despite notable recent improvements, the recycling rate is still rather low, even in developed countries. Nevertheless, packaging represents the largest plastic demand in Europe, corresponding to 40% of the end-use market, with about 20 million ton of plastic used every year.[2] Polyethylene low density (LDPE) and high density (HDPE), polypropylene (PP) and polyethylene terephthalate (PET) are the most used plastic for packaging. They are recyclable to a certain extent, but none of them is biodegradable.

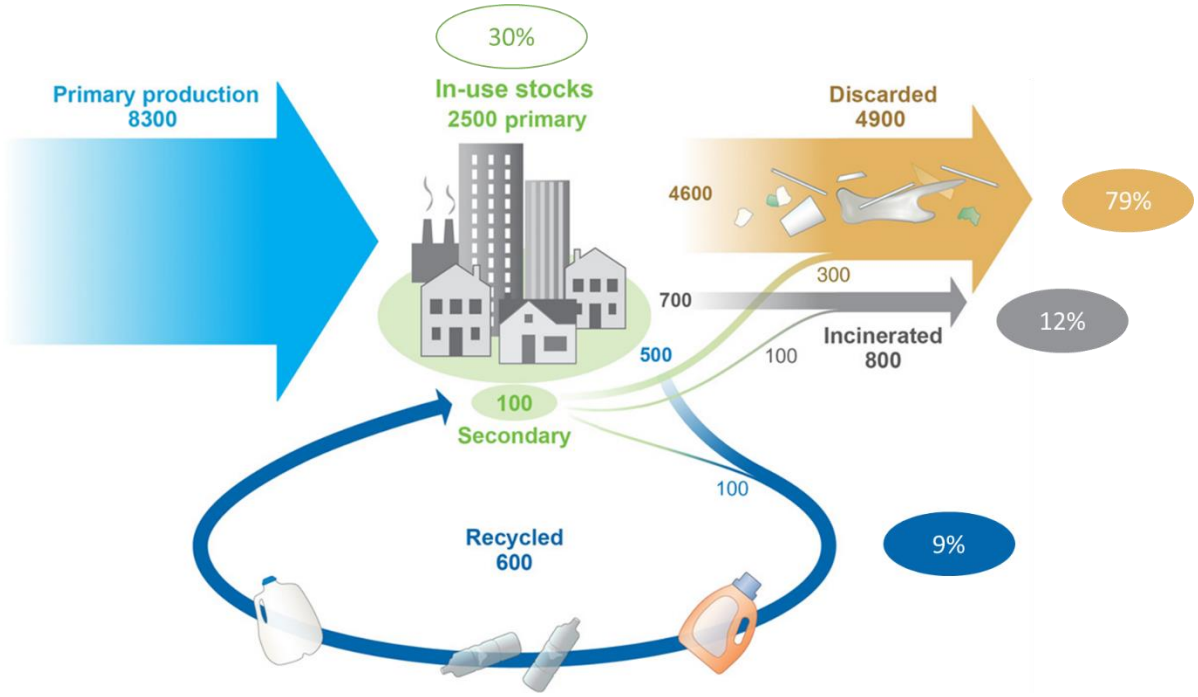

Figure 1. Global production, stocks, and waste of plastics in million tons between 1950 and 2015. Reproduced from[1]

Even though new solutions for recycling emerge and improvements in the quality of recycled plastics are continuously made, plastic recycling rate is still very low. Moreover, most countries are starting to introduce regulations to limit the use of plastic, for example, the single-use plastic directive in the European Union, which considers ten of the most found plastics in the coastline and beaches.

Hence solutions are needed to reduce the reliance on packaging materials, especially single-use packages. However, packaging is essential for food protection, *e.g.*, to reduce food waste, which poses detrimental effects on the environment (carbon emission, land and water use during food production, transformation, and distribution).[3] As result of this, alternatives to plastic packaging, with similar or better properties, are demanded while decreasing the environmental footprint linked to the end-of-life.

Biobased fibers such as those based on cellulose and chitin, which present versatile sources and end-of-life, are great candidates to replace the precursors otherwise used in packaging materials. At the same time, the use of waste, agricultural and industrial by-products as a source of packaging materials could significantly decrease their total environmental footprint. Cellulose can be extracted from several processed or non-processed agricultural by-products, such as straws, bagasse, and husks of several different plants (rice, maize, sugarcane, among others).[4] Chitin is already extracted as a by-product of the crustacean industry and could soon become a useful by-product of the insect farming industry.[5] To meet the increasing demand for biobased fibers, diversification of the sources is expected, and the valorization of every crop, as well as every part of the crops, into high-performance materials, could be part of the solution. It is also promising to observe an increased use of industrial waste along with higher recycling rates for fiber-based materials.[6]

During the last decade, it has been shown that cellulose and chitin can form stable colloids with notable performance for food packaging applications. Cellulose nanofibers (CNF) and chitin nanofibers (ChNF), for instance, can be prepared by mechanical fibrillation of their respective precursor to form gel-like suspension at low concentrations (**Figure 2a** and **2c**).[7] Such nanofibers have characteristic high aspect ratio, high crystallinity, high specific surface area, and can be used to produce films with remarkable mechanical, optical, and barrier properties.[8–10] Furthermore, films made of CNF or ChNF form strong and dense networks that display high barrier properties towards oxygen.

On the other hand, lignin can be sourced from the same plants used to isolate cellulose and is readily available in large quantities. Lignin's aromatic nature gives rise to properties such as antioxidant, antimicrobial, and UV-shielding activity, which are all important for food packaging. Lignin can be shaped into spherical particles (LP, **Figure 2b**), which have become quite popular, as shown by recent reviews about the subject.[11–15] When shaped into LP, lignin can be easily processed in water and endow colloidal stability in nanofibers matrices.[16]

CNF, ChNF, and LP are three biobased colloids that are potentially available in large quantities and represent promising candidates for food packaging applications. They all have been studied individually during the two last decades; however, the interactions between each other have been so far overlooked. In this thesis, we take advantage of their individual properties and interactions to assemble them into more complex and functional materials.

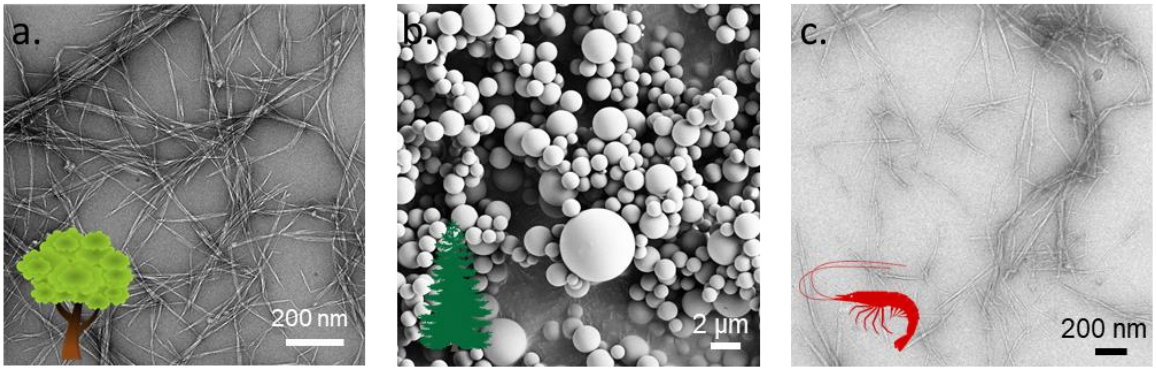

Figure 2. Images of some of the most abundant biobased colloids sourced from nature: cellulose nanofibers (a.), lignin particles (b.) and chitin nanofibers (c.), associated with an image of their source.

This PhD project started at the end of 2018 from a collaboration between the Laboratory of Pulp and Paper Science and Graphic Arts (LGP2, Grenoble, France) and the Biobased Colloids and Materials group of Aalto University (Finland). The project was supported by the "Bourse Présidence" program from Grenoble INP made to promote international collaborations as well as the European "BioElCell" project funded by the European Research Council under the European Union's Horizon 2020 research and innovation program. The time was divided equally between the two laboratories and joint meetings were held regularly to discuss the progress and to synergize collaborative efforts between the two teams.

The project focuses on the preparation of biobased colloids and their interactions in the wet and dry states. Particular attention was given to the relevant properties of the polysaccharide and lignin colloids for food packaging applications. Hence, this PhD thesis is organized into four chapters (see **Figure 3**): the first one describes the background literature associated with the three colloids (LP, CNF and ChNF) and their use in packaging applications. The following chapters discuss the research performed during the PhD thesis, which follow the format of published and submitted papers as well as manuscripts in preparation.

Chapter I describes the recent literature related to the three colloids and the gaps of knowledge associated with them. This chapter is divided into two parts, the first one relates to the sources, extraction, and preparation methods used to produce the colloids as well as their properties in suspension. The second part reviews the recent progress achieved so far with regards to fiber-based packaging and how nanopolysaccharides and lignin particles can improve their properties. Their limitations are also considered.

Chapter II focuses on the preparation of the different colloids. The first sub-chapter relates to the preparation of chitin nanofibers (ChNF) from three different sources. Chitin is extracted from fly larvae as well as from the waste of mealworm farming and ChNF are then prepared. ChNF suspension and film properties are compared to ChNF from shrimp shells, a conventional source of chitin. The second part of Chapter II deals with the preparation of lignin microparticles and the first trials to mix them with cellulose nanofibers.

Chapter III introduces a new method to prepare lignin nanoparticles and to improve their compatibility with nanofiber matrices, whereby the particles are produced *in-situ*, in the presence of nanofibers that acted as templating agents. In the first part of Chapter III, LP size effect on CNF film properties is investigated and we highlight the interest of nanosized particles compared to lignin microparticles. The second sub-chapter dives into the method of LP *in-situ* preparation and studies the interactions between LP and the different nanofibers used (CNF or ChNF).

Finally, **Chapter IV** combines the CNF and lignin particles obtained *in-situ* on chitin nanofibers to construct multilayer films that present high barrier properties. A layer of wax is also added to endow the system with water vapor barrier properties. The first part deals with the optimization of the wax layer towards high water vapor barrier while the second part describes the combination of the different layers (CNF, wax, and LP with ChNF) in one film and presents results of the barrier properties towards oxygen, water vapor, and UV light.

This PhD thesis brings an understanding of the different stages of colloid preparation, interactions, and assembly into films. Characterizations are oriented towards food packaging applications where colloidal assembly into films is a critical aspect.

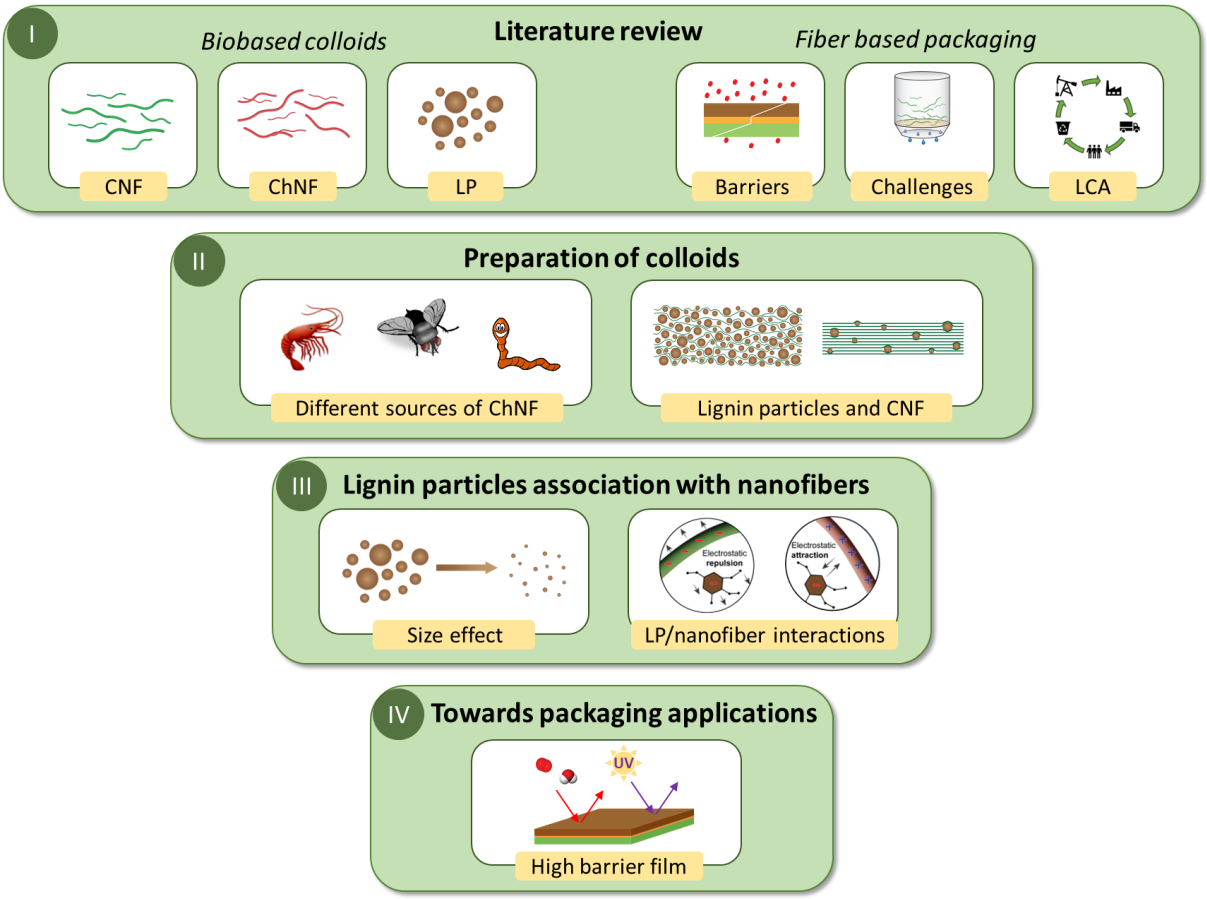

Figure 3. General schematic illustration of the manuscript organization and the respective thesis chapters.

REFERENCES

(1) Geyer, R.; Jambeck, J. R.; Law, K. L. Production, Use, and Fate of All Plastics Ever Made. *Science Advances* **2017**, *3* (7), e1700782. https://doi.org/10.1126/sciadv.1700782.

(2) Market data :: PlasticsEurope https://www.plasticseurope.org/en/resources/market-data (accessed 2021 -05 -20).

(3) Otoni, C. G.; Azeredo, H. M. C.; Mattos, B. D.; Beaumont, M.; Correa, D. S.; Rojas, O. J. The Food–Materials Nexus: Next Generation Bioplastics and Advanced Materials from Agri-Food Residues. *Advanced Materials* **2021**, 2102520. https://doi.org/10.1002/adma.202102520.

(4) García, A.; Gandini, A.; Labidi, J.; Belgacem, N.; Bras, J. Industrial and Crop Wastes: A New Source for Nanocellulose Biorefinery. *Industrial Crops and Products* **2016**, *93*, 26–38. https://doi.org/10.1016/j.indcrop.2016.06.004.

(5) Hahn, T.; Tafi, E.; Paul, A.; Salvia, R.; Falabella, P.; Zibek, S. Current State of Chitin Purification and Chitosan Production from Insects. *Journal of Chemical Technology & Biotechnology* **2020**, *95* (11), 2775–2795. https://doi.org/10.1002/jctb.6533.

(6) Josset, S.; Orsolini, P.; Siqueira, G.; Tejado, A.; Tingaut, P.; Zimmermann, T. Energy Consumption of the Nanofibrillation of Bleached Pulp, Wheat Straw and Recycled Newspaper through a Grinding Process. *Nordic Pulp & Paper Research Journal* **2014**, *29* (1), 167–175. https://doi.org/10.3183/npprj-2014-29-01-p167-175.

(7) Rol, F.; Belgacem, M. N.; Gandini, A.; Bras, J. Recent Advances in Surface-Modified Cellulose Nanofibrils. *Progress in Polymer Science* **2019**, *88*, 241–264. https://doi.org/10.1016/j.progpolymsci.2018.09.002.

(8) Ahankari, S. S.; Subhedar, A. R.; Bhadauria, S. S.; Dufresne, A. Nanocellulose in Food Packaging: A Review. *Carbohydrate Polymers* **2021**, *255*, 117479. https://doi.org/10.1016/j.carbpol.2020.117479.

(9) Ling, S.; Kaplan, D. L.; Buehler, M. J. Nanofibrils in Nature and Materials Engineering. *Nat Rev Mater* **2018**, *3* (4), 1–15. https://doi.org/10.1038/natrevmats.2018.16.

(10) Salaberria, A. M.; Labidi, J.; Fernandes, S. C. M. Different Routes to Turn Chitin into Stunning Nano-Objects. *European Polymer Journal* **2015**, *68*, 503–515. https://doi.org/10.1016/j.eurpolymj.2015.03.005.

(11) Österberg, M.; Sipponen, M. H.; Mattos, B. D.; Rojas, O. J. Spherical Lignin Particles: A Review on Their Sustainability and Applications. *Green Chem.* **2020**, *22* (9), 2712–2733. https://doi.org/10.1039/D0GC00096E.

(12) Schneider, W. D. H.; Dillon, A. J. P.; Camassola, M. Lignin Nanoparticles Enter the Scene: A Promising Versatile Green Tool for Multiple Applications. *Biotechnology Advances* **2021**, *47*, 107685. https://doi.org/10.1016/j.biotechadv.2020.107685.

(13) Ago, M.; Tardy, B. L.; Wang, L.; Guo, J.; Khakalo, A.; Rojas, O. J. Supramolecular Assemblies of Lignin into Nano- and Microparticles. *MRS Bulletin* **2017**, *42* (5), 371–378. https://doi.org/10.1557/mrs.2017.88.

(14) Beisl, S.; Miltner, A.; Friedl, A.; Beisl, S.; Miltner, A.; Friedl, A. Lignin from Micro- to Nanosize: Production Methods. *International Journal of Molecular Sciences* **2017**, *18* (6), 1244. https://doi.org/10.3390/ijms18061244.

(15) Gao, W.; Fatehi, P. Lignin for Polymer and Nanoparticle Production: Current Status and Challenges. *The Canadian Journal of Chemical Engineering* **2019**, *97* (11), 2827–2842. https://doi.org/10.1002/cjce.23620.

(16) Liu, Y. Strong and Flexible Nanocomposites of Carboxylated Cellulose Nanofibril Dispersed by Industrial Lignin. *ACS Sustainable Chem. Eng.* **2018**, *6* (4), 5524–5532. https://doi.org/10.1021/acssuschemeng.8b00402.

Chapter I

Literature review

Table of content – Chapter I

1. Introduction 23

2. Cellulose, chitin and lignin colloids: sources, processing and properties 24

2.1 Cellulose rich residues and their conversion into nanocelluloses 25
2.1.1 Nanocellulose sources 25
2.1.2 Extraction of nanocellulose from unconventional sources 27
2.1.3 Properties of CNF suspensions obtained from residues 31
2.2 Chitin rich residues as precursors for nanochitin 34
2.2.1 Conventional and emerging sources 34
2.2.2 Production of chitin nanofibers 38
2.2.3 Properties of chitin nanofiber suspensions 40
2.3 Lignin-rich biomasses as sources of active molecules and colloids 43
2.3.1 Conventional and alternative sources of lignin 43
2.3.2 Production of lignin particles 44
2.3.3 Properties of lignin and LP relevant for packaging 46

3. Biobased colloids in packaging: developments and challenges 49

3.1 Nanofibers in packaging 49
3.1.1 Requirements for packaging 49
3.1.2 Advantages and limitations of nanofiber-based packaging 50
3.2 Impact of water on nanofiber films 50
3.2.1 Water surface interactions 51
3.2.2 Mechanical properties and impact of humidity 52
3.3 Relevance of barriers properties in packaging 54
3.3.1 Gas barrier 55
3.3.2 Grease barrier properties 60
3.3.3 Light management (UV barrier and visible light transparency) 61
3.4 Active packaging 63
3.5 Challenges related to fiber-based packaging 65
3.5.1 Availability of materials for scale up preparation of packaging 65
3.5.2 Processing of nanofiber-based materials with fiber-based packaging 66
3.5.3 End of life of fiber-based packaging 70
3.6 Environmental impact through LCA analysis 73
3.6.1 Biopolymers sources and impact on land use 75
3.6.2 Cellulose nanofibers 75
3.6.3 Chitin and chitosan 77
3.6.4 Lignin and lignin particles 78
3.6.5 Insights on environmental impact of packaging 79

4. Conclusion 81

1. Introduction

This first chapter aims at introducing the different topics that will be discussed in the following chapters. It gives the context of the PhD through an extensive review of the recent literature covering the three biobased colloids (cellulose, lignin and chitin) and their use in food packaging applications. The main concepts are defined to adapt to experts and non-experts in the field.

Figure I.1 shows how biobased colloids could be integrated in a life cycle from their source to their end of life. The first part of this Chapter discusses the different sources available for each polymer. The extraction methods, processes to prepare cellulose and chitin nanofibers and synthesis methods for lignin particles production will be thoroughly described. The colloids properties will also be reviewed and linked to the source and preparation methods.

The second part is focused on how these colloids perform in packaging application and their limitations. The properties of the films formed with cellulose and chitin nanofibers will be reviewed including their mechanical properties, surface-water interactions, and barrier properties. Impact of lignin as residues or particles will be described notably to make active packaging. Processability, end-of-life and environmental impact will also be discussed to put the use of these materials into perspective.

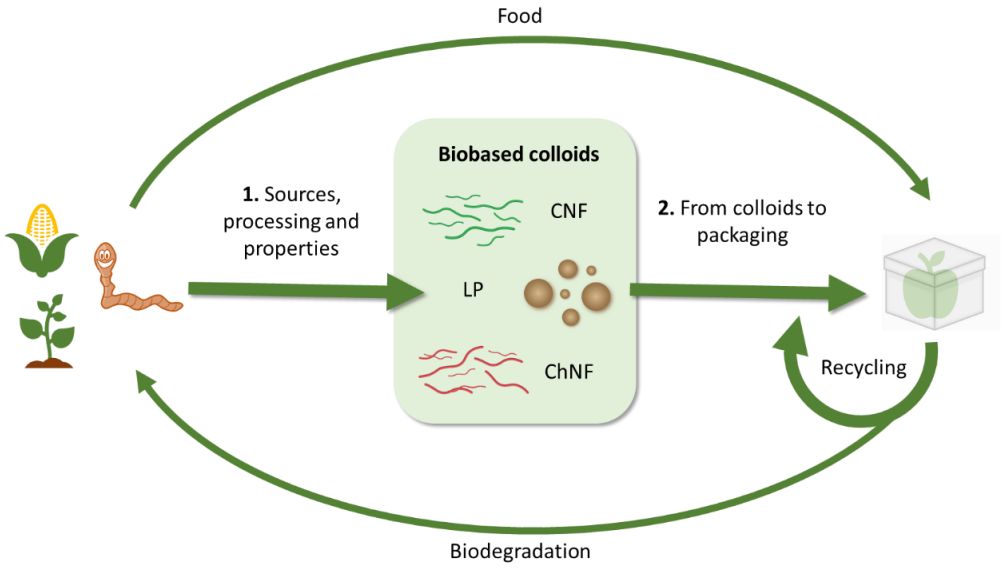

Figure I.1. Biobased colloids (cellulose nanofibers (CNF), lignin particles (LP) and chitin nanofibers (ChNF)

2. Cellulose, chitin, and lignin colloids: sources, processing, and properties

This chapter addresses the preparation of packaging materials from the three most abundant biobased polymers that can form stable colloids in water: cellulose, chitin and lignin (**Figure I.2**). They will be further referred as biocolloids for they are all biobased and form stable suspensions. The extraction and properties of such biocolloids from conventional sources has been thoroughly discussed recently in many venues;[1–5] however, here we highlight their extraction processes and properties when obtained from unconventional sources, namely biomass residues. Cellulose, chitin, and lignin are produced by nature in billions of tons per year and can be extracted from by-products of already existing industries. The intrinsic properties of colloids obtained from these three biomacromolecules can be harnessed towards several high value applications. Cellulose (CNF) and chitin nanofibers (ChNF) (**Figure I.2c-d**), for instance, are flexible, high-aspect ratio particles that can form high-performance films for packaging industry that have potential to replace plastics partially or fully in the food packaging sector. Nanofibers' suspensions often contain microfibers, but they will here be referred as nanofibers as the difference is still not well defined. Moreover, lignin molecules form bioactive colloids/particles (**Figure I.2b**) and could bring additional functions to the packaging materials, such as antioxidant, antimicrobial and UV-shielding. Cellulose nanocrystals (CNC) and chitin nanocrystals (ChNC), although highly effective fillers, cannot form strong and flexible self-standing materials that are required for packaging applications. Therefore, in this Chapter we assess their effects as fillers in fiber-based composite packaging materials, where CNC and ChNC are minor components.

Currently most of agricultural operations generate residues, waste or by-products that are either under-valorized in applications aiming at energy recover by thermal means or represent an elevated cost for their disposal and management in landfills that also includes transportation. These approaches hinder remarkably circularity of the resources. Interestingly, such natural resources display a wide variety of chemical composition and physicochemical aspects that serve as an extremely versatile toolbox for the preparation of sustainable building blocks for packaging materials of the future bioeconomy. Their complex, composited, chemical structures, however, need to be considered when defining their individual role within the packaging materials, in terms of performance but also as extraction yield. In **Figure I.3**, we demonstrate a few common plant-based biomass residues (including wastes and byproducts), putting into perspective their natural compositions emphasizing their major component that

would directly influence the selection of the precursor for a given colloid. Animal-based biomasses are described in **Figure I.7** following the same approach.

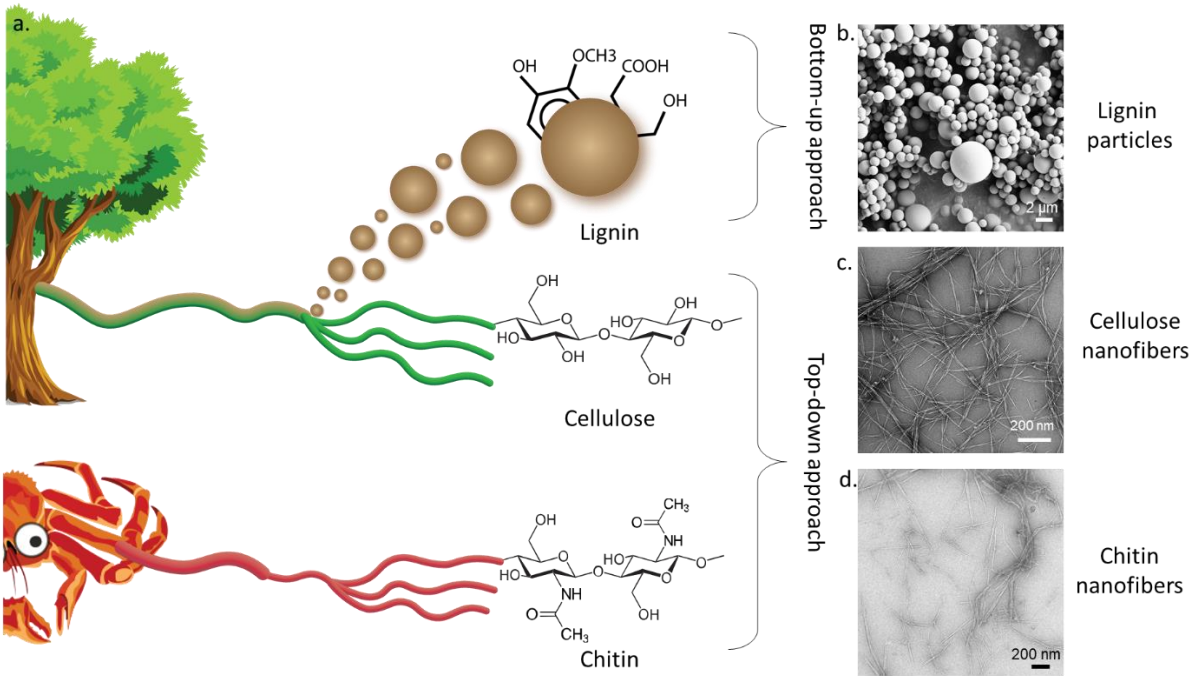

Figure I.2. a. Structure of lignin, cellulose and chitin associated with one of their sources. Lignin particles are obtained by bottom-up approach while cellulose and chitin nanofibers are produced by fiber deconstruction processes. SEM (**b.**) and TEM (**c.** and **d.**) images of the different colloids: lignin particles (**b**.), cellulose nanofibers (**c**.) and chitin nanofibers (**d**.).

2.1 Cellulose rich residues and their conversion into nanocelluloses

2.1.1 Nanocellulose sources

Cellulose has been mostly extracted from wood for the pulp and paper industry or from cotton for the textile industry; however, cellulose represents a major fraction on biomass from several annual plants as it plays an important role in the plant structure together with hemicellulose and lignin. Alternative cellulose sources must be considered given the increased demand for biopolymers. They include agricultural residues, waste from industrial food production but also algae or annual plants like reeds that can be valorized (**Figure I.3**). Additionally, municipal waste such as paper and textiles from cotton are available in large quantities and currently are not fully valorized.[6]

The use of agricultural residues and industrial waste offers several advantages over wood, including low initial value, high volumes and short growth cycles.[7] It also prevents waste and the costs associated with their disposal in landfills or management, as well as their utilization

contributes to efforts towards a circular economy. Decrease in resource waste takes place by following two complementary strategies, namely i) the valorization of every part of a crop and ii) the valorization of every crop. Cellulose rich biomass from agricultural crops includes straw, bark, shells, leaves, husk, roots of different crops such as corn, pineapple, soybeans, almonds and wheat. Wastes from food production are usually already processed waste such as bagasse, pomace, coffee spent or peels. The latter tends to impose more technological challenges in their utilization given the alteration of their physicochemical properties during food processing.[8] Nowadays, plant-based biomass residues are utilized in low added value products such as feed, compost, energy recovery or even disposed in landfills. Already processed waste could lead to reduce amounts of steps for extraction and purification but final quality of nanocellulose could also be impacted by a high processing degree. Textile waste derived from cotton may contain more than 90% of cellulose, and therefore it must be considered as a potential source for nanocelluloses. In fact, the production of textiles is increasing worldwide, and cotton is still the most consumed fibers.[9] It was reported that only 15 to 18% of textiles are recovered (reused or recycled) in Europe and in the US which represents large quantities of textile waste for further valorization. Another atypic cellulose source is algae, as it can contain as much as 40% cellulose, it is a great alternative source with high potential for cellulose extraction.[10] It is sometimes considered as an invasive species while for example it strands in high amounts on beaches. Often, municipal efforts are directed for the removal of algae from coastal areas, especially touristic ones, which is typically an expensive operation with no further utilization of the recovered biomass.

Overall, cellulose could be extracted from a variety of unconventional sources in different quantity and quality depending on their isolation processes. The source will influence the fibers properties such as purity, length, crystallinity, and mechanical strength; however, this does not necessarily apply to the nanofibers and nanocrystals obtained from these sources as they require further deconstruction of the plant cell wall. We discuss next the processes to obtain nanocelluloses from such unconventional sources as well as their properties, putting into perspective with nanocelluloses obtained from wood pulp – a more traditional source for nanocellulose in general.

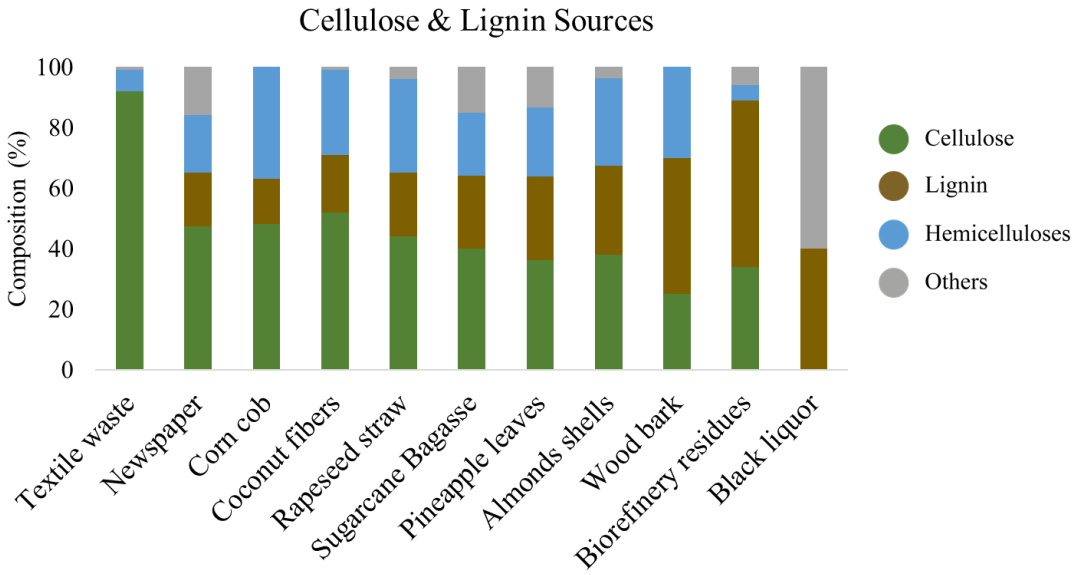

Figure I.3. Examples of sources for cellulose and lignin and their composition. Data extracted from[11–19]

2.1.2 Extraction of nanocellulose from unconventional sources

In plants, cellulose is arranged in a hierarchical fibrillar structure in the primary cell wall. The fiber bundles comprise microfibrils, themselves assembled by elementary nanofibrils. The latter, sizing *ca.* 5 nm in diameter, are composed of cellulose chains arranged parallelly and interconnected by hydrogen bonding. The fibrillar and semi-crystalline structure of cellulose in nature gives rise to the possibility of making two kinds of nanocelluloses: nanofibers and nanocrystals. Their intrinsic properties are highly connected to their extraction process. Cellulose nanofibers (CNF) production involves mechanical treatment while cellulose nanocrystals (CNC) are made by chemical hydrolysis of the amorphous part of cellulose. Disintegration of fibers suspensions in nanofibers results in high aspect ratio, flexible nanofibers (length over 1 micron and diameter of 20-100 nm) while the acid hydrolysis of cellulose fiber leads to rod-like, rigid nanocrystals with length between 50 and 350 nm and diameter of 5-20 nm.[20] Here we focus primarily on CNF, as it has the ability to form self-standing, strong and flexible films that are suitable for food packaging applications.

The production of nanocelluloses from agricultural and industrial wastes have increased in the past few years and recent reviews have summarized the different sources and processes to prepare such colloids (Garcìa *et al.* (2016),[11] Boufi (2017),[7] Pires *et al.* (2019),[21] Pennells *et al.* (2020)[22]). According to Pennells *et al.* over the 2669 publications on the production of CNF between 2004 and 2018, 34% of them were about non-wood sources. The major sources of non-wood CNF were reported to be cotton, bamboo, palm, sugarcane, rice, and algae but in

total 100 different sources were identified. We cross-referenced the number of papers with the annual production of each source to obtain an estimate of the most promising agricultural sources for CNF production. Residues from sugarcane, maize, rice, wheat, and palm fruit stand as the most promising as shown in **Figure I.4**.

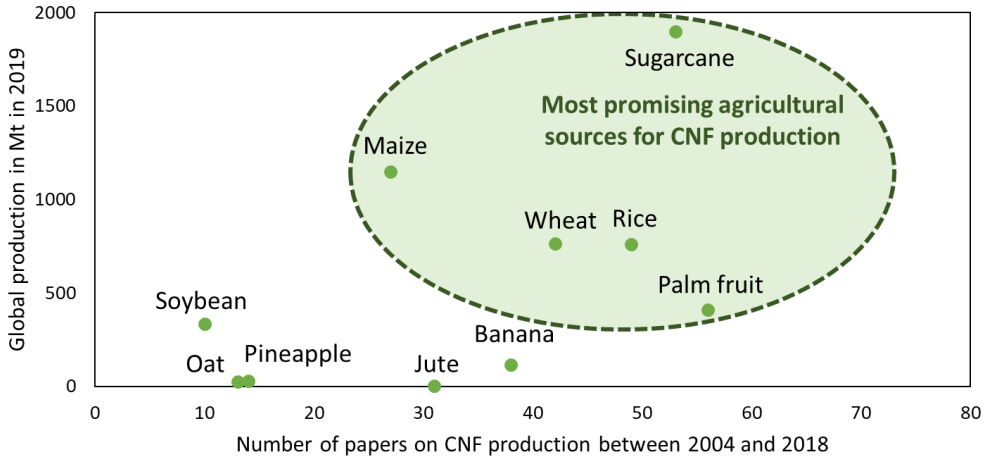

Figure I.4. Global production of the most studied sources for CNF production. (Annual production for 2019 from FAO statistics and number of papers per sources extracted from Pennells *et al*.[22]).

Whether for wood or unconventional sources, processes to produce cellulose nanofibers are centered on mechanical treatments using grinder, microfluidizer or homogenizer.[23] High energy consumption is a major issue in mechanical processing (**Figure I.5**), being the focus of optimization studies aiming at more sustainable nanocellulose production.[24] To decrease the energy consumption, chemical and mechanical pre-treatments of the cellulose fibers have been developed, whereas enzymatic hydrolysis, steam explosion, ionic liquid and twin-screw extruder are among the greenest ones. Espinosa *et al*. compared different mechanical treatment for the production of CNF from wheat straw and concluded that twin-screw extrusion used 5 times less energy than conventional methods (high pressure homogenizer and ultrafine grinder).[25] Furthermore, combination of enzymatic pre-treatment and twin-screw extrusion further decreased the energy consumed for making nanocellulose out of wheat. Berto *et al*. have shown that optimized enzymatic treatments, with endoglucanases, lead to up to 25% energy saving in the production of cellulose nanofibers by mechanical grinding (Masuko). Moreover, the authors highlighted that in most of the recent efforts the pretreating solution is overloaded with enzymes, reaching values 10 times higher than what is required for an efficient

enzymatic pretreatment.[26] The energy consumption depends on the process but also on its duration as nanofibers with smaller sizes will demand longer time and higher energy for their production, hence well identifying the need in CNF dimensions is key for optimizing the energy input.[27]

CNF display high surface area which combined with their high-water absorption capacity leads to the formation of a gel at low consistency (1-2%). The high-water content in CNF suspensions results in large volumes of material, thus inducing extensive costs for transportation or for drying before transportation. For that reason, processes that produce CNF at high consistency have been developed in the past years, and it is expected that more process will emerge given the promising applications for CNF. The HefCel method, developed by VTT (Finland), consists in enzymatic hydrolysis of cellulose at high consistency (20-40%) with constant agitation. The enzyme activity combined with the fiber-fiber friction results in CNF with high yield (>90%).[28] With a different approach, in 2015, Ho *et al*. reported for the first time the fibrillation of pulp at 28% with twin-screw extrusion with control over their defibrillation degree, which depended on the number of passes in the extruder. However degradation of the CNF due to heating at long processing conditions was also reported.[29] Since then, different pre-treatments combined with twin-screw extrusion have been studied leading to high consistency functionalized CNF associated with decrease in energy consumption compared with conventional grinder.[30,31]

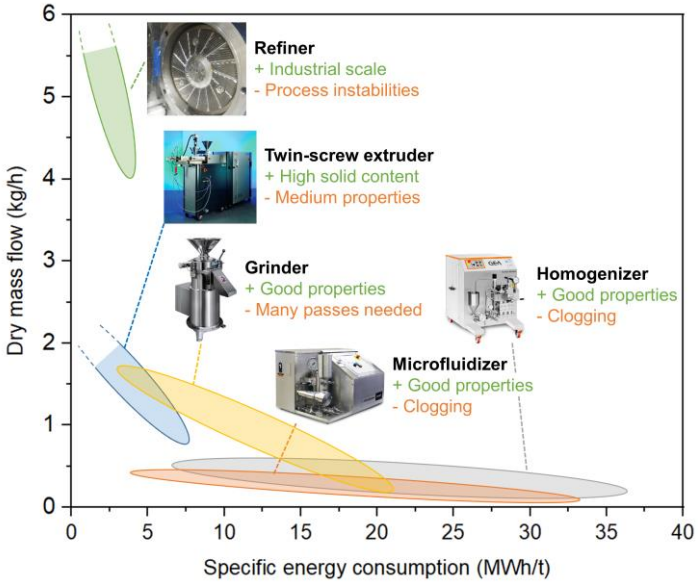

Figure I.5. Different processes used to produce CNF associated with their energy consumption and main advantage and drawback. Reproduced from[32]

On the other hand, the steps that consume the highest amount of chemicals and water are the extraction and bleaching of the cellulose fibers however this step has already been optimized throughout many years of research and industrial practice. A route to reduce the chemicals and water used during extraction of cellulose is the preparation of non-pure system by only partial removal of lignin. Mechanical disintegration of the lignocellulosic biomass leads to lignocellulose nanofibers, called LCNF. Espinosa *et al*. showed that the energy used to produce CNF from unbleached pulp from wheat straw was similar than for bleached pulp, however the size of the nanofibers were smaller for LCNF and their assembled films had higher mechanical properties.[33] Lower energy is then required to obtain LCNF with similar quality than CNF.

Among the non-plant sources, algae is a promising future source for CNF production.[10,34,35] However the process of extraction and CNF preparation might differ from those optimized for plant resources as cellulose from algae has high crystallinity (>95%) and high molecular weight. As a matter of fact, Xiang *et al*.[34] showed that the addition of an enzymatic pre-treatment to cellulose from green algae did not show any significant difference on the nanofibers size but it decreased the crystallinity of the final CNF. CNF obtained from algae by micro-fluidization only already displayed sizes at the elementary fibrils level (*ca.* 10-30 nm). Therefore, processes for obtaining CNF are somewhat universal, but they should be optimized to every new source and depending on targeted application. The processes for obtaining CNF from algae resources should account for the presence of plant protein in the initial precursors. Guo *et al*. have shown that even with chemical pretreatments (with maleic acid hydrolysis or $NaClO_2$ oxidation) prior defibrillation of green macroalgae biomass, the resulting CNF contained residual proteins.[35] Interestingly, the low amount of proteins in the CNF resulted in films with enhanced thermal performance. Therefore, similarly to the benefits observed for residual hemicelluloses and lignin in CNF matrices[36,37] and their materials, protein in algae could infer multiple advantages as far as simpler processing (without extensive purification), but also better materials properties.

Municipal solid waste such as textiles and paper were also investigated as raw material for nanocellulose production.[13,38,39] Production of nanocellulose from such materials is considered as a recycling operation as the product needs to be processed for a second time. Newspaper, old corrugated containers and office papers are the most reported sources for nanocelluloses production.[40] The high amount of cellulose in these wastes make them interesting for nanocelluloses production however purification is still needed as the presence of impurities such as dyes, ink, fillers, plasticizers, additives, and oil would influence the final nanocelluloses quality.[40] Even though, initial state of fibers from recycled newspaper appeared more fibrillated

than bleached softwood pulp fibers, Josset *et al*. showed that grinding of recycled newspaper without purification used slightly higher energy than bleached softwood pulp (6.75 kWh/kg compared to 5.25 kWh/kg) due to the presence of impurities.

2.1.3 Properties of CNF suspensions obtained from residues

The great majority of processes for obtaining CNFs from unconventional (residues) sources has been adapted from those created to extract CNF from highly purified systems (*e.g*. cotton, wood pulp). On that note, it is expected that CNFs from residues, depending on their degree of processing, will contain a varied of co-components that even at low fractions can significantly impact the CNF properties. CNF from biomass residues may contain hemicelluloses, pectin, monomeric sugars, lignin, tannins, minerals, and secondary metabolites. The number of publications addressing the topic directly is not large, and straight comparisons are not always possible. However, we identified the major residual components present in CNFs from biomass residues to further discuss their effects on the CNF properties using idealized/model systems, which are often artificially composited with a given biomolecule for given purpose. Additionality to the short number of publications on the field, there are not straightforward methods to compare quality of CNFs obtained from different sources, as it also depends on their final application. However, Foster *et al*. gave a good overview of the different technics used to characterize nanocelluloses suspensions from surface charge density to rheology including surface modification characterizations, which could be used as comparative starting points.[20] In that sense, Desmaisons *et al*. created a quality index that indicates a level of quality for the CNF based on both suspension and films analyses.[41] For packaging applications, the film forming capacity of cellulose nanofibers and the properties of these are the key factors, which are strictly related to the physicochemical properties of CNFs, *e.g*. size, surface and bulk chemistry and charge, and how they behave collectively in suspension, *e.g*. rheology.

CNFs dimensions are key features driving their colloidal behavior as well as their ability to make strong films. CNFs with diameter between 5-10 nm and length up to several microns leads to nanofibers with high aspect ratio as well as high surface area. Both properties are tethered to the CNF extraction process, pretreatments taken, and the composition of initial biomass as it can affect its recalcitrance. The latter is extremely important in the context of valorization of biomass residues into CNFs for packaging applications, as such precursors are usually complex mixtures.

In this context, Josset *et al*. prepared CNF from wood pulp, wheat straw and recycled newspaper (**Figure I.6**), and measured the surface area with BET as an indicative of their

dimensions.[14] Wheat straw has higher inorganic content when compared to wood, whereas newspaper has been consolidated into packed fiber networks added of other components (*e.g.* inks). The surface area was measured to be 226 m^2/g, 132 m^2/g and 155 m^2/g for CNF from wood pulp, straw and recycled paper respectively.[14] The lower surface area of CNF from recycled newspaper showed the difficulty to separate nanofibers after drying, because of hornification effects. The presence of inorganics – in wheat straw – imposed even higher challenges for the extraction of small CNFs as the minerals are usually highly interacting with cellulose across the plant cell wall.

Due to its high surface area and hydrophilic nature, CNF networks form hydrogel at low concentrations in water which make the processing of highly concentrated suspensions difficult.[42] When shear is applied, these hydrogels present a shear thinning behavior with alignment of the nanofibers with the flow field at high shear leading to decrease in viscosity, it makes nanocelluloses attractive as rheology modifier in a large range of fields (paints, 3D printing, coatings…).

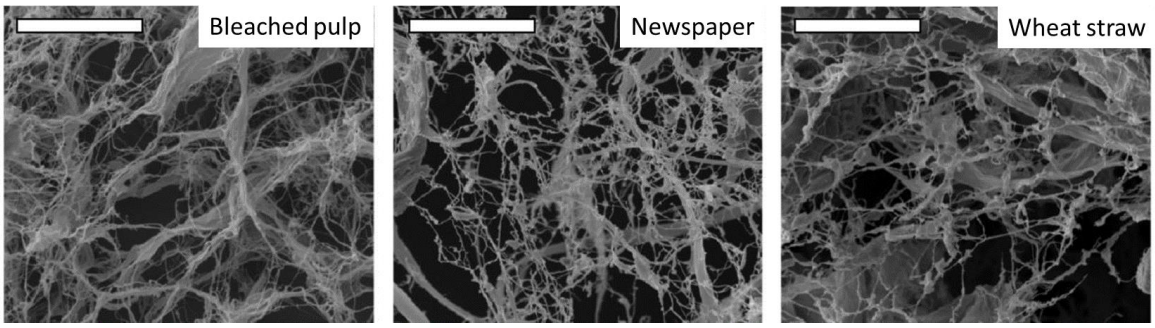

Figure I.6. SEM images of CNF produced from bleached wood-pulp fibers (ECF), recycled newspaper (NP) and wheat straw (WS). Scale bar is 10 μm. Reproduced from[14]

Colloidal stability of CNF is of importance especially for processability, colloidal stability is related to their surface charge and size. To be colloidally stable CNF need to be well individualized otherwise non-fibrillated fibers will sediment. One easy way to measure the stability is by zeta-potential measurement, the highest the charge the highest the stability. Chemical modifications that could be done as pre-treatment or post fibrillation will also affect the sedimentation and aggregation of CNF. Non-modified CNF are negatively charged with zeta-potential around -60 mV while TEMPO oxidized CNF usually have high surface charge of -75 mV.[43]

CNF are semi-crystalline particles; their crystallinity can vary depending on the source of the cellulose. For example, cellulose from algae is known to be highly crystalline.[10] Moreover. it was reported that the crystallinity of soybean-CNF was higher than wood-CNF (78% and 70% respectively) explained by differences in the process used for purification and possibly to different crystallinities of the precursors.

In terms of thermal properties, cellulose is a polymer that doesn't have glass transition temperatures, it degrades before melting. For that reason, the technics used for cellulose processing often differ to one used for classic polymers. However, due to its high crystallinity, cellulose has a high degradation temperature. Ferrer *et al*. demonstrated that CNF from soybean had a higher onset degradation temperature of 305°C and maximum degradation temperature of 361°C, compared to 282°C and 355°C for CNF. The higher amount of hemicelluloses in CNF (22% compared to 10% for soybean CNF) was responsible for the shift in degradation temperature to lower value.[44] LCNF from pine cone showed higher degradation temperature than CNF from the same source.[45] Elsewhere, the impact of the sizes on the degradation was studied and it was found that smaller nanofibers lead to lower degradation temperatures.[46] The high specific surface area of CNF increases the exposition to heat and thermal degradation.

The presence of three hydroxyl groups in the glucose unit is responsible for the hydrogen bonds inter and intra chains that makes the interactions between cellulose chains and fibers highly cohesive. When dried, this network forms films with high strength. Different processes are used to make films, the most common ones are suspension casting and filtration. Films can also be made by regeneration of dissolved cellulose or electro-spinning. In this Chapter, we will talk about films made by casting and filtration as they maintain the nanofibrillar structure of CNF. The drying parameters are of high importance as they will highly influence the films properties (porosity, water interactions, mechanical properties, barrier properties). Sehaqui *et al*. studied the preparation conditions on films properties.[47] The films obtained with a semi-automatic sheet-former (vacuum filtration and drying for 10 min at 93°C and 70 mbar vacuum) presented the highest mechanical strength compare to films made by solvent casting, filtration and oven drying or filtration and hot-pressing.

Regarding packaging applications, CNF films have high strength and toughness, and they were shown to have good barrier properties against oxygen especially at low humidity, these properties will be developed more in details in the second part of this Chapter.

2.2 Chitin rich residues as precursors for nanochitin

2.2.1 Conventional and emerging sources

Chitin is the second most abundant polymer on earth after cellulose. Chitin is a linear polysaccharide derived from glucose; it is composed of N-acetyl-D-glucosamine units linked with β-(1,4) bonding. It differs from cellulose by the substitution of one hydroxyl group by an acetyl amine group which bring positive charge to the fibrils surface. Chitin and cellulose have several similarities in their composition and they both have fibrillar arrangement in nature. However, animal-based biomass and fungi are the main sources for chitin, thus affecting greatly the composition of their sources with a direct impact over the extraction methods. The annual production of chitin in nature is 10^{11} tones/year by every ecosystem[48] which offers a great possibility for chitin industrialization. In **Figure I.7**, we present the major and emerging sources for chitin extraction with their chemical composition. Traditional sources are crustacean shells, which are already generated in significant amounts as waste from the fishing industry. However new sources for chitin are emerging as by-products of the recently born insect industry.

Crustaceans and especially shrimp, crab and lobster are great sources of chitin as their shells is composed of *ca.* 20% of chitin.[49,50] Shrimps and crabs are farmed primarily for their high-valued meat, but a significant amount of biomass is left often unused and landfilled. Today, chitin is industrially produced and commercialized from these sources, with an annual production of *ca.* 30 000 tons in 2015.[51] At the moment, chitin is mainly used in water treatment, food and cosmetic industry or process into chitosan for a larger range of applications. Other sources of chitin that have potential for industrialization are insect cuticles and mushrooms.[52] While at the moment the Asia-Pacific holds two-thirds of the global market of chitin and its derivative,[51] development of chitin from insect farming could equilibrate the market worldwide. Reduced environmental impact of the insect industry could also stimulate the production of insect-based chitin.[53,54]

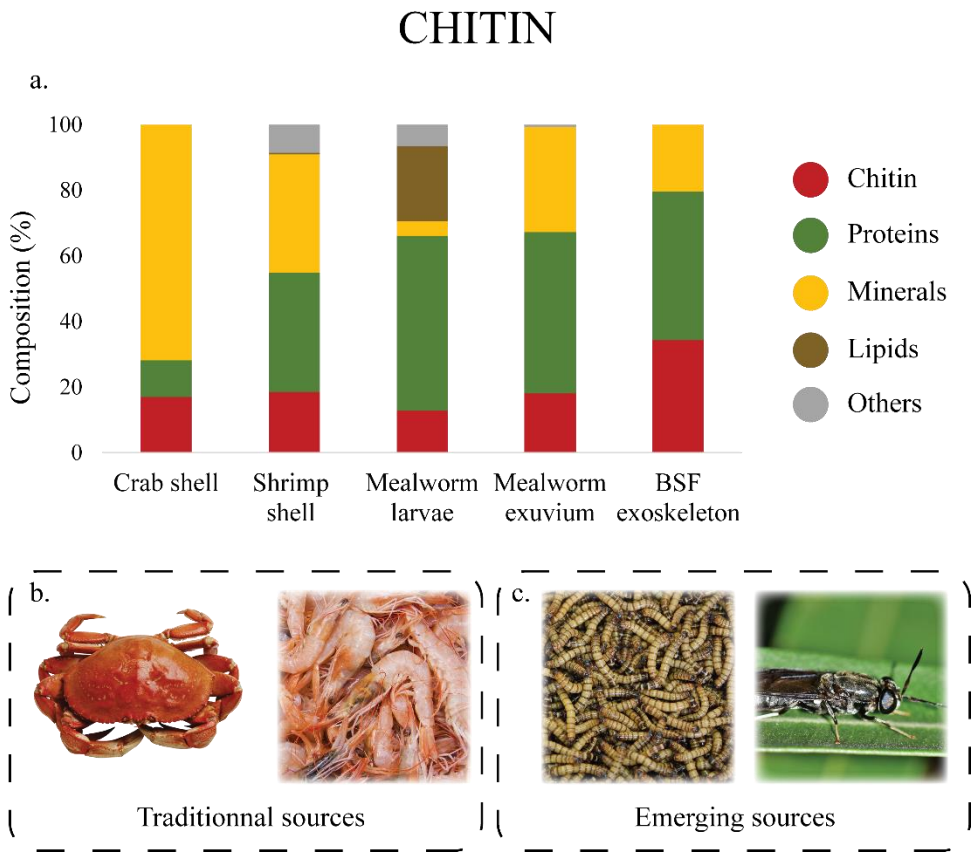

Figure I.7. a. Main chitin sources associated with their compositions. Crustacean shells (**b.**) are traditional sources for chitin nanofibers while insects are emerging as promising sources (**c.**). Data extracted from[49,50,55–57]

In crustacean, chitin fibers are surrounded by proteins and embedded in a mineral-protein matrix that forms a 3D helicoidal structure.[58] The extraction process of chitin in crustacean shells always follow the same major steps of demineralization (acid) and deproteinization (basic). However, there is a wide range of conditions being used within each of these major steps. For instance, acid (HCl) concentration can vary from 0.275 to 2 M, temperature from 25 to 100 °C, during times ranging from 1 to 48 hours for demineralization. For deproteinization, the conditions are less scattered, with 1 M NaOH at 65-100 °C, but the time of reaction is still in a wide range of values, from 1 to 72 hours mainly correlated with the temperature. Percot *et al*. set up a method to optimize the reaction time following the pH after acid addition during the demineralization step. In fact, solubilization of $CaCO_3$ increased the pH, therefore when the pH of the medium was observed to be constant during the further addition of acid, the reaction was considered as complete. Moreover, the deproteinization efficiency was tracked by UV-Vis spectroscopy, following the absorbance at 280 nm that is related to the tryptophan protein present in the crustacean shells. Percot *et al*. optimized the extraction of chitin flakes

from shrimp shells, which resulted in demineralization with 40 mL/g of 0.25 M HCl during 15 min at room temperature, and deproteinization with 1 M NaOH at 70°C for 24 h. Controlled demineralization allowed to minimize the hydrolysis of the glycosidic bonds and decrease in molecular weight while following the deproteinization conditions enable control on the degree of acetylation.[59] However, these parameters should be handled with care and only relate to specific initial material, optimization should be performed for each new source. The amount of acid and base used for purification of chitin are considerable and to make the process the more profitable, the extracted proteins and calcium carbonate in the shells should be valorized as well. Chitin extraction is tethered to the recalcitrance of the initial materials, which affects solvent accessibility, dissolution kinetics and mass transport of products. Degree of processing of the biomass also greatly affects recalcitrance.

Dissolution with ionic liquids is an alternative to the acid/base extraction of chitin from the arthropod's cuticles. Qin *et al.* extracted chitin from shrimp shells using 1-Ethyl-3-methyl-imidazolium acetate ([C2min][Oac]) ionic liquid[60] and Shamshina *et al.* obtained chitin from shrimp shells with hydroxylammonium acetate ([NH_3OH][OAc]).[61] Chitin extracted with ionic liquid has high molecular weight and high purity, with a remarkable technical benefit that relates to the recyclability of ionic liquids. However, these procedures are still at experimental scales and need more time to be implemented at larger scale.

Usually insects contain between 5% and 25% chitin, but chitin can account to 35 wt.% of the exoskeleton of Black Solider Flies (BSF), which is a by-product from the insect farming industry.[52] Insects are promising sources of chitin for the future due to the fast development of insect factories all around the world. The first aim of these factories is to produce proteins that could replace, in a near future, soy for animal feed or even meat for humans.[62] They have several great advantages regarding actual ecological concerns: their protein yield to surface ratio is incredibly high compare to current proteins sources,[54] they also have lower water and land footprint, and faster growing rates. Additionally, the current business model aims at taking advantage of the whole insect. The frass produced by the insects is sold as fertilizer, whereas the lipids extracted alongside the proteins is commercialized as oil. This promising industry is growing as several new companies are entering the market (InnovaFeed, Agronutris, Protix, Enterra, Ynsect) as the legal framework is being implemented.[63] Recently, mealworm which is characterized as a *"novel food"* was considered safe for human consumption by the European Food Safety Authority.[64] As far as insect farming, black soldier fly (Hermetia Illucens) and the mealworm (Tenebrio Molitor)[62,63] are the most relevant species. Besides the production of proteins, lipids and fertilizer, the insect farming gives another alternative for upcycling biomass

(agricultural and food) residues as feed. Thus, decreasing mostly water and land footprint of the biorefinery. On that note, insect farming can ultimately become carbon negative. To minimize the waste production, every part of the insects should be valued. The insect shell that is removed during molting is also a side stream that contains higher amount of chitin,[65] and it could be directly used for chitin extraction in parallel to the insect breeding.

The main constituents present in chitinous crustaceans and insects are similar, but the ratios differ greatly among them (see **Figure I.7**). Whereas crustaceans contain mainly minerals, insects have more proteins and lipids. The extraction of chitin from insects should then be adapted to their initial composition that is not rich in minerals. The demineralization step is shorter and milder while an additional step for lipid extraction is usually done as first step, for instance, Huet *et al.* extracted chitin from *Bombyx eri* larvae and obtained chitin with different purities (45%, 90% and 93%). After juice (lipids and proteins) removal by extrusion, residues containing 45% chitin were deproteinized with 1M NaOH at 80°C during 24 h. At this stage chitin with 90% purity was obtained mainly due to the low mineral content of the larva (1.9%). Purity was slightly increased to 93% with an additional demineralization step (1M HCl at 80°C for 35 min). Brigode *et al.* extracted chitin from three different processing stages of *Hermetia Illucens* farming, puparia (pupa exuviae), adult insect and chitinous flakes obtained after oil extraction. Acid-base extraction (1M HCl, 100°C, 30 min for demineralization and 1M NaOH, 24h for deproteinization) was done and chitin contents of 25%, 8% and 21% were obtained respectively.[66] In several studies, chitin from insects showed comparable properties (purity, crystallinity, thermal properties) to chitin extracted from crustaceans,[57,66–69] and only differences is flakes morphology have been observed (**Figure I.8**).[57,68]

Mushrooms are another potential source of chitin as they are mainly composed of chitin, glucans, and proteins. In mushrooms, chitin nanofibers are embedded in a glucan matrix and act as reinforcing agents in the organism cell walls similarly to cellulose in plants. Fungi are already produced at industrial scale but mainly for food purposes. Moreover, the glucans present in high quantities are difficult to separate from the chitin and additional purification steps are usually required to obtain chitin with high purity. The difficulty to obtain high purity chitin, the low yield of extraction, and most importantly the competition with food do not make them the most promising source of chitin for materials. However, glucan-chitin synergies have led to materials with higher mechanical properties thus raising an interest for mushroom-based materials and further discussion on the food *versus* materials nexus in the bioeconomy landscape.[70] Nawawi *et al.* extracted chitin flakes containing high amount of glucans (50% for the mushroom cap and 65% for the stalk) from the common mushroom (*Agaricus bisporus*).

The extraction consisted of initial blending step of 5 min followed by hot water extraction at 85°C for 30 min and an alkali treatment with 1 M NaOH at 65°C for 3 h. For redispersion, 1 min blending was used as final step. Compared to chitin extraction from crustacean and insect, the conditions were quite mild with short reaction time and no need for demineralization. Other animals that contain large amount of chitin in their exoskeleton or shells, such as squid, mollusks, and riftia tubes, will not be discussed as they are not available in large scales, and especially as a side stream of any industry.

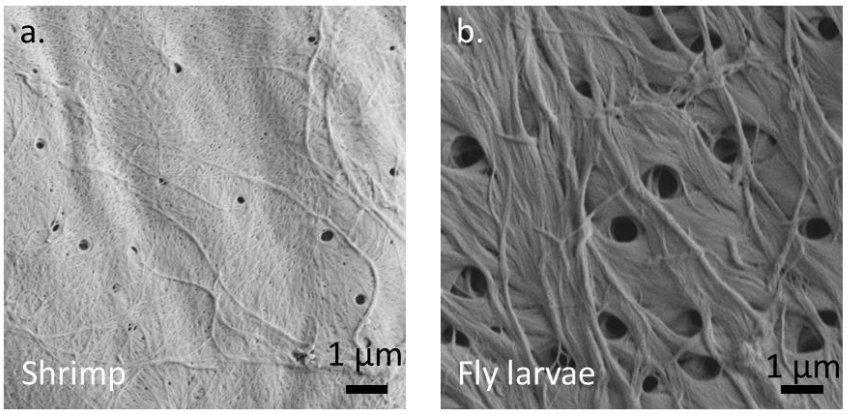

Figure I.8. Microstructures of chitin flakes extracted from shrimp shells (**a.**) and fly larvae (**b.**). Reproduced from[71]

2.2.2 Production of chitin nanofibers

The production of chitin nanofibers (ChNF) and nanocrystals (ChNC) is analogous to the processes for nanocellulose production. Chitin nanofibers are obtained by mechanical treatments of chitin flakes at acidic pH to protonate the amine groups and enhance repulsion between nanofibers. Microfluidizer,[72,73] ultra-fine grinder,[74,75] high pressure homogenizer[76] have been used to mechanically fibrillate chitin into single nanofibers. Combination of the above-mentioned with pre-treatments such as blender or high-shear disperser and post-treatment such as ultra-sonication is often reported.[3] Nanofibers with length over one micron and width between 10 to 50 nm are obtained with these methods. Furthermore, deacetylation of the chitin before fibrillation is often used as pre-treatment in order to obtain smaller nanofibers. With partial deacetylation of the nanofibers, electrostatic repulsion between the positively charged amine groups improves the defibrillation efficiency. Shorter mechanical treatments and decreased energy are then required. Bai *et al.* obtained deacetylated chitin nanofibers after only one pass through microfluidizer under 1500 bar. Long nanofibers with length over 1 micron and deacetylation degree of 27% were obtained.[73] However, the

deacetylation process is performed with harsh chemical conditions, usually NaOH at 30% to 50% during 2-4 h at 70-90 °C.[77,78] Looking for greener alternatives, Ye *et al.* has recently developed a bacterial enzyme, chitin deacetylases, to deacetylate chitin flakes under milder conditions (30 °C, pH 7 for 96 h). They increased the DA from 6.5% to 30.6% and were able to produce chitin nanofibers by sonication of the flake suspension.[79] Deacetylation is often heterogenous[77] and happens on the surface of the nanofibers.[80] Bai *et al.* showed that after 90 min of acid hydrolysis (to prepare ChNC) of already deacetylated chitin, the deacetylation degree was the same than the initial chitin.[81] This was confirmed by Narkevicius *et al.* and is explained by the deacetylation mechanism occurring mainly on the weakest part of the nanofibers which are the disordered part of chitin which are also dissolved during the acid hydrolysis.[82]

To further tune the nanofibers surface properties, other chemical pre-treatments similar to the ones used for cellulose have been also performed on chitin flakes (TEMPO oxidation[83], acetylation[84]). Fan *et al.* investigated the influence of the chitin pre-treatment on final nanochitin morphology after homogenization.[85] TEMPO oxidation and acid hydrolysis led to nanocrystals aggregated in bundles while deacetylated chitin formed a mixture of nanocrystals and nanofibers well individualized with a diameter of 4 nm (**Figure I.9**). In addition, with the idea of optimizing the fibrillation process efficiency, Mushi *et al.* added chitosan during the fibrillation and obtained ChNF that were fully individualized and more stable suspension without aggregation of the nanofibers.[86]

The results discussed so far focus on the extraction of chitin nanofibers and nanocrystals from crustaceans; however, emerging or non-traditional sources should follow same protocols. In 2002, Morin and Dufresne extracted chitin nanocrystals from Riftia tubes.[87] Similarly, in 2011, Ifuku *et al.* were the first to prepare chitin nanofibers from mushrooms. After fibrillation with ultra-fine grinder, nanofibers with similar morphology than ChNF from prawn and crab shells were obtained.[88] Moreover, to our knowledge only one paper reports the production of chitin nanofibers from insect and showed that chitin nanofibers can be produced from *Hermetia Illucens* larvae with higher degree of fibrillation than ChNF from shrimp shells for similar energy of fibrillation.[71] This encourages the production of chitin nanocolloids from emerging sources, such as insects, thus further promoting new investments in insect farming. Overall, the production of nanochitins out of chitin flakes from a variety of sources is a universal method following somewhat standard mechanical protocols that can be further enhanced or facilitated following a few known pre-treatments.

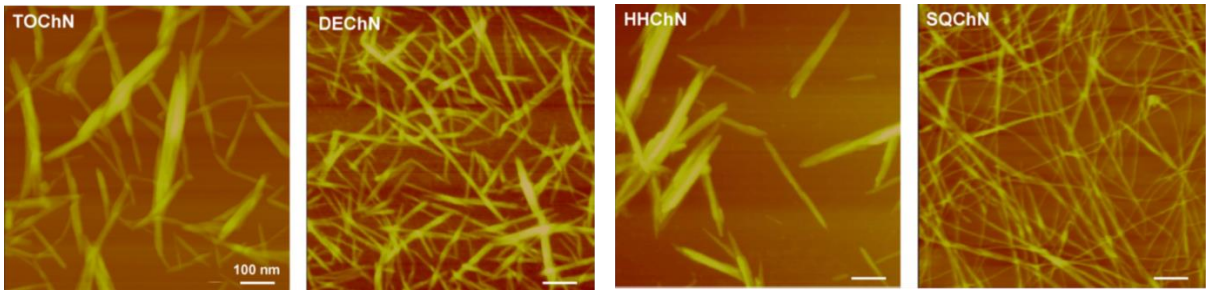

Figure I.9. AFM images of nanochitins obtained by homogenization of chitin from crab shells after different pre-treatment (Tempo oxidation (TOChN), partial deacetylation (DEChN), acid hydrolysis (HHChN)) and chitin nanofibers obtained from squid pens (SQChN). Reproduced from[85].

2.2.3 Properties of chitin nanofiber suspensions

Chitin sources have an influence on the polymeric chitin chains arrangement. α-chitin, which consists of an anti-parallel arrangement, is present in crustacean, insects and fungi. Such arrangement promotes strong hydrogen bonds inter- and intra-sheets. β-chitin is found in sea tubeworm and squid pen, where chains are arranged parallel to each other, leading to weak intra sheet bonding.[89] γ-chitin is composed of both parallel and anti-parallel arrangement of the chains and might be derived from α-chitin or β-chitin.[70] The chains conformation leads the either 2D (β-chitin) or 3D (α-chitin) structures of the fibers. The difference in allomorph induces differences in crystalline structures and stability/solubility, thus impacting the extraction and defibrillation processes. Here we only discuss α-chitin, as it is present in the most promising chitinous biomasses.

In opposition to cellulose, where residual biomolecules played a big role on the nanocellulose performance, nanochitins properties are mostly impacted by processing, especially the degree of deacetylation. Controlled deacetylation offers a means to tune the surface charge of the nanofibers, which highly impact the colloidal behavior of nanochitins, gel formation, entanglement upon consolidation, and interfacial activity. All these properties are relevant in the context of film formation, and their utilization as packaging.

Chitin nanofibers are usually several microns long and display diameter up to 20 nm, representing high aspect ratio colloids. Nanofibers from squid pen are known to have higher aspect ratios up to 750 while α-chitin usually is limited to 250.[90] The milder acidic treatment needed to extract ChNF from squid pen due to their low mineral content is responsible for the better preservation of the properties of native chitin. The size of nanochitins can be tuned by the processing conditions. For instance, Grande *et al.* have shown that nanochitin with aspect-

ratio of 15, 25 and over 60 could be obtained from crab shells by combining partial deacetylation with ultra-sonication.[91]

The large surface area and presence of hydroxyls group on the surface of the nanofibers result in the formation of hydrogels with high water content. Mushi *et al.* produced hydrogels of ChNF (acetylation degree 86-87%) at concentration as low as 0.4 wt% by slow pH shifting of the ChNF suspensions. The shift from acidic to neutral pH induced protonation of the amino groups leading to stronger fibril-fibril interactions and nanofibers entanglements.[92]

The degree of acetylation of non-deacetylated nanochitin can vary from 90% or higher depending on the methods for chitin extraction. Hence, amine groups are always present on the nanochitins surface which give a positive surface charge to the colloids. The presence of amines groups opens doors for surface modification and chemical grafting with a large variety of molecules. The pK_a of the amino group is around 6 hence, mild acidic solution is necessary to provide colloidal stability to the nanochitin suspensions. Deacetylation usually improves fibrillation efficiency and lead to smaller and more individualized nanofibers that can make stronger films than non-deacetylated ChNF films.

Similarly, to cellulose nanofibers, ChNF have the ability to form films with high cohesion at low humidity. The drying process as well as the solvent used for drying influence the porosity of the films and the properties related to it (mechanical properties, barrier properties).[93] Mushi *et al.* performed solvent exchange on wet ChNF cake obtained by filtration and obtained film with porosities ranging from 22% with water to 58% with acetone.[93] Higher modulus and strength were obtained for low-porosity films (77 MPa and 29 MPa for 22% and 58% porosity film respectively) however the tensile strain at break was lower (1.4% and 2.7% for 22% and 58% porosity film respectively). Furthermore, film made from chitin nanofibers from fly larvae were reported to have similar strength than equivalent films from shrimp shells.[71] The use of temperature during drying was reported to influence the final properties to greater extent than the chitin source.

More recently, people have focused on the characterization of nanochitins that are partially purified. It has several advantages of increasing the yield, reducing the chemicals and energy used for the extraction and therefore it is cost saving. Ifuku *et al.* prepared protein-chitin nanofibers complexes from red crab shells and showed that the presence of proteins on the ChNF surfaces increases the biomineralization chances to occur.[94] Nawawi *et al.* extracted nanofibers from *Agaricus bisporus* and compared to crab nanofibers, less mechanical treatment was needed to form non aggregated nanofibers. Despite the high amounts of glucans in the final nanofibers, 50% for the cap and 65% for the stalk, films showed higher mechanical

properties than ChNF alone.[95] Varying the amount of glucans, they also managed to tune the films mechanical properties (**Figure I.10**).[96] These promising results show that partial removal of components during purification could be beneficial and should always be considered.

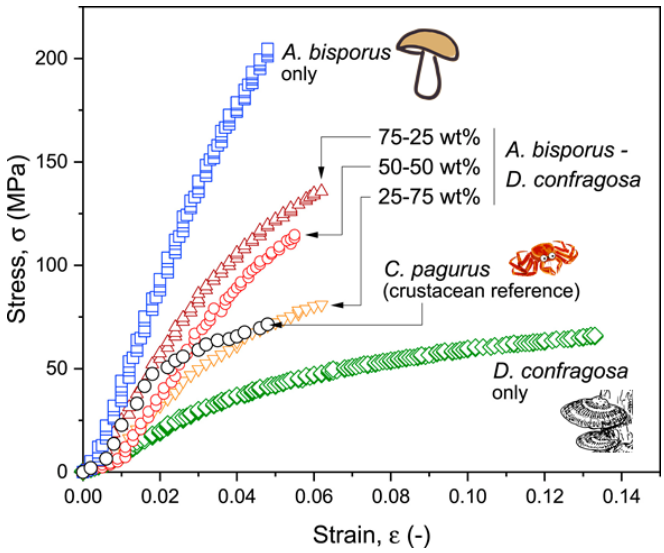

Figure I.10. Mechanical properties of films made from crab shells (*C. pagurus*) compared to common mushroom (*A. bisporus*) and bracket fungus (*D. Confragosa*) and a mix of these two. Adapted from[96].

Chitosan

Further deacetylation (chemically or enzymatically) of chitin leads to chitosan, its polymeric, soluble form that has been used in several applications where solutions (and not colloidal suspensions) are required. Chitosan is characterized by its degree of deacetylation which can vary from 50 to 100% and chain length (molecular weight from 30 to 1000 kDa).[97] The presence of primary amine in the chitosan structure makes it soluble in acidic water (pH 3-4) when the amines are protonated. Chitosan is conventionally obtained from crustacean shells like chitin but its production from mushroom or insects is also possible and have been investigated over the years.[52,57,98] Chitosan produced from *Hermetia Illucens* exoskeleton formed similar films when compared to the one produced from crab shell but had different viscosity and lower yields of conversion from chitin to chitosan. Therefore, extensive deacetylation processes of insect chitin still need optimization.[57] Chitosan have antibacterial property and thus is promising material for biomedical applications.

2.3 Lignin-rich biomasses as sources of active molecules and colloids

2.3.1 Conventional and alternative sources of lignin

Lignin represents 15% to 40% of the dry matter in lignocellulosic biomass.[99] It acts as a reinforcement in the plant cell wall and barrier against micro-organisms. Black liquor, a by-product of the pulping process, is the main industrial source of (technical) lignin. However, lignin from sugar/bioethanol production residues is emerging and has the potential to overtake the production of lignin from wood in the near future.[100,101] Moreover, more recently, lignin-centered biorefineries have been proposed, aiming at the production of well-defined and less degraded lignin that can amplify their utilization in higher end applications.[102] The molecular structure of lignin depends heavily on the separation process. Kraft pulping is the most common process utilized at industrial scale, where the produced black liquors has been primarily used as a (thermal) energy source to power the plant. However, one estimates that valorization of 5 to 20% of the residual lignin into valuable materials or chemicals would benefit the chain without compromising their own energy demands.[100] Other extraction methods exist in the industry such as alkali, sulfite, organosolv processes, each extraction method having a major influence on the lignin chemistry.[103] Moreover, lignin can be extracted from annual plants (*e.g.* crops) and other biomasses (*e.g.* barks, shells) other than wood. For example, Kammoun *et al.* extracted lignin from various residues: marine residues (*Posidonia Oceanica* leaves and aegagropile), agri-food byproducts (almond shells and olive pomace), forest residues (pinecones), and perennial lignocellulosic grasses (*Stipa tenacissima*).[104] In addition, as lignin and cellulose and usually associated in the plant cell wall, agricultural by-products used for cellulose extraction could be directly used for lignin extraction (see **Figure I.3**). In the case of emerging lignin from sugar/bioethanol biorefineries, the residues consist of a mix of lignin and cellulose, thus opening opportunities to full valorization of residues. Rivière *et al.* extracted both lignin and cellulose rich fractions to produce lignin particles and LCNF from recalcitrant hydrolysis lignin from wheat straw biorefinery residues.[17]

Overall, lignin is an aromatic polymer with complex structure that is still not well defined.[105] Lignin is highly heterogeneous in nature and when extracted, its chemical structure is further modified. The monolignol units composing lignin macromolecules are p-hydroxyl phenyl (H), guaiacyl (G) and syringyl (S), linked with different ether or carbon-carbon linkages.[106] Whereas annual plants contains the three different units, softwood is richer in G units, and hardwoods contains mainly G and S units.[107] However, during its extraction, lignin can be fragmented through β-O-4' bond cleavage which generates phenolic units, or lignin can condensate to create more stable C-C bond across the polyaromatic structure. Different solvent

used for extraction will influence in a different way these two reactions and lead to lignin with different phenolic content and different degree of cross-linking.[108] Therefore, based on the intrinsic, natural properties of lignin added of several chemical modifications that can take place during extraction, one can expect a wide variety of properties for lignin precursors and its particles.

2.3.2 Production of lignin particles

As mentioned above, the molecular structure of lignin is complex, and the variety of the extraction processes further modifies its structure. Lignin particles have been of preference to several groups as this is a way of overcoming the molecular heterogeneity of lignin, while keeping its functions. The micro- to nano-sized particles also brings new properties and functionalities to lignin to tackle current challenges by offering sustainable options for a large range of applications. Different preparation methods of lignin particles have been investigated, and they can be divided in two classes: the dry (spray-drying, aerosol reactor, ball milling) and wet methods (solvent shifting, anti-solvent precipitation, ultra-sonication, emulsification and cross-linking) (**Figure I.11**).[1,4,109,110] They result in particles with different size, size distribution, surface chemistry and consequently colloidal stability.

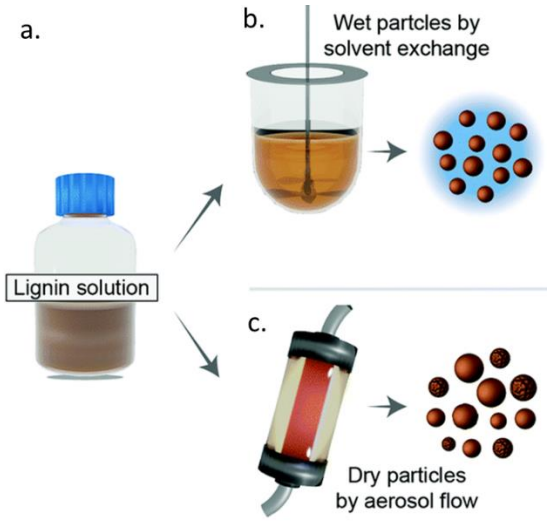

Figure I.11. Solution of dissolved lignin (**a.**) can be used to produce wet particles by solvent exchange (**b.**) or dry particles by aerosol flow reactor (**c.**). Reproduced from[1]

Anti-solvent precipitation method is commonly used as it is simple to set up, scalable and was shown to produce LP at low cost (**Figure I.11a**).[111,112] The process consists of the efficient solubilization of lignin (usually THF or Acetone) followed by the fast mixing of the solution

with an antisolvent, usually water. The mechanism of particles formation has been recently described.[1,113,114] Briefly, the large molecular weight lignin fraction due to their low solubility nucleate first and then smaller molecular weight fractions are adsorbed, and promote particle growth. Spherical particles ranging from tens of nanometers to 500 nm are formed (**Figure I.12a**). Adamcyk *et al*. studied the impact of molecular weight on final particle size (**Figure I.12b**), showing that higher molecular weight lignin produced smaller particles. The low amount of low molecular weight lignin limited the growth of particles and promoted high rate of nucleation in first place. It was also demonstrated that the hydrophilicity of lignin can increase the final particle size.[114] In the same manner than low molecular weight increases the particles size, increased solubility of lignin in the final medium will favor particles growth over nucleation. Other parameters such as surface chemistry, ionic strength of the antisolvent, initial concentration of lignin or rate of addition also have an impact on the LP sizes.[115–117] Richter *et al.* prepared LP by dissolving organosolv lignin at 5 g/L in acetone and water was added to obtain a final ratio of 90:10 (water:acetone) in volume.[115] By varying the addition rate from 1 to 1100 mL/min, particles ranging from 200 nm to 80 nm were obtained.

Aerosol flow reactor to produce lignin particles has also been demonstrated to be scalable.[118,119] The latter offers the possibility of working with dried particles, without the need for extra energy to dry them (**Figure I.11c**). With this method, LP present the advantage of being in a dry state which is attractive in terms of transportation and storage. More importantly they are dispersible in aqueous suspension after short time sonication.[118]Additionally, aerosol flow reactor may yield particles with different surface roughness, which depends on the solvent used for dissolution. Particles made of kraft and organosolv lignin at concentration of 0.5% to 2% in DMF were prepared with the aerosol method.[118] Due to the large range of sizes obtained, from 31 nm to 7.8 µm, particles fractionation, as far as size, was integrated in the process.

Overall, the stability of the lignin particles can be tune by changing the ionic strength of the suspension or the pH.[115] Modification of the surface charge can be achieved by adsorption of cationic polyelectrolyte or cationic lignin and will further influence the particles colloidal stability.[120]

While the first lignin particles were produced from lignin from pulp mills[121,122], more recently several publications reported preparation of LP from waste and by-products including coconut fibers,[123] cocoa shell,[124] woodchips,[125] sugarcane bagasse,[126] bioethanol production residues[17], corncob,[127], wheat straw,[128] and many others.[4] The processes for their assembly is virtually the same, with specific solvent systems adapted to the lignin source. Lignin particles from corncob lignin Posoknistakul *et al.,* produced lignin particles from organosolv lignin extracted from

sugar bagasse and wood by solvent exchange. The resulting particles had similar sizes and shape and the parameters of synthesis (solvent, lignin concentration and dialysis rotational speed) influenced the LP sizes independently from the lignin source.[126] With the same trends, Adamcyk *et al.* prepared lignin particles from wheat straw, spruce and beech with different temperatures of organosolv extraction.[129]

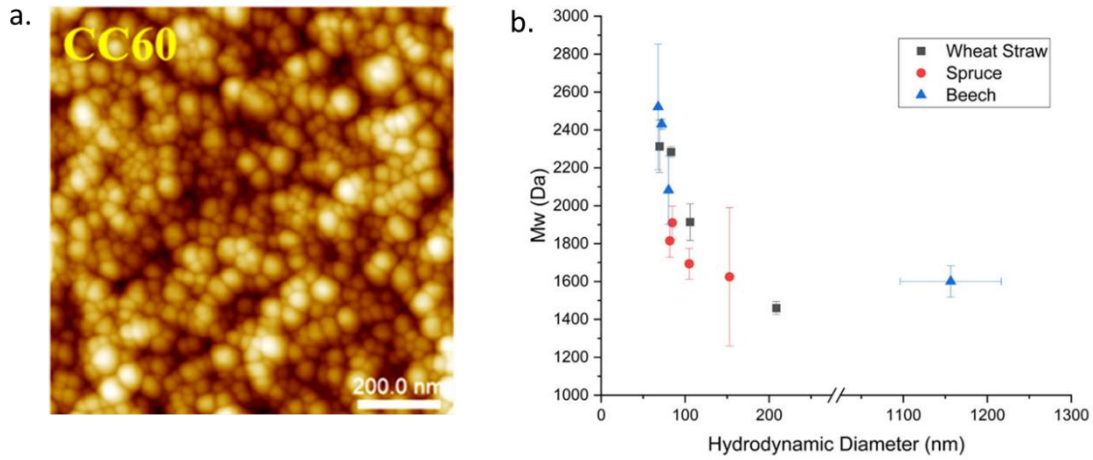

Figure I.12. a. AFM image of lignin particles obtained by solvent shifting of corncob lignin. Reproduced from[127] **b.** Molecular weight of lignin as function of LP hydrodynamic diameter for ethanol organosolv lignin from three different sources (wheat straw, spruce and beech). Reproduced from[129]

2.3.3 Properties of lignin and LP relevant for packaging

The formation of lignin colloids makes easier the incorporation of lignin into structures that are important for materials development. Several applications have been investigated for lignin particles including stabilization of Pickering emulsions,[118] drug encapsulation,[113] sunscreen,[130] water purification[131] and food packaging. Here we focus our discussion on lignin particles as antioxidant agent and UV absorber, both properties linked to the abundant phenolic hydroxyl groups present in lignin and related to food packaging application. The two key parameters to which these properties are tethered are the chemical groups on the surface of the particles and their size (which relates directly with the area exposed). Whereas the chemical structure is mainly influenced by the extraction method, the particles diameter is linked to the molecular weight of lignin and the conditions of preparation while the source of lignin has a relatively low impact on both, especially for particles obtained from anti-solvent method.

Although straight correlations between properties of lignin in its soluble and particle states have not been thoroughly addressed, it is somewhat accepted that lignin particles should mirror

the properties of the lignin macromolecule with a performance correction based on their surface area exposed to function.

Guo *et al.* extracted lignin from poplar with four different methods (DES, organosolv, soda/anthraquinone and hydrotrope), and despite the same source the final contents and types of phenolic hydroxyl groups was different. The antioxidant activity of the lignin was positively correlated with the total phenolic content and more specifically with the amount of syringyl phenolic hydroxyl group.[108] The organosolv and soda/anthraquinone had the highest phenolic content being of 3.37 and 3.25 mmol/g respectively and showed antioxidant capacity of 1250 and 1382 $\mu mol_{Trolox}/g_{lignin}$ respectively. The formation of lignin particles influences the anti-oxidant properties as only the phenolic groups present on the surface of particles participate to the radical scavenging activity, hence lignin particles are less active towards radical than free lignin.[132] However, when lignin particles are formed as the activity is positively correlated to the surface available, the smaller the particles the higher the activity.[127]

The presence of phenolic groups and other chromophores in lignin enables UV shielding capacity, which is promising for food packaging applications. The increase of UV shielding is often associated with a decrease in transparency. For example Zhang *et al.*, lightened kraft lignin by 314% by fractionation and acetylation but this resulted in slight decrease of UV absorbance.[133] Moreover, Zhang and Naebe reviewed the recent improvement in lightening of lignin and the effect on the UV properties. In summary, the critical parameters are the lignin structure (modification during extraction or post extraction), the morphology of the lignin particles and their size.[134] Here again, a smaller size of lignin particles allowed higher transparency and UV absorbance. Moreover, when incorporating lignin particles in film forming matrices, the dispersion should be well controlled as aggregates will decrease the transparency.

The color of the lignin and its particles affects the public perception towards new alternatives for food packaging. Lignin is darken by the harsh conditions of extraction (high pressure and high temperature) which typically leads to condensation and oxidation of lignin (**Figure I.13**).[129] Lee *et al.* managed to obtain light colored lignin by ball milling of rice husks followed by enzymatic treatment and dioxane extraction at room temperature.[135]

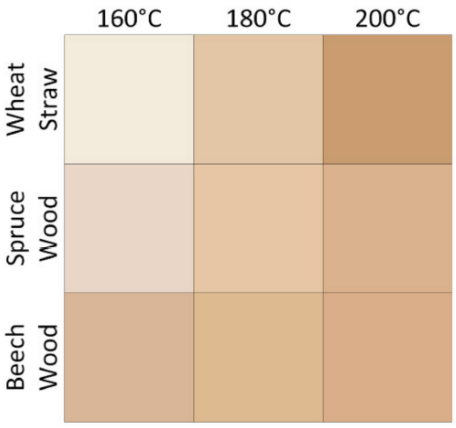

Figure I.13. Color of lignin particles from different sources and different lignin extraction temperatures. Reproduced from[129]

3. Biobased colloids in packaging: developments and challenges

This section discusses the most recent progress on nanofiber-based packaging including films made of nanocellulose and/or nanochitin as well as the incorporation of functional properties using lignin colloids. These films could be considered as biobased packaging because they are made of polymers or molecules extracted from biomass, as opposed to fossil based, but it does not necessarily imply that they are biodegradable. Herein we do not cover synthetic biobased such as PLA, bio-PE, bio-PP that derive from the polymerization of biobased monomers.[136]

3.1 Nanofibers in packaging

3.1.1 Requirements for packaging

The primary goal of food packaging is to protect the food from many external factors, in order to limit food spoilage and extend their shelf-life. External factors comprise microorganisms, light, different gases (oxygen, CO_2, water vapor) and liquids (water, grease) but also mechanical stresses that the packaging will endure during transportation and manipulation.[137] Food packaging also have secondary functions such as providing information for the consumer (nutrition value, preservation time, composition) as well as they enable easy handling and convenient usage of the good. For instance, packaging materials should maintain their structure while pouring liquids, have the possibility to be closed and re-heated for direct consumption. Moreover, a given packaging needs to be adapted to specific requirements of each food, for example dry or wet state, cold temperatures, with permeability or impermeability of certain gases, among others. To fulfill all these requirements, combination of different materials is often used either in a separate form like a plastic pouch and a cardboard box (*e.g.*, for corn flakes packaging), or combined in multilayer films like the Tetra Pak® packaging. The separated solution often requires higher amounts of raw materials but offers advantages in the processing and in the end of life as they can be easily separated and sorted by the consumer for recycling. On the other hand, the multilayer packaging is composed of thin layers with optimized mass of different materials; however, their manufacturing processes are more complex (lamination, co-extrusion, coating) and recyclability can be compromised. This shows the complexity of packaging manufacturing as many requirements need to be fulfill at once while each packaging must comply to one specific type of food and their conditioning requirements. Lindström and Österberg displayed the different oxygen and moisture gain or loss for more than 10 food and beverages.[136] For example, dried foods can tolerate a maximum oxygen gain of 5 to 15 ppm and a maximum water gain of 1% while instant coffee can only

tolerate a oxygen gain of 1 to 5 ppm but a maximum water gain of 2%. On the other side, liquids and canned fruits and vegetables have a limited water loss.

Although there is an urge for reducing packaging materials and replacing them from fossil fuels to those obtained from renewable resources, the existence of innumerous requirements imposes a major technological challenge. However, as we will discuss in this literature review, cellulose, chitin and lignin colloids have the potential to replace packaging in some niches and markets, while their composites may widen their spectrum of applications.

3.1.2 Advantages and limitations of nanofiber-based packaging

Biobased films made of cellulose or chitin nanofibers are still new materials, but they have shown promising results as packaging materials. Fiber-based packaging are made from renewable sources such as wood, plants or animal exoskeleton and can be sourced from by-products from agriculture of food industry as detailed in the first part of this Chapter. They have good thermal stability with high degradation temperatures (around 300°C)[138] which is an advantage for processing. Nanofiber films are often transparent (90% transmittance), have high strength (150-300 MPa) and present high barrier properties against oxygen at low humidity however, when in contact with water the mechanical properties as well as barrier properties are impacted. Nevertheless, the water sensitivity is an advantage when talking about end of life as it improves the biodegradability. Because they do not melt, cellulose and chitin nanofibers cannot be processed with conventional equipment for thermoplastic packaging manufacturing. The implementation of biocolloid-based materials as food packaging relies upon overcoming a few key technical challenges such as the large-scale, and cost-efficient production of nanofibers and particles, as well as development of manufacturing processes that can account for high water content. The environmental impact, from production to end life, of these nanofibers is still not completely understood, but they offer promising and more suitable alternatives at their end-life when compared to petrol-based packaging. In the following section we discuss relevant properties of biobased materials targeted at packaging applications. We discuss the current solutions utilized to overcome the present limitations associated with biobased packaging. Lignin and more specifically lignin particles will be considered as additives in the nanofiber films as property enablers.

3.2 Impact of water on nanofiber films

3.2.1 Water surface interactions

Surface properties such as hydrophobicity and lipophobicity are important parameters for food packaging applications to enable protection against water and grease either from the packed food or from exterior sources. The high amount of hydroxyl groups in cellulose and chitin (even when highly acetylated) nanofibers, leads to hydrophilic behavior, hence research has focused on decreasing or controlling the hydrophilicity of the films made from these polymeric nanofibers. Lignin is a more complex molecule and has a mix of hydrophilic (hydroxyl, carboxyl) and hydrophobic (aromatic, methoxy) groups, thus its surface energy depends on the extraction method used. The water contact angle of milled wood lignin thin film which is considered to be one of the closest to native lignin, was measured to be 53° for softwood and 56° for hardwood compared to 46° for softwood kraft lignin.[139]

Different measurement methods exist to assess water interactions. For surface wetting evaluations, one usually acquires the water contact angle (WCA) whereas Cobb test or gravimetric methods can be used to measure water absorption.[140] Surface chemistry and roughness of the material are the two main parameters to tune its surface energy, with superhydrophobic surfaces (WCA > 150°) being achieved only by controlling both features. When measuring WCA, the porosity of the material should also be assessed as it can influence the result due to water absorption.

Different approaches were reported to increase the WCA of nanofibers-based films including surface treatment or bulk modification of the film. Surface modification of nanofibers after film processing can take place by grafting hydrophobic molecules such as fatty acids or silanes, increased in contact angle from 50° to 90° was observed upon grafting of amino propyl trimethoxy silane on CNF.[141,142] Adsorption of polyelectrolytes or hydrophobic molecules as post-treatment has also been carried out.[143] Intending to create 100% cellulose-based materials for packaging applications, a process was developed to hydrophobized the cellulose or nanocellulose film surface called chromatogeny,[144] which comprises the grafting of fatty acid chlorides on surfaces that contain free OH groups. A small amount of liquid fatty acid is applied to the substrate followed by heating at 180°C. The process is solvent free and can be applied via roll to roll technology to reach water contact angles of 120 °C independently from the grafting density on bleached and unbleached CNF.[142]

The presence of residual lignin and lignin particles was also reported to decrease the water sensitivity of biobased films. Robles *et al.* produced LCNF films from pistachio shells with different lignin content and reported increasing WCA with lignin content (94° for films containing 20 wt% lignin compared to 53° for bleached CNF).[145] In another effort, films of

LCNF from hemp hurd displayed WCA of 103° compared to 66°for films made with bleached CNF from the same source.[146] These results are explained by the surface chemistry of lignin which is less hydrophilic than cellulose. Filling of the film porosity by lignin is also influencing the surface interaction with water.[33] When lignin is added post fibrillation, similar results were obtained. In our recent work, we demonstrated that the addition of 15% lignin nanoparticles to chitin nanofibers film increased the contact angle to 72 ± 5° compared to 32 ± 6° for chitin nanofibers alone.[147] Similarly, as for LCNF, these results are explained by pore filling due to addition of nanosized lignin particles and surface chemistry. Other studies reported that heat treatment of the nanofiber films increased its hydrophobicity by creating irreversible hydrogen bonds, post-treatment of CNF films at 150°C for 3h increased the contact angle from 61 ± 3 ° to 89 ± 4° as well as decreased the water retention value 127 ± 6 g/m^2 to 76 ± 4 g/m^2.[148,149]

3.2.2 Mechanical properties and impact of humidity

Various parameters influence the mechanical properties of neat nanofiber films. Nanofiber size, crystallinity and degree of polymerization, additionally to processing conditions should affect remarkably the porosity of the film and the orientation of the nanofibers within the film, which have a significant impact on barrier and mechanical properties for instance. Moreover, the moisture content in the film promote nanofiber swelling, leading to several nanostructure rearrangements that impact both barrier and mechanical properties as well.[150] It has been reported that nanofiber-based films display elastic modulus of 10 GPa and mechanical strength of *ca.* 150-300MPa under tensile stress; however, their deformation under stress is usually still quite low (< 10%) which is a drawback for the processability of the films.[150] Addition of plasticizer, *e.g.* glycerol, helps to increase the elongation of the films.[151] Ifuku *et al.* were able to tune the mechanical properties of deacetylated ChNF by adding different amount of glycerol. With the addition of 30% glycerol, the ultimate strength decreased by a factor two at the same time that elongation increased by two, while the transparency and thermal expansion of the films were not influenced.[152] The mechanical properties can be further tuned by promoting only a partial purification of the starting nanofibers. For instance, residual lignin in CNF films[33,145] or glucans in ChNF films[96] will affect the mechanical properties. Nawawi *et al.* demonstrated that chitin/glucans films from *Agaricus bisporus* containing 65% glucans had double elongation compared to chitin/glucans film containing 50% glucans while maintaining the same ultimate strength at 200 MPa.[95] Moreover, in nanofiber-based films cohesion arises from the nanofiber-nanofiber supramolecular interactions as well as fiber entanglement at the

nanoscale, therefore the presence of other molecules or particles in the films has to be well devised to avoid a significant disruption in the nanofiber network that is responsible for the high strength of the materials.

Water sensitivity of CNF and ChNF films impacts their mechanical performance. Water acts as a plasticizer, which can be a tool to tailor the mechanical properties of the film. However, when looking at the applications and in particular packaging, sensibility to water is a limitation. When in presence of high humidity (> 50% RH) or liquid water, water decreases the internal cohesion of the films by disrupting the hydrogen bonds network and the film starts to swell. To tackle this challenge in packaging materials, several solutions have been investigated including chemical cross-linking, ionic cross-linking,[153] ionic interactions with oppositely charged polymer,[154] hydrophobization, or physical hindrance.[155] Therein, the main objective is to prevent swelling of the film and/or reduce matrix-water interactions, by preventing hydrogen bonds formation. Moreover, the measurement of wet properties is a current challenge, mostly because the changes in the thickness of the film due to the wet conditions is usually overlooked.[156] In order to physically cross-linked CNF films, Toivonen *et al.* prepared CNF-chitosan mixture at acidic pH by film casting and dipped them in 100 mM NaOH after drying.[154] The change in pH favored the interactions between CNF and chitosan over those with water. With 20 wt% chitosan, wet maximum strength of 100 MPa with strain of 28% were obtained (**Figure I.14a**). Similarly, Kriechbaum *et al.* grafted gelatin on dialdehyde modified CNF and after film formation dipped the film in a tannin solution for gelatin precipitation. The water uptake was reduced from 167% for neat CNF to 25% for the modified film resulting in wet tensile strength of 33 ± 2 MPa and strain at failure of 22 ± 2 % (**Figure I.14b**). This is explained by a physical cross-link between tannins and gelatin to form water insoluble complexes.[157] Moreover, wet strength of cellulose based composite was obtained by making films of microfibrillated cellulose from sugarcane bagasse mixed with CNF (26 wt%) and lignin powder (21 wt%) and treating them at 150 °C for 6h after drying.[158] During heating, the temperature went over glass transition temperature of lignin which infused the lignin in the cellulosic matrix. Water absorption was decreased by 4 to 5 times compared to nontreated samples, thus resulting in wet tensile strength of 30 MPa after 30 min in water.

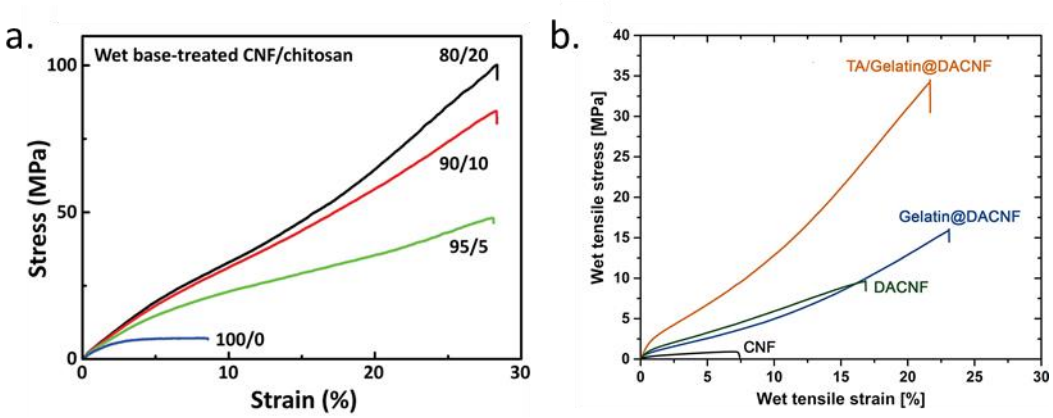

Figure I.14. a. Wet tensile test of CNF/Chitosan films treated with NaOH with different amount of chitosan. Reproduced from[154] **b.** Wet mechanical properties of films made of CNF, dialdehyde modified CNF (DACNF), DACNF grafted with gelatin (Gelatin@DACNF) and Gelatin@DACNF precipitated with tannins. Adapted from[157]

3.3 Relevance of barriers properties in packaging

Several external agents, such as oxidative gases and light, can deteriorate the foodstuff, making barrier properties key in food packaging materials. The different gases that need to be considered are oxygen, carbon dioxide, water vapor, ethylene while liquids mainly account for water and grease. Each food has a different requirement in terms of barrier properties, *i.e.* sometimes high breathability is more suitable than high barrier.[136] While petroleum-based plastics are basically non affected by moisture and display high water vapor barrier, they usually have low barrier against oxygen, a property that could be fulfill by biobased nanofibers that are semi-crystalline and form tight networks efficient to block oxygen permeation. However, water and water vapor sensitivity are limiting factors in the use of biobased polymers as packing materials. The following sections discuss the barrier properties of biobased films, the importance of water, and the current strategies used to overcome water sensitivity in biobased building blocks and its materials. Chitin and cellulose colloids are used as matrices, fillers and coatings to enhance barrier properties in packaging. Herein we put especial attentions to the use of nanofibers as matrices and coatings, where residual lignin and lignin particles are considered as an additive to improve other properties in the nanofiber films.

3.3.1 Gas barrier

When considering gases, the permeation phenomena through the film occurs in three different phases: the adsorption of gases on the surface, their diffusion through the film and their desorption (see **Figure I.15a**). After the equilibration period, the adsorption and desorption are constant over time and the diffusion – following Fick's first law of steady state diffusion – is usually the limiting factor.[159] Moreover, for porous materials, it is most likely that molecules diffuse through the pores and that this phenomenon prevail. In this case, measurement of air permeability under a pressure gradient is relevant to determine the air penetration through the pores of the film. Other defects such as cracks or pinholes will influence the air permeability. Both penetration and permeation usually takes place at the same time and one should understand which phenomenon is dominant in the system.[160] Understanding of the pore network (pore size distribution, tortuosity and pore connectivity) is therefore important in the development of materials aiming at controlled barrier properties. For non-porous materials, permeation of gases through the material is dominant and then permeation tests such as oxygen and water vapor permeability measurements should be assessed.

Water vapor transmission rate (WVTR) and oxygen transmission rate (OTR) represent the transmission rate of the gas through the film and does not consider the thickness of the film while water vaper permeability (WVP) and oxygen permeability (OP) accounts for the thickness of the film (as the permeation path) and pressure gradient. They are calculated following the equations below.[160]

$$WVTR = \frac{\Delta m}{A} \quad \text{(I.1)}$$

$$WP = \frac{WVTR \times thickness}{P_{sat} \times \Delta\%RH} \quad \text{(I.2)}$$

$$OTR = \frac{\Delta v}{A} \quad \text{(I.3)}$$

$$OP = \frac{OTR \times thickness}{\Delta P} \quad \text{(I.4)}$$

Where Δm represents the mass increase in g per day, A the area of the film measured in m^2, P_{sat} the saturation pressure of water vapor at the temperature of measurement, Δ% RH the difference in relative humidity, Δv the oxygen volume variation in cm^3/day and ΔP the oxygen partial pressure difference.

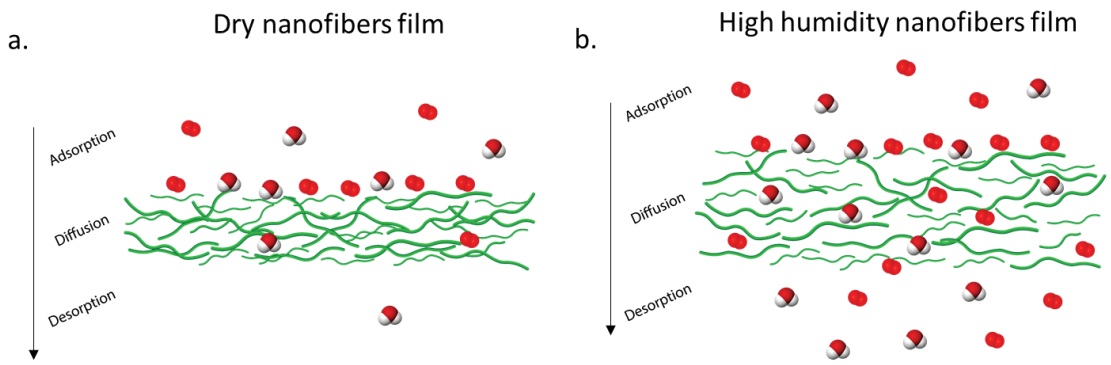

Figure I.15. a. Mechanism of gas propagation through a nanofiber film and **b.** swelling of the film at high humidity with increased porosity and hence gas permeability.

When comparing values among different contributions, one should be careful with units being displayed and test conditions taken (temperature, pressure, humidity), as several combinations have been used to assess barrier properties. WVTR and OTR are usually shown on a logarithmic scale, and they are not always proportional to the film thickness especially for coatings or multilayers where the thickness of the barrier-inducing component does not necessarily correspond to the thickness of the film. Temperature and relative humidity during the measurement are important parameters, mostly because in hydrophilic materials, their barrier properties were shown to increase exponentially with humidity and temperature.[161,162] Requirements for packaging can be divided in three barrier categories depending on their WVTR (38°C, 90% RH) and OTR (23°C, 50% RH): high barrier with WVTR under 1 g/m^2.d and OTR below 1 cc/m^2.d.atm; medium barrier with WVTR between 1 and 5 g/m^2.d and OTR between 1 and 100 cc/m^2.d.atm; and low barrier with WVTR between 5 and 50 g/m^2.d and OTR between 100 and 5000 cc/m^2.d.atm.[163] Each category corresponding to different types of food, from fresh products to dry food. While cellulose nanofibers, due to their high internal cohesion, crystallinity and high aspect ratio,[159] have barrier properties against oxygen that are qualified as high (around 1 cc/m^2.d.atm), when in contact with water or at high relative humidity, the OH binding between the nanofibers that are responsible for the internal cohesion starts to break because of the insertion of water molecules between the nanofibers (**Figure I.15b**). As result the internal cohesion of the fiber mat decreases. This leads to film swelling and increase in porosity and permeability. High-water absorption capacity of cellulosic materials results in exponential increase in their permeability when at humidity above 50% RH.[164,165] Other parameters such as pressure, temperature, crystallinity, chemistry, density, pore size, thickness and structure influence the barrier properties of nanofiber films. Hence,

there are different ways to improve the barrier properties, for example surface chemistry of the nanofibers can be modified, fillers or grafted molecules can be added, physical cross-link can reduce swelling or process of film formation can also be tuned. Examples of these different solutions will be displayed in the following parts (**Figure I.17**). More extensive review on barrier properties of biobased and nanocellulose-based packaging can be found in Helanto *et al.*[159] and Wang *et al.*[160].

Addition of impermeable fillers increases the pathway for gas molecules to go through the film and decreases the transmission rate. Bardet *et al.* added mineral nanoclay (MMT) and TEMPO oxidized CNC as fillers in CNF films to improve the barrier properties by increasing both crystallinity and density to slow down diffusion through the film. MMT were more efficient fillers as the OTR at 90% relative humidity decreased by 70% while it only decreased by 50% in the presence of TEMPO CNC.[166]

Hydrophobization of the film surface or the nanofibers surface has potential in reducing water interactions and improving WVTR. Among others, coating of nanofibers films with hydrophobic wax resulted in high decrease in WVTR from 600 to 40 g/m^2.day and limited the increase of OP at 96% relative humidity by 70%.[161,167] The wax coating decreased drastically the diffusion of water molecules through the films because the formed coating was non-porous and water has low solubility in the hydrophobic wax. It was shown that continuous wax layer was needed to obtain such results, but the brittleness of the wax hinders its wider use in commercial applications. Adhesion between wax layers and the nanofibers substrate is also a key parameter as their surface chemistry differs, a problem that is still unsolved.

Another approach to improve barrier properties is to prevent film swelling at high humidity by chemical or physical cross-linking of the nanofibers film. Larsson *et al.* used internal cross-linked of CNF by periodate oxidation of cellulose to create dialdehydes followed by covalent cross-linking between each other.[168] This approach was capable to limit water sorption and swelling at 80% RH, thus resulting in oxygen permeability at 80% RH of 2 mL.µm/(m^2.day.kPa) compared to 9 mL.µm/(m^2.day.kPa) for untreated CNF. The main drawback of internal cross-linking is a decrease in mechanical properties, with a small decrease in modulus by 40% but significant decrease in tensile strain from 6% to 1% and strength from 225 MPa to 48 MPa, for untreated film and cross-linked film respectively. The main reasons for the decrease in mechanical strength were the decrease in crystallinity due to the periodate oxidation and the increase in fiber sizes. Ionic cross-linking of the nanofibers as post-treatment is another promising solution. Shimizu *et al.* promoted ion exchange in TEMPO-CNF films with different metallic ions (Mg^{2+}, Al^{3+}, Ca^{2+}, H^{+} and Fe^{3+}).[153] Films exchanged with Ca^{2+}

resulted in OTR at 80% RH three orders of magnitude lower than untreated films (0.08 mL.µm.m^{-2}.day^{-1}.kPa^{-1} and 100 mL.µm.m^{-2}.day^{-1}.kPa^{-1} respectively) due to full protons exchange and increase in density (from 1.53 g/cm^3 to 1.68 g/cm^3) (**Figure I.16**). As positive side effect, the mechanical properties of the modified films were slightly impacted in the dry state and were improved in the wet state compared to untreated film.

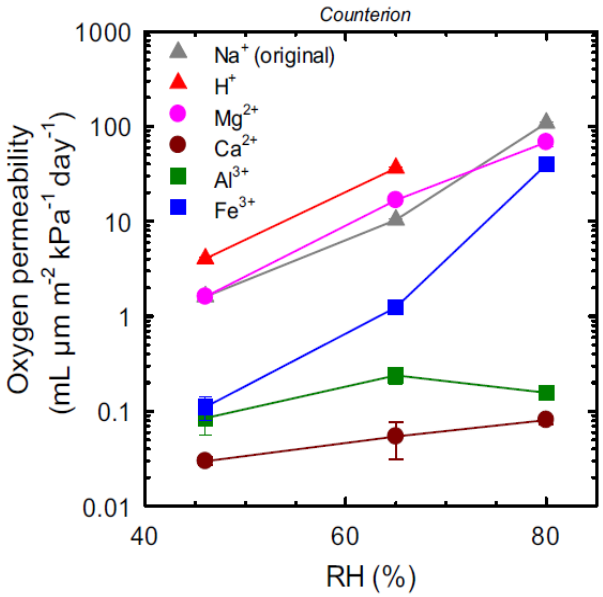

Figure I.16. Oxygen permeability measured at different humidity of tCNF films cross-linked with different ions. Reproduced from[153]

The drying process used during the film formation can significantly influence the barrier properties of the films. Above all, hot pressing of the nanofibers films as post-treatment improves both OTR and WVTR by decreasing porosity and therefore the surface accessibility that promote interactions with water. Formation of irreversible H-bonds within the free OH groups in the network, similar to hornification of cellulose, occurs at temperatures above 100°C and induces decrease in water absorption of the film and surface hydrophilicity leading to improved WVTR and OTR.[148,149] Xia *et al*. used hot press treatment at different temperatures (100°C, 130°C and 145°C) on TEMPO-CNF films, using $NaBH_4$ as reducing agent added before the heat treatment to prevent oxidation and coloring of the films. Treatment at 130°C induced a remarkable decrease in oxygen permeability at 80% RH, going from 1.5 mL.µm.kPa^{-1}.m^{-2}.day^{-1} for untreated sample to 0.85 mL.µm.kPa^{-1}.m^{-2}.day^{-1} with 130°C while maintaining the same mechanical properties than the untreated samples.

The effect of residual lignin on CNF films barrier properties was assessed by Espinosa *et al.* who measured OTR and WVTR in films made with CNF and LCNF from straw containing 1.9% and 9% residual lignin respectively. LCNF displayed slightly better barrier properties due to their higher degree of fibrillation that resulted in lower porosity. The lignin present in the film also promoted pore filling accompanied with a decrease in hydrophilicity, thus resulting in reduced water absorption capacity of the film.[33] However, Rivière *et al.* showed that LCNF had triple oxygen permeability than pure CNF due to the presence of lignin cluster in the nanofibers network.[17] Therefore, the distribution of lignin in the cellulosic network and its influence on porosity of the films are key features that if controlled can induce higher barrier properties.

Given their high performance, biobased nanofibers have been combined with synthetic polymers to improve their barrier properties. PLA is a promising biobased and industrially compostable polymer; however, PLA has poor barrier properties against oxygen. Coating with biobased fibers could improve the OTR without compromising the compostability. Coating of PLA with different nanochitins (TEMPO, deacetylated and hydrolyzed crab ChNC and squid ChNF) decreased the OTR from 184 $mL.\mu m.m^{-2}.day^{-1}.kPa^{-1}$ to between 1.01 and 1.14 $mL.\mu m.m^{-2}.day^{-1}.kPa^{-1}$ after 0.1 µm coating.[85] Neither the source of chitin nor the surface modification had a significant influence on the final OTR. In addition, Kim *et al.* used layer-by-layer deposition by spray coating of TEMPO oxidized CNF and deacetylated ChNC on the surface of polyethylene terephthalate (PET) film to improve barrier properties while keeping their known high transparency. When coating PET with biobased fibers, synergies between CNF and ChNC were observed as the OTR values for CNF and ChNC alone (1.91 ± 0.33 $mL.m^{-2}.day^{-1}$ and 1.46 ± 0.06 $mL.m^{-2}.day^{-1}$) were higher than the equivalent alternated layers (0.48 ± 0.02 $mL.m^{-2}.day^{-1}$).[169] These synergies were explained by ionic interactions between negatively charged CNF and positively charged ChNC that favor tight packing as well as addition of short ChNC that can fill the gaps between long CNF.

Several approaches to improve barrier properties of biobased packaging have been attempted, specially to decrease water vapor transmission rate (WVTR) and oxygen transmission rate (OTR) at high humidity (> 50%). The recent contributions have highlighted the technical potential of biobased nanofibers to enable high barrier materials; however, studies on feasibility and on scaling up strategies are scarce. Additionally, more performance-demanding measurements should be considered, for example, using tropical conditions at 40°C and 90% RH, which are rarely performed but of great industrial importance. Due to the brittleness of the

films, stability of the permeabilities after mechanical stresses would also bring new insights of their viability.

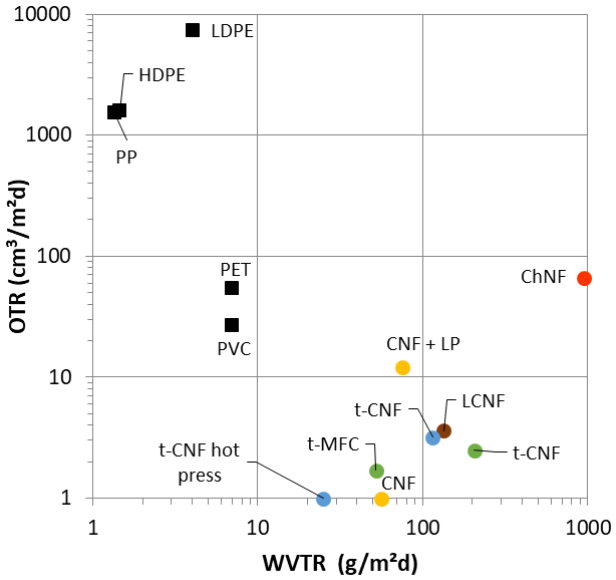

Figure I.17. Oxygen and water vapor transmittance rate of different nanofibers films (●) compared to petroleum-based polymers (■). Effect of residual lignin[170], lignin particles addition, surface modification,[151] hot press post-treatment[148] and nanofiber nature are displayed. Same color relates to same conditions of measurement and same paper. Data extracted from[137,148,151,170]

3.3.2 Grease barrier properties

Grease is another liquid that need to be stopped from crossing the packaging either from inside or outside. Barrier against grease is also important to protect the foodstuff from the packaging itself as mineral oil from the ink printing could migrate to the food. Several methods to measure grease barrier property exist including: Cobb-Ungern method, the Kit-test and the ASTM F119-82 standard test.[159] Measuring the barrier to heptane is also used as equivalent to barrier against mineral oil.[171] The Kit-test consists of 12 solutions with different amount of castor oil, n-heptane and toluene numbered from 1 to 12. For solution 8 and above, if the substrate does not absorb the drop of solution, it is considered as grease resistant. CNF due to their ability to form closed networks are known to have barrier properties against grease. Kumar *et al.* prepared paperboard slot-die coated with CNF and found that 300 µm Slot-Web gap corresponding at 6 g/m^2 and thicker coatings resulted in Kit test of 8 or more.[171] They also measured the heptane vapor transmission rate (HVTR) of the coated paperboard, and showed it exponentially

decreased with the coating weight and no transmission was detected above 9 g/m^2 coating. This was confirmed by Tayeb *et al.* who showed that a grammage of 16 g/m^2 of CNF or LCNF on regular paper improved the kit test number from 0 to 12.[162]

3.3.3 Light management (UV barrier and visible light transparency)

Transparency of food packaging is of great importance especially for consumer convenience and perception. Nanofibrillar films are usually transparent or semi-transparent film due to the size of the nanofibers being below visible wavelengths and the high density of the films. CNF and ChNF films with transparencies as high as 90% can be obtained **(Figure I.18**).[152] Tuning of the transparency can also be obtained by changing the nanofibers sizes and the film density. Toivonen *et al.* tuned the optical performances of CNF films by size fractionation of CNF and by using different solvent for film drying (**Figure I.18a**).[172] The drying solvent influences the porosity of the film by disturbing the hydrogen network, thus resulting in a more porous network that scatters (and reflects) more light when compared to the packed CNF films dried from water.

High transparency, although satisfactory to the consumers, can cause food spoilage as it may cause photo-degradation and photo-oxidation of proteins, fats, vitamins and pigments present in food.[173] The combination of light and oxygen can create reactive oxygen species (ROS) or free radicals that lead to chemical modifications in the food thus altering sensorial aspects, *e.g.* taste, texture and odor, and increase in spoilage speed. Light in the ultraviolet (UV) range can also affect the properties of the packaging itself and make it more brittle, thus decreasing its ability to protect the food. Classically, aluminum foil is used as light and oxygen barrier in packaging.[137] However, it has high cost, it is not transparent and makes recyclability of the whole package more difficult. For that reason, there has been many attempts to develop new light and oxygen barrier materials.

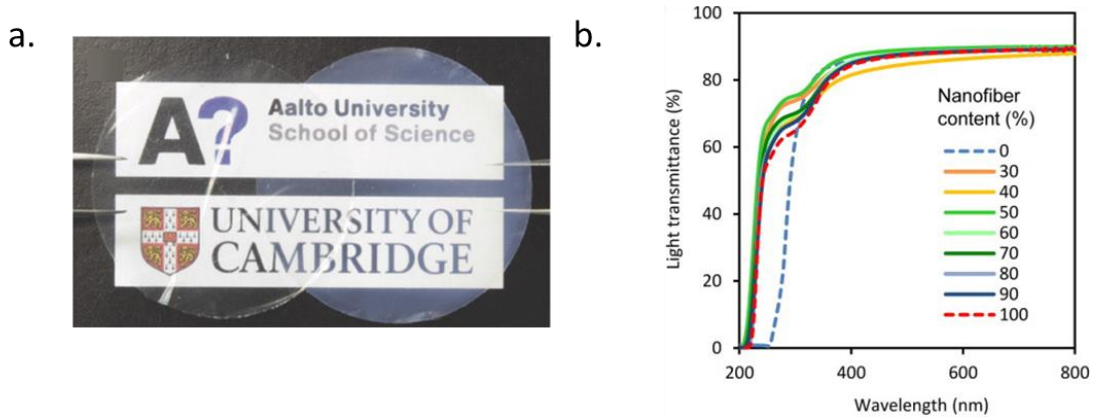

Figure I.18. **a.** Effect of drying solvent on transparency of CNF films, left films was dried in water and right film in octane. Reproduced from[172] **b.** UV-Vis light transmittance of deacetylated ChNF films with different amount of glycerol. Reproduced from[152]

Light absorbers can be divided in two categories: inorganic absorbers usually semi-conductive metal oxide particles such as TiO_2, ZnO, CeO_2, which can absorb and scatter light; and organic absorbers that usually absorb light in a given wavelength range depending on its chromophore groups. Both inorganic and organic have been used as additives in biobased packaging, Abitbol *et al.* incorporated CeO_2 particles in CNC/CNF films and obtained complete UV blocking property that was dependent on the particle content while keeping a high transparency of 80%.[174] Moreover, coffee silverskins from the coffee roasting industry were used as additives in starch films.[175] Coffee silverskins contain chlorogenic acids and caffeine that have UV protecting capacity.

Lignin, a polyphenolic macromolecule, is a promising UV absorber; however, it is brownish colored by nature and hence will influence the transparency of the final material. The UV-shielding capacity of lignin increases with increasing total phenolic content while its color is affected mostly by the molecular weight polydispersity index.[134] Zhang and Naebe discussed the different solutions for whitening the lignin color while increasing its UV blocking capacity.[134] For example, acetylation of lignin is often used to lighten its color however it also decreases the UV blocking capacity (**Figure I.19**).[176,177] The formation of lignin nanoparticles is also a viable approach, the large specific surface of area of nanoparticles increases the UV shielding capacity of lignin while the small size (<100 nm) avoids light scattering in the visible range. It was demonstrated that inclusion of 10 wt.% LP in CNF and ChNF matrices is enough to obtain complete UV shielding properties.[147,178] Additionally, compared to addition of non-particulate lignin, the transparency in the visible range was notably enhanced. In contrast, when LCNF were extracted from willow bark, both UV and visible light were blocked.[170]

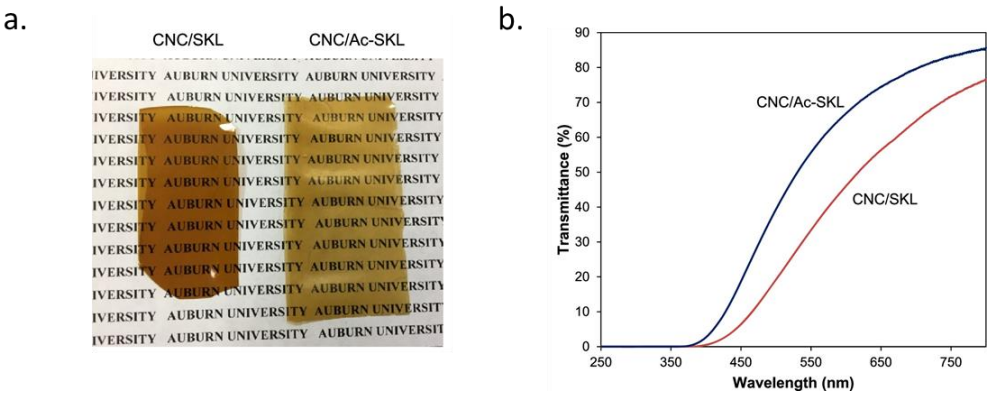

Figure I.19. **a.** Pictures of films made of CNC and softwood kraft lignin (SKL) or acetylated SK associated with their UV-Vis transmittance spectrum (**b.**). Reproduced from[179]

3.4 Active packaging

To increase food life time and reduce spoilage, packaging can be active, meaning that it acts during its lifetime by for example releasing active molecules to the food or headspace or absorbing undesired gases produced by the food.[180] Ideally, functional food packages should enable to decrease the amount of additives and preservatives from the food products. Examples of active packaging are oxygen scavengers, ethylene absorbers, carbon dioxide absorbers, antimicrobial or antioxidant packaging.

Different approaches are used to add active molecules to a packaging material: a thin layer coating inside the package or addition to the bulk during the process to enable controlled release of active or direct surface activity. When active molecules are incorporated in the bulk material, one should be careful that no degradation happens during the processing as high temperature and mechanical stresses are usually required during polymer processing. In addition to thermostability, compatibility with the matrix is also required in order to avoid aggregation. Affinity with the matrix is also key if the aim is to release the active molecule in a controlled manner. Finally, the addition of additives should not deteriorate the barrier properties of the film against gases and liquids.

Among the biopolymers studied in this literature review, lignin has antioxidant properties while chitin and its derivatives can show antibacterial activity.[4,181] Lignin, because of its polyphenolic nature, is known to have antioxidant properties. Lignin can donate electrons to stabilize radicals, it then forms a phenoxy radical that need to be stabilized within the lignin macromolecule. Hence, the amount of phenolic hydroxyl groups is positively correlated to the antioxidant properties of lignin, but the molecular weight and polydispersity could also influence the antioxidant activity.[182] De Menezes Nogueira *et al.* extracted lignin from by-

products of oil palm industry with an acetone-based process.[183] They compared the antioxidant activity of different lignin fractions (methanol, ethanol and acetone soluble fractions) with commercial antioxidant (BHX and Irganox 1010). It was shown that all fractions had superior antioxidant activity than the commercial antioxidants, which was explained by the greater number of phenolic hydroxyl groups of lignin in comparison with commercial antioxidant, as well as the presence of methoxy groups and conjugated double bonds that help with radical stabilization in lignin.

When dissolved in solution lignin has better antioxidant properties than LP as the functional groups are more accessible.[132] For lignin particles the radical scavenging activity occurs on the surface of the particles, hence the specific surface area which is correlated to the particles size is key parameter. Zhang *et al.* demonstrated that the antioxidant properties of LP from corncob were positively correlated to the size of the LP and to the total phenolic content (**Figure I.20a**).[127] Cusola *et al.*[131] prepared films with 90% LPs using CNF for cohesion and polyamidoamine-epichlorohydrin as wet strength agent. Porous membranes for active microfiltration were obtained showing the potential of lignin as antioxidant agent. When the particles are incorporated in cellulose nanofibers films it was demonstrated that the antioxidant activity of the film is limited to the particles on the surface of the film.[178] Also formation of hydrogen bonds with cellulose, decrease the accessibility to the lignin particles distributed across the material bulk.[132]

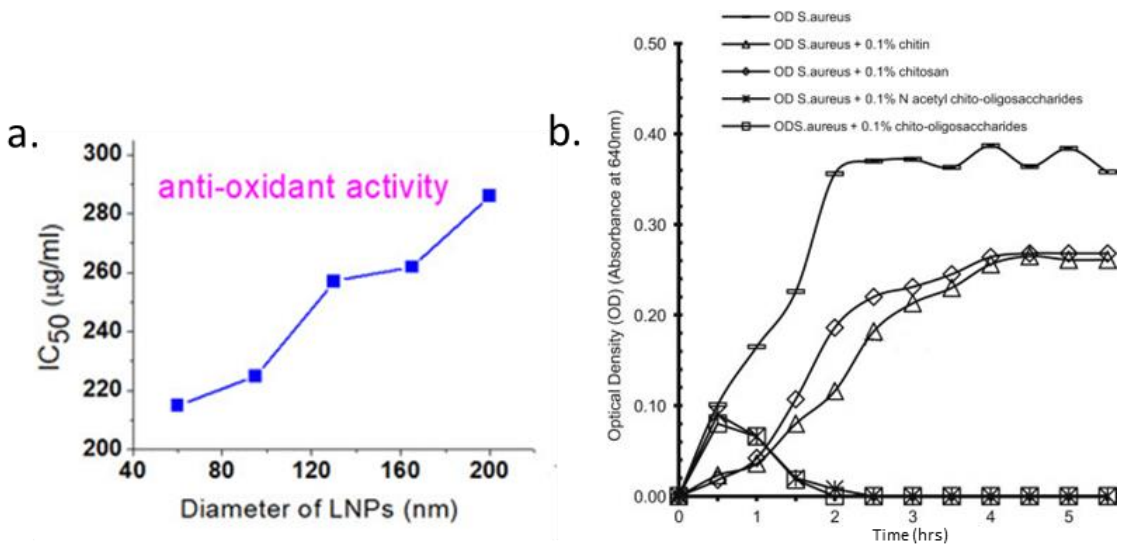

Figure I.20. a. Antioxidant activity of lignin particles from corncob as function of their size. Reproduced from[127] **b.** Antibacterial effect of chitin and its derivatives on *S. Aureus*. Reproduced from[181]

Chitin when highly deacetylated gives chitosan which shows antibacterial activity that depends on its degree of acetylation and molecular weight.[184] Benhabiles *et al.* studied the antibacterial activity of chitin and its derivatives (chitosan, N-acetyl chito-oligosaccharides and chito-oligosaccharides) (see **Figure I.20b**).[181] They demonstrated that chitin and chitosan exhibited bacteriostatic effect especially on Gram-negative bacteria while both oligomers had bactericide effect on E. coli, S. aureus, S. typhimurium and B. subtilis stains among others. For chitin and chitosan, electrostatic interactions with bacteria induce their flocculation and prevented their reproduction. As the mechanism depends on the charge of the polymer, the degree of acetylation is key parameter, which usually leads to chitosan being more bioactive than chitin. Moreover, it was reported that the chito-oligosaccharides were able to pass through the bacteria cell wall and to effectively kill the bacteria. Along the same line, Kaya *et al.* demonstrated that chitosan extracted from grasshoppers showed antibacterial activity especially against Gram-negative bacteria.[185]

On the other hand, it was shown that lignin and lignin particles can inhibit the growth of bacteria especially gram-positive;[110,132,186] however they do not show strong antibacterial activity. Nevertheless, lignin particles have shown more promising results as carrier for drug or metallic nanoparticles for higher performance bactericides.[113,187,188] Richter *et al.* engineered lignin particles with adsorbed silver ions on the surface.[187] Silver ions release was controlled by a cationic polyelectrolyte outer layer for a limited time period, resulting in lignin particles that were more environmentally friendly than pure silver nanoparticles.

3.5 Challenges related to fiber-based packaging

3.5.1 Availability of materials for scale up preparation of packaging

Cellulose and chitin nanofibers, and lignin particles are not completely available at the market in large quantities. CNFs productions has intensified recently, but prices are still high and cannot be compared to those of more traditional polymers used in packaging. Feasibility of manufacturing, and wide utilization, account for both performance and cost. A few techno-economic studies have been performed to estimate the price of cellulose, chitin and lignin colloids. Recently, Clauser *et al.* studied the cost of CNF and microfibrillated cellulose fibers from sawdust taking an industrial-scale biorefinery approach, which also co-produced lignin and xylose syrup.[189] Price of CNF has been estimated to be between USD 1.05/kg and USD 1.90/kg for enzymatic CNF, with the price of enzymes representing 45% of the total production cost. A minimum biomass (sawdust) input of 15 000 t/year is required to make the process profitable. Previously, Abbati de Assis *et al.* estimated the price of CNF prepared from wood

bleached pulp to be between 1.5 USD/kg and 1.9 USD/kg,[190] with the pulp cost representing 60% of the whole manufacturing cost. Given the high costs coming from raw materials, the use of alternative sources (*e.g*. agriculture residues) for the preparation of CNF could have a significant impact on the final price.

In a techno-economic assessment, Ashok *et al.* evaluated the manufacturing price of lignin particles made by solvent precipitation at industrial scale.[112] Different prices were obtained depending on the integration or not to a pulp-mill or biorefinery. If integrated, the cost of LP is estimated to be 0.99 €/kg, whereas in an isolated production line the manufacturing price would be 1.59 €/kg. The price difference between integrated and non-integrated plant shows the importance of the price of raw lignin on the final product. Manufacturing of LP by aerosol atomization was estimated to cost between 0.87 and 1.17 USD/kg depending on the lignin type and the solvent used for solubilization.[119] In addition, only one study reported the price of potential ChNF and ChNC to be 6.7 €/kg and 11.9 €/kg respectively.[74] However, these results should be taken with care as the calculation was based on lab-scale data.

In general, only few studies reported price estimation of biobased nanofibers and nanoparticles, one can note that the price of the raw material takes an important part of the final price and that using by-products or integrated plant in a biorefinery approach could help reduce the final price of the nano materials as shown by Clauser *et al.* and Ashok *et al.*.[112,189] Comparison with existing products for specific applications also need to be conducted in more details to know if the biocolloids are competitive with the market.

3.5.2 Processing of nanofiber-based materials with fiber-based packaging

Thermal processing is central in the current packaging manufacturing, therefore thermal properties of the biobased building blocks need to be considered. Cellulose does not melt but degrades at temperatures varying between 275 and 300°C, whereas cellulose nanofibers are more sensitive to thermal degradation due to their high specific surface. The presence of lignin in LCNF improves the thermal stability of the nanofibers,[138] due to the higher thermal degradation temperature of lignin. Thermal degradation of chitin peaks at 369 and 378°C for chitin from insect and crustacean respectively.[69] The absence of melting temperature of cellulose and chitin makes it impossible to use the traditional processing used for manufacturing plastic food packaging like thermoforming or melt extrusion. Processes that are analogous to papermaking are used instead (**Figure I.21**). When processed as fillers in plastic matrices, the thermostability of these biopolymers are an advantage as they do not degrade and

stay unaltered within the molten polymer matrix. These nanofibers are usually processed in high water contents (>90%), therefore there are several efforts to enable efficient compositing of nanocelluloses and nanochitin with polyolefins for example.[191,192] These efforts focus on reducing water content, and *in situ* preparation of the nanofiber, as well as chemical modification to enable strong interfacial interactions between the hydrophilic filler and hydrophobic matrix. In this section, we focus on processing nanofibers as self-standing films or coatings, as well as we discuss the different processes under study at different scales.

Nanofibers films can be formed as self-standing films or as coatings on various substrates. At the lab-scale, many studies have been done on self-standing nanofiber films. It is a convenient and easily reproducible process that enables the study of pure films that can be used as model to further improve films properties. The typical process to make self-standing films at lab scale are bench casting and filtration assisted with vacuum or over pressure (**Figure I.21 a-b)**. The bench casting method has the advantage of retaining soluble additives and nanoparticles. However, it is time consuming as because the water-holding capacity of both cellulose and chitin makes the drying process slow, reaching over one week at ambient temperature and decreasing while increasing the drying temperature. On the other hand, filtration is a faster process but more energy consuming as energy is needed to remove water from the film with vacuum or pressure first and then the drying step require heat and pressure or vacuum depending on the method used.[47] Recently, Shanmugam *et al.* prepared self-standing films by spraying of CNF on stainless steel plates moving on a conveyor.[193] The velocity of the conveyor and the concentration of CNF were tuned to obtain different films thicknesses resulting in grammage between 50 and 200 g/m^2. With optimized parameters, films with elastic modulus comparable (around 6 GPa) to vacuum filtrated films were obtained. Spraying at high concentrations avoids high dewatering times that are common in vacuum filtration method for film consolidation.

At a larger scale, continuous casting of CNF film has been investigated (**Figure I.21e**). In 2012, Peresin *et al.* reported the continuous casting of CNF films on a pilot scale.[194] Casting was done on a plastic substrate and peeling was carried out after drying leading to roll-to-roll film manufacturing. More recently, Claro *et al.* reported the preparation of CNF/CNC films by continuous casting.[195] Nanocelluloses were oriented in the films leading to anisotropic mechanical properties. Films with low density (0.5 g/cm3) were obtained due to the absence of packing, *i.e.* nanofiber accommodation, before the fast drying. Continuous processes to make roll-to-roll self-standing films of nanofibers need to be further developed to be further

transfer at industrial scale. Decrease in the filtration time and optimization of the drying conditions for casting are determinant parameters that need to be considered.

Moreover, due to the brittleness of the films, the price and availability of nanofibers, it seems still too early to consider self-standing films as market ready. The production of thin layer coatings of nanofibers on already existing substrates used in packaging applications (*e.g.* cardboard) is closer to the market. Different coating techniques haves been developed on different substrates including paper, board or plastic (**Figure I.21 c-d** and **g-h**). The high viscosity at low concentration (< 1 wt%) is a limiting factor for some coating methods, *i.e.* low mass fraction indicates high water content that needs to be removed during drying. At lab scale, rod coating has been the most used technique; rod coating allows the deposition of layers of a few g/m^2 with suspension from 0.5 to 2 wt%.[196–198] If needed, multiple layers can be coated to increase the grammage. Layer-by-layer (LbL) coating consists of alternating monolayer of polyelectrolytes or colloids with opposite surface charges, it is usually done by alternating dipping of a substrate in suspensions followed by washing. Kim *et al.* used LbL spray coating of TEMPO oxidized CNF and deacetylated ChNC on PET, with each layer comprising 5 sprayings, yielding a 2.6 µm coating when applying 20 bilayers. Even if automated dipping system exists, the high number of layers needed to achieve a reasonable thickness makes it difficult to scale up LbL coatings. Spray-coating is another widely used method where a nozzle sprays a nanofiber suspension on a substrate, with an automatic system that allows either the substrate or the nozzle to move steadily to yield a homogeneous coating. Beneventi *et al.* used spray-coating to add 2 wt% CNF on never dried paper surface, it was shown that a high retention of CNF on the paper was obtained and a homogeneous film was observed for a coating weight above 6 g/m^2.[199]

When upscaling coating processes, roll-to-roll coating is needed which often includes coating and drying units – combination of several drying units is usually required to have completely dried coating before re-winding the film (**Figure I.21 g-h**). Slot-die coating is a promising approach that has been implemented for roll-to-roll coating of CNF.[171,200] The method consists of a pressurized suspension that is fed into a slot-die and applied on a substrate. There is always a gap between the slot-die and the substrate usually referred as Slot-Web gap (SWG), which is the parameter that controls the thickness of the final coating, whereas the slot gap, speed and concentration of the suspension are also important parameters to control the coating properties. With this coating technique, deposition can be done at low speed which gives time for drying the water-rich CNF suspension. Roll-to-roll slot-die coating allowed uniform deposition of CNF of different grammage from 1 to 16 g/m^2 by tuning the Slot-Web gap.[171] CMC was needed

in small amount (5 pph) to decrease the viscosity at high shear rate to be able to pump high concentration of CNF (1 to 3 wt%). It also helped dispersing the CNF to reduce phase separation and increase coating homogeneity. Uniform coatings with high barrier properties against mineral oil, grease, and air were obtained; however, the coating speed (3 m/min) is still low compared to industrial processes and the drying of high-water content CNF required high energy consumption.

Other processes have been combining the formation of paper and CNF coating without intermediate drying using filtration system[162], spray-coating[199] or dynamic sheet former.[201] Wet lamination of CNF on board is also under study.[142] To conclude, several techniques have been developed and adapted to nanofibers suspension to make films and coatings at different scales.[202,203] The major obstacle of processing hydrophilic nanofibers is the formation of a gel at low concentration that limits the grammage and makes water removal more laborious and energy consuming. Other challenges such as sealing of packaging have been raised concerning fiber-based packaging, when no hot sealing is possible, glue and/or folding are needed. Development of new techniques such as ultra-sound welding can lead to sealing performances comparable to hot-melt adhesives for papers containing lignin and hemi-celluloses without any adhesives.[204]

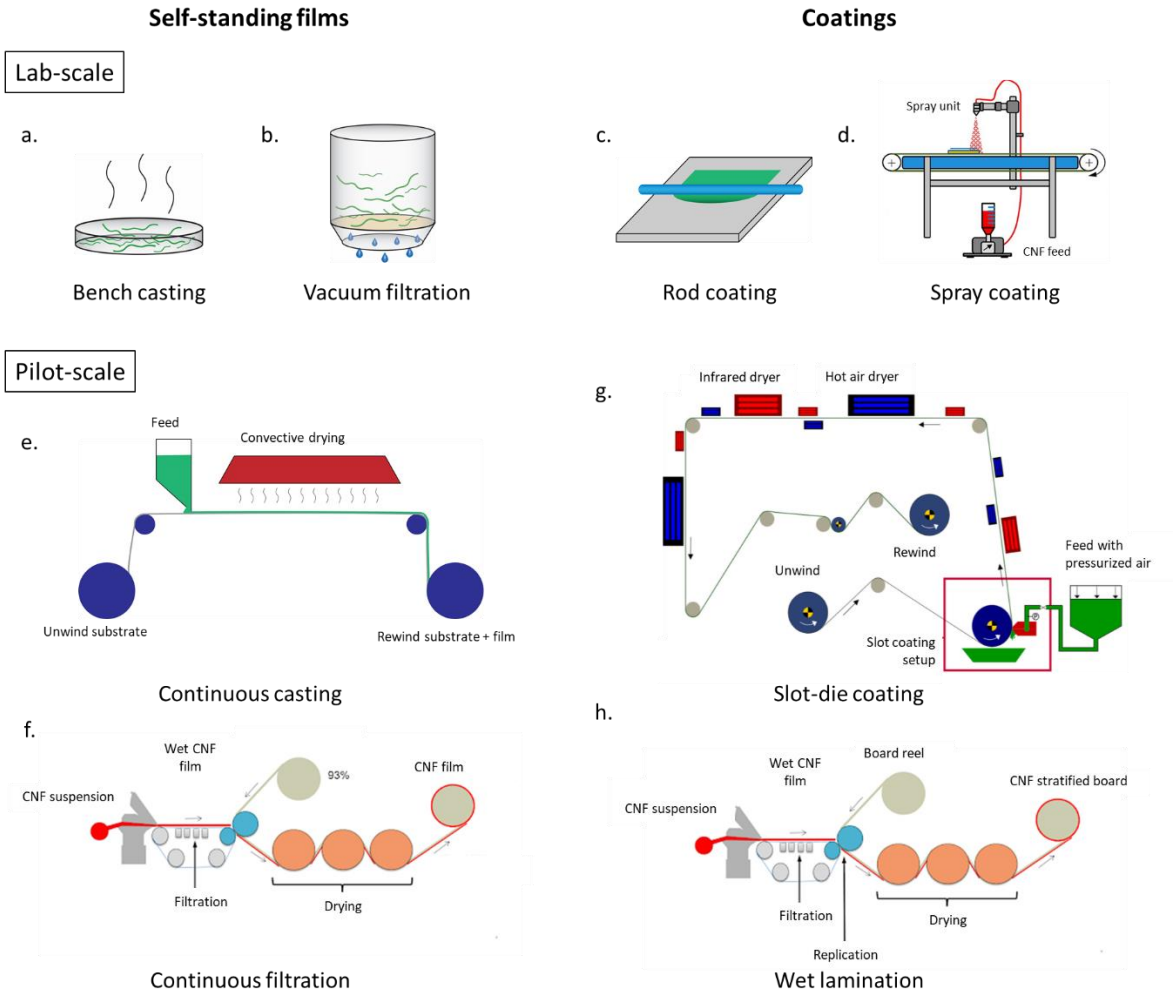

Figure I.21. Different processes used to make self-standing nanofibers films and coatings at lab-scale and pilot scale. Lab-scale processes are **a.** bench casting **b.** vacuum filtration, **c.** rod coating and **d.** spray coating. Pilot-scale processes comprised **e.** continuous casting and **f.** continuous filtration to make self-standing films and **g.** slot-die coating and **h.** wet lamination for films coatings. Reproduced from[142,199,205]

3.5.3 End of life of fiber-based packaging

Circular economy principles points at reutilization practices as the first, best option for end-of life of packaging.[206] Reusable containers should be promoted in first place; however, single use packaging and food containers sometimes cannot be reused. Recycling, in those cases, comes as the second-best option. Recycling of packaging is an optimal end of life scenario, but it is not straight forward. Several steps need to be fulfilled to obtain desired results, presence of sorting facilities and proper sorting by the consumer followed by industrial sorting and

finally recycling, ideally without loss of material, and in an equivalent quality. Nowadays, this optimal scheme is mainly observed for glass and metal packaging that can be recycled an unlimited number of times.[207] Whereas plastic and paper based packaging are usually recycled in non-food contact products due to the presence of contaminants.[207] However, the advantage of pure paper-based packaging over most plastics is its ability to biodegrade when landfilled or discarded in nature without the release of microplastics.

If nanomaterials are included in the fabrication process of fiber-based packaging, assessment of their impact on the end-of-life of the packaging needs to be consider including both recyclability and biodegradability. While several studies have shown the positive impact of addition of CNF in recycled paper,[25,208] only few studies looked at the recyclability of CNF-based materials.[209,210] While paper and cardboard are known to be recyclable; it might not be the case for CNF because their assemblies are often much stronger than macrofiber assemblies (*e.g.* paper). In the recycling of fiber-based packaging, first the fiber network is deconstructed to be later reassembled, but the energy required to deconstruct the strong nanofiber assemblies is much higher than for paper, which can negatively impact their recycling. Recently, Shanmugan *et al.* demonstrated the recyclability of CNF films by comparing virgin CNF films and mechanically recycled films.[209] They showed that films with lower density were obtained as higher amounts of aggregates were found in the films and thus less hydrogen bonds were formed. This resulted in reduction of mechanical strength by 30%. Recyclability could be further optimized by adding a fluidization or homogenization step. With the same trends, Ang *et al.*, showed that recycled films showed strength 80% as high as the virgin CNF films.[210] Reduced mechanical properties was due to the presence of non-fully fibrillated aggregates of CNF. In addition, hornification of the CNF during drying reduced the swelling properties when rewetting the CNF. The impact of additives such as plasticizer or functional nanoparticles has not been assessed so far. The effect of CNF as coating or reinforcing agent in paper should also be evaluated.

As they are natural polymers and in its pure forms degrade in nature, biodegradability is often claimed for cellulose, chitin and lignin materials. However, chemical and physical modifications take place during processing, which raises legitimate questions as far as their biodegradability. Biodegradability is difficult to assess, because the absence of a unified protocol and the intrinsic complexity of the biodegradability concept that can include biodegradation in natural environment (terrestrial or marine), composting in residential (ambient temperature) and industrial compost (high temperature 50-70°C). In compostability, one should always specify the conditions taken, for example, PLA is considered as

biodegradable, but it only degrades in industrial compost. Helanto *et al.* listed the different existing standards for biodegradability in compost, soil and marine environment.[159]

Only few studies investigated the biodegradation of biobased nanomaterials. Leppänen *et al.* studied the enzymatic biodegradability and compostability of different cellulose based materials including non-modified nanocelluloses.[211] Enzymatic hydrolysis was done during two days with a mixture of four different enzymes: cellulase, mannase, xylanase and β-glucosidase. An exponential decrease of the hydrolysis degree was shown as a function of the degree of substitution of the different films, regardless of the chemical modification. Following the same logic, one wonders if chemically modified CNF are biodegradable. Compostability tests were also assessed in semi-industrial compost conditions, and degradation was measured on a macroscale visualization. After four weeks composting, the CNF films were fully degraded. However, visual degradation tests do not report the possible formation of resilient micro or nanoparticles that are not fully degraded into organic matter, water or gas. In another study, Homma *et al.* investigated the degradability of TEMPO oxidized cellulose fibers and nanofibers by their enzymatic hydrolysis using cellulase,[212] to show that the presence of sodium counter-ion was found to be determinant on the degradability. TEMPO CNF with free carboxyl groups were not degraded by cellulase, which could be due to the locally low pH close to the carboxylate groups. Degradability of TEMPO CNF was positively correlated to the charge content, but a clear conclusion could not be achieved because higher charge could have led to higher surface area and therefore higher enzymatic hydrolysis efficiency. Unlike the previous study, the degree of substitution had a positive impact on the enzymatic degradability however the presence of sodium counter-ion was determinant to achieve degradability. Other factors that could influence the degradability of cellulose are degree of crystallinity, structure, functional groups, cross-linking and molecular weight.[211] Hence, biodegradability of natural polymers should not be taken as granted especially if they were subjected to deep chemical modifications. However, if the modification is limited to the surface then the biodegradable character remains although with a small delay of initiation.[213]

Though biodegradability in nature offers the advantage of short time pollution if accidentally disposed in the environment, it is not an optimal option when considering the end of life of a product.[214,215] and for that reason, it should not be the targeted end-life of packaging.

3.6 Environmental impact through LCA analysis

The most acceptable way to measure the environmental impact of a product is conducting a Life Cycle Assessment (LCA). It can be used to compare and identify the best environmental performer among several materials. Many procedural frameworks have been developed to perform LCA, but generally it allows to evaluate a certain number of environmental impacts including greenhouse gas (GHG) emission, global warming potential, climate change, acidification, land use change (LUC), eutrophication, water use, photo-oxidant formation among others. However, one should be careful when comparing results from different contributions as the definition of boundaries usually vary from study to study. Moreover, comparison could be made by weight or by material performance giving different results, also putting in perspective the processing scale. For example, lab-scale is not an optimized process and has higher energy consumption compared to industrial scale.[216] The origin of electricity (country and sources) can also influence the final results as fossil based electricity production will highly increase the CO_2 emissions while hydropower plants will increase the water usage.[216,217]

Different models have been developed. Cradle-to-grave is the full LCA, considering from extraction of the raw materials to end of life, while cradle-to-gate is a partial LCA which stops at the end of the fabrication process, *i.e.*, in the latter the use and disposal phases are not considered. It is also possible to make a cradle-to-customer study where transportation to the customer is included. In the case of our materials, nanofibers and nanoparticles are only starting to have industrial applications hence mainly cradle-to-gate studies have been done. The comparison displayed here are made within the studies presented in **Table I.1** so that data are comparable. Comparison between studies is not made as the scales, boundaries, LCA methods, energy sources are different from one study to another. For exact numbers and details on each impact, we recommend a further read of each contribution.

Table I.1. List of publications reporting the LCA of CNF, LP or chitin and their main specificities.

Colloid	Source	Pre-treatment	Process	Functional Unit	Boundaries	Scale	Reference
CNF	Wood pulp	Enzymatic or TEMPO	Refinement or homogenization	1 t CNF	Cradle to gate	Pilot scale	Hohenthal *et al.*, 2012[218]
CNF	Kraft pulp	TEMPO or chloroacetic acid etherification	Sonication or homogenization	10 g CNF	Cradle to gate	Lab scale	Li *et al.*, 2013[219]
CNF	Wood pulp (ECF, TCF, unbleached sulfate, chlorine bleached sulfite)	Enzymatic or carboxymethylation or no pretreatment	Microfluidization or homogenization	1 kg CNF	Cradle to gate	Pilot scale	Arvidsson *et al.*, 2015
CNF	Never-dried bleached birch kraft pulp	No pre-treatment	Masuko grinding	Mechanical performance	Cradle to grave	Mix of lab and industrial scales	Hervy *et al.*, 2015
CNF	Carrot residues	Enzymatic	Homogenization	1 g CNF	Cradle to gate	Lab scale	Piccinno *et al.*, 2015
CNF	Wood logging residues	No pre-treatment	Grinding	1 kg CNF	Cradle to gate	Industrial scale	Moon *et al.*, 2017
CNF	Carrot residues	Enzymatic	Homogenization	1 kg spun yarn	Cradle to gate	Assumption at industrial scale	Piccinno *et al.*, 2018
CNF	Carrot residues	No pre-treatment	Ultrafine grinding	20g CNF	Cradle to gate	Pilot scale	Berglund *et al.*, 2020
CNF	Thermoground wood	TEMPO	Homogenization	1 kg CNF	Cradle to gate	Lab scale + assumption at industrial scale	Turk *et al.*, 2020
CNF	Virgin hardwood kraft pulp, cotton, and industrial waste sludge	Enzymatic or TEMPO	Sonication or homogenization	10 g CNF	Cradle to gate	Lab scale	Gallo Stampino *et al.*, 2021
		Chitin extraction					
Chitosan	Shrimp shells	Acid/base		1 m^2 packaging	Cradle to grave	Lab scale	Leceta *et al.*, 2013
Chitosan	Shrimp and crab shells	Acid/base		1 kg chitosan	Cradle to gate	Industrial scale	Munoz *et al.*, 2018
Chitin	Black Soldier Fly prepupae	Acid/base and enzymatic extraction		0.5 g protein	Cradle to grave	Lab scale	Rosa *et al.*, 2020
		Lignin extraction	LP preparation method				
LP	Wheat straw	Ethanol/water extraction	Solvent and pH precipitation	1 kg LP	Cradle to gate	Lab scale	Koch *et al.*, 2020
LP	Wheat straw	Steam explosion and enzymatic hydrolysis	Solvent shifting	1 kg composite	Cradle to gate	Lab scale + assumption at industrial scale	Riviére *et al.*, 2021

3.6.1 Biopolymers sources and impact on land use

When assessing LCA of biobased materials, direct and indirect land change use is an important aspect that has not been systematically evaluated while it can significantly increase the GHG emissions especially for biobased polymers.[220,221] Several studies looked at the LCA of nanocelluloses from residues[217,222–227] however none of them looked at the impact of the source or compared with wood source.

Land use change takes into account the impact on loss of biodiversity, deforestation, soil carbon depletion and soil erosion. Distinction between first-generation and second-generation bio plastics should be made as second generation do not compete with food and feed and can be a waste of the first-generation feedstock. The sources of cellulose and lignin considered in this literature review are second generation feedstock which offers reduced impact compared to first generation. However even when derived from residues, the land use is inherent to their source, and it is always higher than petroleum-based materials. On the other hand, algae are considered as third generation feedstock as its farming does not use land, fertilizer or pesticides, thus representing a promising feedstock for cellulose and lignin extraction.[228] Moreover, extraction of chitin has a relatively low impact on land use. When sourced from crustacean waste, the land use impact is relative to the type of farming (extensive, semi-intensive, intensive)[229] while for insects vertical farming as well as the possibility the feed the insects with food and agricultural waste significantly reduce their land use footprint.[54]

Improvement in agricultural and forest management practices (improving yields, regulating the use of pesticides, fertilizers and water) have a positive impact on LCA of biobased materials. Biorefinery approach can also improve the land use impact and general impact as higher yield of products are usually obtained. Nascimento *et al.* showed that the use of lignin as by-product instead of burning it for energy recovery had a positive impact on four over six impacts.[225] Using recycled materials as source also offers great advantage on the final impact. Comparison between virgin cellulose and recycled cellulose from industrial waste sludge as source for CNF production showed that on average of the 16 impact categories studied recycled fibers had a lower impact (**Figure I.22**).[227]

3.6.2 Cellulose nanofibers

Five main stages are accounted in LCA of CNFs: cultivation, extraction, manufacturing, use phase, end of life.[230] The studies found on LCA of CNF mainly aimed at comparing different pre-treatments and mechanical treatments for CNF production, whereas fewer information was found on cultivation, use phase and end of life. A recent review on LCA of cellulose and its

derivatives by Foroughi *et al.* summarized the main studies on LCA of nanocelluloses.[231] The addition of chemical pre-treatment to reduce energy consumption did not always result in lower environmental impact as chemicals production, high amount of water for washing, wastewater treatment and use of solvent increased significantly the environmental impact.[227,232] It was shown that carboxymethylation pre-treatment had the same cumulative energy demand than no pre-treatment, resulting in CNF with an overall impact higher than CNF obtained with no pretreatment or enzymatic pretreatment.[232] Moreover, Gallo Stampino showed that enzymatic pre-treatment had lower impact, for every factor studied, than TEMPO-oxidization when the same mechanical treatment was applied (see **Figure I.22**).[227] This was due to the absence of chemicals and reduction in electricity consumption.

The impact of processing route taken for CNF production, such as homogenization, sonication, microfluidization and refinement, have been studied.[218,219,227,232] Sonication was demonstrated to have high energy demand and is not easily scalable thus not being a promising route for industrialization. Mechanical disintegration of cellulose fibers is energy consuming hence the environmental impact of the process step will be highly dependent on the electricity grid mix.[218] Concerning the scale of production, Piccinno *et al.* predicted a scale-up of CNF production to industrial scales would reduce its impact by up to 6.5 times.[233] With these results, a comparison with commercial products would be more reasonable. The relative contribution of the different steps of the process also changed, leading to misleading results at lab scale if one wants to optimize the process for better environmental impact. This was confirmed by Turk *et al.* who found a decreased environmental footprint from 60 to 85% when going from lab-scale to industrial scale.[234] Cradle-to-grave study of CNF and bacterial cellulose (BC) was also done by Hervy *et al.* considering CNF and BC as reinforcing agents in epoxy resin for automobile applications.[235] Comparison with PLA and glass fibers/PP was made as reference materials. They concluded that the cradle-to-gate impact of CNF and BC epoxy reinforced composite were higher than that of the reference materials while the cradle-to-grave impact was equivalent, the end-of-life was beneficial to the CNF composite. Moreover, increasing the CNF or BC content in the epoxy resin resulted in decrease in total impact.

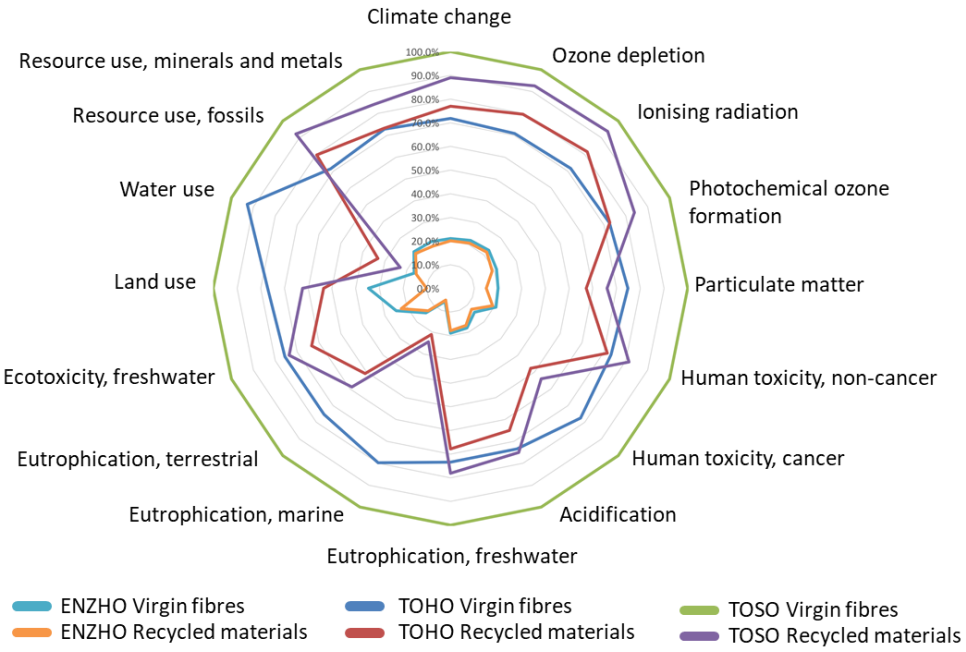

Figure I.22. LCA of CNF production, impact of pre-treatment and production process. Reproduced from[227]

3.6.3 Chitin and chitosan

Few papers investigated the LCA of chitin or chitosan,[236–238] all being sourced from crustacean waste and processed under conventional (demineralization/deproteinization) extraction method. Munoz *et al.* compared LCA of chitosan from different biomasses (shrimp and crab), locations (locally produced and global supply chain) and applications (agricultural and medical) with data from producers. In one case, the production of NaOH and HCl was identified as the hot spot while in the second case the energy use (coal for heat and electricity mix) was the limiting factor. In another contribution, Leceta *et al.* compared the LCA of chitosan and PP films for packaging applications. Chitosan film had higher land use impact due to the addition of biobased glycerol in the film as plasticizer. Hydrochloric acid used for demineralization of chitin was identified as a hot spot being responsible for high burden in respiratory inorganics and mineral resources. This could be overcome by using insect as source as they comprise significantly less minerals. However, the presence of lipids in insect biomasses requires the use of organic solvents that would then impact other factors that are considered in LCA.

For the chitin extraction from insects, several studies compared the protein efficiency of insect to other protein sources,[54] but no contribution was found on the LCA of chitin extracted from insect. However, Rosa *et al.* investigated the LCA of black soldier fly (BSF) rearing associated

with the extraction of different biomolecules and found out that the BSF larvae rearing phase represented 60% of the total impact which included the rearing of the larvae, the extraction and fractionation of proteins, lipids and chitin from prepupae, and the production of film from the protein fraction.[53] When comparing two extraction methods, an enzymatic route was 32% more environmentally impacting than the conventional (acid-base) method mainly due to low yield and high reaction time. These results give insights on the LCA of crustacean and insect-based chitin showing promising results that need to be consolidated. Concerning the fibrillation of chitin into nanofibers studies are still needed; however, one can expect that insect based chitin would potentially demand less energy as higher fibrillation degree can be obtain with similar mechanical treatment.[71]

3.6.4 Lignin and lignin particles

A recent review[239] on lignin and its derivatives showed that lignin-based products often have better environmental performances than their fossil-based counterpart. However, one should be careful that if the lignin studied was used as fuel for the biorefinery or pulp mill, the energy source used to replace this energy demand will highly influence the impact of the lignin product.[239] Only two studies reported LCA of lignin particles. Koch *et al.* studied the LCA of lignin particles biorefinery. The major steps were the extraction of lignin from wheat straw with ethanol: water (60:40) at 180°C and the precipitation with acidic water. Ethanol and thermal energy for the extraction were the identified hot spots concerning the global warming potential and human toxicity potential. The use of bioethanol could lower the total impact. Rivière *et al.* studied the global warming potential of composite films made of CNF, LCNF incorporated with 10% of lignin particles. Most of the greenhouse gas emissions (98.9%) came from the energy consumption at lab scale, which could be estimated that after scale-up of the process the GHG would decrease by 85.4%, while shifting to renewable energy source would further decrease the carbon footprint (see **Figure I.23**). The valorization of lignin could also reduce the impact of other products from biorefineries. Nascimiento *et al.* showed that valorization of lignin as chemical by-product of CNC production was favorable over burning it for energy recovery.[225]

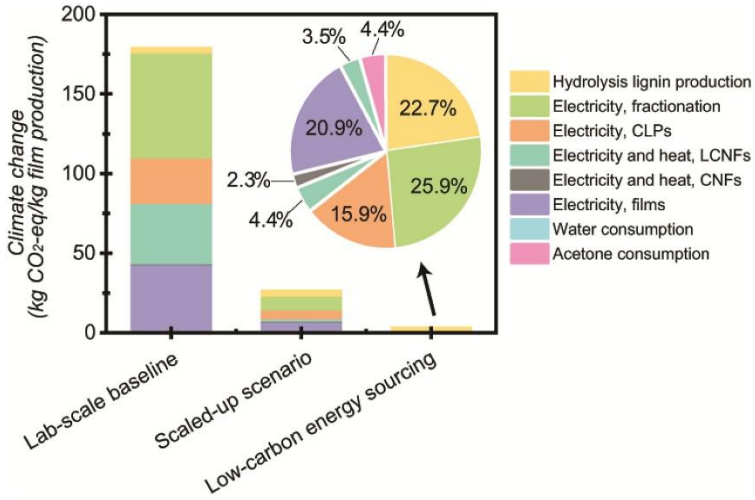

Figure I.23. Influence of process scale and energy source on the carbon footprint of CNF/LCNF/LP films. Reproduced from[17]

3.6.5 Insights on environmental impact of packaging

During the assessment of environmental impact of packaging, comparisons should be made with equivalent properties (*e.g.* barrier performance) rather than material amount, grammage or weight. No studies were found on the LCA of pure nanofiber-based packaging, therefore we reviewed studies comparing biobased and petroleum-based packaging to get insights on the impact of biobased packaging from cellulose, chitin, and lignin biocolloids.

Hermann *et al.* compared environmental impact of biobased packaging (paper, PLA, bio-PE, bio-PET) and conventional packaging (PP, PET).[240] Differentiation between Outer Packs and Inner Packs was made and comparison was done per m^2 of packaging, the end of life of the packaging was taken into account with different scenarios (incineration with or without energy recovery, landfilling, composting or digestion). The low barrier properties of biobased materials lead to a need for higher amount of material which has a negative influence on the general environmental impact. Biobased materials were more beneficial for Outer Packs as no barrier properties were needed. This emphasizes the need to improve barrier properties of biobased materials. For Inner Pack, the best material was reported to be hybrid paper (paper/PE/metalized oriented PP) and for the Outer Packs paper with biobased polyester. At the time of the study (2010), PLA and cellulose films did not offer any environmental advantages compared to conventional packaging. However, for both polymer new technologies and larger scale production are expected to improve their global impact. In addition, it was reported that land use can vary considerably depending on the type for biobased materials.

Evaluation of the LCA of fiber-based packaging and comparison with their fossil-based counterpart was done by Schenker *et al.*.[163] The impact of fossil based between 3 and 5 kg CO_2eq/kg while cellulosic fiber packaging is under 1.5 kg CO_2eq/kg. However, one should be careful when comparing these numbers as usually it depends on the mass needed to produce packaging with equivalent properties. Hence, regardless of the chosen material, minimizing the packaging weight is key to reduce its environmental impact. In another study, Hohenthal *et al.* investigated the impact of replacing latex by CNF in coated board for packaging. As the coating represented less than 1% of the total product, no significant changed in environmental impact was observed. Moreover, if the replacement was done with a 1:1 ratio no significant economic impact was found.

The end-of-life of chitosan and PP films was included in another study by Leceta *et al.*,[237] where composting was considered as the only option for chitosan while recycling (21%), landfilling (58 %) and incineration (21%) were considered for PP film. Composting of chitosan had positive impact in all categories (climate change, acidification/eutrophication, and fossil fuels among others) studied as it provided useful soil and carbon emissions were considered as part of the biological carbon cycle. In the case of PP end-of-life, the recycled part resulted in reduction of fossil fuel impact while the landfill and incineration had a negative impact on carcinogen due to the gases emissions. Fiber-based materials have potential in packaging applications due to their versatile end-of-life; however, improvement of barrier properties is still needed to outperform their fossil counterpart.

To conclude, LCA studies are relatively new but they allow a global overview on environmental impact of a product. Such studies being made ahead of scientific research and product development would allow focusing on key parameters and avoiding general, uninformed belief. Iterations between process, material optimization and LCA are beneficial for the final impact of the product. Some studies have been conducted on the LCA of fiber-based materials and packaging; however, their number is still small, and one cannot reach to any conclusive information at the moment. The use of biobased nanomaterials is still new and scale up to pilot or industrial scale would benefit their environmental impact, while linear scale up calculations are not accurate.[231] For example, at large scale, energy recovery or continuous process can be considered. Moreover, because we are aiming at negative footprint and positive impact, new concepts such as handprint are arising. When footprint needs to reduce as close to zero as possible, handprint quantifies the positive impact and should be maximize without any limit.[241]

4. Conclusion

Environmental impact of biobased materials is limited by their lower properties, hence there is a need to improve the mechanical and barrier properties of biobased materials while minimizing the mass of materials needed. Going towards this direction, biobased colloids show great potential to improve fiber-based packaging as cellulose and chitin nanofibers can bring high strength and barrier properties. Water interactions with biobased fibers has always been a challenge and many studies demonstrated improvements towards water and water vapor interactions with either chemical modification or physical interactions. Incorporation of active molecules such as lignin is the form of residue or particles could be used to further improve the functionality of packaging. Progress on up scaling the production of these colloids as well as the processes to integrate them in packaging production is still needed.

However, to answer the increasing demand of biobased fiber and tackle the environmental footprint of these materials, research need to go towards diversifying the sources and using biorefinery approach where biomass is fully valorized. Colloids from unusual sources were shown to have properties similar with sometimes additional features compare to the ones produced from conventional sources. Diversifying the sources also encourage diversification of biomass production which allow local production in large part of the world.

On top of all the technical requirements for new packaging development, consumer acceptability in terms of price and perception should also be considered when designing new packaging. To further improve the consumers perception, proper labeling and education campaigns should be set up to orient the consumers so that they make fully informed choices.

REFRENCES

(1) Österberg, M.; Sipponen, M. H.; Mattos, B. D.; Rojas, O. J. Spherical Lignin Particles: A Review on Their Sustainability and Applications. *Green Chem.* **2020**, *22* (9), 2712–2733. https://doi.org/10.1039/D0GC00096E.

(2) Jin, T.; Liu, T.; Lam, E.; Moores, A. Chitin and Chitosan on the Nanoscale. *Nanoscale Horiz.* **2021**, *6* (7), 505–542. https://doi.org/10.1039/D0NH00696C.

(3) Salaberria, A. M.; Labidi, J.; Fernandes, S. C. M. Different Routes to Turn Chitin into Stunning Nano-Objects. *Eur. Polym. J.* **2015**, *68*, 503–515. https://doi.org/10.1016/j.eurpolymj.2015.03.005.

(4) Schneider, W. D. H.; Dillon, A. J. P.; Camassola, M. Lignin Nanoparticles Enter the Scene: A Promising Versatile Green Tool for Multiple Applications. *Biotechnol. Adv.* **2021**, *47*, 107685. https://doi.org/10.1016/j.biotechadv.2020.107685.

(5) Rol, F.; Belgacem, M. N.; Gandini, A.; Bras, J. Recent Advances in Surface-Modified Cellulose Nanofibrils. *Prog. Polym. Sci.* **2019**, *88*, 241–264. https://doi.org/10.1016/j.progpolymsci.2018.09.002.

(6) Niinimäki, K.; Peters, G.; Dahlbo, H.; Perry, P.; Rissanen, T.; Gwilt, A. The Environmental Price of Fast Fashion. *Nat. Rev. Earth Environ.* **2020**, *1* (4), 189–200. https://doi.org/10.1038/s43017-020-0039-9.

(7) Boufi, S. Agricultural Crop Residue as a Source for the Production of Cellulose Nanofibrils. In *Cellulose-Reinforced Nanofibre Composites*; Jawaid, M., Boufi, S., H.p.s., A. K., Eds.; Woodhead Publishing, 2017; pp 129–152. https://doi.org/10.1016/B978-0-08-100957-4.00006-1.

(8) Otoni, C. G.; Azeredo, H. M. C.; Mattos, B. D.; Beaumont, M.; Correa, D. S.; Rojas, O. J. The Food–Materials Nexus: Next Generation Bioplastics and Advanced Materials from Agri-Food Residues. *Adv. Mater.* **2021**, 2102520. https://doi.org/10.1002/adma.202102520.

(9) Ütebay, B.; Çelik, P.; Çay, A. Effects of Cotton Textile Waste Properties on Recycled Fibre Quality. *J. Clean. Prod.* **2019**, *222*, 29–35. https://doi.org/10.1016/j.jclepro.2019.03.033.

(10) Ross, I. L.; Shah, S.; Hankamer, B.; Amiralian, N. Microalgal Nanocellulose – Opportunities for a Circular Bioeconomy. *Trends Plant Sci.* **2021**, *26* (9), 924–939. https://doi.org/10.1016/j.tplants.2021.05.004.

(11) García, A.; Gandini, A.; Labidi, J.; Belgacem, N.; Bras, J. Industrial and Crop Wastes: A New Source for Nanocellulose Biorefinery. *Ind. Crops Prod.* **2016**, *93*, 26–38. https://doi.org/10.1016/j.indcrop.2016.06.004.

(12) Köhnke, J.; Rennhofer, H.; Lichtenegger, H.; Mahendran, A. raj; Unterweger, C.; Prats-Mateu, B.; Gierlinger, N.; Schwaiger, E.; Mahler, A.-K.; Potthast, A.; Gindl-Altmutter, W. Electrically Conducting Carbon Microparticles by Direct Carbonization of Spent Wood Pulping Liquor. *ACS Sustain. Chem. Eng.* **2018**, *6* (3), 3385–3391. https://doi.org/10.1021/acssuschemeng.7b03582.

(13) Wang, Z.; Yao, Z.; Zhou, J.; Zhang, Y. Reuse of Waste Cotton Cloth for the Extraction of Cellulose Nanocrystals. *Carbohydr. Polym.* **2017**, *157*, 945–952. https://doi.org/10.1016/j.carbpol.2016.10.044.

(14) Josset, S.; Orsolini, P.; Siqueira, G.; Tejado, A.; Tingaut, P.; Zimmermann, T. Energy Consumption of the Nanofibrillation of Bleached Pulp, Wheat Straw and Recycled Newspaper through a Grinding Process. *Nord. Pulp Pap. Res. J.* **2014**, *29* (1), 167–175. https://doi.org/10.3183/npprj-2014-29-01-p167-175.

(15) Chaker, A.; Mutjé, P.; Vilar, M. R.; Boufi, S. Agriculture Crop Residues as a Source for the Production of Nanofibrillated Cellulose with Low Energy Demand. *Cellulose* **2014**, *21* (6), 4247–4259. https://doi.org/10.1007/s10570-014-0454-5.

(16) Slavutsky, A. M.; Bertuzzi, M. A. Water Barrier Properties of Starch Films Reinforced with Cellulose Nanocrystals Obtained from Sugarcane Bagasse. *Carbohydr. Polym.* **2014**, *110*, 53–61. https://doi.org/10.1016/j.carbpol.2014.03.049.

(17) Rivière, G. N.; Pion, F.; Farooq, M.; Sipponen, M. H.; Koivula, H.; Jayabalan, T.; Pandard, P.; Marlair, G.; Liao, X.; Baumberger, S.; Österberg, M. Toward Waste Valorization by Converting

Bioethanol Production Residues into Nanoparticles and Nanocomposite Films. *Sustain. Mater. Technol.* **2021**, *28*, e00269. https://doi.org/10.1016/j.susmat.2021.e00269.

(18) Li, X.; Liu, Y.; Hao, J.; Wang, W. Study of Almond Shell Characteristics. *Materials* **2018**, *11* (9), 1782. https://doi.org/10.3390/ma11091782.

(19) Santos, R. M. dos; Flauzino Neto, W. P.; Silvério, H. A.; Martins, D. F.; Dantas, N. O.; Pasquini, D. Cellulose Nanocrystals from Pineapple Leaf, a New Approach for the Reuse of This Agro-Waste. *Ind. Crops Prod.* **2013**, *50*, 707–714. https://doi.org/10.1016/j.indcrop.2013.08.049.

(20) Foster, E. J.; Moon, R. J.; Agarwal, U. P.; Bortner, M. J.; Bras, J.; Camarero-Espinosa, S.; Chan, K. J.; Clift, M. J. D.; Cranston, E. D.; Eichhorn, S. J.; Fox, D. M.; Hamad, W. Y.; Heux, L.; Jean, B.; Korey, M.; Nieh, W.; Ong, K. J.; Reid, M. S.; Renneckar, S.; Roberts, R.; Shatkin, J. A.; Simonsen, J.; Stinson-Bagby, K.; Wanasekara, N.; Youngblood, J. Current Characterization Methods for Cellulose Nanomaterials. *Chem. Soc. Rev.* **2018**, *47* (8), 2609–2679. https://doi.org/10.1039/C6CS00895J.

(21) Pires, J. R. A.; Souza, V. G. L.; Fernando, A. L. Valorization of Energy Crops as a Source for Nanocellulose Production – Current Knowledge and Future Prospects. *Ind. Crops Prod.* **2019**, *140*, 111642. https://doi.org/10.1016/j.indcrop.2019.111642.

(22) Pennells, J.; Godwin, I. D.; Amiralian, N.; Martin, D. J. Trends in the Production of Cellulose Nanofibers from Non-Wood Sources. *Cellulose* **2020**, *27* (2), 575–593. https://doi.org/10.1007/s10570-019-02828-9.

(23) Nechyporchuk, O.; Belgacem, M. N.; Bras, J. Production of Cellulose Nanofibrils: A Review of Recent Advances. *Ind. Crops Prod.* **2016**, *93*, 2–25. https://doi.org/10.1016/j.indcrop.2016.02.016.

(24) Li, T.; Chen, C.; Brozena, A. H.; Zhu, J. Y.; Xu, L.; Driemeier, C.; Dai, J.; Rojas, O. J.; Isogai, A.; Wågberg, L.; Hu, L. Developing Fibrillated Cellulose as a Sustainable Technological Material. *Nature* **2021**, *590* (7844), 47–56. https://doi.org/10.1038/s41586-020-03167-7.

(25) Espinosa, E.; Rol, F.; Bras, J.; Rodríguez, A. Production of Lignocellulose Nanofibers from Wheat Straw by Different Fibrillation Methods. Comparison of Its Viability in Cardboard Recycling Process. *J. Clean. Prod.* **2019**, *239*, 118083. https://doi.org/10.1016/j.jclepro.2019.118083.

(26) Berto, G. L.; Mattos, B. D.; Rojas, O. J.; Arantes, V. Single-Step Fiber Pretreatment with Monocomponent Endoglucanase: Defibrillation Energy and Cellulose Nanofibril Quality. *ACS Sustain. Chem. Eng.* **2021**, *9* (5), 2260–2270. https://doi.org/10.1021/acssuschemeng.0c08162.

(27) Spence, K. L.; Venditti, R. A.; Rojas, O. J.; Habibi, Y.; Pawlak, J. J. A Comparative Study of Energy Consumption and Physical Properties of Microfibrillated Cellulose Produced by Different Processing Methods. *Cellulose* **2011**, *18* (4), 1097–1111. https://doi.org/10.1007/s10570-011-9533-z.

(28) Kangas, H.; Pere, J.; Qvintus, P. High-Consistency Enzymatic Fibrillation (HefCel) – a Cost-Efficient Way to Produce Cellulose Nanofibrils (CNF). *TechConnect Briefs* **2016**, *1* (2016), 181–183.

(29) Ho, T. T. T.; Abe, K.; Zimmermann, T.; Yano, H. Nanofibrillation of Pulp Fibers by Twin-Screw Extrusion. *Cellulose* **2015**, *22* (1), 421–433. https://doi.org/10.1007/s10570-014-0518-6.

(30) Rol, F.; Karakashov, B.; Nechyporchuk, O.; Terrien, M.; Meyer, V.; Dufresne, A.; Belgacem, M. N.; Bras, J. Pilot-Scale Twin Screw Extrusion and Chemical Pretreatment as an Energy-Efficient Method for the Production of Nanofibrillated Cellulose at High Solid Content. *ACS Sustain. Chem. Eng.* **2017**, *5* (8), 6524–6531. https://doi.org/10.1021/acssuschemeng.7b00630.

(31) Banvillet, G.; Gatt, E.; Belgacem, N.; Bras, J. Cellulose Fibers Deconstruction by Twin-Screw Extrusion with in Situ Enzymatic Hydrolysis via Bioextrusion. *Bioresour. Technol.* **2021**, *327*, 124819. https://doi.org/10.1016/j.biortech.2021.124819.

(32) Banvillet, G. Industrial Application of Pretreatments for Obtaining High Quality Cellulose Nanofibrils. These de doctorat, Université Grenoble Alpes, 2021.

(33) Espinosa, E.; Rol, F.; Bras, J.; Rodríguez, A. Use of Multi-Factorial Analysis to Determine the Quality of Cellulose Nanofibers: Effect of Nanofibrillation Treatment and Residual Lignin Content. *Cellulose* **2020**, *27* (18), 10689–10705. https://doi.org/10.1007/s10570-020-03136-3.
(34) Xiang, Z.; Gao, W.; Chen, L.; Lan, W.; Zhu, J. Y.; Runge, T. A Comparison of Cellulose Nanofibrils Produced from Cladophora Glomerata Algae and Bleached Eucalyptus Pulp. *Cellulose* **2016**, *23* (1), 493–503. https://doi.org/10.1007/s10570-015-0840-7.
(35) Guo, J.; Uddin, K. M. A.; Mihhels, K.; Fang, W.; Laaksonen, P.; Zhu, J. Y.; Rojas, O. J. Contribution of Residual Proteins to the Thermomechanical Performance of Cellulosic Nanofibrils Isolated from Green Macroalgae. *ACS Sustain. Chem. Eng.* **2017**, *5* (8), 6978–6985. https://doi.org/10.1021/acssuschemeng.7b01169.
(36) Imani, M.; Ghasemian, A.; Dehghani-Firouzabadi, M. R.; Afra, E.; Borghei, M.; Johansson, L. S.; Gane, P. A. C.; Rojas, O. J. Coupling Nanofibril Lateral Size and Residual Lignin to Tailor the Properties of Lignocellulose Films. *Adv. Mater. Interfaces* **2019**, *6* (19), 1900770. https://doi.org/10.1002/admi.201900770.
(37) Claro, F. C.; Matos, M.; Jordão, C.; Avelino, F.; Lomonaco, D.; Magalhães, W. L. E. Enhanced Microfibrillated Cellulose-Based Film by Controlling the Hemicellulose Content and MFC Rheology. *Carbohydr. Polym.* **2019**, *218*, 307–314. https://doi.org/10.1016/j.carbpol.2019.04.089.
(38) Orue, A.; Santamaria-Echart, A.; Eceiza, A.; Peña-Rodriguez, C.; Arbelaiz, A. Office Waste Paper as Cellulose Nanocrystal Source. *J. Appl. Polym. Sci.* **2017**, *134* (35), 45257. https://doi.org/10.1002/app.45257.
(39) Huang, S.; Tao, R.; Ismail, A.; Wang, Y. Cellulose Nanocrystals Derived from Textile Waste through Acid Hydrolysis and Oxidation as Reinforcing Agent of Soy Protein Film. *Polymers* **2020**, *12* (4), 958. https://doi.org/10.3390/polym12040958.
(40) Kumar, V.; Pathak, P.; Bhardwaj, N. K. Waste Paper: An Underutilized but Promising Source for Nanocellulose Mining. *Waste Manag.* **2020**, *102*, 281–303. https://doi.org/10.1016/j.wasman.2019.10.041.
(41) Desmaisons, J.; Boutonnet, E.; Rueff, M.; Dufresne, A.; Bras, J. A New Quality Index for Benchmarking of Different Cellulose Nanofibrils. *Carbohydr. Polym.* **2017**, *174*, 318–329. https://doi.org/10.1016/j.carbpol.2017.06.032.
(42) Ajdary, R.; Tardy, B. L.; Mattos, B. D.; Bai, L.; Rojas, O. J. Plant Nanomaterials and Inspiration from Nature: Water Interactions and Hierarchically Structured Hydrogels. *Adv. Mater.* **2021**, *33* (28), 2001085. https://doi.org/10.1002/adma.202001085.
(43) Isogai, A.; Saito, T.; Fukuzumi, H. TEMPO-Oxidized Cellulose Nanofibers. *Nanoscale* **2011**, *3* (1), 71–85. https://doi.org/10.1039/C0NR00583E.
(44) Ferrer, A.; Salas, C.; Rojas, O. J. Physical, Thermal, Chemical and Rheological Characterization of Cellulosic Microfibrils and Microparticles Produced from Soybean Hulls. *Ind. Crops Prod.* **2016**, *84*, 337–343. https://doi.org/10.1016/j.indcrop.2016.02.014.
(45) Trifol, J.; Marin Quintero, D. C.; Moriana, R. Pine Cone Biorefinery: Integral Valorization of Residual Biomass into Lignocellulose Nanofibrils (LCNF)-Reinforced Composites for Packaging. *ACS Sustain. Chem. Eng.* **2021**, *9* (5), 2180–2190. https://doi.org/10.1021/acssuschemeng.0c07687.
(46) Espinosa, E.; Sánchez, R.; Otero, R.; Domínguez-Robles, J.; Rodríguez, A. A Comparative Study of the Suitability of Different Cereal Straws for Lignocellulose Nanofibers Isolation. *Int. J. Biol. Macromol.* **2017**, *103*, 990–999. https://doi.org/10.1016/j.ijbiomac.2017.05.156.
(47) Sehaqui, H.; Liu, A.; Zhou, Q.; Berglund, L. A. Fast Preparation Procedure for Large, Flat Cellulose and Cellulose/Inorganic Nanopaper Structures. *Biomacromolecules* **2010**, *11* (9), 2195–2198. https://doi.org/10.1021/bm100490s.
(48) Kurita, K. Chitin and Chitosan: Functional Biopolymers from Marine Crustaceans. *Mar. Biotechnol.* **2006**, *8* (3), 203. https://doi.org/10.1007/s10126-005-0097-5.

(49) Rødde, R. H.; Einbu, A.; Vårum, K. M. A Seasonal Study of the Chemical Composition and Chitin Quality of Shrimp Shells Obtained from Northern Shrimp (Pandalus Borealis). *Carbohydr. Polym.* **2008**, *71* (3), 388–393. https://doi.org/10.1016/j.carbpol.2007.06.006.
(50) Boßelmann, F.; Romano, P.; Fabritius, H.; Raabe, D.; Epple, M. The Composition of the Exoskeleton of Two Crustacea: The American Lobster Homarus Americanus and the Edible Crab Cancer Pagurus. *Thermochim. Acta* **2007**, *463* (1), 65–68. https://doi.org/10.1016/j.tca.2007.07.018.
(51) Oyatogun, G. M.; Esan, T. A.; Akpan, E. I.; Adeosun, S. O.; Popoola, A. P. I.; Imasogie, B. I.; Soboyejo, W. O.; Afonja, A. A.; Ibitoye, S. A.; Abere, V. D.; Oyatogun, A. O.; Oluwasegun, K. M.; Akinwole, I. E.; Akinluwade, K. J. Chapter 11 - Chitin, Chitosan, Marine to Market. In *Handbook of Chitin and Chitosan*; Gopi, S., Thomas, S., Pius, A., Eds.; Elsevier, 2020; pp 341–381. https://doi.org/10.1016/B978-0-12-817966-6.00011-X.
(52) Hahn, T.; Tafi, E.; Paul, A.; Salvia, R.; Falabella, P.; Zibek, S. Current State of Chitin Purification and Chitosan Production from Insects. *J. Chem. Technol. Biotechnol.* **2020**, *95* (11), 2775–2795. https://doi.org/10.1002/jctb.6533.
(53) Rosa, R.; Spinelli, R.; Neri, P.; Pini, M.; Barbi, S.; Montorsi, M.; Maistrello, L.; Marseglia, A.; Caligiani, A.; Ferrari, A. M. Life Cycle Assessment of Chemical vs Enzymatic-Assisted Extraction of Proteins from Black Soldier Fly Prepupae for the Preparation of Biomaterials for Potential Agricultural Use. *ACS Sustain. Chem. Eng.* **2020**, *8* (39), 14752–14764. https://doi.org/10.1021/acssuschemeng.0c03795.
(54) Oonincx, D. G. A. B.; Boer, I. J. M. Environmental Impact of the Production of Mealworms as a Protein Source for Humans – A Life Cycle Assessment. *PLOS ONE* **2012**, *7* (12), e51145. https://doi.org/10.1371/journal.pone.0051145.
(55) Song, Y.-S.; Kim, M.-W.; Moon, C.; Seo, D.-J.; Han, Y. S.; Jo, Y. H.; Noh, M. Y.; Park, Y.-K.; Kim, S.-A.; Kim, Y. W.; Jung, W.-J. Extraction of Chitin and Chitosan from Larval Exuvium and Whole Body of Edible Mealworm, Tenebrio Molitor. *Entomol. Res.* **2018**, *48* (3), 227–233. https://doi.org/10.1111/1748-5967.12304.
(56) Purschke, B.; Brüggen, H.; Scheibelberger, R.; Jäger, H. Effect of Pre-Treatment and Drying Method on Physico-Chemical Properties and Dry Fractionation Behaviour of Mealworm Larvae (Tenebrio Molitor L.). *Eur. Food Res. Technol.* **2018**, *244* (2), 269–280. https://doi.org/10.1007/s00217-017-2953-8.
(57) Hahn, T.; Roth, A.; Ji, R.; Schmitt, E.; Zibek, S. Chitosan Production with Larval Exoskeletons Derived from the Insect Protein Production. *J. Biotechnol.* **2020**, *310*, 62–67. https://doi.org/10.1016/j.jbiotec.2019.12.015.
(58) Ling, S.; Kaplan, D. L.; Buehler, M. J. Nanofibrils in Nature and Materials Engineering. *Nat. Rev. Mater.* **2018**, *3* (4), 1–15. https://doi.org/10.1038/natrevmats.2018.16.
(59) Percot, A.; Viton, C.; Domard, A. Optimization of Chitin Extraction from Shrimp Shells. *Biomacromolecules* **2003**, *4* (1), 12–18. https://doi.org/10.1021/bm025602k.
(60) Qin, Y.; Lu, X.; Sun, N.; Rogers, R. D. Dissolution or Extraction of Crustacean Shells Using Ionic Liquids to Obtain High Molecular Weight Purified Chitin and Direct Production of Chitin Films and Fibers. *Green Chem.* **2010**, *12* (6), 968–971. https://doi.org/10.1039/C003583A.
(61) Shamshina, J. L.; Barber, P. S.; Gurau, G.; Griggs, C. S.; Rogers, R. D. Pulping of Crustacean Waste Using Ionic Liquids: To Extract or Not To Extract. *ACS Sustain. Chem. Eng.* **2016**, *4* (11), 6072–6081. https://doi.org/10.1021/acssuschemeng.6b01434.
(62) Parodi, A.; Leip, A.; De Boer, I. J. M.; Slegers, P. M.; Ziegler, F.; Temme, E. H. M.; Herrero, M.; Tuomisto, H.; Valin, H.; Van Middelaar, C. E.; Van Loon, J. J. A.; Van Zanten, H. H. E. The Potential of Future Foods for Sustainable and Healthy Diets. *Nat. Sustain.* **2018**, *1* (12), 782–789. https://doi.org/10.1038/s41893-018-0189-7.
(63) Baiano, A. Edible Insects: An Overview on Nutritional Characteristics, Safety, Farming, Production Technologies, Regulatory Framework, and Socio-Economic and Ethical Implications. *Trends Food Sci. Technol.* **2020**, *100*, 35–50. https://doi.org/10.1016/j.tifs.2020.03.040.

(64) Turck, D.; Castenmiller, J.; Henauw, S. D.; Hirsch-Ernst, K. I.; Kearney, J.; Maciuk, A.; Mangelsdorf, I.; McArdle, H. J.; Naska, A.; Pelaez, C.; Pentieva, K.; Siani, A.; Thies, F.; Tsabouri, S.; Vinceti, M.; Cubadda, F.; Frenzel, T.; Heinonen, M.; Marchelli, R.; Neuhäuser-Berthold, M.; Poulsen, M.; Maradona, M. P.; Schlatter, J. R.; Loveren, H. van; Ververis, E.; Knutsen, H. K. Safety of Dried Yellow Mealworm (Tenebrio Molitor Larva) as a Novel Food Pursuant to Regulation (EU) 2015/2283. *EFSA J.* **2021**, *19* (1), e06343. https://doi.org/10.2903/j.efsa.2021.6343.

(65) Hahn, T.; Roth, A.; Febel, E.; Fijalkowska, M.; Schmitt, E.; Arsiwalla, T.; Zibek, S. New Methods for High-Accuracy Insect Chitin Measurement. *J. Sci. Food Agric.* **2018**, *98* (13), 5069–5073. https://doi.org/10.1002/jsfa.9044.

(66) Brigode, C.; Hobbi, P.; Jafari, H.; Verwilghen, F.; Baeten, E.; Shavandi, A. Isolation and Physicochemical Properties of Chitin Polymer from Insect Farm Side Stream as a New Source of Renewable Biopolymer. *J. Clean. Prod.* **2020**, *275*, 122924. https://doi.org/10.1016/j.jclepro.2020.122924.

(67) Sanandiya, N. D.; Ottenheim, C.; Phua, J. W.; Caligiani, A.; Dritsas, S.; Fernandez, J. G. Circular Manufacturing of Chitinous Bio-Composites via Bioconversion of Urban Refuse. *Sci. Rep.* **2020**, *10* (1), 1–8. https://doi.org/10.1038/s41598-020-61664-1.

(68) Kaya, M.; Baublys, V.; Can, E.; Šatkauskienė, I.; Bitim, B.; Tubelytė, V.; Baran, T. Comparison of Physicochemical Properties of Chitins Isolated from an Insect (Melolontha Melolontha) and a Crustacean Species (Oniscus Asellus). *Zoomorphology* **2014**, *133* (3), 285–293. https://doi.org/10.1007/s00435-014-0227-6.

(69) Huet, G.; Hadad, C.; Husson, E.; Laclef, S.; Lambertyn, V.; Araya Farias, M.; Jamali, A.; Courty, M.; Alayoubi, R.; Gosselin, I.; Sarazin, C.; Van Nhien, A. N. Straightforward Extraction and Selective Bioconversion of High Purity Chitin from Bombyx Eri Larva: Toward an Integrated Insect Biorefinery. *Carbohydr. Polym.* **2020**, *228*, 115382. https://doi.org/10.1016/j.carbpol.2019.115382.

(70) Nawawi, W. M. F. B. W.; Jones, M.; Murphy, R. J.; Lee, K.-Y.; Kontturi, E.; Bismarck, A. Nanomaterials Derived from Fungal Sources—Is It the New Hype? *Biomacromolecules* **2020**, *21* (1), 30–55. https://doi.org/10.1021/acs.biomac.9b01141.

(71) Pasquier, E.; Beaumont, M.; Mattos, B. D.; Otoni, C. G.; Winter, A.; Rosenau, T.; Belgacem, M. N.; Rojas, O. J.; Bras, J. Upcycling Byproducts from Insect (Fly Larvae and Mealworm) Farming into Chitin Nanofibers and Films. *ACS Sustain. Chem. Eng.* **2021**, *9* (40), 13618–13629. https://doi.org/10.1021/acssuschemeng.1c05035.

(72) Mushi, N. E.; Butchosa, N.; Salajkova, M.; Zhou, Q.; Berglund, L. A. Nanostructured Membranes Based on Native Chitin Nanofibers Prepared by Mild Process. *Carbohydr. Polym.* **2014**, *112*, 255–263. https://doi.org/10.1016/j.carbpol.2014.05.038.

(73) Bai, L.; Huan, S.; Xiang, W.; Liu, L.; Yang, Y.; Nugroho, R. W. N.; Fan, Y.; Rojas, O. J. Self-Assembled Networks of Short and Long Chitin Nanoparticles for Oil/Water Interfacial Superstabilization. *ACS Sustain. Chem. Eng.* **2019**, *7* (7), 6497–6511. https://doi.org/10.1021/acssuschemeng.8b04023.

(74) Larbi, F.; García, A.; del Valle, L. J.; Hamou, A.; Puiggalí, J.; Belgacem, N.; Bras, J. Comparison of Nanocrystals and Nanofibers Produced from Shrimp Shell α-Chitin: From Energy Production to Material Cytotoxicity and Pickering Emulsion Properties. *Carbohydr. Polym.* **2018**, *196*, 385–397. https://doi.org/10.1016/j.carbpol.2018.04.094.

(75) Ifuku, S.; Nogi, M.; Abe, K.; Yoshioka, M.; Morimoto, M.; Saimoto, H.; Yano, H. Preparation of Chitin Nanofibers with a Uniform Width as α-Chitin from Crab Shells. *Biomacromolecules* **2009**, *10* (6), 1584–1588. https://doi.org/10.1021/bm900163d.

(76) Salaberria, A. M.; Fernandes, S. C. M.; Diaz, R. H.; Labidi, J. Processing of α-Chitin Nanofibers by Dynamic High Pressure Homogenization: Characterization and Antifungal Activity against A. Niger. *Carbohydr. Polym.* **2015**, *116*, 286–291. https://doi.org/10.1016/j.carbpol.2014.04.047.

(77) Lamarque, G.; Viton, C.; Domard, A. Comparative Study of the First Heterogeneous Deacetylation of α- and β-Chitins in a Multistep Process. *Biomacromolecules* **2004**, *5* (3), 992–1001. https://doi.org/10.1021/bm034498j.
(78) Fan, Y.; Saito, T.; Isogai, A. Individual Chitin Nano-Whiskers Prepared from Partially Deacetylated α-Chitin by Fibril Surface Cationization. *Carbohydr. Polym.* **2010**, *79* (4), 1046–1051. https://doi.org/10.1016/j.carbpol.2009.10.044.
(79) Ye, W.; Ma, H.; Liu, L.; Yu, J.; Lai, J.; Fang, Y.; Fan, Y. Biocatalyzed Route for the Preparation of Surface-Deacetylated Chitin Nanofibers. *Green Chem.* **2019**, *21* (11), 3143–3151. https://doi.org/10.1039/C9GC00857H.
(80) Goto, K.; Teramoto, Y. Distribution of the Degree of Deacetylation of Surface-Deacetylated Chitin Nanofibers: Effects on Crystalline Structure and Cell Adhesion and Proliferation. *ACS Appl. Bio Mater.* **2020**, *3* (12), 8650–8657. https://doi.org/10.1021/acsabm.0c01040.
(81) Bai, L.; Kämäräinen, T.; Xiang, W.; Majoinen, J.; Seitsonen, J.; Grande, R.; Huan, S.; Liu, L.; Fan, Y.; Rojas, O. J. Chirality from Cryo-Electron Tomograms of Nanocrystals Obtained by Lateral Disassembly and Surface Etching of Never-Dried Chitin. *ACS Nano* **2020**, *14* (6), 6921–6930. https://doi.org/10.1021/acsnano.0c01327.
(82) Narkevicius, A.; Steiner, L. M.; Parker, R. M.; Ogawa, Y.; Frka-Petesic, B.; Vignolini, S. Controlling the Self-Assembly Behavior of Aqueous Chitin Nanocrystal Suspensions. *Biomacromolecules* **2019**, *20* (7), 2830–2838. https://doi.org/10.1021/acs.biomac.9b00589.
(83) Fan, Y.; Saito, T.; Isogai, A. Chitin Nanocrystals Prepared by TEMPO-Mediated Oxidation of α-Chitin. *Biomacromolecules* **2008**, *9* (1), 192–198. https://doi.org/10.1021/bm700966g.
(84) Ifuku, S.; Morooka, S.; Morimoto, M.; Saimoto, H. Acetylation of Chitin Nanofibers and Their Transparent Nanocomposite Films. *Biomacromolecules* **2010**, *11* (5), 1326–1330. https://doi.org/10.1021/bm100109a.
(85) Fan, Y.; Fukuzumi, H.; Saito, T.; Isogai, A. Comparative Characterization of Aqueous Dispersions and Cast Films of Different Chitin Nanowhiskers/Nanofibers. *Int. J. Biol. Macromol.* **2012**, *50* (1), 69–76. https://doi.org/10.1016/j.ijbiomac.2011.09.026.
(86) Mushi, N. E.; Nishino, T.; Berglund, L. A.; Zhou, Q. Strong and Tough Chitin Film from α-Chitin Nanofibers Prepared by High Pressure Homogenization and Chitosan Addition. *ACS Sustain. Chem. Eng.* **2019**, *7* (1), 1692–1697. https://doi.org/10.1021/acssuschemeng.8b05452.
(87) Morin, A.; Dufresne, A. Nanocomposites of Chitin Whiskers from Riftia Tubes and Poly(Caprolactone). *Macromolecules* **2002**, *35* (6), 2190–2199. https://doi.org/10.1021/ma011493a.
(88) Ifuku, S.; Nomura, R.; Morimoto, M.; Saimoto, H. Preparation of Chitin Nanofibers from Mushrooms. *Materials* **2011**, *4* (8), 1417–1425. https://doi.org/10.3390/ma4081417.
(89) Susana Cortizo, M.; Berghoff, C. F.; Alessandrini, J. L. Characterization of Chitin from Illex Argentinus Squid Pen. *Carbohydr. Polym.* **2008**, *74* (1), 10–15. https://doi.org/10.1016/j.carbpol.2008.01.004.
(90) Wu, Q.; Jungstedt, E.; Šoltésová, M.; Mushi, N. E.; Berglund, L. A. High Strength Nanostructured Films Based on Well-Preserved β-Chitin Nanofibrils. *Nanoscale* **2019**, *11* (22), 11001–11011. https://doi.org/10.1039/C9NR02870F.
(91) Grande, R.; Bai, L.; Wang, L.; Xiang, W.; Ikkala, O.; Carvalho, A. J. F.; Rojas, O. J. Nanochitins of Varying Aspect Ratio and Properties of Microfibers Produced by Interfacial Complexation with Seaweed Alginate. *ACS Sustain. Chem. Eng.* **2020**, *8* (2), 1137–1145. https://doi.org/10.1021/acssuschemeng.9b06099.
(92) Mushi, N. E.; Kochumalayil, J.; Cervin, N. T.; Zhou, Q.; Berglund, L. A. Nanostructurally Controlled Hydrogel Based on Small-Diameter Native Chitin Nanofibers: Preparation, Structure, and Properties. *ChemSusChem* **2016**, *9* (9), 989–995. https://doi.org/10.1002/cssc.201501697.
(93) Mushi, N. E.; Butchosa, N.; Zhou, Q.; Berglund, L. A. Nanopaper Membranes from Chitin–Protein Composite Nanofibers—Structure and Mechanical Properties. *J. Appl. Polym. Sci.* **2014**, *131* (7). https://doi.org/10.1002/app.40121.

(94) Ifuku, S.; Urakami, T.; Izawa, H.; Morimoto, M.; Saimoto, H. Preparation of a Protein–Chitin Nanofiber Complex from Crab Shells and Its Application as a Reinforcement Filler or Substrate for Biomineralization. *RSC Adv.* **2015**, *5* (79), 64196–64201. https://doi.org/10.1039/C5RA12761K.
(95) Fazli Wan Nawawi, W. M.; Lee, K.-Y.; Kontturi, E.; Murphy, R. J.; Bismarck, A. Chitin Nanopaper from Mushroom Extract: Natural Composite of Nanofibers and Glucan from a Single Biobased Source. *ACS Sustain. Chem. Eng.* **2019**, *7* (7), 6492–6496. https://doi.org/10.1021/acssuschemeng.9b00721.
(96) Nawawi, W. M. F. W.; Jones, M. P.; Kontturi, E.; Mautner, A.; Bismarck, A. Plastic to Elastic: Fungi-Derived Composite Nanopapers with Tunable Tensile Properties. *Compos. Sci. Technol.* **2020**, *198*, 108327. https://doi.org/10.1016/j.compscitech.2020.108327.
(97) Younes, I.; Rinaudo, M. Chitin and Chitosan Preparation from Marine Sources. Structure, Properties and Applications. *Mar. Drugs* **2015**, *13* (3), 1133–1174. https://doi.org/10.3390/md13031133.
(98) Di Mario, F.; Rapanà, P.; Tomati, U.; Galli, E. Chitin and Chitosan from Basidiomycetes. *Int. J. Biol. Macromol.* **2008**, *43* (1), 8–12. https://doi.org/10.1016/j.ijbiomac.2007.10.005.
(99) Domínguez-Robles, J.; Cárcamo-Martínez, Á.; Stewart, S. A.; Donnelly, R. F.; Larrañeta, E.; Borrega, M. Lignin for Pharmaceutical and Biomedical Applications – Could This Become a Reality? *Sustain. Chem. Pharm.* **2020**, *18*, 100320. https://doi.org/10.1016/j.scp.2020.100320.
(100) Balakshin, M. Y.; Capanema, E. A.; Sulaeva, I.; Schlee, P.; Huang, Z.; Feng, M.; Borghei, M.; Rojas, O. J.; Potthast, A.; Rosenau, T. New Opportunities in the Valorization of Technical Lignins. *ChemSusChem* **2021**, *14* (4), 1016–1036. https://doi.org/10.1002/cssc.202002553.
(101) Bajwa, D. S.; Pourhashem, G.; Ullah, A. H.; Bajwa, S. G. A Concise Review of Current Lignin Production, Applications, Products and Their Environmental Impact. *Ind. Crops Prod.* **2019**, *139*, 111526. https://doi.org/10.1016/j.indcrop.2019.111526.
(102) Lourencon, T. V.; Greca, L. G.; Tarasov, D.; Borrega, M.; Tamminen, T.; Rojas, O. J.; Balakshin, M. Y. Lignin-First Integrated Hydrothermal Treatment (HTT) and Synthesis of Low-Cost Biorefinery Particles. *ACS Sustain. Chem. Eng.* **2020**, *8* (2), 1230–1239. https://doi.org/10.1021/acssuschemeng.9b06511.
(103) Duval, A.; Lawoko, M. A Review on Lignin-Based Polymeric, Micro- and Nano-Structured Materials. *React. Funct. Polym.* **2014**, *85*, 78–96. https://doi.org/10.1016/j.reactfunctpolym.2014.09.017.
(104) Kammoun, M.; Berchem, T.; Richel, A. Ultrafast Lignin Extraction from Unusual Mediterranean Lignocellulosic Residues. *JoVE J. Vis. Exp.* **2021**, No. 169, e61997. https://doi.org/10.3791/61997.
(105) Balakshin, M.; Capanema, E. A.; Zhu, X.; Sulaeva, I.; Potthast, A.; Rosenau, T.; Rojas, O. J. Spruce Milled Wood Lignin: Linear, Branched or Cross-Linked? *Green Chem.* **2020**, *22* (13), 3985–4001. https://doi.org/10.1039/D0GC00926A.
(106) Tao, J.; Li, S.; Ye, F.; Zhou, Y.; Lei, L.; Zhao, G. Lignin – An Underutilized, Renewable and Valuable Material for Food Industry. *Crit. Rev. Food Sci. Nutr.* **2020**, *60* (12), 2011–2033. https://doi.org/10.1080/10408398.2019.1625025.
(107) Gil-Chávez, J.; Gurikov, P.; Hu, X.; Meyer, R.; Reynolds, W.; Smirnova, I. Application of Novel and Technical Lignins in Food and Pharmaceutical Industries: Structure-Function Relationship and Current Challenges. *Biomass Convers. Biorefinery* **2021**, *11* (6), 2387–2403. https://doi.org/10.1007/s13399-019-00458-6.
(108) Guo, Y.; Tian, D.; Shen, F.; Yang, G.; Long, L.; He, J.; Song, C.; Zhang, J.; Zhu, Y.; Huang, C.; Deng, S. Transparent Cellulose/Technical Lignin Composite Films for Advanced Packaging. *Polymers* **2019**, *11* (9). https://doi.org/10.3390/polym11091455.
(109) Ago, M.; Tardy, B. L.; Wang, L.; Guo, J.; Khakalo, A.; Rojas, O. J. Supramolecular Assemblies of Lignin into Nano- and Microparticles. *MRS Bull.* **2017**, *42* (5), 371–378. https://doi.org/10.1557/mrs.2017.88.

(110) Freitas, F. M. C.; Cerqueira, M. A.; Gonçalves, C.; Azinheiro, S.; Garrido-Maestu, A.; Vicente, A. A.; Pastrana, L. M.; Teixeira, J. A.; Michelin, M. Green Synthesis of Lignin Nano- and Micro-Particles: Physicochemical Characterization, Bioactive Properties and Cytotoxicity Assessment. *Int. J. Biol. Macromol.* **2020**, *163*, 1798–1809. https://doi.org/10.1016/j.ijbiomac.2020.09.110.

(111) Leskinen, T.; Smyth, M.; Xiao, Y.; Lintinen, K.; Mattinen, M. L.; Kostiainen, M. A.; Oinas, P.; Österberg, M. Scaling up Production of Colloidal Lignin Particles. *Nord Pulp Pap. Res. J.* **2017**, *32* (4), 586–596. https://doi.org/10.3183/NPPRJ-2017-32-04-p586-596.

(112) Ashok, R. P. B.; Oinas, P.; Lintinen, K.; Sarwar, G.; Kostiainen, M. A.; Österberg, M. Techno-Economic Assessment for the Large-Scale Production of Colloidal Lignin Particles. *Green Chem.* **2018**, *20* (21), 4911–4919. https://doi.org/10.1039/C8GC02805B.

(113) Sipponen, M. H.; Lange, H.; Ago, M.; Crestini, C. Understanding Lignin Aggregation Processes. A Case Study: Budesonide Entrapment and Stimuli Controlled Release from Lignin Nanoparticles. *ACS Sustain. Chem. Eng.* **2018**, *6* (7), 9342–9351. https://doi.org/10.1021/acssuschemeng.8b01652.

(114) Zwilling, J. D.; Jiang, X.; Zambrano, F.; Venditti, R. A.; Jameel, H.; Velev, O. D.; Rojas, O. J.; Gonzalez, R. Understanding Lignin Micro- and Nanoparticle Nucleation and Growth in Aqueous Suspensions by Solvent Fractionation. *Green Chem.* **2021**, *23* (2), 1001–1012. https://doi.org/10.1039/D0GC03632C.

(115) Richter, A. P.; Bharti, B.; Armstrong, H. B.; Brown, J. S.; Plemmons, D.; Paunov, V. N.; Stoyanov, S. D.; Velev, O. D. Synthesis and Characterization of Biodegradable Lignin Nanoparticles with Tunable Surface Properties. *Langmuir* **2016**, *32* (25), 6468–6477. https://doi.org/10.1021/acs.langmuir.6b01088.

(116) Lievonen, M.; José Valle-Delgado, J.; Mattinen, M.-L.; Hult, E.-L.; Lintinen, K.; A. Kostiainen, M.; Paananen, A.; R. Szilvay, G.; Setälä, H.; Österberg, M. A Simple Process for Lignin Nanoparticle Preparation. *Green Chem.* **2016**, *18* (5), 1416–1422. https://doi.org/10.1039/C5GC01436K.

(117) Pang, T.; Wang, G.; Sun, H.; Wang, L.; Liu, Q.; Sui, W.; Parvez, A. M.; Si, C. Lignin Fractionation for Reduced Heterogeneity in Self-Assembly Nanosizing: Toward Targeted Preparation of Uniform Lignin Nanoparticles with Small Size. *ACS Sustain. Chem. Eng.* **2020**, *8* (24), 9174–9183. https://doi.org/10.1021/acssuschemeng.0c02967.

(118) Ago, M.; Huan, S.; Borghei, M.; Raula, J.; Kauppinen, E. I.; Rojas, O. J. High-Throughput Synthesis of Lignin Particles (∼30 Nm to ∼2 Mm) via Aerosol Flow Reactor: Size Fractionation and Utilization in Pickering Emulsions. *ACS Appl. Mater. Interfaces* **2016**, *8* (35), 23302–23310. https://doi.org/10.1021/acsami.6b07900.

(119) Abbati de Assis, C.; Greca, L. G.; Ago, M.; Balakshin, M. Yu.; Jameel, H.; Gonzalez, R.; Rojas, O. J. Techno-Economic Assessment, Scalability, and Applications of Aerosol Lignin Micro- and Nanoparticles. *ACS Sustain. Chem. Eng.* **2018**, *6* (9), 11853–11868. https://doi.org/10.1021/acssuschemeng.8b02151.

(120) Sipponen, M. H.; Smyth, M.; Leskinen, T.; Johansson, L.-S.; Österberg, M. All-Lignin Approach to Prepare Cationic Colloidal Lignin Particles: Stabilization of Durable Pickering Emulsions. *Green Chem.* **2017**, *19* (24), 5831–5840. https://doi.org/10.1039/C7GC02900D.

(121) Frangville, C.; Rutkevičius, M.; Richter, A. P.; Velev, O. D.; Stoyanov, S. D.; Paunov, V. N. Fabrication of Environmentally Biodegradable Lignin Nanoparticles. *ChemPhysChem* **2012**, *13* (18), 4235–4243. https://doi.org/10.1002/cphc.201200537.

(122) Qian, Y.; Deng, Y.; Qiu, X.; Li, H.; Yang, D. Formation of Uniform Colloidal Spheres from Lignin, a Renewable Resource Recovered from Pulping Spent Liquor. *Green Chem.* **2014**, *16* (4), 2156–2163. https://doi.org/10.1039/C3GC42131G.

(123) Juikar, S. J.; Vigneshwaran, N. Extraction of Nanolignin from Coconut Fibers by Controlled Microbial Hydrolysis. *Ind. Crops Prod.* **2017**, *109*, 420–425. https://doi.org/10.1016/j.indcrop.2017.08.067.

(124) Cuthill, H.; Elleman, C.; Curwen, T.; Wolf, B. Colloidal Particles for Pickering Emulsion Stabilization Prepared via Antisolvent Precipitation of Lignin-Rich Cocoa Shell Extract. *Foods* **2021**, *10* (2), 371. https://doi.org/10.3390/foods10020371.

(125) Matsakas, L.; Gerber, M.; Yu, L.; Rova, U.; Christakopoulos, P. Preparation of Low Carbon Impact Lignin Nanoparticles with Controllable Size by Using Different Strategies for Particles Recovery. *Ind. Crops Prod.* **2020**, *147*, 112243. https://doi.org/10.1016/j.indcrop.2020.112243.

(126) Posoknistakul, P.; Tangkrakul, C.; Chaosuanphae, P.; Deepentham, S.; Techasawong, W.; Phonphirunrot, N.; Bairak, S.; Sakdaronnarong, C.; Laosiripojana, N. Fabrication and Characterization of Lignin Particles and Their Ultraviolet Protection Ability in PVA Composite Film. *ACS Omega* **2020**, *5* (33), 20976–20982. https://doi.org/10.1021/acsomega.0c02443.

(127) Zhang, X.; Yang, M.; Yuan, Q.; Cheng, G. Controlled Preparation of Corncob Lignin Nanoparticles and Their Size-Dependent Antioxidant Properties: Toward High Value Utilization of Lignin. *ACS Sustain. Chem. Eng.* **2019**, *7* (20), 17166–17174. https://doi.org/10.1021/acssuschemeng.9b03535.

(128) Beisl, S.; Loidolt, P.; Miltner, A.; Harasek, M.; Friedl, A.; Beisl, S.; Loidolt, P.; Miltner, A.; Harasek, M.; Friedl, A. Production of Micro- and Nanoscale Lignin from Wheat Straw Using Different Precipitation Setups. *Molecules* **2018**, *23* (3), 633. https://doi.org/10.3390/molecules23030633.

(129) Adamcyk, J.; Beisl, S.; Amini, S.; Jung, T.; Zikeli, F.; Labidi, J.; Friedl, A. Production and Properties of Lignin Nanoparticles from Ethanol Organosolv Liquors—Influence of Origin and Pretreatment Conditions. *Polymers* **2021**, *13* (3), 384. https://doi.org/10.3390/polym13030384.

(130) Qian, Y.; Qiu, X.; Zhu, S. Lignin: A Nature-Inspired Sun Blocker for Broad-Spectrum Sunscreens. *Green Chem.* **2014**, *17* (1), 320–324. https://doi.org/10.1039/C4GC01333F.

(131) Cusola, O.; Rojas, O. J.; Roncero, M. B. Lignin Particles for Multifunctional Membranes, Antioxidative Microfiltration, Patterning, and 3D Structuring. *ACS Appl. Mater. Interfaces* **2019**, *11* (48), 45226–45236. https://doi.org/10.1021/acsami.9b16931.

(132) Gerbin, E.; Rivière, G. N.; Foulon, L.; Frapart, Y. M.; Cottyn, B.; Pernes, M.; Marcuello, C.; Godon, B.; Gainvors-Claisse, A.; Crônier, D.; Majira, A.; Österberg, M.; Kurek, B.; Baumberger, S.; Aguié-Béghin, V. Tuning the Functional Properties of Lignocellulosic Films by Controlling the Molecular and Supramolecular Structure of Lignin. *Int. J. Biol. Macromol.* **2021**, *181*, 136–149. https://doi.org/10.1016/j.ijbiomac.2021.03.081.

(133) Zhang, H.; Liu, X.; Fu, S.; Chen, Y. High-Value Utilization of Kraft Lignin: Color Reduction and Evaluation as Sunscreen Ingredient. *Int. J. Biol. Macromol.* **2019**, *133*, 86–92. https://doi.org/10.1016/j.ijbiomac.2019.04.092.

(134) Zhang, Y.; Naebe, M. Lignin: A Review on Structure, Properties, and Applications as a Light-Colored UV Absorber. *ACS Sustain. Chem. Eng.* **2021**, *9* (4), 1427–1442. https://doi.org/10.1021/acssuschemeng.0c06998.

(135) Lee, S. C.; Yoo, E.; Lee, S. H.; Won, K. Preparation and Application of Light-Colored Lignin Nanoparticles for Broad-Spectrum Sunscreens. *Polymers* **2020**, *12* (3), 699. https://doi.org/10.3390/polym12030699.

(136) Lindström, T.; Österberg, F. Evolution of Biobased and Nanotechnology Packaging – a Review. *Nord. Pulp Pap. Res. J.* **2020**, *35* (4), 491–515. https://doi.org/10.1515/npprj-2020-0042.

(137) Robertson, G. L. Food Packaging. In *Encyclopedia of Agriculture and Food Systems*; Van Alfen, N. K., Ed.; Academic Press: Oxford, 2014; pp 232–249. https://doi.org/10.1016/B978-0-444-52512-3.00063-2.

(138) Wen, Y.; Yuan, Z.; Liu, X.; Qu, J.; Yang, S.; Wang, A.; Wang, C.; Wei, B.; Xu, J.; Ni, Y. Preparation and Characterization of Lignin-Containing Cellulose Nanofibril from Poplar High-

Yield Pulp via TEMPO-Mediated Oxidation and Homogenization. *ACS Sustain. Chem. Eng.* **2019**, *7* (6), 6131–6139. https://doi.org/10.1021/acssuschemeng.8b06355.

(139) Notley, S. M.; Norgren, M. Surface Energy and Wettability of Spin-Coated Thin Films of Lignin Isolated from Wood. *Langmuir* **2010**, *26* (8), 5484–5490. https://doi.org/10.1021/la1003337.

(140) Beaumont, M.; Otoni, C. G.; Mattos, B. D.; Koso, T. V.; Abidnejad, R.; Zhao, B.; Kondor, A.; King, A. W. T.; Rojas, O. J. Regioselective and Water-Assisted Surface Esterification of Never-Dried Cellulose: Nanofibers with Adjustable Surface Energy. *Green Chem.* **2021**, *23* (18), 6966–6974. https://doi.org/10.1039/D1GC02292J.

(141) Reverdy, C.; Belgacem, N.; Moghaddam, M. S.; Sundin, M.; Swerin, A.; Bras, J. One-Step Superhydrophobic Coating Using Hydrophobized Cellulose Nanofibrils. *Colloids Surf. Physicochem. Eng. Asp.* **2018**, *544*, 152–158. https://doi.org/10.1016/j.colsurfa.2017.12.059.

(142) Martinez, P.; Rol, F.; Guerin, D. Chromatogeny Applied to MFC Wet Laminated Papers & Boards; 2020.

(143) Gustafsson, E.; Larsson, P. A.; Wågberg, L. Treatment of Cellulose Fibres with Polyelectrolytes and Wax Colloids to Create Tailored Highly Hydrophobic Fibrous Networks. *Colloids Surf. Physicochem. Eng. Asp.* **2012**, *414*, 415–421. https://doi.org/10.1016/j.colsurfa.2012.08.042.

(144) Samain, D. Procede de traitement d'un materiau solide pour le rendre hydrophobe, materiau obtenu et applications. CA2301073A1, February 25, 1999.

(145) Robles, E.; Izaguirre, N.; Martin, A.; Moschou, D.; Labidi, J. Assessment of Bleached and Unbleached Nanofibers from Pistachio Shells for Nanopaper Making. *Molecules* **2021**, *26* (5), 1371. https://doi.org/10.3390/molecules26051371.

(146) Tyagi, P.; Gutierrez, J. N.; Nathani, V.; Lucia, L. A.; Rojas, O. J.; Hubbe, M. A.; Pal, L. Hydrothermal and Mechanically Generated Hemp Hurd Nanofibers for Sustainable Barrier Coatings/Films. *Ind. Crops Prod.* **2021**, *168*, 113582. https://doi.org/10.1016/j.indcrop.2021.113582.

(147) Pasquier, E.; Mattos, B. D.; Belgacem, N.; Bras, J.; Rojas, O. J. Lignin Nanoparticle Nucleation and Growth on Cellulose and Chitin Nanofibers. *Biomacromolecules* **2021**, *22* (2), 880–889. https://doi.org/10.1021/acs.biomac.0c01596.

(148) Xia, J.; Zhang, Z.; Liu, W.; Li, V. C. F.; Cao, Y.; Zhang, W.; Deng, Y. Highly Transparent 100% Cellulose Nanofibril Films with Extremely High Oxygen Barriers in High Relative Humidity. *Cellulose* **2018**, *25* (7), 4057–4066. https://doi.org/10.1007/s10570-018-1843-y.

(149) Sharma, S.; Zhang, X.; Nair, S. S.; Ragauskas, A.; Zhu, J.; Deng, Y. Thermally Enhanced High Performance Cellulose Nano Fibril Barrier Membranes. *RSC Adv.* **2014**, *4* (85), 45136–45142. https://doi.org/10.1039/C4RA07469F.

(150) J. Benítez, A.; Walther, A. Cellulose Nanofibril Nanopapers and Bioinspired Nanocomposites: A Review to Understand the Mechanical Property Space. *J. Mater. Chem. A* **2017**, *5* (31), 16003–16024. https://doi.org/10.1039/C7TA02006F.

(151) Kumar, V.; Bollström, R.; Yang, A.; Chen, Q.; Chen, G.; Salminen, P.; Bousfield, D.; Toivakka, M. Comparison of Nano- and Microfibrillated Cellulose Films. *Cellulose* **2014**, *21* (5), 3443–3456. https://doi.org/10.1007/s10570-014-0357-5.

(152) Ifuku, S.; Ikuta, A.; Izawa, H.; Morimoto, M.; Saimoto, H. Control of Mechanical Properties of Chitin Nanofiber Film Using Glycerol without Losing Its Characteristics. *Carbohydr. Polym.* **2014**, *101*, 714–717. https://doi.org/10.1016/j.carbpol.2013.09.076.

(153) Shimizu, M.; Saito, T.; Isogai, A. Water-Resistant and High Oxygen-Barrier Nanocellulose Films with Interfibrillar Cross-Linkages Formed through Multivalent Metal Ions. *J. Membr. Sci.* **2016**, *500*, 1–7. https://doi.org/10.1016/j.memsci.2015.11.002.

(154) Toivonen, M. S.; Kurki-Suonio, S.; Schacher, F. H.; Hietala, S.; Rojas, O. J.; Ikkala, O. Water-Resistant, Transparent Hybrid Nanopaper by Physical Cross-Linking with Chitosan. *Biomacromolecules* **2015**, *16* (3), 1062–1071. https://doi.org/10.1021/acs.biomac.5b00145.

(155) Benselfelt, T.; Engström, J.; Wågberg, L. Supramolecular Double Networks of Cellulose Nanofibrils and Algal Polysaccharides with Excellent Wet Mechanical Properties. *Green Chem.* **2018**, *20* (11), 2558–2570. https://doi.org/10.1039/C8GC00590G.

(156) Walther, A.; Lossada, F.; Benselfelt, T.; Kriechbaum, K.; Berglund, L.; Ikkala, O.; Saito, T.; Wågberg, L.; Bergström, L. Best Practice for Reporting Wet Mechanical Properties of Nanocellulose-Based Materials. *Biomacromolecules* **2020**, *21* (6), 2536–2540. https://doi.org/10.1021/acs.biomac.0c00330.

(157) Kriechbaum, K.; Bergström, L. Antioxidant and UV-Blocking Leather-Inspired Nanocellulose-Based Films with High Wet Strength. *Biomacromolecules* **2020**, *21* (5), 1720–1728. https://doi.org/10.1021/acs.biomac.9b01655.

(158) Wang, X.; Xia, Q.; Jing, S.; Li, C.; Chen, Q.; Chen, B.; Pang, Z.; Jiang, B.; Gan, W.; Chen, G.; Cui, M.; Hu, L.; Li, T. Strong, Hydrostable, and Degradable Straws Based on Cellulose-Lignin Reinforced Composites. *Small* **2021**, *17* (18), 2008011. https://doi.org/10.1002/smll.202008011.

(159) Helanto, K.; Matikainen, L.; Talja, R.; Rojas, O. J. Bio-Based Polymers for Sustainable Packaging and Biobarriers: A Critical Review. *BioRessources* **2019**, *14* (2), 4902–4951.

(160) Wang, J.; Gardner, D. J.; Stark, N. M.; Bousfield, D. W.; Tajvidi, M.; Cai, Z. Moisture and Oxygen Barrier Properties of Cellulose Nanomaterial-Based Films. *ACS Sustain. Chem. Eng.* **2018**, *6* (1), 49–70. https://doi.org/10.1021/acssuschemeng.7b03523.

(161) Österberg, M.; Vartiainen, J.; Lucenius, J.; Hippi, U.; Seppälä, J.; Serimaa, R.; Laine, J. A Fast Method to Produce Strong NFC Films as a Platform for Barrier and Functional Materials. *ACS Appl. Mater. Interfaces* **2013**, *5* (11), 4640–4647. https://doi.org/10.1021/am401046x.

(162) H. Tayeb, A.; Tajvidi, M.; Bousfield, D. Paper-Based Oil Barrier Packaging Using Lignin-Containing Cellulose Nanofibrils. *Molecules* **2020**, *25* (6), 1344. https://doi.org/10.3390/molecules25061344.

(163) Schenker, U.; Chardot, J.; Missoum, K.; Vishtal, A.; Bras, J. Short Communication on the Role of Cellulosic Fiber-Based Packaging in Reduction of Climate Change Impacts. *Carbohydr. Polym.* **2021**, *254*, 117248. https://doi.org/10.1016/j.carbpol.2020.117248.

(164) Bedane, A. H.; Eić, M.; Farmahini-Farahani, M.; Xiao, H. Water Vapor Transport Properties of Regenerated Cellulose and Nanofibrillated Cellulose Films. *J. Membr. Sci.* **2015**, *493*, 46–57. https://doi.org/10.1016/j.memsci.2015.06.009.

(165) Fukuzumi, H.; Saito, T.; Isogai, A. Influence of TEMPO-Oxidized Cellulose Nanofibril Length on Film Properties. *Carbohydr. Polym.* **2013**, *93* (1), 172–177. https://doi.org/10.1016/j.carbpol.2012.04.069.

(166) Bardet, R.; Reverdy, C.; Belgacem, N.; Leirset, I.; Syverud, K.; Bardet, M.; Bras, J. Substitution of Nanoclay in High Gas Barrier Films of Cellulose Nanofibrils with Cellulose Nanocrystals and Thermal Treatment. *Cellulose* **2015**, *22* (2), 1227–1241. https://doi.org/10.1007/s10570-015-0547-9.

(167) Spence, K. L.; Venditti, R. A.; Rojas, O. J.; Pawlak, J. J.; Hubbe, M. A. Water Vapor Barrier Properties of Coated and Filled Microfibrillated Cellulose Composite Films. *BioResources* **2011**, *6* (4), 4370–4388. https://doi.org/10.15376/biores.6.4.4370-4388.

(168) Larsson, P. A.; Kochumalayil, J. J.; Wågberg, L. Oxygen and Water Vapour Barrier Films with Low Moisture Sensitivity Fabricated from Self-Crosslinking Fibrillated Cellulose. *Adv. Pulp Pap. Res.* **2013**, 851–866. https://doi.org/10.15376/frc.2013.2.851.

(169) Kim, T.; Tran, T. H.; Hwang, S. Y.; Park, J.; Oh, D. X.; Kim, B.-S. Crab-on-a-Tree: All Biorenewable, Optical and Radio Frequency Transparent Barrier Nanocoating for Food Packaging. *ACS Nano* **2019**, *13* (4), 3796–3805. https://doi.org/10.1021/acsnano.8b08522.

(170) Dou, J.; Vuorinen, T.; Koivula, H.; Forsman, N.; Sipponen, M.; Hietala, S. Self-Standing Lignin-Containing Willow Bark Nanocellulose Films for Oxygen Blocking and UV Shielding. *ACS Appl. Nano Mater.* **2021**, *4* (3), 2921–2929. https://doi.org/10.1021/acsanm.1c00071.

(171) Kumar, V.; Elfving, A.; Koivula, H.; Bousfield, D.; Toivakka, M. Roll-to-Roll Processed Cellulose Nanofiber Coatings. *Ind. Eng. Chem. Res.* **2016**, *55* (12), 3603–3613. https://doi.org/10.1021/acs.iecr.6b00417.

(172) Toivonen, M. S.; Onelli, O. D.; Jacucci, G.; Lovikka, V.; Rojas, O. J.; Ikkala, O.; Vignolini, S. Anomalous-Diffusion-Assisted Brightness in White Cellulose Nanofibril Membranes. *Adv. Mater.* **2018**, *30* (16), 1704050. https://doi.org/10.1002/adma.201704050.

(173) Kwon, S.; Orsuwan, A.; Bumbudsanpharoke, N.; Yoon, C.; Choi, J.; Ko, S. A Short Review of Light Barrier Materials for Food and Beverage Packaging. *KOREAN J. Packag. Sci. Technol.* **2018**, *24* (3), 141–148. https://doi.org/10.20909/kopast.2018.24.3.141.

(174) Abitbol, T.; Ahniyaz, A.; Álvarez-Asencio, R.; Fall, A.; Swerin, A. Nanocellulose-Based Hybrid Materials for UV Blocking and Mechanically Robust Barriers. *ACS Appl. Bio Mater.* **2020**, *3* (4), 2245–2254. https://doi.org/10.1021/acsabm.0c00058.

(175) Oliveira, G.; Gonçalves, I.; Barra, A.; Nunes, C.; Ferreira, P.; Coimbra, M. A. Coffee Silverskin and Starch-Rich Potato Washing Slurries as Raw Materials for Elastic, Antioxidant, and UV-Protective Biobased Films. *Food Res. Int.* **2020**, *138*, 109733. https://doi.org/10.1016/j.foodres.2020.109733.

(176) Wang, B.; Sun, D.; Wang, H.-M.; Yuan, T.-Q.; Sun, R.-C. Green and Facile Preparation of Regular Lignin Nanoparticles with High Yield and Their Natural Broad-Spectrum Sunscreens. *ACS Sustain. Chem. Eng.* **2019**, *7* (2), 2658–2666. https://doi.org/10.1021/acssuschemeng.8b05735.

(177) Qian, Y.; Zhong, X.; Li, Y.; Qiu, X. Fabrication of Uniform Lignin Colloidal Spheres for Developing Natural Broad-Spectrum Sunscreens with High Sun Protection Factor. *Ind. Crops Prod.* **2017**, *101*, 54–60. https://doi.org/10.1016/j.indcrop.2017.03.001.

(178) Farooq, M.; Zou, T.; Riviere, G.; Sipponen, M. H.; Österberg, M. Strong, Ductile, and Waterproof Cellulose Nanofibril Composite Films with Colloidal Lignin Particles. *Biomacromolecules* **2019**, *20* (2), 693–704. https://doi.org/10.1021/acs.biomac.8b01364.

(179) Parit, M.; Saha, P.; Davis, V. A.; Jiang, Z. Transparent and Homogenous Cellulose Nanocrystal/Lignin UV-Protection Films. *ACS Omega* **2018**, *3* (9), 10679–10691. https://doi.org/10.1021/acsomega.8b01345.

(180) Gómez-Estaca, J.; López-de-Dicastillo, C.; Hernández-Muñoz, P.; Catalá, R.; Gavara, R. Advances in Antioxidant Active Food Packaging. *Trends Food Sci. Technol.* **2014**, *35* (1), 42–51. https://doi.org/10.1016/j.tifs.2013.10.008.

(181) Benhabiles, M. S.; Salah, R.; Lounici, H.; Drouiche, N.; Goosen, M. F. A.; Mameri, N. Antibacterial Activity of Chitin, Chitosan and Its Oligomers Prepared from Shrimp Shell Waste. *Food Hydrocoll.* **2012**, *29* (1), 48–56. https://doi.org/10.1016/j.foodhyd.2012.02.013.

(182) García, A.; Toledano, A.; Andrés, M. Á.; Labidi, J. Study of the Antioxidant Capacity of Miscanthus Sinensis Lignins. *Process Biochem.* **2010**, *45* (6), 935–940. https://doi.org/10.1016/j.procbio.2010.02.015.

(183) de Menezes Nogueira, I.; Avelino, F.; de Oliveira, D. R.; Souza, N. F.; Rosa, M. F.; Mazzetto, S. E.; Lomonaco, D. Organic Solvent Fractionation of Acetosolv Palm Oil Lignin: The Role of Its Structure on the Antioxidant Activity. *Int. J. Biol. Macromol.* **2019**, *122*, 1163–1172. https://doi.org/10.1016/j.ijbiomac.2018.09.066.

(184) Younes, I.; Sellimi, S.; Rinaudo, M.; Jellouli, K.; Nasri, M. Influence of Acetylation Degree and Molecular Weight of Homogeneous Chitosans on Antibacterial and Antifungal Activities. *Int. J. Food Microbiol.* **2014**, *185*, 57–63. https://doi.org/10.1016/j.ijfoodmicro.2014.04.029.

(185) Kaya, M.; Baran, T.; Asan-Ozusaglam, M.; Cakmak, Y. S.; Tozak, K. O.; Mol, A.; Mentes, A.; Sezen, G. Extraction and Characterization of Chitin and Chitosan with Antimicrobial and Antioxidant Activities from Cosmopolitan Orthoptera Species (Insecta). *Biotechnol. Bioprocess Eng.* **2015**, *20* (1), 168–179. https://doi.org/10.1007/s12257-014-0391-z.

(186) Lourençon, T. V.; de Lima, G. G.; Ribeiro, C. S. P.; Hansel, F. A.; Maciel, G. M.; da Silva, K.; Winnischofer, S. M. B.; de Muniz, G. I. B.; Magalhães, W. L. E. Antioxidant, Antibacterial and Antitumoural Activities of Kraft Lignin from Hardwood Fractionated by Acid Precipitation. *Int. J. Biol. Macromol.* **2021**, *166*, 1535–1542. https://doi.org/10.1016/j.ijbiomac.2020.11.033.

(187) Richter, A. P.; Brown, J. S.; Bharti, B.; Wang, A.; Gangwal, S.; Houck, K.; Hubal, E. A. C.; Paunov, V. N.; Stoyanov, S. D.; Velev, O. D. An Environmentally Benign Antimicrobial Nanoparticle Based on a Silver-Infused Lignin Core. *Nat. Nanotechnol.* **2015**, *10* (9), 817–823. https://doi.org/10.1038/nnano.2015.141.

(188) Lintinen, K.; Luiro, S.; Figueiredo, P.; Sakarinen, E.; Mousavi, Z.; Seitsonen, J.; Rivière, G. N. S.; Mattinen, U.; Niemelä, M.; Tammela, P.; Österberg, M.; Johansson, L.-S.; Bobacka, J.; Santos, H. A.; Kostiainen, M. A. Antimicrobial Colloidal Silver–Lignin Particles via Ion and Solvent Exchange. *ACS Sustain. Chem. Eng.* **2019**, *7* (18), 15297–15303. https://doi.org/10.1021/acssuschemeng.9b02498.

(189) Clauser, N. M.; Felissia, F. E.; Area, M. C.; Vallejos, M. E. Design of Nano and Micro Fibrillated Cellulose Production Processes from Forest Industrial Wastes in a Multiproduct Biorefinery. *Chem. Eng. Res. Des.* **2021**, *167*, 1–14. https://doi.org/10.1016/j.cherd.2020.12.003.

(190) Assis, C. A. de; Iglesias, M. C.; Bilodeau, M.; Johnson, D.; Phillips, R.; Peresin, M. S.; Bilek, E. M. (Ted); Rojas, O. J.; Venditti, R.; Gonzalez, R. Cellulose Micro- and Nanofibrils (CMNF) Manufacturing - Financial and Risk Assessment. *Biofuels Bioprod. Biorefining* **2018**, *12* (2), 251–264. https://doi.org/10.1002/bbb.1835.

(191) Lee, K.-Y.; Aitomäki, Y.; Berglund, L. A.; Oksman, K.; Bismarck, A. On the Use of Nanocellulose as Reinforcement in Polymer Matrix Composites. *Compos. Sci. Technol.* **2014**, *105*, 15–27. https://doi.org/10.1016/j.compscitech.2014.08.032.

(192) Wang, L.; Roach, A. W.; Gardner, D. J.; Han, Y. Mechanisms Contributing to Mechanical Property Changes in Composites of Polypropylene Reinforced with Spray-Dried Cellulose Nanofibrils. *Cellulose* **2018**, *25* (1), 439–448. https://doi.org/10.1007/s10570-017-1556-7.

(193) Shanmugam, K.; Doosthosseini, H.; Varanasi, S.; Garnier, G.; Batchelor, W. Flexible Spray Coating Process for Smooth Nanocellulose Film Production. *Cellulose* **2018**, *25* (3), 1725–1741. https://doi.org/10.1007/s10570-018-1677-7.

(194) Peresin, M.; Vartiainen, J.; Kunnari, V.; Kaljunen, T.; Tammelin, T.; Qvintus, P. Large-Scale Nanofibrillated Cellulose Film: An Overview on Its Production, Properties, and Potential Applications; Nanjing, China, 2012.

(195) Claro, P.; de Campos, A.; Corrêa, A.; Rodrigues, V.; Luchesi, B.; Silva, L.; Tonoli, G.; Mattoso, L.; Marconcini, J. Curaua and Eucalyptus Nanofiber Films by Continuous Casting: Mixture of Cellulose Nanocrystals and Nanofibrils. *Cellulose* **2019**, *26* (4), 2453–2470. https://doi.org/10.1007/s10570-019-02280-9.

(196) Lavoine, N.; Bras, J.; Desloges, I. Mechanical and Barrier Properties of Cardboard and 3D Packaging Coated with Microfibrillated Cellulose. *J. Appl. Polym. Sci.* **2014**, *131* (8). https://doi.org/10.1002/app.40106.

(197) Lavoine, N.; Desloges, I.; Khelifi, B.; Bras, J. Impact of Different Coating Processes of Microfibrillated Cellulose on the Mechanical and Barrier Properties of Paper. *J. Mater. Sci.* **2014**, *49* (7), 2879–2893. https://doi.org/10.1007/s10853-013-7995-0.

(198) Mazhari Mousavi, S. M.; Afra, E.; Tajvidi, M.; Bousfield, D. W.; Dehghani-Firouzabadi, M. Cellulose Nanofiber/Carboxymethyl Cellulose Blends as an Efficient Coating to Improve the Structure and Barrier Properties of Paperboard. *Cellulose* **2017**, *24* (7), 3001–3014. https://doi.org/10.1007/s10570-017-1299-5.

(199) Beneventi, D.; Chaussy, D.; Curtil, D.; Zolin, L.; Gerbaldi, C.; Penazzi, N. Highly Porous Paper Loading with Microfibrillated Cellulose by Spray Coating on Wet Substrates. *Ind. Eng. Chem. Res.* **2014**, *53* (27), 10982–10989. https://doi.org/10.1021/ie500955x.

(200) Ottesen, V.; Kumar, V.; Toivakka, M.; Carrasco, G. C.; Syverud, K.; Gregersen, Ø. W. Viability and Properties of Roll-to-Roll Coating of Cellulose Nanofibrils on Recycled Paperboard. *Nord. Pulp Pap. Res. J.* **2017**, *32* (2), 179–188. https://doi.org/10.3183/npprj-2017-32-02-p179-188.

(201) Syverud, K.; Stenius, P. Strength and Barrier Properties of MFC Films. *Cellulose* **2008**, *16* (1), 75. https://doi.org/10.1007/s10570-008-9244-2.

(202) Hubbe, M. A.; Ferrer, A.; Tyagi, P.; Yin, Y.; Salas, C.; Pal, L.; Rojas, O. J. Nanocellulose in Thin Films, Coatings, and Plies for Packaging Applications: A Review. *BioResources* **2017**, *12* (1), 2143–2233. https://doi.org/10.15376/biores.12.1.2143-2233.

(203) Fotie, G.; Limbo, S.; Piergiovanni, L. Manufacturing of Food Packaging Based on Nanocellulose: Current Advances and Challenges. *Nanomaterials* **2020**, *10* (9), 1726. https://doi.org/10.3390/nano10091726.

(204) Regazzi, A.; Viguié, J.; Harthong, B.; Dumont, P. J. J.; Imbault, D.; Peyroux, R.; Rueff, M.; Charlier, Q.; Guérin, D.; Leroy, L.; Krouit, M.; Petit-Conil, M. Ultrasonic Welding of 100% Lignocellulosic Papers. *J. Mater. Sci.* **2019**, *54* (19), 12938–12950. https://doi.org/10.1007/s10853-019-03763-7.

(205) Koppolu, R.; Abitbol, T.; Kumar, V.; Jaiswal, A. K.; Swerin, A.; Toivakka, M. Continuous Roll-to-Roll Coating of Cellulose Nanocrystals onto Paperboard. *Cellulose* **2018**, *25* (10), 6055–6069. https://doi.org/10.1007/s10570-018-1958-1.

(206) Ghisellini, P.; Cialani, C.; Ulgiati, S. A Review on Circular Economy: The Expected Transition to a Balanced Interplay of Environmental and Economic Systems. *J. Clean. Prod.* **2016**, *114*, 11–32. https://doi.org/10.1016/j.jclepro.2015.09.007.

(207) Geueke, B.; Groh, K.; Muncke, J. Food Packaging in the Circular Economy: Overview of Chemical Safety Aspects for Commonly Used Materials. *J. Clean. Prod.* **2018**, *193*, 491–505. https://doi.org/10.1016/j.jclepro.2018.05.005.

(208) Bascón-Villegas, I.; Espinosa, E.; Sánchez, R.; Tarrés, Q.; Pérez-Rodríguez, F.; Rodríguez, A. Horticultural Plant Residues as New Source for Lignocellulose Nanofibers Isolation: Application on the Recycling Paperboard Process. *Molecules* **2020**, *25* (14), 3275. https://doi.org/10.3390/molecules25143275.

(209) Shanmugam, K.; Doosthosseini, H.; Varanasi, S.; Garnier, G.; Batchelor, W. Nanocellulose Films as Air and Water Vapour Barriers: A Recyclable and Biodegradable Alternative to Polyolefin Packaging. *Sustain. Mater. Technol.* **2019**, *22*, e00115. https://doi.org/10.1016/j.susmat.2019.e00115.

(210) Ang, S.; Ghosh, D.; Haritos, V.; Batchelor, W. Recycling Cellulose Nanofibers from Wood Pulps Provides Drainage Improvements for High Strength Sheets in Papermaking. *J. Clean. Prod.* **2021**, *312*, 127731. https://doi.org/10.1016/j.jclepro.2021.127731.

(211) Leppänen, I.; Vikman, M.; Harlin, A.; Orelma, H. Enzymatic Degradation and Pilot-Scale Composting of Cellulose-Based Films with Different Chemical Structures. *J. Polym. Environ.* **2020**, *28* (2), 458–470. https://doi.org/10.1007/s10924-019-01621-w.

(212) Homma, I.; Isogai, T.; Saito, T.; Isogai, A. Degradation of TEMPO-Oxidized Cellulose Fibers and Nanofibrils by Crude Cellulase. *Cellulose* **2013**, *20* (2), 795–805. https://doi.org/10.1007/s10570-013-9872-z.

(213) Paquet, O.; Krouit, M.; Bras, J.; Thielemans, W.; Belgacem, M. N. Surface Modification of Cellulose by PCL Grafts. *Acta Mater.* **2010**, *58* (3), 792–801. https://doi.org/10.1016/j.actamat.2009.09.057.

(214) Rossi, V.; Cleeve-Edwards, N.; Lundquist, L.; Schenker, U.; Dubois, C.; Humbert, S.; Jolliet, O. Life Cycle Assessment of End-of-Life Options for Two Biodegradable Packaging Materials: Sound Application of the European Waste Hierarchy. *J. Clean. Prod.* **2015**, *86*, 132–145. https://doi.org/10.1016/j.jclepro.2014.08.049.

(215) Kakadellis, S.; Harris, Z. M. Don't Scrap the Waste: The Need for Broader System Boundaries in Bioplastic Food Packaging Life-Cycle Assessment – A Critical Review. *J. Clean. Prod.* **2020**, *274*, 122831. https://doi.org/10.1016/j.jclepro.2020.122831.
(216) Kargarzadeh, H.; Mariano, M.; Gopakumar, D.; Ahmad, I.; Thomas, S.; Dufresne, A.; Huang, J.; Lin, N. Advances in Cellulose Nanomaterials. *Cellulose* **2018**, *25* (4), 2151–2189. https://doi.org/10.1007/s10570-018-1723-5.
(217) Berglund, L.; Breedveld, L.; Oksman, K. Toward Eco-Efficient Production of Natural Nanofibers from Industrial Residue: Eco-Design and Quality Assessment. *J. Clean. Prod.* **2020**, *255*, 120274. https://doi.org/10.1016/j.jclepro.2020.120274.
(218) Hohenthal, C.; Ovaskainen, M.; Bussini, D.; Sadocco, P.; Pajula, T.; Lehtinen, H.; Kautto, J.; Salmenkivi, K. *Final Assessment of Nano Enhanced New Products*; The research leading to these results has received funding from the European Community's 7thFrame work Programme under grantagreementno228802Scale-up Nanoparticles in Modern Papermaking-SUNPAP; VTT, 2012; p 56.
(219) Li, Q.; McGinnis, S.; Sydnor, C.; Wong, A.; Renneckar, S. Nanocellulose Life Cycle Assessment. *ACS Sustain. Chem. Eng.* **2013**, *1* (8), 919–928. https://doi.org/10.1021/sc4000225.
(220) Ita-Nagy, D.; Vázquez-Rowe, I.; Kahhat, R.; Chinga-Carrasco, G.; Quispe, I. Reviewing Environmental Life Cycle Impacts of Biobased Polymers: Current Trends and Methodological Challenges. *Int. J. Life Cycle Assess.* **2020**, *25* (11), 2169–2189. https://doi.org/10.1007/s11367-020-01829-2.
(221) Weiss, M.; Haufe, J.; Carus, M.; Brandão, M.; Bringezu, S.; Hermann, B.; Patel, M. K. A Review of the Environmental Impacts of Biobased Materials. *J. Ind. Ecol.* **2012**, *16* (s1), S169–S181. https://doi.org/10.1111/j.1530-9290.2012.00468.x.
(222) Piccinno, F.; Hischier, R.; Seeger, S.; Som, C. Life Cycle Assessment of a New Technology To Extract, Functionalize and Orient Cellulose Nanofibers from Food Waste. *ACS Sustain. Chem. Eng.* **2015**, *3* (6), 1047–1055. https://doi.org/10.1021/acssuschemeng.5b00209.
(223) Bauli, C. R.; Rocha, D. B.; de Oliveira, S. A.; Rosa, D. S. Cellulose Nanostructures from Wood Waste with Low Input Consumption. *J. Clean. Prod.* **2019**, *211*, 408–416. https://doi.org/10.1016/j.jclepro.2018.11.099.
(224) Leão, R. M.; Miléo, P. C.; Maia, J. M. L. L.; Luz, S. M. Environmental and Technical Feasibility of Cellulose Nanocrystal Manufacturing from Sugarcane Bagasse. *Carbohydr. Polym.* **2017**, *175*, 518–529. https://doi.org/10.1016/j.carbpol.2017.07.087.
(225) Nascimento, D. M. do; Dias, A. F.; Araújo Junior, C. P. de; Rosa, M. de F.; Morais, J. P. S.; Figueirêdo, M. C. B. de. A Comprehensive Approach for Obtaining Cellulose Nanocrystal from Coconut Fiber. Part II: Environmental Assessment of Technological Pathways. *Ind. Crops Prod.* **2016**, *93*, 58–65. https://doi.org/10.1016/j.indcrop.2016.02.063.
(226) de Figueirêdo, M. C. B.; Rosa, M. de F.; Ugaya, C. M. L.; Souza Filho, M. de S. M. de; Silva Braid, A. C. C. da; Melo, L. F. L. de. Life Cycle Assessment of Cellulose Nanowhiskers. *J. Clean. Prod.* **2012**, *35*, 130–139. https://doi.org/10.1016/j.jclepro.2012.05.033.
(227) Gallo Stampino, P.; Riva, L.; Punta, C.; Elegir, G.; Bussini, D.; Dotelli, G. Comparative Life Cycle Assessment of Cellulose Nanofibres Production Routes from Virgin and Recycled Raw Materials. *Molecules* **2021**, *26* (9), 2558. https://doi.org/10.3390/molecules26092558.
(228) Rodionova, M. V.; Poudyal, R. S.; Tiwari, I.; Voloshin, R. A.; Zharmukhamedov, S. K.; Nam, H. G.; Zayadan, B. K.; Bruce, B. D.; Hou, H. J. M.; Allakhverdiev, S. I. Biofuel Production: Challenges and Opportunities. *Int. J. Hydrog. Energy* **2017**, *42* (12), 8450–8461. https://doi.org/10.1016/j.ijhydene.2016.11.125.
(229) Cao, L.; Diana, J. S.; Keoleian, G. A.; Lai, Q. Life Cycle Assessment of Chinese Shrimp Farming Systems Targeted for Export and Domestic Sales. *Environ. Sci. Technol.* **2011**, *45* (15), 6531–6538. https://doi.org/10.1021/es104058z.

(230) Yang, N.; Zhang, W.; Ye, C.; Chen, X.; Ling, S. Nanobiopolymers Fabrication and Their Life Cycle Assessments. *Biotechnol. J.* **2019**, *14* (1), 1700754. https://doi.org/10.1002/biot.201700754.

(231) Foroughi, F.; Rezvani Ghomi, E.; Morshedi Dehaghi, F.; Borayek, R.; Ramakrishna, S. A Review on the Life Cycle Assessment of Cellulose: From Properties to the Potential of Making It a Low Carbon Material. *Materials* **2021**, *14* (4), 714. https://doi.org/10.3390/ma14040714.

(232) Arvidsson, R.; Nguyen, D.; Svanström, M. Life Cycle Assessment of Cellulose Nanofibrils Production by Mechanical Treatment and Two Different Pretreatment Processes. *Environ. Sci. Technol.* **2015**, *49* (11), 6881–6890. https://doi.org/10.1021/acs.est.5b00888.

(233) Piccinno, F.; Hischier, R.; Seeger, S.; Som, C. Predicting the Environmental Impact of a Future Nanocellulose Production at Industrial Scale: Application of the Life Cycle Assessment Scale-up Framework. *J. Clean. Prod.* **2018**, *174*, 283–295. https://doi.org/10.1016/j.jclepro.2017.10.226.

(234) Turk, J.; Oven, P.; Poljanšek, I.; Lešek, A.; Knez, F.; Malovrh Rebec, K. Evaluation of an Environmental Profile Comparison for Nanocellulose Production and Supply Chain by Applying Different Life Cycle Assessment Methods. *J. Clean. Prod.* **2020**, *247*, 119107. https://doi.org/10.1016/j.jclepro.2019.119107.

(235) Hervy, M.; Evangelisti, S.; Lettieri, P.; Lee, K.-Y. Life Cycle Assessment of Nanocellulose-Reinforced Advanced Fibre Composites. *Compos. Sci. Technol.* **2015**, *118*, 154–162. https://doi.org/10.1016/j.compscitech.2015.08.024.

(236) Muñoz, I.; Rodríguez, C.; Gillet, D.; M. Moerschbacher, B. Life Cycle Assessment of Chitosan Production in India and Europe. *Int. J. Life Cycle Assess.* **2018**, *23* (5), 1151–1160. https://doi.org/10.1007/s11367-017-1290-2.

(237) Leceta, I.; Guerrero, P.; Cabezudo, S.; Caba, K. de la. Environmental Assessment of Chitosan-Based Films. *J. Clean. Prod.* **2013**, *41*, 312–318. https://doi.org/10.1016/j.jclepro.2012.09.049.

(238) Leceta, I.; Etxabide, A.; Cabezudo, S.; de la Caba, K.; Guerrero, P. Bio-Based Films Prepared with by-Products and Wastes: Environmental Assessment. *J. Clean. Prod.* **2014**, *64*, 218–227. https://doi.org/10.1016/j.jclepro.2013.07.054.

(239) Moretti, C.; Corona, B.; Hoefnagels, R.; Vural-Gürsel, I.; Gosselink, R.; Junginger, M. Review of Life Cycle Assessments of Lignin and Derived Products: Lessons Learned. *Sci. Total Environ.* **2021**, *770*, 144656. https://doi.org/10.1016/j.scitotenv.2020.144656.

(240) Hermann, B. G.; Blok, K.; Patel, M. K. Twisting Biomaterials around Your Little Finger: Environmental Impacts of Bio-Based Wrappings. *Int. J. Life Cycle Assess.* **2010**, *15* (4), 346–358. https://doi.org/10.1007/s11367-010-0155-8.

(241) Pajula, T.; Vatanen, S.; Behm, K.; Grönman, K.; Lakanen, L.; Kasurinen, H.; Soukka, R. *Carbon Handprint Guide: V. 2.0 Applicable for Environmental Handprint*; VTT Technical Research Centre of Finland, 2021; p 28.

Chapter II
Preparation of colloids and first assembly into films

Table of content – Chapter II

Introduction to Chapter II 103

Chapter II.1 Production of chitin nanofibers and films from insects (fly larvae and mealworm) 105

INTRODUCTION 105
EXPERIMENTAL SECTION 107
Chitin Purification. 108
Characterization of the raw and purified chitin flakes. 108
Nanofiber suspension preparation. 108
Suspension characterization. 109
Film preparation. 110
Film characterization. 110
RESULTS AND DISCUSSION 111
Analysis of the purified materials 111
Structural analysis of the chitin nanofibers. 114
Analysis of the films' properties depending on the ChNF source and drying process. . 119
Overall sustainability, insights on potential applications, and prospects for insect based ChNF. 125
CONCLUSION 129

Chapter II.2 Preparation of lignin microparticles and their incorporation in CNF films 131

INTRODUCTION 131
EXPERIMENTAL SECTION 133
Dried lignin particles preparation. 133
Characterization of the suspensions. 134
Preparation of CNF film containing lignin particles. 135
Characterization of the films. 135
RESULTS AND DISCUSSION 136
Properties of tCNF. 136
Lignin particles prepared with an aerosol reactor. 136
Influence of LPs on the nanostructure of the films. 138
CONCLUSION 142

Conclusion to Chapter II 143

References 144

Introduction to Chapter II

Chapter I presented the different biobased colloids available in large quantities as well as their relevance for the preparation of food packaging. The PhD project is then divided into three chapters presenting results following **Figure II.1**. In **Chapter II**, we focus on the preparation of colloids in particular the preparation of ChNF from different sources and the preparation of LP with an aerosol reactor. First CNF films containing LP are also produced and characterized.

Chapter II.1 reports the preparation of chitin nanofibers from three different sources. Chitin is extracted from by-products of mealworm farming composed of mealworm exuviae as well as food residues, the second source is chitin already extracted from fly larvae. Finally, shrimp chitin is used as a reference. Characterization of the purified chitin and fibrillated chitin nanofibers is carried out regarding the suspension stability, nanofibers size, and crystallinity. Suspensions and ChNF films are compared in terms of structure, surface, and mechanical properties.

In **Chapter II.2**, lignin particles (LP) are prepared with an aerosol reactor and mixed with TEMPO oxidized CNF. Films with different content of LP are formed and the structure of the films is assessed.

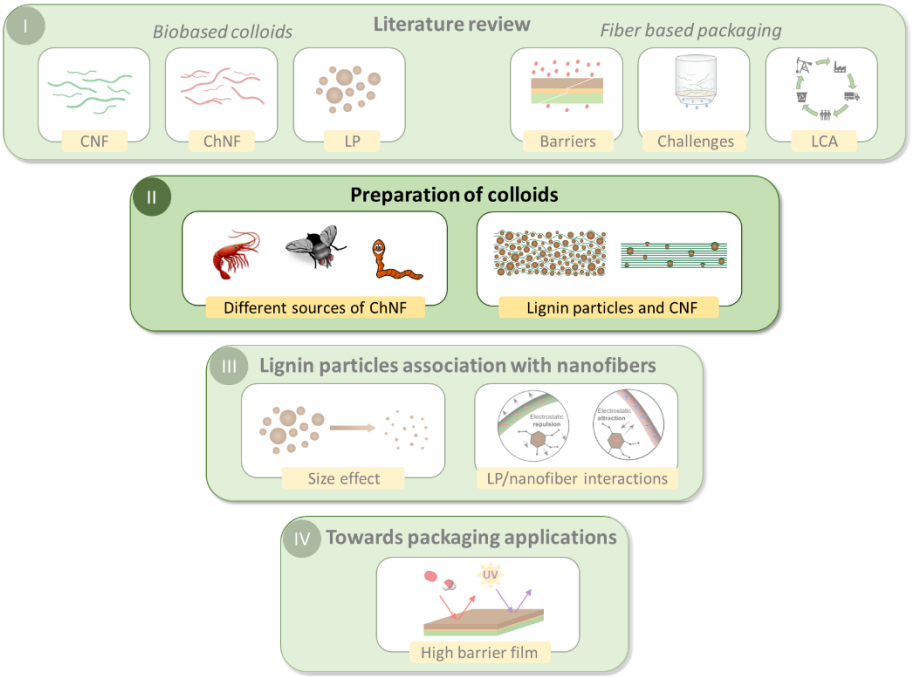

Figure II.1. Global scheme of the PhD project, Chapter II is highlighted.

Chapter II.1 Production of chitin nanofibers and films from insects (fly larvae and mealworm)

Adapted from "Upcycling Byproducts from Insect (Fly Larvae and Mealworm) Farming into Chitin Nanofibers and Films", E. Pasquier, B. D. Mattos, C. G. Otoni, A. Winter, T. Rosenau, N. Belgacem, O. J. Rojas, J. Bras, published in ACS Sustainable Chemistry, 2021.

INTRODUCTION

Today's environmental crisis has urged scientist to find alternatives to conventional sources of proteins. With their high protein content, insects are promising food[1–3] and feed[4] alternatives, and their composition also includes high amounts of lipids and structural polysaccharides, notably chitin. Insects are considered as future foods to potentially replace conventional animal sources of protein,[2] also having great advantages regarding current environmental issues. One reason is the incredibly high protein yield per production space in comparison to other protein sources, mainly due to the possibility of vertical farming: One kilogram of edible protein from mealworm requires 18 m^2, differing in one order of magnitude from beef cattle (200 m^2/kg).[5] In addition, the amount of water needed for insect farming is low as some insects can grow without water and can be fed in a very sustainable manner, *e.g.* with crop waste.[6] Moreover, it was shown that frass from mealworm larvae farming has similar fertilizing potential as conventional mineral fertilizers.[7] All these arguments explain the advancement of insect farming. Although the pertinent business models are still under development, it is obvious that valorization of all components is needed to meet the demands of sustainable biorefinery approaches.[8] Chitin is one of the insects´ main components, representing 5 to 10% of their dry matter.[9,10] Chitin possesses a high potential in agriculture, waste treatment, cosmetic, healthcare, food, or materials application and its utilization could further enhance the sustainability of insect farming. The chitin presents in the insects´ body, larvae, or shells can be readily separated from the protein-rich fractions. Caligiani *et al.* showed that black soldier fly prepupae can be integrated in a biorefinery approach as source of proteins, lipids, and chitin.[11] In addition, during the different life stages (larvae, pupae, prepupae, adult), insects molt, leaving behind shells (exoskeletons) as a chitin-rich side stream[12,13] that could be directly used for chitin extraction.

Colloidal nanofibers can be obtained from chitinous biomass by mechanical treatment at high pressure or sonication of purified chitin suspensions.[14] Chitin nanofibers (ChNFs) have a

tremendous potential in the fabrication of materials given their unique properties. Compared to nanocellulose, nanochitin is less hydrophilic and can bear cationic surface groups due to deacetylation of the *N*-acetyl moieties, which support, *via* electrostatic repulsion, the individualization into nanofibers. Moreover, the presence of primary amino groups on the fibril surface after partial deacetylation opens many doors for chemical functionalization absent in nanocelluloses. When protonated, these groups also offer the opportunity of physical functionalization through the electrostatic toolbox and render ChNF suspensions colloidally stable. Its fibrillar nature, biodegradability as well as natural cationic surface make deacetylated chitin/chitosan a promising, versatile building block for material development, as demonstrated in composites,[15] membranes,[16] platforms for waste water treatment, and emulsion stabilization.[17]

Many studies have shown the extraction of nanochitin from shrimps, crabs,[18] squid pen,[19] mushrooms,[20] and *Riftia tube*,[21] but the production and comparison of ChNFs from different insect sources has been overlooked so far. In fact, chitin has been extracted from insects, but only few comparisons between crustacean and insect chitin have been reported and no nanofibers have been obtained from insect chitin.[12,22–24] The chitins possess similar chemical structures, crystalline arrays, and thermal properties,[23] but differences in morphology, in particular the accessibility of the fibers, were noted.[12,22] Also, given the unique chemical composition and therefore recalcitrance of each chitin source (either from crustaceans or insects), the extraction and purification processes should be tuned accordingly. Whereas crustacean shells are mainly composed of calcium carbonate, exoskeletons of insects contain relatively more proteins and lipids. The conventional demineralization/deproteinization steps should therefore be adapted.[25] Fungi are another source of chitin, from which ChNFs have been extracted, though with low purity due to glucans present on the fibers´ surface.[26]

In this work, we have studied the effects of the chitinous raw material on the purification of chitin and the subsequent isolation of nanofibers and their properties. ChNFs were produced from chitin of black soldier fly (*Hermetia illucens*) larvae and chitinous waste from mealworm (*Tenebrio molitor*) farming. These two species are among the most promising insects for industrial farming,[9] being both considered as future foods,[2] which has triggered several companies (*e.g.*, Ynsect, Alpha Chitin, InnovaFeed, Enterra, Die Wurm Farm, and Protix) to start efforts at pilot and industrial scales. In addition, mealworm has recently been considered safe for human consumption as food by the European Food Safety Authority (EFSA).[27] In our work, purification of the chitins from different sources was followed by mechanical

disintegration to form nanofibers (see **Figure II.2**). Comparisons of the structural properties of the extracted nanofibers and their ability to form self-standing films are presented. The influence of impurities was also considered and discussed. With this work we hope to encourage efforts to upcycle insect farming waste into high-performance building blocks for colloidal and solid-state materials.

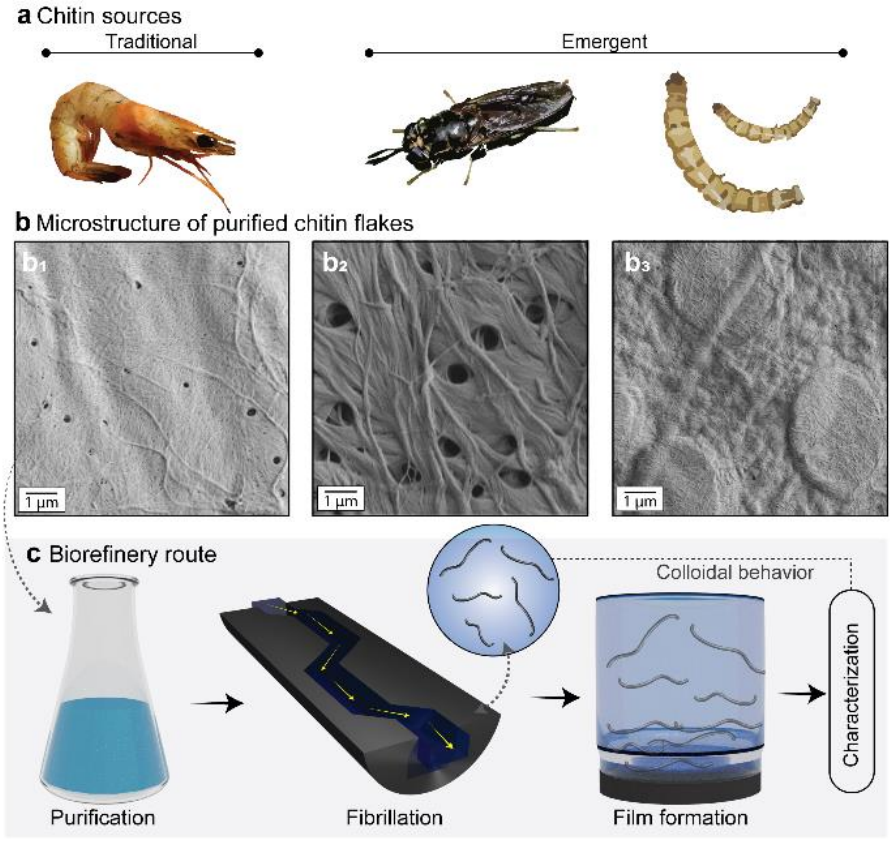

Figure II.2: Different chitin sources used in this study (**a**). Microstructure of the purified chitin fibers from shrimp shells (**b1**), fly larvae (**b2**) and mealworm exuviae (**b3**) shown by SEM images (**b**). Different process steps conducted before characterization of the materials (**c**).

EXPERIMENTAL SECTION

Materials. Chitin flakes from shrimp were obtained from Sigma-Aldrich. Chitin from fly larvae (*Hermetia illucens*) was provided by S-Fly (France), and the chitinous waste from mealworm (*Tenebrio molitor*) farming was provided by Die Wurm Farm (Austria). All chitinous samples were received as dried powder. Bleached Kraft Hardwood pulp was used as never dried raw materials to produce the reference cellulose nanofibers (CNF) following microfluidization (M-110P, Microfluidics In., USA, 2000 bar with 200- and 100-µm chambers) using six passes and with no chemical pretreatment. All reagents and solvents were purchased from Sigma-Aldrich and used as received.

Chitin Purification.

Chitin from fly and mealworm were first purified with a Soxhlet extraction with hexane for 6 h. Chitin purification was optimized following the procedure described by Percot at al.[28] First, acid hydrolysis at 0.25 M and room temperature was controlled following the increase of pH that occurred upon dissolution of calcium carbonate. In the same way, deproteinization with NaOH 1 M at 50 °C was controlled by UV absorption at 280 nm, characteristic of the tryptophan protein. A final bleaching step, with sodium chlorite at 80 °C for 2 h, was used to remove any residual pigments. Only one cycle was needed for the chitin from shrimp while three were needed to obtain white chitin from fly. Four bleaching cycles separated by sodium hydroxide purification step at 70 °C for 1 h were needed to obtain white chitin from the mealworm waste. The yield was calculated by dividing the final dry mass of the obtained material by the initial mass of the purified biomass.

Characterization of the raw and purified chitin flakes.

Purity. Solid state ^{13}C NMR was used to analyze the purity of the extracted chitinous fibers. Before measurement, fiber samples were hydrated in DI water for 24 h at room temperature and excess water was removed by squeezing the wet samples between tissue paper. Solid state ^{13}C NMR experiments were performed according to Beaumont *et al*.[29] on a Bruker Avance III HD 400 spectrometer (resonance frequency of ^{13}C of 100.61 MHz), equipped with a 4-mm dual broadband CP-MAS probe. The degree of acetylation was calculated by comparing the integrals of **C2** (51-58 ppm region) and **C**H_3 (acetyl) (21.3-23.7 ppm) peaks. The amount of cellulose in the mealworm sample was estimated by relating the integral of the **C2** with the **C1** (96-109 ppm region) peak.

Ash content. A thermogravimetric analyzer (Q500, TA instruments) was used to measure the ash content of the different samples before and after purification. For that purpose, 10 mg of biomass were dried and then carbonized at 600 °C for 15 min within an oxygen-containing atmosphere.

Nanofiber suspension preparation.

The purified chitins were diluted to 0.6% and acidified with acetic acid to reach pH 3. The fibers were pre-treated with an Ultra-Turrax homogenizer (IKA, Germany) for 10 min at room temperature, then fibrillated with six passes in a microfluidizer (M-110P, Microfluidics In., USA) at 1500 bar using sequentially the 400- and 200-µm chambers. Nanochitin suspensions are herein referred to as S-ChNF, F-ChNF, and W-NF for the ChNF suspension coming

respectively from shrimp, fly larvae, and chitinous waste from mealworm farming. Part of W-NF suspension was dialyzed (6-8 kDa membrane) in deionized water to obtain a suspension of neutral pH.

Suspension characterization.

Chemical structure. To analyze the changes in chemical structure of the fibers after purification and fibrillation, Fourier-transform infrared (FTIR) spectra were acquired on a Perkin Elmer spectrometer in ATR mode. Samples were dried at 105 °C before analyses. The resolution was 2 cm^{-1} and the spectra shown are the cumulative data after at least 10 scans.

Surface charge measurement. Zeta potential of the nanofibers suspensions at different pH was measured with a Malvern Zetasizer Nano using a dip cell. The suspensions were diluted to 0.05% and pH was adjusted with NaOH and HCl or buffer solutions, conductivity was corrected with NaCl 1 M to 0.25 mS/cm. At least duplicate samples were analyzed.

Conductometric titrations were done with an automatic titrator (Metrohm). Before titration, nanofiber suspensions were dialyzed as described above to remove acetic acid. Then, 0.1 g of nanofibers were dispersed in 100 mL water, 0.2 mL HCl 0.1 M, and 0.1 mL NaCl 0.5 M were added. The suspension was then titrated against NaOH 0.02 M at 0.1 mL/min and the conductivity was measured under continuous magnetic stirring. The surface charge was calculated from the volume of NaOH added corresponding to the difference between the two inflection points representing the change in conductivity of the solution (V_{eq}). The degree of acetylation (DA) of the suspensions was then calculated using the equation below:

$$DA = 1 - \frac{M_a}{M_a - M_d + \frac{m}{[NaOH] \times V_{eq}}} \quad \text{(II.1)}$$

where *m* represents the mass of nanofibers and M_a and M_d correspond to the molar mass of the acetylated (203 g/mol) and deacetylated (161 g/mol) chitin.

Morphology. The morphology of the nanofibers was analyzed with atomic force microscopy (Bruker MultiMode 8 AFM). For sample preparation, PEI was drop cast on silica substrates, after 1 min contact, the substrate was rinsed and then dipped in diluted nanofiber suspension (0.001 wt%) to deposit nanofibers on the surface. NanoScope Anaylsis software was used to measure the fibers height. At least 50 different nanofibers were measured, and the average was calculated.

UV-Vis transmittance of suspension at pH 3 and 0.1% was measured with a spectrophotometer (Shimadzu UV-2550) to obtain information on the fiber's behavior in suspension. To obtain a ratio of fine fibers, the suspensions were diluted to 0.1% and centrifuged at 3000 rpm (4.2 x g) for 15 min.[30] Then, the supernatant was removed and weighted. The ratio of fines was calculated following the equation below:

$$Fines\ (\%) = \frac{m_{sup}}{m_{tot}} \times 100 \qquad \text{(II.2)}$$

where m_{sup} represents the mass of nanofibers in the supernatant and m_{tot} the total mass of initial nanofibers. The measurement was performed in triplicate.

Film preparation.

Films (30 g/m^2) were produced using a positive pressure filtration unit with 0.45-µm PVDF membranes. To better understand the role of the drying process, some films were hot pressed (HP) at 100 °C and 70 bar for 30 min and others cold-pressed with a 3.4 kg load (0.012 bar) and dried overnight at room temperature. Films were processed at pH 3 and for the W-NF sample, one additional film was made at pH 7 after dialysis of the suspension.

Films containing CNF. To better understand the mechanical behavior of the W-NF films, a film with 50 wt% of S-ChNF and CNF was prepared. For that purpose, the desired mass of nanofibers was weighted and mixed with an Ultra-Turrax homogenizer for 5 min at room temperature followed by over-pressure filtration and cold pressing and drying overnight at room temperature, using the same conditions than those use for the chitin films. A film containing only CNF was also processed.

Film characterization.

Density. The density of the films was measured gravimetrically by weighting the films at 23 °C and 50% relative humidity and measuring their thicknesses and surfaces in the same conditions.

Crystallinity. X-ray diffraction pattern of the chitin films was measured, and their crystallinity indexes were calculated. Rigaku Smart-Lab diffractometer with Cu anode operated at 45 kV and 200 mA was used to measure the X-ray diffraction intensities between 5 and 65° in 2Θ. Films of ChNF were dried at 105 °C overnight before measurement in reflection mode. The crystallinity index was calculated following Càrdenas *et al*.[31] method using the ratio between

the crystalline peak intensity at 19.2° corresponding to the (110) diffraction plan and the amorphous part at 12.6°. The crystalline index was then calculated with the following equation:

$$CI = \frac{(I_{110} - I_{am})}{I_{110}} \times 100 \quad \text{(II.3)}$$

Morphology. Scanning electron microscopy (SEM) images of the cross-sections after mechanical tests were made to observe the homogeneity of the films. Zeiss, Sigma VP SEM was operated at 1.5 kV. A 4-nm-thick Au/Pd layer was sputtered on the sample before analysis. Most representative SEM images were selected for the discussion among at least 10 images in different zones of observation.

Wettability. Contact angle of the films was measured with a Theta Flex optical tensiometer (Biolin Scientific) using 5-µL drops. The recorded contact angles were measured after 120 s of drop contact on different zones. At least triplicate was performed.

Transparency. A UV-Vis spectrophotometer (Shimadzu UV-2550) was utilized to measure the transparency of the films between 200 and 800 nm. The average of triplicate is proposed for discussion.

Mechanical properties. Tensile tests of 50 x 5 mm^2 samples were carried out on an Instron 5944 with a 2-kN load cell at 1 mm/min with an initial gap of 30 mm. Before measurements, specimen thicknesses and width were measured with a micrometer and a caliper, respectively. Every sample was conditioned at 23 °C and 50% relative humidity for at least 24 h before and during the measurements. At least triplicate was performed for each film.

RESULTS AND DISCUSSION

Analysis of the purified materials

We first compared the properties of chitin fibers obtained from the larvae and residual biomass of emerging farming of fly (*Hermetia illucens*) larvae and mealworm (*Tenebrio molitor*) with those of chitin purified from shrimp shell, a conventional commercial source of this polysaccharide. We analyzed the chemical composition and purity of the raw materials using Fourier-Transform Infrared (FTIR) and solid-state ^{13}C Nuclear Magnetic Resonance (NMR) spectroscopies (**Figure II.3**). The results were also used to adapt the conditions of purification applied to each chitinous biomass (fly, mealworm, and shrimp). According to the NMR spectra both fly and shrimp raw chitin samples did not contain significant amount of protein or lipid

while that from the mealworm production contained considerable amounts of lipids and proteins (**Figure II.3b**). This is also visible in the IR spectrum of the mealworm chitin which displayed a significantly lower intensity of the C–O IR band at *ca.* 1000 cm^{-1} (corresponding mostly to polysaccharide moieties, see **Table II.1** for further details) than the other raw materials, whereas the intensity of C=O band at 1450-1700 cm^{-1} was similar (**Figure II.3a**). Moreover, NMR indicated that the mealworm waste sample was a mixture of chitin and cellulose. The cellulose fraction originated from the cereal-based feed of the mealworm (residual husk as feed leftover) which was mixed with the mealworm exuviae. The inorganic residues in the samples were analyzed thermogravimetrically: the ash contents of the as-received materials were 0.3, 4.0, and 4.8 wt%, for S-Ch, F-Ch, and W-Fiber, respectively.

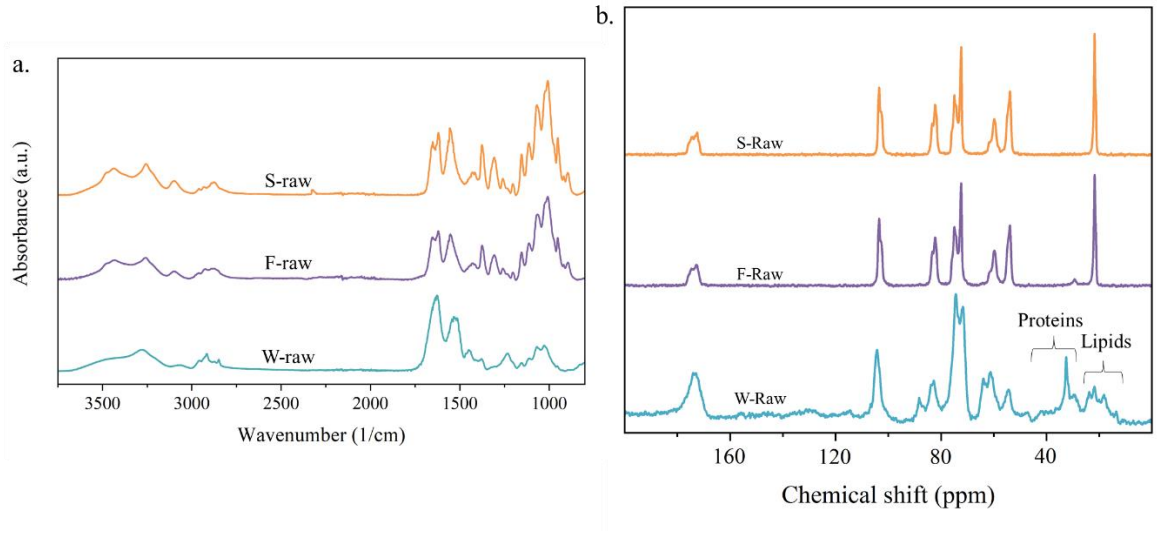

Figure II.3. FTIR spectra (**a.**) and ^{13}C NMR spectra (**b.**) of the raw materials, from top to bottom: shrimp chitin (S-raw), chitin from fly larvae (F-raw), and mealworm waste (W-raw).

The conventional demineralization, deproteinization, and bleaching steps that are usually applied for crustacean shells were carried out using similar concentrations and temperatures, but the time was adapted to each source following the optimization method of Percot *et al.*[28] A mild demineralization step with 0.25 M HCl at room temperature was followed by a treatment with 1M NaOH at 50 °C between 4 and 24 h, depending on the source, and sodium chlorite bleaching cycles (2 h at 80 °C). Although the fly and shrimp raw chitins were of considerable purity, these steps were required to remove remaining inorganic and protein contaminants. The purification yields were 90% for the shrimp and 68% for the fly. For the mealworm sample, we used a different protocol and first extracted the lipid fraction with *n*-hexane. After extraction, we applied the same protocol as for the other chitin samples but added an alkaline

purification step due to the high protein content of the material, applying 1 M NaOH for 1 h at 70 °C between two bleaching cycles. The yield after extraction was 11%.

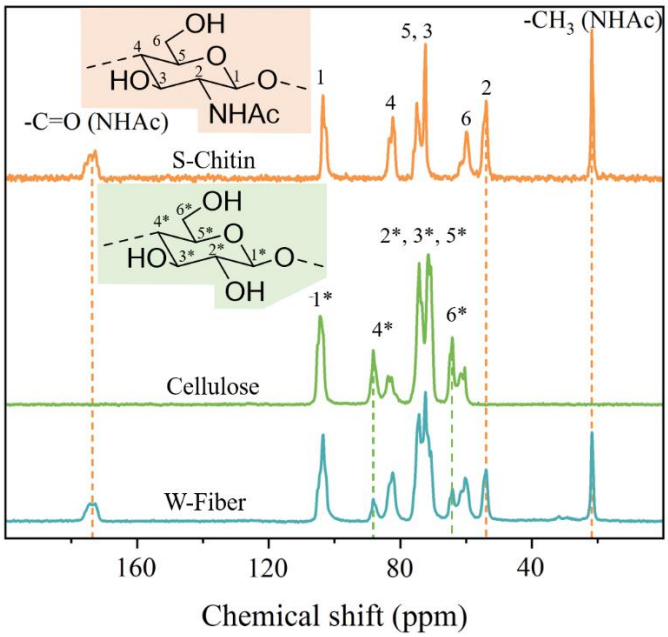

Figure II.4. ^{13}C NMR spectrum of the purified mealworm sample in comparison to respective spectra of cellulose and shrimp chitin.

The solid-state ^{13}C NMR spectra of all chitin samples after purification are shown in **Figure II.5a**. The chitins extracted from shrimp (S-Chitin) and fly (F-Chitin) were almost identical, apart from protein traces in the fly sample (in the range of 30 ppm).[32] Comparable resonances assigned to proteins were also present in the NMR spectra of the mealworm sample (W-Fiber) in which the cellulose fraction was clearly identified (**Figure II.4**). The amount of cellulose in the sample was estimated to approx. 44 wt% (50 mol%) by comparing the peak intensity of the C2 of the chitin fraction at around 55 ppm to the combined C1 peak intensity of chitin and cellulose at about 102 ppm.

The ash contents after purification of the three materials were 0.1%, 1.4%, and 1.2% for S-Ch, F-Ch, and W-Fiber, respectively. Although the initial ash content in every sample was already low (0.3, 4.0, and 4.8 wt%, respectively), it further decreased through removal of inorganic residues.

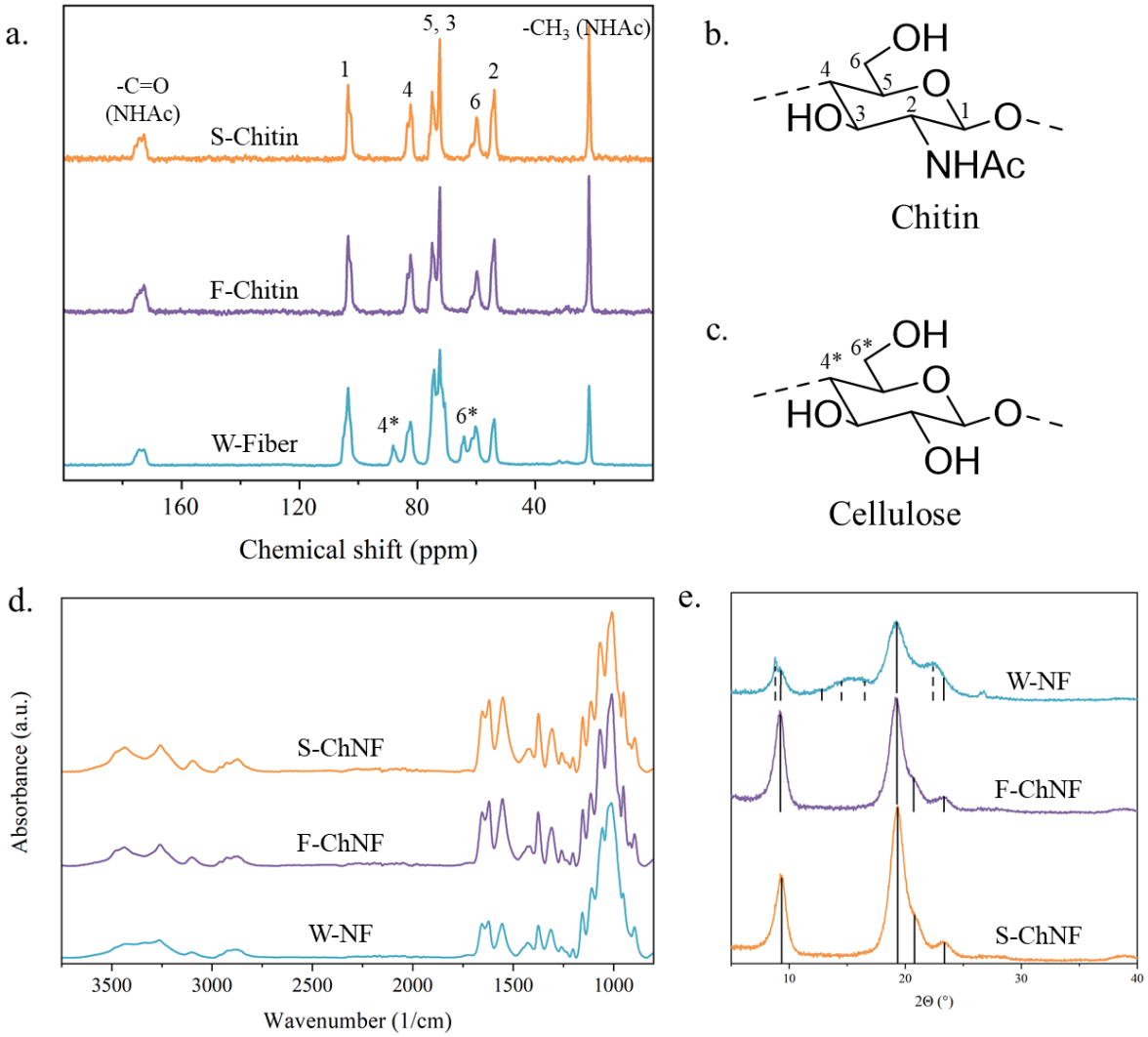

Figure II.5. ^{13}C NMR spectra of the purified fibers from shrimp (S-Chitin), fly (F-Chitin), and mealworm (W-Fiber) (**a**), the latter encompassing cellulose (**c**) in addition to chitin (**b**, respective carbons are numbered and assigned to the NMR spectra). FTIR (**d**) and XRD (**e**) spectra of the dried nanofibers (S-ChNF, F-ChNF, and W-NF). Solid lines in the diffractograms indicate chitin and dashed lines cellulose peaks.

Structural analysis of the chitin nanofibers.

After purification, the chitins were processed into nanofibers by fibrillation under mild acidic conditions. The suspensions were passed six times through a microfluidizer at 1500 bar without any chemical pretreatment. After defibrillation, white gel-like nanofiber suspensions were obtained from S-Chitin (S-ChNF), F-Chitin (F-ChNF), and W-Fiber (W-NF).

FTIR of the fibrillated nanofibers allowed tracking possible chemical changes arising from the purification and processing steps (see **Table II.1** for peak assignment). **Figure II.5d** shows that the three materials have the fingerprint regions of glucopyranoxylamine (and

glucopyranose in case of W-NF) rings in the 1000-1155 cm^{-1} region related to C–O and C–O–C bonds.[31] The amide I and II bands of chitin (1555, 1620, and 1660 cm^{-1}) were also present in all of the three different materials, although having lower intensity in W-NF due to the presence of cellulose. The peaks at 1630 and 1530 cm^{-1}, related to amide bonds in proteins,[23] were predominant in the raw mealworm samples, but were remarkably less intense in W-NF, indicating efficient deproteinization (see **Figure II.3a**).

Table II.1. Assignation table of IR peaks of chitin nanofibers

Peak	Group	Molecule
950	CH_3	Chitin
1010-1110	C-O	Chitin/Cellulose
1155	C-O-C (ring)	Chitin/ Cellulose
1420, 1540		Proteins
1555	Amide II	Chitin
1620	Amide I	Chitin
1660	Amide I	Chitin
2880	CH_3	Chitin
3260	N-H	Chitin
3435	O-H	Chitin/cellulose

Figure II.5e displays the XRD spectra of the three different nanofibers. The typical pattern of α-chitin was present in all samples, with a peak of maximum intensity at 19.2° and a second peak at 9.2°, which is in accordance with results reported for insect chitin.[33] The crystallinity was found to be 94% and 93% for S-ChNF and F-ChNF, respectively. Peaks from both cellulose and chitin were visible in the XRD profile of W-NF. The peaks at 14.5°, 16.5°, and 22.5° corresponded to the cellulose Iα planes (100), (010), and (110), respectively,[34] and those at 9.3°, 12.8°, 19.3°, 20.9°, and 23.4° to the α-chitin planes (020), (101), (110), (120), and (130), respectively.[35] Due to the mix of cellulose and chitin and the fact that peaks were overlapping, it was not possible to calculate the crystallinity index of W-NF.

The surface chemistry of the nanofibers with regard to charged groups was assessed by zeta potential measurements at different pH. S-ChNF and F-ChNF are negatively charged at basic pH and positively charged at acidic pH, with an isoelectric point of approx. 6 (see **Table II.2** and **Figure II.6**). The negative zeta-potential of F-ChNF at pH 7 could be explained by the

higher fibrillation degree of the F-ChNF and the high variation of zeta-potential around the iso-electric points. The presence of acetamide groups on the surface of the nanofibers, and in particular amino groups by deacetylation, leads to positively charged nanofibers in acidic media. The positive charge and the presence of amine are advantages of ChNF over their cellulosic counterparts, as this opens many opportunities regarding functionalization or interaction with molecules containing carboxylic acids or other anionic moieties.[36] Further deacetylation, which is usually done prior to defibrillation, allows tuning the amine content on the surface of ChNFs.[37] Although W-NF was a mix of chitin and cellulose, it displayed a negatively charged surface. The cellulosic contribution was predominant in the blend, leading to a net negative zeta potential throughout the studied pH range. Cellulose fibers are naturally negatively charged at a wide pH range because of the presence of residual hemicelluloses.[38] Classically, the zeta potential of cellulose fibers ranges from -20 to -50 mV depending on the source; hence the value of -7.2 mV confirms a mix of positive and negative charges from chitin and cellulose, respectively.

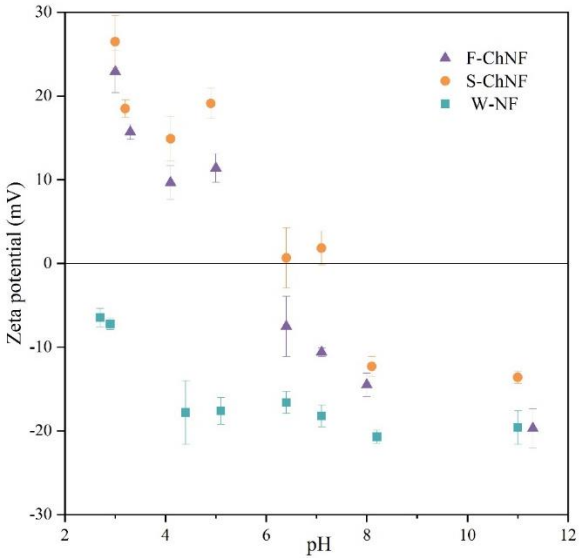

Figure II.6. Zeta potential as function of pH for the different nanoparticle suspensions.

To further study the surface charge of the nanofibers, conductometric titration was performed and the degree of acetylation was determined. The surface charge densities of S-ChNF, F-ChNF, and W-NF were 215 ± 13, 209 ± 5 and 293 ± 18 µmol/g, respectively. Associated degrees of *N*-acetylation (DA) were 96%, 95%, and *ca.* 90% for S-ChNF, F-ChNF, and W-NF, respectively. The DA of W-NF was estimated for its chitin fraction. From the calculated DA (conductometric titration), displayed in **Table II.2**, we conclude a relatively low content of primary amine groups in the nanofibers, probably due to the mild purification steps. This is in

accordance with Ifuku *et al*., who measured a DA of 95% for non-deacetylated ChNFs from crab[39] and Huet *et al*., who calculated a DA of 93% for chitin from insects.[23] The approximated DA of W-NF was slightly lower, which might be reasoned by the additional and more severe caustic treatment.

Table II.2. Zeta potential at different pH and charge content measured by conductometric titration and associated degree of *N*-acetylation. *Degree of *N*-acetylation of W-NF was estimated for its chitin fraction.

	Zeta potential pH 3	Zeta potential pH 7	Charge density	Degree of *N*-acetylation
	mV	mV	µmol/g	-
S-ChNF	27 ± 3	2 ± 2	215 ± 13	95.7 ± 0.3%
F-ChNF	23 ± 3	-11 ± 1	209 ± 5	95.1 ± 0.1%
W-NF	-7 ± 1	-18 ± 1	293 ± 18	≈ 90%*

The morphology of the chitinous nanofibers was investigated by AFM **(Figure II.7a-c)**, from which the height distribution (**Figure II.7d-f**) was obtained. Overall, well separated nanofibers, with average height between 4 and 35 nm were obtained, regardless of the chitin source. Additionally, the transmittance of the aqueous suspensions of nanofibers was measured at pH 3 and 0.1 wt% concentration to gain further insights into their colloidal behavior, in terms of aggregation and stability (**Table II.3**). A remarkable difference in transmittance was observed between S-ChNF (15.2 ± 0.6%) and F-ChNF (28.7 ± 0.8%), indicating that the nanofibers from fly larvae were fibrillated to a greater extent, even though they showed seemingly similar morphologies in the AFM images (**Figure II.7)**. To confirm such difference, the ratio between fine and coarse fractions in the suspensions was measured gravimetrically (**Table II.3**). A higher amount of fine fraction, meaning smaller nanofibers that remain in suspension under centrifugal forces, was measured for F-ChNF (35 ± 2%) compared to S-ChNF (24 ± 10%). Chitins from insects have been reported to be more accessible than those from crustacean,[22,40] which could have facilitated the fibrillation, explaining the difference.

To increase the density of repulsive charges, ChNF suspensions are usually processed at pH 3 to protonate the primary amino groups and kinetically stabilize the suspensions. Due to the mix

of cellulose and chitin nanofibers in W-NF, the stability of this suspension might differ with pH, as shown by the zeta potential. To investigate the pH-dependency in the aggregation phenomena of the W-NF suspension, we measured the transmittance at pH 3 and 7. The transmittance at pH 3 (18.2 ± 0.5%) was slightly lower than at pH 7 (20.9 ± 0.5%), which indicates no remarkable aggregation of the nanofibers at pH 3.

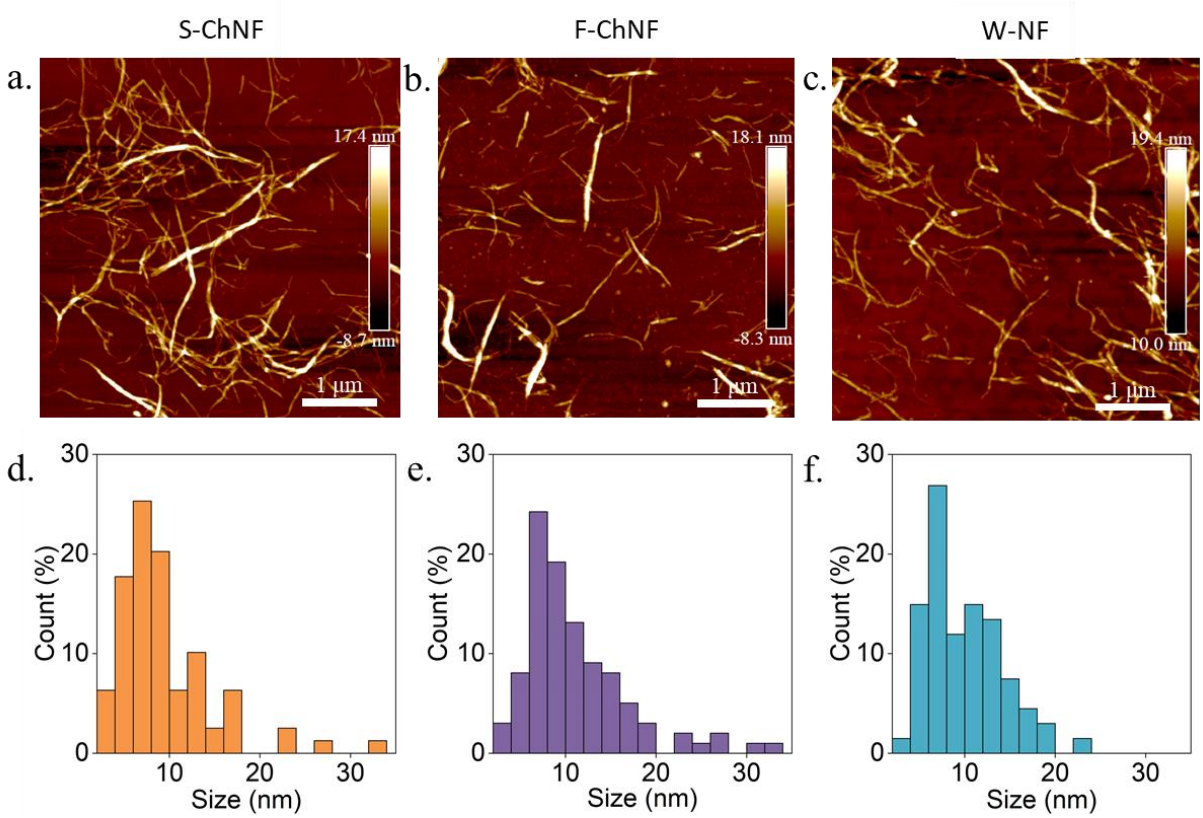

Figure II.7. AFM images of S-ChNF (**a**), F-ChNF (**b**), and W-NF (**c**) and the corresponding height distributions (**d**, **e**, and **f** respectively) (see also **Table II.3**).

Table II.3. Height average of the nanofibers from the AFM images and transmittance of the suspensions at 0.1% and pH 3.

	Height average	Transmittance at 550 nm	Fine fraction
	nm	%	%
S-ChNF	9 ± 6	15.2 ± 0.6	17 ± 1
F-ChNF	11 ± 6	28.7 ± 0.8	27 ± 1
W-NF	10 ± 4	18.2 ± 0.5	1 ± 2

In summary, ChNFs were successfully prepared from all three sources, fly larvae, mealworm waste, and commercial shrimp shell chitin, having only small traces of proteins as noted by NMR spectra. The purification and fibrillation processes did not affect the chitin structure, resulting in highly *N*-acetylated ChNFs. The ChNF extracted from fly and shrimp were structurally similar, with no significant differences in terms of crystallinity, degree of *N*-acetylation, and charge density. One major difference was the presence of non-fully fibrillated species in S-ChNF, as shown by the low transmittance of the suspension and the fine-to-coarse ratio. Additional energy would be required to obtain a more homogeneous and finer S-ChNF.

W-NF consisted of 56 wt% chitin and 44 wt% cellulose, which is a result of the source biomass, a non-purified waste. Both polysaccharides were purified using the same purification steps leading to blended nanofibers. The negative surface charge of the cellulose fibers dominated the colloidal properties and resulted in negatively charged particles in suspension throughout a wide pH range. We could not identify the real state of the cellulosic colloids in the W-NF systems; however, it is likely that they were in the form of nanofibers given the AFM observation. The colloidal behavior at different pHs indicates that the surface of the nanofibers was dominated by cellulose, and that reactive amine groups do not contribute significantly. An advantage for future applications of the mealworm exuviae mixed waste is that both cellulose and chitin could be utilized as reactive moieties.

Analysis of the films' properties depending on the ChNF source and drying process.

Films were formed by overpressure filtration of ChNF suspensions followed by drying under two different conditions. One group of films was hot-pressed (HP) at 70 bar and 100 °C for 30

min and another was cold-pressed (CP), *i.e.*, dried overnight at room temperature under a much smaller pressure (0.012 bar). The density of the obtained films was similar and ranged from 1.2 to 1 g/cm^3, with that of cold-pressed ones being slightly higher (below 10% increase) than their hot-pressed counterparts. The transparency of the films depended both on the source and the processing conditions (**Figure II.8a**). The transmittance at 550 nm for films obtained by cold (CP) and hot pressing (HP) ranged from 7.2 ± 0.5% to 0.8 ± 0.06% for S-ChNF and from 21 ± 2% to 1.8 ± 0.2% for F-ChNF, respectively (see **Figure II.8b**). The opacity of the films was likely a result from the high structural porosity.[41] When the films were hot pressed, the speed of drying and water evaporation was considerably higher compared to that from overnight cold drying. Thus, the nanofibers in hot pressing had little time to rearrange and entangle, leaving a porous or defective structure in the packed lamellas. The F-ChNF CP film had higher transparency than the S-ChNF CP film, which was expected due to the higher homogeneity of F-ChNF and the smaller concentration of fiber aggregates in the suspension.

Water contact angles were measured for each film to gain insights into the surface energy of the different chitins. The films were highly hydrophilic, with contact angles ranging from 29 ± 0.3° to 40 ± 2° for S-ChNF HP and F-ChNF CP films, respectively. However, differences were noticed between the film-forming procedures: HP films trended towards lower contact angles due to their smoother surfaces in comparison with the CP counterparts. W-NF had a slightly higher contact angle compared to their shrimp and fly counterparts (**Figure II.8c**). This is due to the presence of constituents of opposite surface charge (chitin and cellulose), leading to partial charge neutralization and fewer groups to possibly interact with water.[42] Consolidation of the W-NF suspension at different pH did not alter the water contact angle, and neither the transmittance of the resulting films (**Figure II.8**).

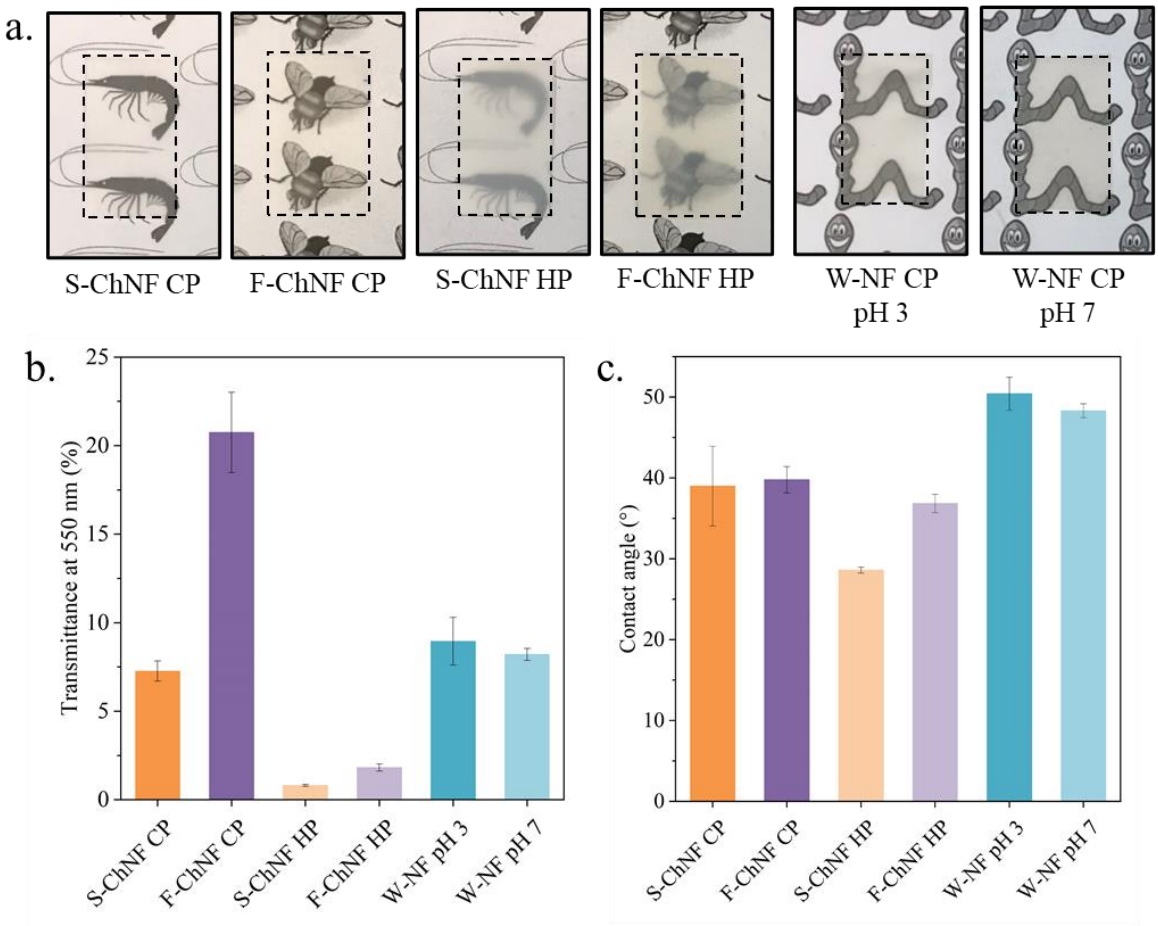

Figure II.8. Images of the different films processed with cold (CP) or hot pressing (HP) at pH 3 or 7 for W-NF (**a**). Transmittances of the films measured by UV-Vis spectrophotometry (**b**) and contact angles measured 2 min after drop deposition (**c**).

All the films were subjected to tensile tests to evaluate their mechanical performances (**Figure II.10**). Following the previous results, the strength of the chitinous nanofibrillar networks was influenced mostly by the assembling conditions (CP or HP) rather than by the nature of the chitin precursor. The HP process induced an increase in Young's modulus from 5.2 ± 0.7 GPa to 8.0 ± 0.2 GPa for S-ChNF and from 4.8 ± 0.4 GPa to 7.2 ± 0.3 GPa for F-ChNF. However, the maximum tensile strain and hence the toughness were greatly reduced by the hot-pressing process, going from 5.5 ± 0.7% to 1.9 ± 0.2% for S-ChNF and from 5.0 ± 0.6% to 1.4 ± 0.1% for F-ChNF. The decrease in toughness could be explained by the reduced amount of water present in the films after the hot pressing. Indeed, water is known for its plasticizing role in cellulosic films. Sharma *et al*. showed that treatment of films at 100 °C or higher decreased the water retention of the film.[43] SEM images of the cross-sections of the films obtained after the

tensile tests showed a paper-like structure, with fibers aligned in the plane and without visible aggregation of nanofibers (see **Figure II.9** and **Figure II.10b-c**).

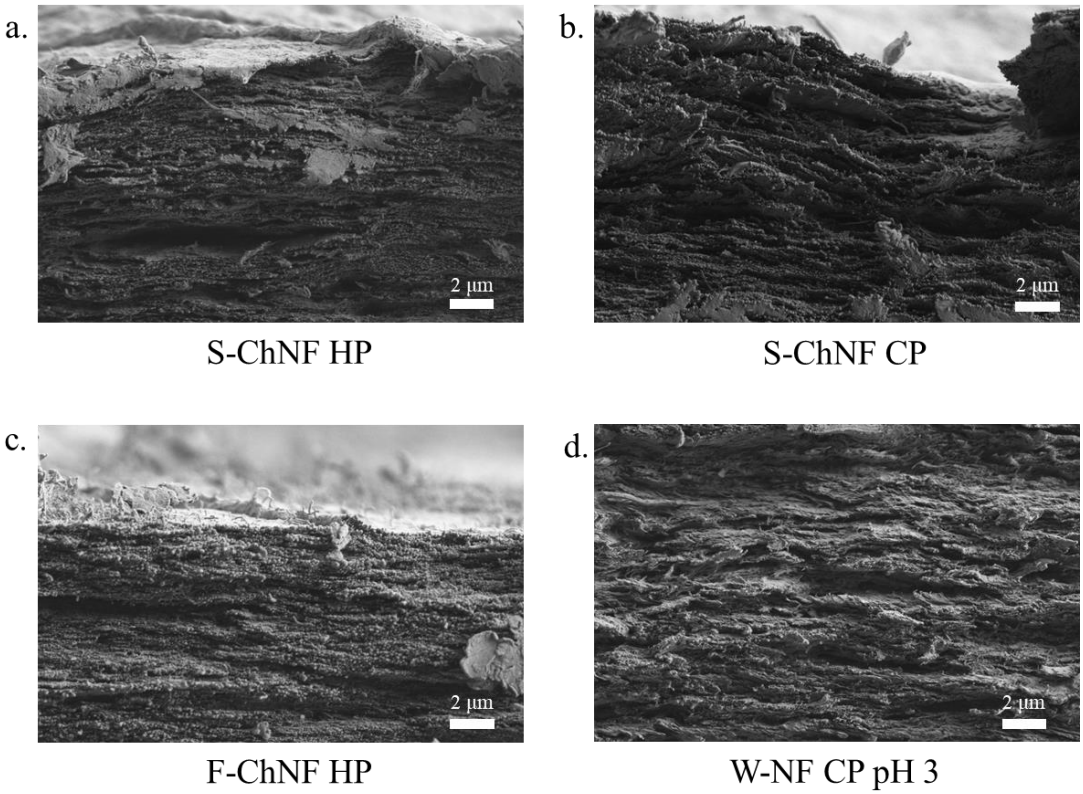

Figure II.9. Cross-section images of **a.** S-ChNF HP, **b.** S-ChNF CP, **c.** F-ChNF HP, and **d.** W-NF CP pH 3 films.

W-NF, with its composite nature, was processed at pH 3 and 7, but only under cold-pressing conditions. As noted, CP offered products with superior mechanical properties compared to the films assembled from F-ChNF and S-ChNF. Two pH values were used to determine the effect of the amine protonation on the film properties. Even with a slightly higher toughness, given the higher elongation, the mechanical properties of the W-NF films were independent of the pH prevalent during film formation, as concluded from the variance of the results. In addition, the SEM image of the cross-section of the films did not show any clear difference with regard to porosity or nanofiber aggregation (**Figure II.9d** and **II.10c**). Moreover, films from W-NF showed an elongation and toughness twice those observed for S-ChNF and F-ChNF. To better understand the mechanical properties of W-NF films, we produced a reference film containing 50 wt% of cellulose nanofibers (CNF) and 50% of ChNF and compared its mechanical properties to films of neat ChNF and CNF (see **Figure II.11**). The CNF film showed higher toughness, Young's modulus, and tensile strength than the ChNF film. The film with 50:50 ChNF:CNF displayed intermediate properties, between those of CNF and ChNF. Therefore,

one can speculate that the cellulose component in W-NF was not in the same state as traditional CNF, but possibly smaller or highly infused or entangled nanofibers. While the films from the ChNF:CNF mixture nearly followed the rule of mixtures, our W-NF displayed reinforcing synergies between the chitin and cellulose components, given the better mechanical performance compared to the other chitin nanofibers.

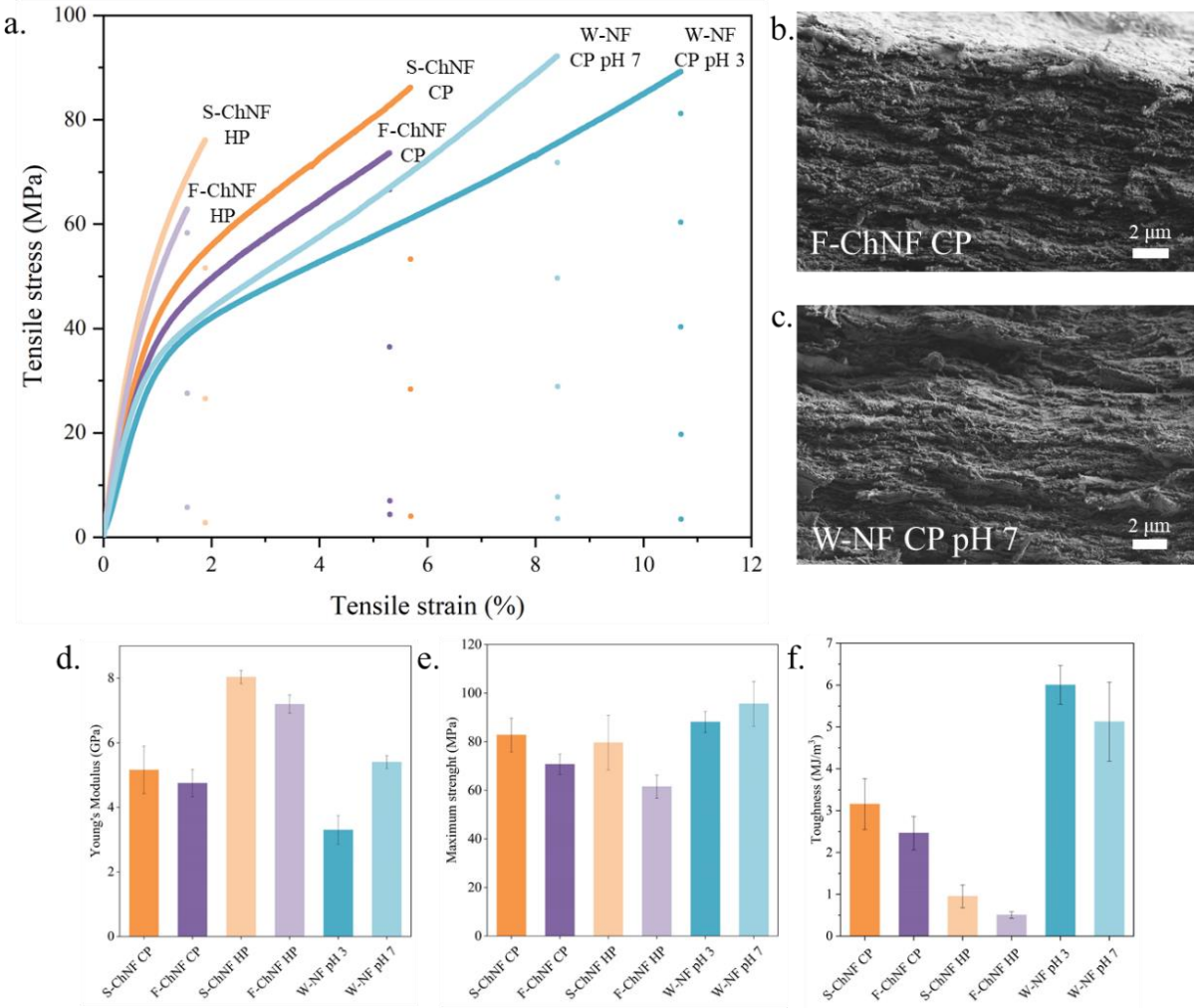

Figure II.10. Tensile stress *vs*. strain profiles of the different films (**a**). Cross-section images of F-ChNF CP (**b**) and W-NF pH 7 (**c**). Young's Modulus (**d**), maximum strength (**e**) and toughness of the films (**f**).

The association of ChNF with other polymers, either towards new functionalities or enhanced properties of the films, has been considered. For instance, Zhang *et al*. showed that contact between cationic chitin nanocrystals and anionic TEMPO-oxidized CNF led to interfacial complexation, allowing dry-spinning of microfibers.[44] The same phenomenon was observed by Grande *et al*. with deacetylated ChNF and anionic seaweed alginate, filaments with wet

strength close to 50 MPa were obtained although the components were both hydrophilic.[45] Kim *et al*. achieved lower oxygen transmission rates using layer-by-layer (LbL) deposition on PET of CNF and chitin nanocrystals compared to the individual biopolymers. The nanoscale blending by LbL assembly led to synergies between the two polymers.[46] Therefore, our substrates present an alternative to explore a synergism between the nanofibrillar matrices, e.g., by taking advantage of W-NF, which contains both chitin and cellulose. Co-grinding biopolymers with nanofibers has been shown to lead to high-performance nanofibers, where the biopolymers are fully infused in the nanofibrillar matrix.[47] Moreover, it seems that the advantages arising from co-grinding techniques may also hold true for insoluble biocolloids, as it was the case of the resulting suspensions obtained by co-homogenization from the mealworm waste.

In summary, ChNF from insects showed similar properties than those obtained from shrimp, with additional features depending on the nature of the starting precursor. The method of film assembly was most relevant as far as the mechanical properties of the obtained films. Hence, the process needs to be chosen depending on the desired application.

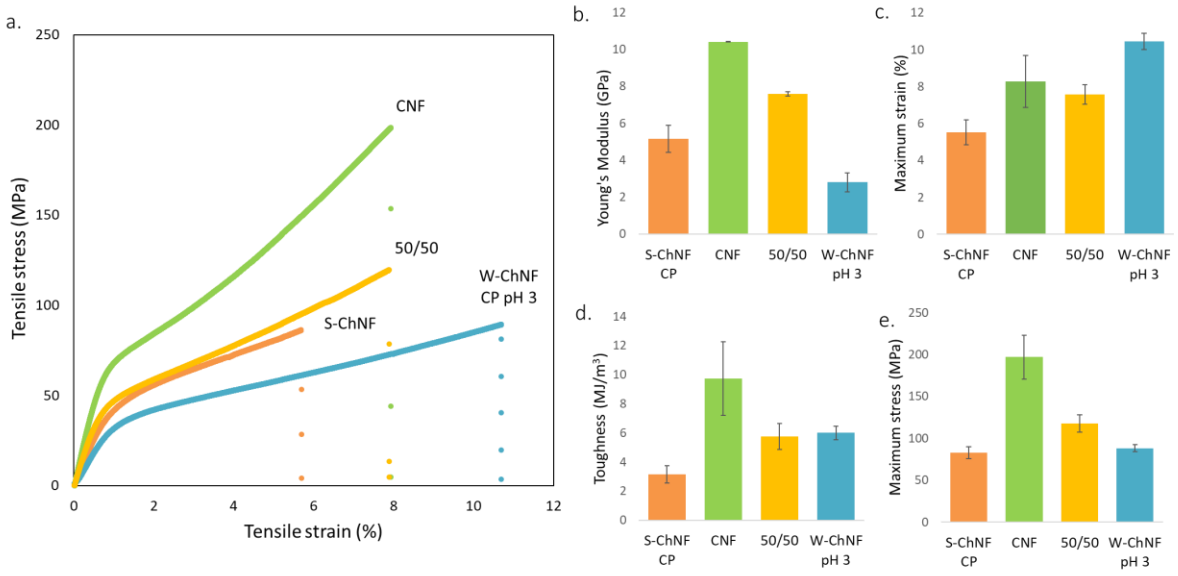

Figure II.11. a. Tensile stress *versus* strain profiles of CNF film, mix of 50% S-ChNF and 50% CNF film, S-ChNF CP and W-NF pH 3 associated with their **b.** Young's modulus, **c.** maximum strain, **d.** toughness, and **e.** maximum stress.

Overall sustainability, insights on potential applications, and prospects for insect based ChNF.

ChNFs present several application prospects, both as suspensions and films. For instance, ChNFs can kinetically stabilize oil-in-water Pickering emulsions at concentrations as low as 0.1 wt%, making them good candidates to replace petrochemical surfactants.[17,48] Mixtures of cellulose and chitin at different ratios have also been studied for Pickering stabilization and resulted in super-stable emulsions.[49] ChNFs have also demonstrate their ability for high-barrier films or coatings.[50] Another way to valorize chitin from residual biomass is by complete or partial deacetylation into chitosan, which is soluble in water at mildly acidic pH and boasts applications in food packaging,[51] biomedical materials,[52] food additives *etc*.[16,53]

Also, some environmental aspects of using waste to produce ChNFs should be put forward here. This study shows that ChNFs from *Hermetia illucens* larvae have similar properties than ChNFs from shrimp shells. ChNF isolation from fishery waste is by common sense already sustainable, and we herein enable the isolation of this biocolloid from insects *via* an equally green (if not greener) procedure and propose its use in materials with superior performance. It is not among our goals, though, to indicate quantitatively which route is more sustainable, but to provide insights on their overall sustainability relying on qualitative indicators of environmental footprint (**Figure II.12**).

The starting biomasses can be compared in terms of availability, including geographical restrictions, seasonality, and lifecycle duration. Overall, insects reproduce at high rates and boast short maturation periods,[2] producing leftover streams that are abundant in chitin. Each mealworm female, for instance, reaches adulthood in 10 weeks and generates nearly 160 eggs throughout the 3-month lifespan.[5] In the case of BSF larvae, the transition to adulthood gives rise to chitin-rich larval exoskeletons (ecdysis) and pupal exuviae (skin renewal),[12] also at a high rate.[5] For shrimp, this cycle of course depends on species among other variables, but typically lasts for 7-8 months before harvesting, and 9-14 months until broodstock. Although important, the chitin yield is rather difficult to compare among the different sources as it varies with species, parts used for isolation, and the isolation protocol itself. Because of their short lifecycle and the growing insect economy, insect biomass appears more available.

Also relevant from the environmental angle is the biomass recalcitrance, which will affect not only extraction time, but also energy input, consumption of chemicals, and inevitably, costs. Even if using an abundant, inexpensive waste, fractionation of crustacean shells is wasteful,

expensive, and involves highly corrosive sodium hydroxide (for protein removal) and hydrochloric acid (for decomposition of calcium carbonate).[54] Insects comprise lower loads of minerals compared to crustacean shells (<6% *vs* 30-50%).[23] Yet, insect chitin may also be recalcitrant to some extent owing to sclerotization, *i.e.*, when proteins are covalently crosslinked to catecholic compounds and chitin.[12] This is true for pupal exuviae, but not for larval exoskeletons, making chitin isolation from the latter preferable.

Lower recalcitrance means not only less energy input, but also less use of harsh chemicals, including HCl, which has a negative impact on acidification of complex environments,[55] leaving behind a solid chemical footprint. The isolation of 1 kg chitin from shrimp shells requires *ca.* 2.5 kg of HCl and 1.3 kg of NaOH, plus 167 L of water.[55] HCl has been traditionally the acid of choice for the demineralization of crustacean shell-derived chitin, but milder, less corrosive acids (*e.g.*, formic acid) have been used for less recalcitrant larval exoskeletons.[12] Such a replacement is also relevant from the technical angle, as strong acid treatment is responsible for chitin depolymerization, hence milder acidic treatments from insect purification can lead to better preserved chitin fibers. Recovery and recyclability of the acid can also be developed as it is classically the case in industry. Moreover, new extraction processes with ionic liquid are emerging,[56] which are considered green solvents. It was demonstrated that chitin extracted with ionic had high molecular weight and high purity.

Importantly, the acid demineralization of the calcium carbonate-rich shrimp shells releases *ca.* 0.7 kg CO_2/kg chitin, this CO_2 being considered as of fossil origin.[55] Not only fractionation operations, but also logistics involved in the supply chain ought to be considered when assessing emissions. If CO_2 emission is to be avoided in the case of crabs and shrimps, the prevalent commercial sources of chitin, availability is concentrated in coastal regions as most species are marine.[12] Only shell transportation and bulldozer operations have been shown to consume 20+ L diesel per ton of chitin,[55] although the emissions of greenhouse gases (GHG) in fisheries are dominated by feed production.[57] Insect farming, on the other hand, is globally suitable and has the great advantage of no geographical restrictions.[11] Additionally, the technological features of highly deacetylated chitin derived from insect depend neither on the geographical location nor on the organic substrate, as showcased for food waste-fed insects.[11] Indeed, organic (*e.g.*, agricultural and urban) waste is abundantly available all year-round, denoting another plus of insects over crustaceans as the chitin source. The global warming potential – typically expressed in CO_2-equivalents, considering CO_2, CH_4, and N_2O emissions, which is already low for mealworms (2.7 kg of CO_2-eq/kg edible protein) compared to other

animals – may be further decreased in a straightforward fashion by using local leftover stream, as this indicator is dominated by production and transportation of feeding (*ca.* 56%) followed by gas and electricity for heating the rearing environment (*ca.* 43%).[5] When optimized, insects farms can become even carbon neutral or negative; their handprint could therefore be calculated to measure the positive impact of their production on the environment.[58]

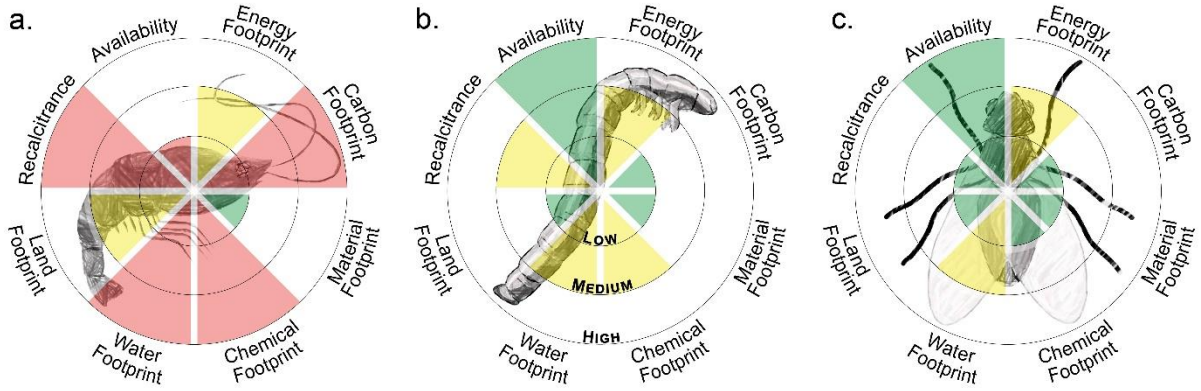

Figure II.12. Overall qualitative evaluation of shrimp **(a)**, pupal exuviae **(b)**, and larval exoskeleton **(c)** sustainability as sources of nanochitin. *Availability* considers geographical restrictions, seasonality, and lifecycle duration for biomass generation. *Energy footprint* relates to any energy input in the production chain, renewable energy contributing less to the ultimate footprint than its fossil analogue. *Carbon footprint* encompasses emissions of greenhouse gases, including carbon dioxide, methane, nitrous oxide, and ozone. *Material footprint* accounts for the depletion of natural resources for use in biomass generation and fractionation, while *chemical and water footprints* relate to emissions of chemicals and use of freshwater in these processes, respectively. Finally, *land footprint* translates the use of land to isolate nanochitin, including that for feed cultivation, to absorb the waste generated in the processes, and the land use change induced by a change in current practices. The levels (low, green; medium, yellow; high, red) were attributed in relative terms to illustrate qualitatively the comparison between the three scenarios, relying on our data and literature reports. Note that they are not meant to be compared with other procedures and goods (the carbon footprint of nanochitin isolation from shrimp is the highest among the three resources, but is significantly lower than that of livestock, as an example). Several of these indicators are intricately connected with biomass recalcitrance.

While mealworms do not produce enteric CH_4,[59] *H. illucens* outstands owing to the ability of its larvae to digest organic matter. The biodigesting approach further fits the insect biorefinery into the circular bioeconomy by opening up the possibility of feeding larvae with nutritious agri-food side streams (*e.g.*, brewery spent grains and okara),[11] which may denote not only a major environmental issue but also an opportunity to upcycle food waste into economically

valuable biomass,[60] including nanochitin. This also applies to municipal waste that, when decomposed by *H. illucens* larvae, will generate less malodors, potential diseases, and methane emission. Notably, between egg hatching and the prepupal stage (two weeks), *H. illucens* converts *ca.* 20 times their own weight of waste.[61] While most of worldwide commercialization of chitin derives from crustacean shells as by-product of the fishery industry, chitin isolation from organic leftover stream-fed insects can be consider a by-product of the by-product, rendering a milder material footprint owing to the diminished extraction of raw materials from nature.

Whereas biogenic CO_2 emissions arising from degrading organic matter do not contribute to a net increase in atmospheric CO_2, as biogenic carbon is scavenged and released rapidly, biogenic CO_2 emissions resulting from land use change denotes a net addition to atmospheric CO_2.[55] The latter includes clearing of land for crop production. As mentioned above, mealworms can be fed organic waste, eliminating the need for feeding with crops. Although the land use for shrimp farming is virtually null when farming is extensive, there is an induced land use change (iLUC) associated with diverting its shells from their traditional use as animal feed. This iLUC, in turn, augments the need to deforest land for crop cultivation (further emitting CO_2) and/or to increase the yield in cultivated land using nitrogen fertilizers (boosting acidification).[55] When shrimp farming is intensive, additional land use due to earthen ponds and feed production should be considered.[57,62] The already low land footprint of insect farming can be further reduced by vertical farming.

This study has also demonstrated that a direct valorization of untreated waste from the mealworm industry, comprising chitin-rich exuviae and cellulose-rich rearing substrate, is viable and can lead to strong biobased films.

In a more sustainable perspective, partial purification of chitin could also be achieved giving rise to both energy and chemicals saving compared to complete purification as well as new properties due to the presence of impurities. For example, Nawawi *et al.*[26] extracted ChNF from mushroom with only partial removal of glucans to maintain the chitin-glucan complexes naturally present in mushrooms. Films with tensile strengths up to 200 MPa were produced and two times higher Young's moduli than for ChNF from crab were reported. Following the same idea, Ifuku *et al.* did not deproteinate chitin fibers from crab to yield protein-rich ChNF, which displayed similar reinforcing properties than neat, highly purified ChNF.[63] Finally, one must

consider the need for highly purified systems, as non-purified fibers have been performing similar, if not better, given natural synergies present on the precursors.

CONCLUSION

In this study, we prepared nanofibers from chitin-rich biomass. Chitin from fly larvae and an industrial mealworm waste stream were compared to that from commercially available chitin (from shrimp shells). Fly-derived chitin nanofibers (F-ChNF) showed similar properties compared to shrimp chitin nanofibers (S-ChNF), for example, in terms of crystallinity, degree of acetylation and film mechanical properties. Moreover, F-ChNF featured superior fibrillation behavior which resulted in suspensions with higher transmittance and produced films with higher transparency. In contrast, the nanofibers prepared from the mealworm waste (W-NF) differed considerably from the other samples, due to the presence of cellulose from feeding residues, which was incorporated in the form of composite nanofibers. The surface charge of the colloidal suspension was dominated by the cellulose component, explaining a colloidal stability over a large pH range. Films from W-NF were less brittle than the other ChNF films and had a higher toughness (double the value) than those from the F- and S-ChNF samples.

Taking all together, ChNF from fly larvae shows high promise as alternative to commercial chitin, but the valorization of mealworm waste as W-NF is expected to further open a new field of applications given the synergistic effects between the two components, chitin and cellulose. Our results demonstrate that side streams from the emerging insect industry can be valuable sources for future materials.

Chapter II.2 Preparation of lignin microparticles and their incorporation in CNF films

INTRODUCTION

Lignin is a natural polyphenolic polymer present in the cell wall of wood and various lignocellulosic biomass.[64] Lignin has long been considered as by-product from the pulp and paper industry and is still often burnt for energy recovery.[65] Lignin is a chemically complex molecule that contains several interesting functional groups (phenol, carbonyl, stilbene, methoxy),[66] and it could be valorized as functional polymer or deconstructed into high-value molecules.[65] Its renewability as well as biodegradability makes it a good candidate as an active molecule for materials applications. However, lignin is typically found in the form of irregular powder and cannot form self-standing materials by itself, thus needing a supporting matrix to function to its full potential.

Cellulose shares the same properties in terms of renewability and biodegradability, and it is an ideal matrix for lignin because they naturally coexist in wood cell wall. Cellulose nanofibers (CNF) and more specifically TEMPO oxidized CNF (tCNF) have been demonstrated to form packed transparent films with high performance for several applications ranging from packaging to electronic.[67–69] CNF are made by mechanical fibrillation of cellulose fibers (e.g. pulp), and recent advances in their productions favored their increasing industrialization during the last decade.[70] Pre-treatment such as TEMPO oxidation add charges on the fibers surface and results in reduction of energy consumption necessary for the fibrillation.[71] The nanofibers obtained are well individualized with diameters around 5 nm and approximately 1 µm in length, and present a high surface charge up to 2 mmol/g.[72] When dried into films, tCNF form strong network with high mechanical properties due to the formation of multiple hydrogen bonds inter and intra fibrils.[73]

Addition of functionalities to such tCNF films is needed to compete with existing materials. The presence of active molecules like lignin could provide better stability towards relative humidity but also antioxidant properties and shielding against UV light.[74,75] These properties, when combined with the high oxygen barrier of CNF, make lignin-containing CNF films promising for food packaging applications.[76] There are different ways to integrate lignin into CNF matrices.[77] For instance, partial bleaching of cellulose before fibrillation leads to lignin-containing cellulose nanofibers (LCNF) where lignin is present in its natural form and covalently linked to cellulose. A second method is to mix lignin powder that has been extracted

beforehand and CNF, this opens possibilities of new electrostatic interactions and hydrogen bonds linkages. Using extracted lignin allows tuning of the lignin surface chemistry, which depends on the method used for extraction.[78] However, to be integrated homogeneously in a matrix, lignin powder need to be solubilized in organic solvent. To address this problem and improve the integration of lignin in matrices, the preparation of lignin particles has been recently reported.[79–81] When shaped into particles, the size, colloidal stability, and surface chemistry of lignin can be controlled to improve their interactions with the supporting matrix. As recently reviewed, lignin particles can be shaped into spherical colloids that are stable in water,[82] which allow mixing with CNF suspension without addition of any organic solvent. Such solvent could indeed disrupt the hydrogen bonding among nanofibers and therefore the film cohesion. Different methods have been used to prepare lignin particles, which can be divided between dry and wet process conditions.[83] One of the advantage of producing LP in dry conditions is to save storage space and transport energy, as well as to facilitate LP incorporation in hydrophobic matrices. There is also no need for washing or purification which limits the use of high volume of water associated with these steps. Among the dry methods used to produce LP, the aerosol reactor is to our knowledge the most promising one, as dry lignin particles can be obtained in one-step process.[84] The process was demonstrated to have high yield (> 60%) and can be scalable.[85] Moreover, such dry lignin particles can be dispersible in water under high shear forces.

Only few papers reported the addition of LP to CNF for film preparation and only with LP present in wet state.[86–88] It was shown that the addition of LP to tCNF suspension improved the colloidal stability and reduced the tCNF aggregation during film formation.[86] Here, we demonstrate the dispersion of dry LP in water and their incorporation in CNF matrices to form homogeneous composite films. In this study, dried lignin particles were prepared by aerosol reactor and characterized. Then they were mixed with tCNF and assembled into films (see **Figure II.13**). We studied the modification of the tCNF assembly and film structure depending on the LP content.

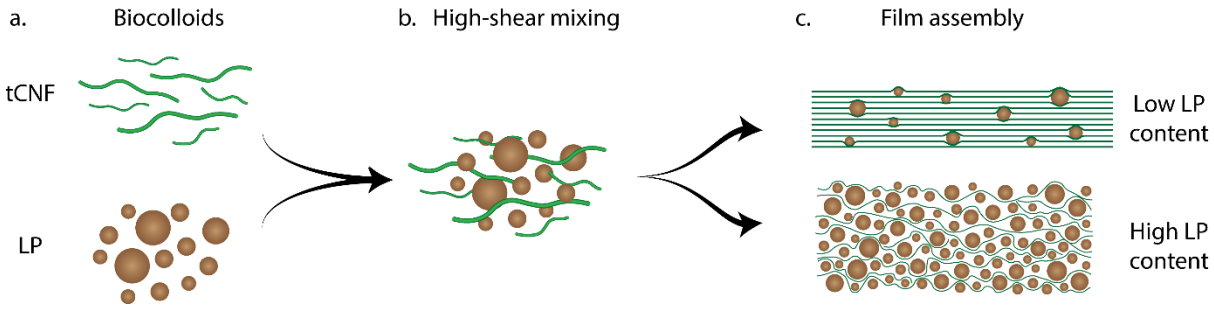

Figure II.13. Different steps taken for the preparation of the LP-tCNF films. **a.** Preparation of the TEMPO oxidized CNF (tCNF) and lignin particles (LP). **b.** High-shear mixing of the biocolloids with different ratios and **c.** assembly into films with different structure depending on the LP content.

EXPERIMENTAL SECTION

Materials. Technical Kraft lignin (Indulin AT) from softwood was purchased from MeadWestvaco (USA). TEMPO cellulose nanofibers (tCNF) at 1 wt% were purchased from University of Maine, they were obtained from wood pulp and sodium was used as counter-ion. Ammonium hydroxide was provided by Sigma-Aldrich.

Dried lignin particles preparation.

The preparation of dry lignin particles (LP) with an aerosol flow reactor was reported by Abbati de Assis *et al.* (see **Figure II.14**).[85] In brief, 2% (w/v) lignin was dissolved in ammonium hydroxide 14% w/w. Lignin solution was fed in the ultrasonic nebulizer and small droplets (e.g. aerosol) were carried with nitrogen through the heated tube (150°C) to allow evaporation of the solvent and formation of solid dried lignin particles. LP were collected in a cyclone collector at 100 °C and stored at room temperature. The preparation of LP was done in collaboration with Luiz G. Greca from Aalto University.

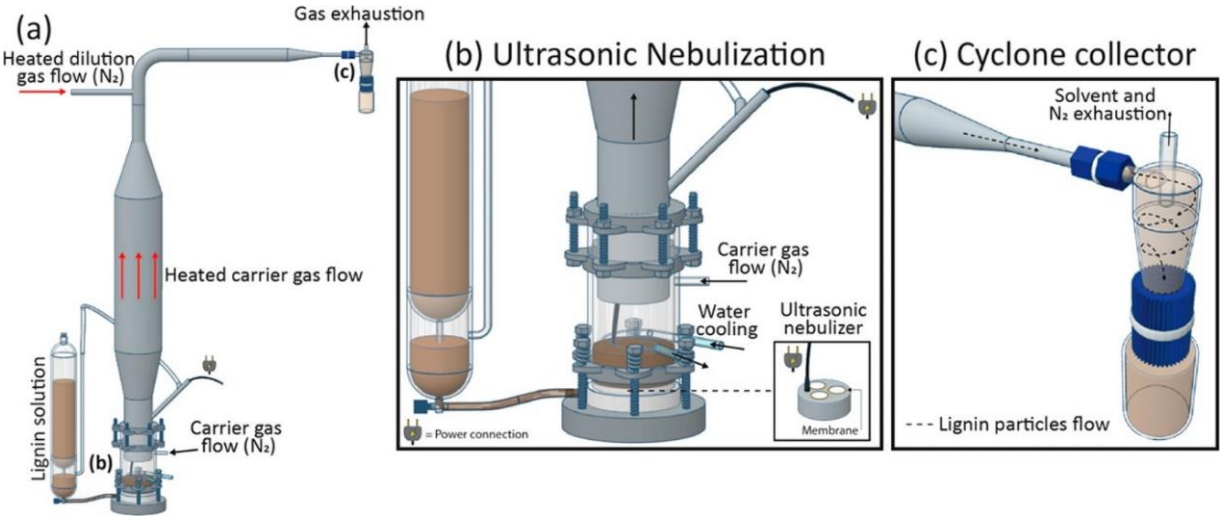

Figure II.14. Aerosol flow reactor used to produce lignin particles. Global scheme of the reactor (**a**). Detailed schemes of the ultrasonic nebulization device (**b**) and cyclone collector (**c**). Reproduced from[85]

Characterization of the suspensions.

Morphology of the nanoparticles. Because of their size difference, lignin particles were imaged with scanning electron microscopy (SEM) while tCNF were imaged with transmission electron microscopy (TEM). Zeiss Sigma VP was used to assess the morphology of the lignin particles. Dry lignin particles were deposited on carbon tape and 4 nm Au/Pd coating was sputtered to make the sample conductive. The size of at least 100 particles was measured with ImageJ software and the size distribution is presented.

TEM images were acquired with a JEOL JEM 2100-Plus microscope operating at 200 kV. Diluted suspension was cast on copper grid and uranyl acetate was added for negative staining. At least 10 images were obtained in different zones of the grid and the most representative were used for the discussion.

Surface charge measurement. The zeta-potential of the lignin particles and tCNF was measured with a Malvern Zetasizer Nano using a dip cell. LP suspension was diluted to 0.05% and sonicated with an ultrasonic probe at (30%, 2 min) before measurement, tCNF was diluted at 0.1% and mixed for 2 min with a high shear homogenizer (Ultra-Turrax) before any analyses. Triplicate samples were analyzed.

The charge content of tCNF was measured by conductimetric titration. Briefly, 0.2 g dry mass of tCNF were dispersed in 200 mL water and concentrated HCl was added to reach pH 3. The suspension was then titrated with NaOH 0.03 M. The total charge content (cc) was calculated using the equation below.

$$cc = \frac{[NaOH] \times (V_2 - V_1)}{m} \quad \text{(II.4)}$$

Where *[NaOH]* is the concentration of sodium hydroxide used for titration, V_1 and V_2 are equivalent volumes of sodium hydroxide needed to titrate excess of HCl (V_1) and the charge content of the fibers (V_2) and *m* the dry mass of tCNF. The average of three measurements is reported.

Hydrodynamic size measurement. The size of the lignin particles was assessed by DLS using a Malvern Zetasizer Nano. LP suspension at 0.05% was sonicated by ultrasonic probe for 2 min at 30% amplitude before measurement.

Preparation of CNF film containing lignin particles.

Suspensions with different ratios of LP and tCNF (0%, 5%, 9%, 23%, 33% and 50%) were prepared. For that purpose, lignin particles were dispersed in water with an ultrasonic bath for 10 min followed by ultrasonic probe for 2 min at 50% amplitude. After addition of a given amount of LP to constant amount of tCNF suspension, the mixture was homogenized with a high shear homogenizer (Ultra-Turax) for 2 min followed by casting in petri dish. Films were dried at 23°C and 50% RH until constant mass. The films will be further referred as "tCNF + X% LP", X representing the amount of LP relative to the total mass of the films. Every percentage mentioned are weight percentage.

Characterization of the films.

All films were stored at least 24 h in 50% RH and 23 °C before any characterization.

Morphology of the films. Cross-sections of the films were imaged by Scanning Electron Microscopy (SEM). Zeiss Sigma VP was used to image the films and a conductive coating of 4 nm of Au/Pd was sputtered on the cross-sections.

Thicknesses. Thicknesses of the films were measured with ImageJ software from the SEM cross-section images. At least 50 measurements were done per film on different images.

Mechanical properties. Tensile strength of the films was measured using a dynamic mechanical analyzer (DMA) (TA Instruments RSA 3). Strips of 0.5 cm x 3 cm were cut in the films and elongated at 0.1 mm/s. The gap between the clamps was set at 1.5 cm.

Optical properties. Transmittance of the films at 550 nm was measured with a UV-Vis spectrophotometer (UV-1800, Shimadzu).

RESULTS AND DISCUSSION

Properties of tCNF.

Figure II.15a shows the TEM image of tCNF, which were well fibrillated and mostly present as single nanofibers. The charge density of tCNF was measured by conductimetric titration (**Figure II.15b**). The total charge density was 1.2 ± 0.1 mmol/g, mainly attributed to the carboxylic groups present on the surface of the nanofibers. The zeta potential of tCNF was –48 ± 2 mV confirming the presence of negatively charged groups on the surface of the nanofibers.

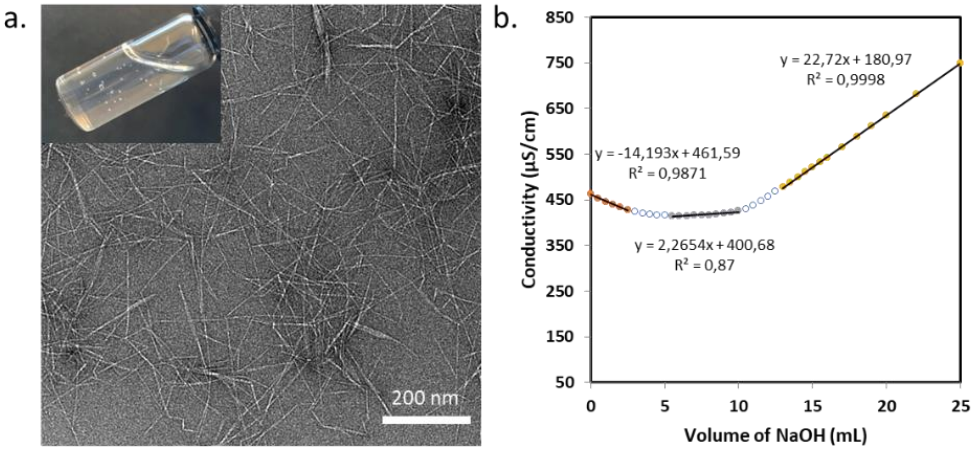

Figure II.15. a. TEM image of tCNF with picture of the suspension at 1 wt%. **b.** Example of a conductimetric titration curve used to measure the charge density of the nanofibers.

Lignin particles prepared with an aerosol reactor.

Commercial Kraft lignin from pine (Indulin AT) was used to produce lignin particles. During extraction of lignin from wood, the structure of lignin is modified as fragmentation and condensation occur. Characterization of Indulin AT lignin has been reported elsewhere.[66] Briefly, it is composed of 93 wt% of lignin, 2 wt% ashes and 1.5 wt% sugars and has a weight average molecular weight of 6549 g/mol. The phenolic content was estimated to be 59-60 phenolic OH per 100 aromatic rings. Compared to milled wood lignin, which is today known as the closest to natural lignin, kraft lignin has more phenolic hydroxyls and carboxyl groups and less aliphatic hydroxyls.[89] The high content of carboxyl and phenolic hydroxyl of Kraft lignin decreases lignin hydrophobicity and increases its solubility in polar solvents. Compatibility with highly hydrophilic cellulose could then be enhanced and formation of hydrogen bonds facilitated.

Lignin particles (LP) were prepared from this Kraft lignin using an aerosol flow reactor, the process consisted first in the dissolution of lignin in ammonium hydroxide 14% and atomization of the suspension to form droplets. Micrometric particles were formed upon drying and particles were collected with a cyclone collector. This process resulted in spherical particles with smooth surface as shown is **Figure II.16a**. Particles with sizes ranging from 250 nm to 4 µm were obtained, with an average size measured from SEM images of 1.4 ± 0.6 µm (see **Figure II.16b**). High polydispersity is inherent to the aerosol flow reactor process and Ago *et al*. showed that fractionation of the particles by size at the output was possible with a Berner-type low-pressure impactor.[84] Moreover, the cyclone collector does not collect the smallest particles that are carried with the nitrogen flow, using another kind of collector would allow the recovery of these smaller particles.

After dispersion in water by sonication, DLS and zeta potential measurements were done. For the DLS measurement, the polydispersity index was too high and hence the measurement was not considered as valid. The average zeta potential of LP was -28 ± 2 mV. These results should be taken with care due to the high polydispersity and micrometric size of the particles. The suspension was not colloidally stable and tended to sediment over time.

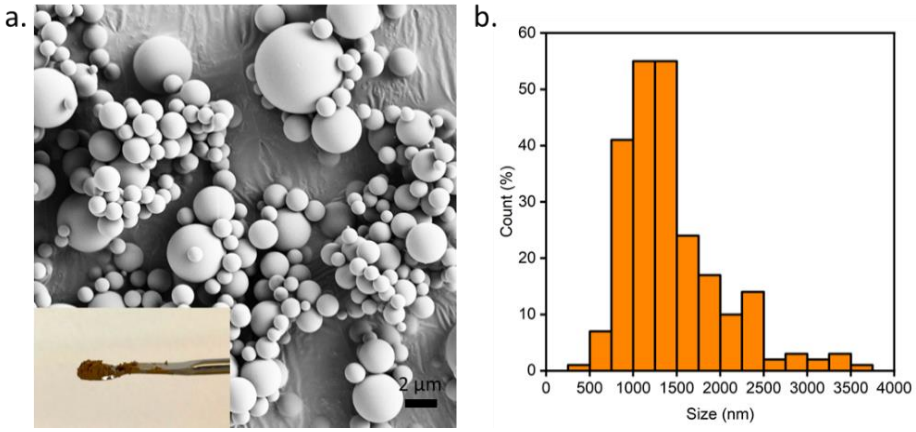

Figure II.16. a. SEM image of lignin particles obtained with the aerosol reactor associated with a picture of the powder and their size distribution measured from SEM images (**b**.).

Surface chemistry and size of lignin particles are highly dependent on the type of lignin used and the preparation method. Characteristics of particles made by aerosol reactor are perfectly spherical, polydisperse in size and dry state. Other more common method like solvent precipitation allow to obtain narrow size distribution of different sizes from tenth of nanometers to micrometers depending on the process conditions.[90,91] Richter *et al*. obtained LP with

average sizes between 50 nm and 200 nm by varying the lignin concentration and dilution rate.[91] Furthermore, methods like ultrasonication or ball milling led to particles with irregular shapes.[82] On the other hand, the surface chemistry depends mostly on the method used to extract the lignin, which influences the surface charge of the particles, hydrophilicity, molecular weight. all influencing the size and suspension stability of the LP.[92] Lourencon *et al.* showed that LP obtained from acetone extracted lignin had a zeta-potential of -35 mV while similar LP from Kraft lignin had a surface charge of -50 mV showing the higher stability of the LP obtained from Kraft lignin.[93]

Influence of LPs on the nanostructure of the films.

Films containing various amount of LP from 5% to 50% were prepared by mixing tCNF and LP followed by evaporation drying. Water evaporation induced densification of the structure and formation of cohesive self-standing films. The films obtained are homogeneous (see **Figure 11.17**). While CNF films are transparent due to the high density and small sizes of the fibers, the addition of micrometric and brown LP significantly reduced the transparency. Films without LP had a transmittance at 550 nm of 89% while addition of 9% LP decreased the transmittance to 0.8%. The films containing high amount of LP (33% and 50%) shrunk during drying to a great extent. No external stress was applied during drying, hence only internal stresses were responsible for the shrinkage, higher stresses in the highly LP loaded films could be explained by the lower amount of tCNF and thus the fewer possibilities for interfibrillar hydrogen bonds which brought fibers closer. Moreover, during the water evaporation from the particle network, tCNF is pulled into interparticle spaces, *i.e.*, interstices, by capillary action thus resulting in in-plan stresses of the tCNF network. Shrinking could be avoided/reduced by drying the films under stress (weight or vacuum).

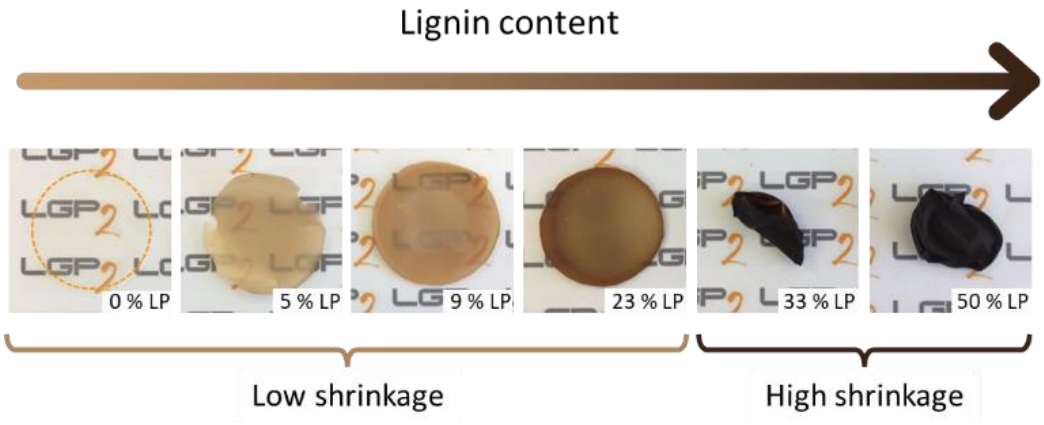

Figure II.17. Images of the films of tCNF and LP prepared with lignin content from 0 to 50%. Low shrinkage upon drying of the films was observed for films from 0% to 23% LP while high shrinkage was noticed for films with 33% and 50% LP.

To better understand the structure of the films, SEM images of the cross-sections were done. **Figure II.18b** and **c** display the cross-section images of the film containing 50% LP and 9% LP respectively. Both films have homogeneous structures with good dispersion of the LP in the tCNF matrix, displaying no visible aggregation. Repulsion between negatively charged tCNF and LP fostered the high stability of the suspension and prevented aggregation is solution. Moreover, films were cohesive even at high LP content showing the strong interactions between tCNF and LP due to the formation of hydrogen bonds between hydroxyls groups present on the surface of LP and hydroxyls of tCNF.

The film with 9% LP had a sheet like structure specific to fiber-based films and LPs were well dispersed in the tCNF network (**Figure II.18e**). On the other hand, the film containing 50% LP had a structure dominated by the LP and tCNF were interpenetrated in between the LP (**Figure II.18d**). The difference in size between nanometric tCNF and micrometric LP could explain the disruption of the tCNF network. From the film's thicknesses (**Figure II.18a**), it was possible to extrapolate to which lignin content the change of structure occurs. In fact, the SEM cross-section of tCNF + 23% LP contained both domains with sheet like structure and disrupted network and 23% can be considered as the threshold amount between the two structures.

Using LP from aerosol reactor, Cusola *et al*. observed segregation of LP by size upon evaporation-induced self-assembly of 100% LP coatings due to the large polydispersity of the LP.[94] Here, sedimentations of large LPs was avoided during casting with the presence of high viscosity tCNF hydrogel network and a homogeneous dispersion of the LP through the cross-section of the films was observed. Furthermore, with the idea of making high LP content

membranes, Cusola *et al.* found that 8% of CNF was the minimum amount needed to form a cohesive membrane.[95] The structure of such membranes were similar to our high LP content films.

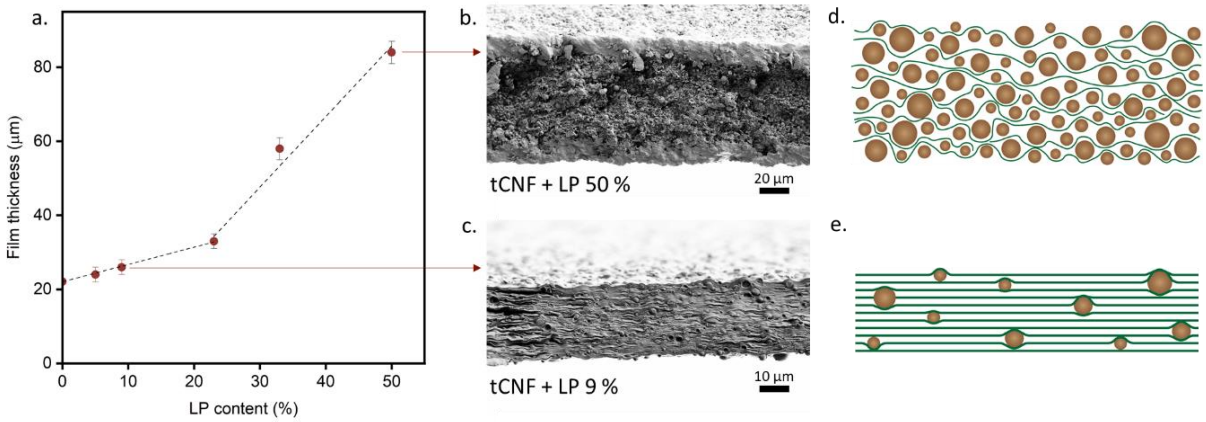

Figure II.18. a. Thicknesses of the films (measured on SEM images) as function of LP content. SEM images of the film containing 50% LP (**b.**) and 9% LP (**c.**) associated with scheme of their structure. The structure of film containing 50% LP is dominated by the LP (**d.**) while a sheet like structure characteristic of CNF films is observed in the film with 9% LP (**e.**).

Films with LP amount lower than 23% seemed promising for further experiments as they resulted in dense cohesive films with homogeneous LP dispersion. **Table II.4** shows the elastic modulus, maximum stress and strain of the tCNF and tCNF + LP 9% films. The addition of 9% LP to tCNF film decreased the elastic modulus two times while the stress and strain at break also decreased. The poor mechanical properties of the film containing LP could be explained by the presence of microparticles that acted as defects in the tCNF matrix, as well as the weak particle-fiber interactions when compared to the strong interfibrillar entangled interactions of tCNF.

Comparison with literature showed that inclusion of LP in CNF matrix does not necessarily have negative impact on the mechanical properties of the films. In fact, Farooq *et al.* prepared LP with diameter of 102 nm by solvent precipitation of Kraft lignin. After mixing them with CNF at 10 wt%, films with equivalent elastic modulus and increased strength and maximum strain compared to CNF alone were obtained (**Table II.4**). The improved mechanical properties were explained by the ability of LP to transfer stress through hydrogen bonding between LP and CNF. In another study, Liu *et al.* obtained LP of 4.8 ± 1.7 nm by solvent shifting by dialysis of Kraft lignin. Then, films containing 7.7 wt% of LP and 92.3 wt% of tCNF were prepared by

solvent casting. The resulting films displayed Young's modulus almost three times higher than tCNF alone as well as double maximum strength. The nanosized LP were able to fill the pores and increase film density as well as to increase the suspension stability by hindering fibrils aggregation, both leading to improved mechanical properties.

Table II.4. Mechanical properties of the tCNF and tCNF + LP 9 % films and comparison with similar films in literature.

	tCNF	tCNF + LP 9 wt%	CNF	CNF + LP 10 wt%	tCNF	tCNF + LP 7.7 wt%
Ref	Our work		Farooq *et al.*[87]		Liu *et al.*[86]	
Elastic modulus (GPa)	3.3 ± 0.3	1.6 ± 0.1	5.7 ± 1.2	5.5 ± 0.6	2.9	8.6
Maximum stress (MPa)	155 ± 15	43 ± 13	132 ± 15	160 ± 12	120	245
Strain at break (%)	4.8 ± 0.5	3.1 ± 0.6	9 ± 2	16 ± 2	≈13.5	≈14
LP size (nm)	1.4 ± 0.6 µm		102 nm		4.8 ± 1.7 nm	

Comparing the three previous examples, one can notice that the size of LP was of different order of magnitude and the explanations for improved mechanical properties could not apply to micrometric particles. The presence of micrometric particles in our films prevented pore filling or increased number of interactions, the larger the particles the smaller the specific surface area and the possibilities to interact and form hydrogen bonds. We thus suggest that the micrometric size of LP was responsible for the weak mechanical properties of the film rather than the surface chemistry. The mechanical properties of the films containing LP was not promising. The size of the LP being one factor that highly influence the film structure, in the next chapter, we will present a novel method to prepare LP with smaller size and their integration in CNF matrix. The structure and properties of the films will be investigated as function of LP size, amongst other parameters.

CONCLUSION

LP were obtained by an aerosol flow reactor from dissolved Kraft lignin, which had an average diameter of 1.4 ± 0.6 µm. We successfully prepared cohesive and homogeneous films by mixing tCNF and LP with different LP content from 5% to 50%. For LP content below 23%, films had a sheet like structure characteristic of fiber-based films while above 23% the films' structure was dominated by the particles. Mechanical properties of the film containing 9% LP were decreased compared to tCNF film mostly due to the micrometric size of LP. In the next chapter, nanometric LP will be prepared and integrated to CNF films for comparison. More properties relevant to packaging applications such as transparency, water interaction and gas barrier properties will also be studied.

Conclusion to Chapter II

The goal of this chapter was to study the influence of the source on chitin nanofibers preparation as well as prepare lignin particles and first films of LP and CNF.

We successfully prepared chitin nanofibers from insects for the first time. Two different insect sources were used and resulted in ChNF with similar properties to ChNF from shrimp shells. ChNF from fly larvae showed higher degree of fibrillation compared to ChNF from shrimp shells for similar degree of processing. Moreover, a mix of cellulose and chitin nanofibers was obtained from mealworm farming by-product. The obtained suspension presented improved stability throughout a high range of pH. While processed into films, interesting elongation properties were obtained compared to similar films containing a mix of CNF and ChNF. Further study of the interactions between chitin and cellulose at the nanoscale should be done to further understand the synergies between the nanofibers. Furthermore, a sustainability study of different sources was also done and showed that insects have a lower impact than shrimp on several criteria including carbon, water, and chemical footprints mainly due to their fast life cycle and lower recalcitrance. Optimization of the extraction of chitin from insects should be further studied to even lower the fabrication footprint. Partial purification of the chitin could also result in improved film properties and lower the total material footprint.

Despite the equivalent properties of ChNF from fly compared to shrimp shells, in the next chapters, ChNF from shrimp are used as the quantity of F-ChNF was limited. However, we believe that similar results could be obtained with F-ChNF.

In the second part of this chapter, lignin particles were prepared with an aerosol reactor. Round and polydisperse particles with an average diameter of 1.4 µm were obtained. Films of tCNF were prepared with different amounts of LP. It was found that 23% of LP in tCNF films was the threshold between the typical tCNF lamellar structure and a structure dominated by the particles. Poor mechanical properties were obtained with only 9% of LP. After comparison with the literature, we hypothesized that the size of the LP was responsible for the weak film properties. In the next chapter, lignin nanoparticles are prepared and the influence of the LP size on the film properties is studied.

References

(1) Payne, C. L. R.; Scarborough, P.; Rayner, M.; Nonaka, K. Are Edible Insects More or Less 'Healthy' than Commonly Consumed Meats? A Comparison Using Two Nutrient Profiling Models Developed to Combat over- and Undernutrition. *European Journal of Clinical Nutrition* **2016**, *70* (3), 285–291. https://doi.org/10.1038/ejcn.2015.149.

(2) Parodi, A.; Leip, A.; De Boer, I. J. M.; Slegers, P. M.; Ziegler, F.; Temme, E. H. M.; Herrero, M.; Tuomisto, H.; Valin, H.; Van Middelaar, C. E.; Van Loon, J. J. A.; Van Zanten, H. H. E. The Potential of Future Foods for Sustainable and Healthy Diets. *Nature Sustainability* **2018**, *1* (12), 782–789. https://doi.org/10.1038/s41893-018-0189-7.

(3) McClements, D. J. *Future Foods: How Modern Science Is Transforming the Way We Eat*; Copernicus, 2019. https://doi.org/10.1007/978-3-030-12995-8.

(4) Sánchez-Muros, M.-J.; Barroso, F. G.; Manzano-Agugliaro, F. Insect Meal as Renewable Source of Food for Animal Feeding: A Review. *Journal of Cleaner Production* **2014**, *65*, 16–27. https://doi.org/10.1016/j.jclepro.2013.11.068.

(5) Oonincx, D. G. A. B.; Boer, I. J. M. Environmental Impact of the Production of Mealworms as a Protein Source for Humans – A Life Cycle Assessment. *PLOS ONE* **2012**, *7* (12), e51145. https://doi.org/10.1371/journal.pone.0051145.

(6) Varelas, V. Food Wastes as a Potential New Source for Edible Insect Mass Production for Food and Feed: A Review. *Fermentation* **2019**, *5* (3), 81. https://doi.org/10.3390/fermentation5030081.

(7) Houben, D.; Daoulas, G.; Faucon, M.-P.; Dulaurent, A.-M. Potential Use of Mealworm Frass as a Fertilizer: Impact on Crop Growth and Soil Properties. *Scientific Reports* **2020**, *10* (1), 4659. https://doi.org/10.1038/s41598-020-61765-x.

(8) Rosa, R.; Spinelli, R.; Neri, P.; Pini, M.; Barbi, S.; Montorsi, M.; Maistrello, L.; Marseglia, A.; Caligiani, A.; Ferrari, A. M. Life Cycle Assessment of Chemical vs Enzymatic-Assisted Extraction of Proteins from Black Soldier Fly Prepupae for the Preparation of Biomaterials for Potential Agricultural Use. *ACS Sustainable Chem. Eng.* **2020**, *8* (39), 14752–14764. https://doi.org/10.1021/acssuschemeng.0c03795.

(9) Spranghers, T.; Ottoboni, M.; Klootwijk, C.; Ovyn, A.; Deboosere, S.; Meulenaer, B. D.; Michiels, J.; Eeckhout, M.; Clercq, P. D.; Smet, S. D. Nutritional Composition of Black Soldier Fly (Hermetia Illucens) Prepupae Reared on Different Organic Waste Substrates. *Journal of the Science of Food and Agriculture* **2017**, *97* (8), 2594–2600. https://doi.org/10.1002/jsfa.8081.

(10) Hahn, T.; Roth, A.; Febel, E.; Fijalkowska, M.; Schmitt, E.; Arsiwalla, T.; Zibek, S. New Methods for High-Accuracy Insect Chitin Measurement. *Journal of the Science of Food and Agriculture* **2018**, *98* (13), 5069–5073. https://doi.org/10.1002/jsfa.9044.

(11) Sanandiya, N. D.; Ottenheim, C.; Phua, J. W.; Caligiani, A.; Dritsas, S.; Fernandez, J. G. Circular Manufacturing of Chitinous Bio-Composites via Bioconversion of Urban Refuse. *Sci Rep* **2020**, *10* (1), 1–8. https://doi.org/10.1038/s41598-020-61664-1.

(12) Hahn, T.; Roth, A.; Ji, R.; Schmitt, E.; Zibek, S. Chitosan Production with Larval Exoskeletons Derived from the Insect Protein Production. *Journal of Biotechnology* **2020**, *310*, 62–67. https://doi.org/10.1016/j.jbiotec.2019.12.015.

(13) Song, Y.-S.; Kim, M.-W.; Moon, C.; Seo, D.-J.; Han, Y. S.; Jo, Y. H.; Noh, M. Y.; Park, Y.-K.; Kim, S.-A.; Kim, Y. W.; Jung, W.-J. Extraction of Chitin and Chitosan from Larval Exuvium and Whole Body of Edible Mealworm, Tenebrio Molitor. *Entomological Research* **2018**, *48* (3), 227–233. https://doi.org/10.1111/1748-5967.12304.

(14) Salaberria, A. M.; Labidi, J.; Fernandes, S. C. M. Different Routes to Turn Chitin into Stunning Nano-Objects. *European Polymer Journal* **2015**, *68*, 503–515. https://doi.org/10.1016/j.eurpolymj.2015.03.005.
(15) Biswas, S. K.; Shams, Md. I.; Das, A. K.; Islam, Md. N.; Nazhad, M. M. Flexible and Transparent Chitin/Acrylic Nanocomposite Films with High Mechanical Strength. *Fibers Polym* **2015**, *16* (4), 774–781. https://doi.org/10.1007/s12221-015-0774-6.
(16) Ahmad, S. I.; Ahmad, R.; Khan, Mohd. S.; Kant, R.; Shahid, S.; Gautam, L.; Hasan, G. M.; Hassan, Md. I. Chitin and Its Derivatives: Structural Properties and Biomedical Applications. *International Journal of Biological Macromolecules* **2020**, *164*, 526–539. https://doi.org/10.1016/j.ijbiomac.2020.07.098.
(17) Zhu, Y.; Huan, S.; Bai, L.; Ketola, A.; Shi, X.; Zhang, X.; Ketoja, J. A.; Rojas, O. J. High Internal Phase Oil-in-Water Pickering Emulsions Stabilized by Chitin Nanofibrils: 3D Structuring and Solid Foams. *ACS Appl. Mater. Interfaces* **2020**, *12*, 11240–11251. https://doi.org/10.1021/acsami.9b23430.
(18) Ifuku, S.; Morooka, S.; Morimoto, M.; Saimoto, H. Acetylation of Chitin Nanofibers and Their Transparent Nanocomposite Films. *Biomacromolecules* **2010**, *11* (5), 1326–1330. https://doi.org/10.1021/bm100109a.
(19) Fan, Y.; Saito, T.; Isogai, A. Preparation of Chitin Nanofibers from Squid Pen β-Chitin by Simple Mechanical Treatment under Acid Conditions. *Biomacromolecules* **2008**, *9* (7), 1919–1923. https://doi.org/10.1021/bm800178b.
(20) Ifuku, S.; Nomura, R.; Morimoto, M.; Saimoto, H. Preparation of Chitin Nanofibers from Mushrooms. *Materials* **2011**, *4* (8), 1417–1425. https://doi.org/10.3390/ma4081417.
(21) Morin, A.; Dufresne, A. Nanocomposites of Chitin Whiskers from Riftia Tubes and Poly(Caprolactone). *Macromolecules* **2002**, *35* (6), 2190–2199. https://doi.org/10.1021/ma011493a.
(22) Kaya, M.; Baublys, V.; Can, E.; Šatkauskienė, I.; Bitim, B.; Tubelytė, V.; Baran, T. Comparison of Physicochemical Properties of Chitins Isolated from an Insect (Melolontha Melolontha) and a Crustacean Species (Oniscus Asellus). *Zoomorphology* **2014**, *133* (3), 285–293. https://doi.org/10.1007/s00435-014-0227-6.
(23) Huet, G.; Hadad, C.; Husson, E.; Laclef, S.; Lambertyn, V.; Araya Farias, M.; Jamali, A.; Courty, M.; Alayoubi, R.; Gosselin, I.; Sarazin, C.; Van Nhien, A. N. Straightforward Extraction and Selective Bioconversion of High Purity Chitin from Bombyx Eri Larva: Toward an Integrated Insect Biorefinery. *Carbohydrate Polymers* **2020**, *228*, 115382. https://doi.org/10.1016/j.carbpol.2019.115382.
(24) Brigode, C.; Hobbi, P.; Jafari, H.; Verwilghen, F.; Baeten, E.; Shavandi, A. Isolation and Physicochemical Properties of Chitin Polymer from Insect Farm Side Stream as a New Source of Renewable Biopolymer. *Journal of Cleaner Production* **2020**, *275*, 122924. https://doi.org/10.1016/j.jclepro.2020.122924.
(25) Hahn, T.; Tafi, E.; Paul, A.; Salvia, R.; Falabella, P.; Zibek, S. Current State of Chitin Purification and Chitosan Production from Insects. *Journal of Chemical Technology & Biotechnology* **2020**, *95* (11), 2775–2795. https://doi.org/10.1002/jctb.6533.
(26) Fazli Wan Nawawi, W. M.; Lee, K.-Y.; Kontturi, E.; Murphy, R. J.; Bismarck, A. Chitin Nanopaper from Mushroom Extract: Natural Composite of Nanofibers and Glucan from a Single Biobased Source. *ACS Sustainable Chem. Eng.* **2019**, *7* (7), 6492–6496. https://doi.org/10.1021/acssuschemeng.9b00721.
(27) Turck, D.; Castenmiller, J.; Henauw, S. D.; Hirsch-Ernst, K. I.; Kearney, J.; Maciuk, A.; Mangelsdorf, I.; McArdle, H. J.; Naska, A.; Pelaez, C.; Pentieva, K.; Siani, A.; Thies, F.; Tsabouri, S.; Vinceti, M.; Cubadda, F.; Frenzel, T.; Heinonen, M.; Marchelli, R.; Neuhäuser-Berthold, M.; Poulsen, M.; Maradona, M. P.; Schlatter, J. R.; Loveren, H.

van; Ververis, E.; Knutsen, H. K. Safety of Dried Yellow Mealworm (Tenebrio Molitor Larva) as a Novel Food Pursuant to Regulation (EU) 2015/2283. *EFSA Journal* **2021**, *19* (1), e06343. https://doi.org/10.2903/j.efsa.2021.6343.

(28) Percot, A.; Viton, C.; Domard, A. Optimization of Chitin Extraction from Shrimp Shells. *Biomacromolecules* **2003**, *4* (1), 12–18. https://doi.org/10.1021/bm025602k.

(29) Beaumont, M.; Rennhofer, H.; Opietnik, M.; Lichtenegger, H. C.; Potthast, A.; Rosenau, T. Nanostructured Cellulose II Gel Consisting of Spherical Particles. *ACS Sustainable Chem. Eng.* **2016**, *4* (8), 4424–4432. https://doi.org/10.1021/acssuschemeng.6b01036.

(30) Desmaisons, J.; Boutonnet, E.; Rueff, M.; Dufresne, A.; Bras, J. A New Quality Index for Benchmarking of Different Cellulose Nanofibrils. *Carbohydrate Polymers* **2017**, *174*, 318–329. https://doi.org/10.1016/j.carbpol.2017.06.032.

(31) Cárdenas, G.; Cabrera, G.; Taboada, E.; Miranda, S. P. Chitin Characterization by SEM, FTIR, XRD, and 13C Cross Polarization/Mass Angle Spinning NMR. *Journal of Applied Polymer Science* **2004**, *93* (4), 1876–1885. https://doi.org/10.1002/app.20647.

(32) King, C.; Stein, R. S.; Shamshina, J. L.; Rogers, R. D. Measuring the Purity of Chitin with a Clean, Quantitative Solid-State NMR Method. *ACS Sustainable Chem. Eng.* **2017**, *5* (9), 8011–8016. https://doi.org/10.1021/acssuschemeng.7b01589.

(33) Waśko, A.; Bulak, P.; Polak-Berecka, M.; Nowak, K.; Polakowski, C.; Bieganowski, A. The First Report of the Physicochemical Structure of Chitin Isolated from Hermetia Illucens. *International Journal of Biological Macromolecules* **2016**, *92*, 316–320. https://doi.org/10.1016/j.ijbiomac.2016.07.038.

(34) French, A. D. Idealized Powder Diffraction Patterns for Cellulose Polymorphs. *Cellulose* **2014**, *21* (2), 885–896. https://doi.org/10.1007/s10570-013-0030-4.

(35) Lu, Y.; Sun, Q.; She, X.; Xia, Y.; Liu, Y.; Li, J.; Yang, D. Fabrication and Characterisation of α-Chitin Nanofibers and Highly Transparent Chitin Films by Pulsed Ultrasonication. *Carbohydrate Polymers* **2013**, *98* (2), 1497–1504. https://doi.org/10.1016/j.carbpol.2013.07.038.

(36) Yang, R.; Su, Y.; Aubrecht, K. B.; Wang, X.; Ma, H.; Grubbs, R. B.; Hsiao, B. S.; Chu, B. Thiol-Functionalized Chitin Nanofibers for As (III) Adsorption. *Polymer* **2015**, *60*, 9–17. https://doi.org/10.1016/j.polymer.2015.01.025.

(37) Lamarque, G.; Viton, C.; Domard, A. Comparative Study of the First Heterogeneous Deacetylation of α- and β-Chitins in a Multistep Process. *Biomacromolecules* **2004**, *5* (3), 992–1001. https://doi.org/10.1021/bm034498j.

(38) Shak, K. P. Y.; Pang, Y. L.; Mah, S. K. Nanocellulose: Recent Advances and Its Prospects in Environmental Remediation. *Beilstein J Nanotechnol* **2018**, *9*, 2479–2498. https://doi.org/10.3762/bjnano.9.232.

(39) Ifuku, S.; Nogi, M.; Abe, K.; Yoshioka, M.; Morimoto, M.; Saimoto, H.; Yano, H. Preparation of Chitin Nanofibers with a Uniform Width as α-Chitin from Crab Shells. *Biomacromolecules* **2009**, *10* (6), 1584–1588. https://doi.org/10.1021/bm900163d.

(40) Marei, N. H.; El-Samie, E. A.; Salah, T.; Saad, G. R.; Elwahy, A. H. M. Isolation and Characterization of Chitosan from Different Local Insects in Egypt. *International Journal of Biological Macromolecules* **2016**, *82*, 871–877. https://doi.org/10.1016/j.ijbiomac.2015.10.024.

(41) Toivonen, M. S.; Onelli, O. D.; Jacucci, G.; Lovikka, V.; Rojas, O. J.; Ikkala, O.; Vignolini, S. Anomalous-Diffusion-Assisted Brightness in White Cellulose Nanofibril Membranes. *Advanced Materials* **2018**, *30* (16), 1704050. https://doi.org/10.1002/adma.201704050.

(42) Toivonen, M. S.; Kurki-Suonio, S.; Schacher, F. H.; Hietala, S.; Rojas, O. J.; Ikkala, O. Water-Resistant, Transparent Hybrid Nanopaper by Physical Cross-Linking with

Chitosan. *Biomacromolecules* **2015**, *16* (3), 1062–1071. https://doi.org/10.1021/acs.biomac.5b00145.

(43) Sharma, S.; Zhang, X.; Nair, S. S.; Ragauskas, A.; Zhu, J.; Deng, Y. Thermally Enhanced High Performance Cellulose Nano Fibril Barrier Membranes. *RSC Adv.* **2014**, *4* (85), 45136–45142. https://doi.org/10.1039/C4RA07469F.

(44) Zhang, K.; Ketterle, L.; Järvinen, T.; Hong, S.; Liimatainen, H. Conductive Hybrid Filaments of Carbon Nanotubes, Chitin Nanocrystals and Cellulose Nanofibers Formed by Interfacial Nanoparticle Complexation. *Materials & Design* **2020**, *191*, 108594. https://doi.org/10.1016/j.matdes.2020.108594.

(45) Grande, R.; Bai, L.; Wang, L.; Xiang, W.; Ikkala, O.; Carvalho, A. J. F.; Rojas, O. J. Nanochitins of Varying Aspect Ratio and Properties of Microfibers Produced by Interfacial Complexation with Seaweed Alginate. *ACS Sustainable Chem. Eng.* **2020**, *8* (2), 1137–1145. https://doi.org/10.1021/acssuschemeng.9b06099.

(46) Kim, T.; Tran, T. H.; Hwang, S. Y.; Park, J.; Oh, D. X.; Kim, B.-S. Crab-on-a-Tree: All Biorenewable, Optical and Radio Frequency Transparent Barrier Nanocoating for Food Packaging. *ACS Nano* **2019**, *13* (4), 3796–3805. https://doi.org/10.1021/acsnano.8b08522.

(47) Missio, A. L.; Mattos, B. D.; Otoni, C. G.; Gentil, M.; Coldebella, R.; Khakalo, A.; Gatto, D. A.; Rojas, O. J. Cogrinding Wood Fibers and Tannins: Surfactant Effects on the Interactions and Properties of Functional Films for Sustainable Packaging Materials. *Biomacromolecules* **2020**, *21* (5), 1865–1874. https://doi.org/10.1021/acs.biomac.9b01733.

(48) Bai, L.; Huan, S.; Xiang, W.; Liu, L.; Yang, Y.; Nugroho, R. W. N.; Fan, Y.; Rojas, O. J. Self-Assembled Networks of Short and Long Chitin Nanoparticles for Oil/Water Interfacial Superstabilization. *ACS Sustainable Chem. Eng.* **2019**, *7* (7), 6497–6511. https://doi.org/10.1021/acssuschemeng.8b04023.

(49) Lv, S.; Zhou, H.; Bai, L.; Rojas, O. J.; McClements, D. J. Development of Food-Grade Pickering Emulsions Stabilized by a Mixture of Cellulose Nanofibrils and Nanochitin. *Food Hydrocolloids* **2021**, *113*, 106451. https://doi.org/10.1016/j.foodhyd.2020.106451.

(50) Fan, Y.; Fukuzumi, H.; Saito, T.; Isogai, A. Comparative Characterization of Aqueous Dispersions and Cast Films of Different Chitin Nanowhiskers/Nanofibers. *International Journal of Biological Macromolecules* **2012**, *50* (1), 69–76. https://doi.org/10.1016/j.ijbiomac.2011.09.026.

(51) Wang, H.; Qian, J.; Ding, F. Emerging Chitosan-Based Films for Food Packaging Applications. *J. Agric. Food Chem.* **2018**, *66* (2), 395–413. https://doi.org/10.1021/acs.jafc.7b04528.

(52) Santos, V. P.; Marques, N. S. S.; Maia, P. C. S. V.; Lima, M. A. B. de; Franco, L. de O.; Campos-Takaki, G. M. de. Seafood Waste as Attractive Source of Chitin and Chitosan Production and Their Applications. *International Journal of Molecular Sciences* **2020**, *21* (12), 4290. https://doi.org/10.3390/ijms21124290.

(53) Younes, I.; Rinaudo, M. Chitin and Chitosan Preparation from Marine Sources. Structure, Properties and Applications. *Marine Drugs* **2015**, *13* (3), 1133–1174. https://doi.org/10.3390/md13031133.

(54) Yan, N.; Chen, X. Sustainability: Don't Waste Seafood Waste. *Nature* **2015**, *524* (7564), 155–157. https://doi.org/10.1038/524155a.

(55) Muñoz, I.; Rodríguez, C.; Gillet, D.; M. Moerschbacher, B. Life Cycle Assessment of Chitosan Production in India and Europe. *Int J Life Cycle Assess* **2018**, *23* (5), 1151–1160. https://doi.org/10.1007/s11367-017-1290-2.

(56) Shamshina, J. L.; Barber, P. S.; Gurau, G.; Griggs, C. S.; Rogers, R. D. Pulping of Crustacean Waste Using Ionic Liquids: To Extract or Not To Extract. *ACS Sustainable Chem. Eng.* **2016**, *4* (11), 6072–6081. https://doi.org/10.1021/acssuschemeng.6b01434.
(57) Cao, L.; Diana, J. S.; Keoleian, G. A.; Lai, Q. Life Cycle Assessment of Chinese Shrimp Farming Systems Targeted for Export and Domestic Sales. *Environ. Sci. Technol.* **2011**, *45* (15), 6531–6538. https://doi.org/10.1021/es104058z.
(58) Pajula, T.; Vatanen, S.; Behm, K.; Grönman, K.; Lakanen, L.; Kasurinen, H.; Soukka, R. *Carbon Handprint Guide: V. 2.0 Applicable for Environmental Handprint*; VTT Technical Research Centre of Finland, 2021; p 28.
(59) Oonincx, D. G. A. B.; Itterbeeck, J. van; Heetkamp, M. J. W.; Brand, H. van den; Loon, J. J. A. van; Huis, A. van. An Exploration on Greenhouse Gas and Ammonia Production by Insect Species Suitable for Animal or Human Consumption. *PLOS ONE* **2010**, *5* (12), e14445. https://doi.org/10.1371/journal.pone.0014445.
(60) Otoni, C. G.; Azeredo, H. M. C.; Mattos, B. D.; Beaumont, M.; Correa, D. S.; Rojas, O. J. The Food–Materials Nexus: Next Generation Bioplastics and Advanced Materials from Agri-Food Residues. *Advanced Materials* **2021**, 2102520. https://doi.org/10.1002/adma.202102520.
(61) Gao, Z.; Wang, W.; Lu, X.; Zhu, F.; Liu, W.; Wang, X.; Lei, C. Bioconversion Performance and Life Table of Black Soldier Fly (Hermetia Illucens) on Fermented Maize Straw. *Journal of Cleaner Production* **2019**, *230*, 974–980. https://doi.org/10.1016/j.jclepro.2019.05.074.
(62) Järviö, N.; Henriksson, P. J. G.; Guinée, J. B. Including GHG Emissions from Mangrove Forests LULUC in LCA: A Case Study on Shrimp Farming in the Mekong Delta, Vietnam. *Int J Life Cycle Assess* **2018**, *23* (5), 1078–1090. https://doi.org/10.1007/s11367-017-1332-9.
(63) Ifuku, S.; Urakami, T.; Izawa, H.; Morimoto, M.; Saimoto, H. Preparation of a Protein–Chitin Nanofiber Complex from Crab Shells and Its Application as a Reinforcement Filler or Substrate for Biomineralization. *RSC Adv.* **2015**, *5* (79), 64196–64201. https://doi.org/10.1039/C5RA12761K.
(64) Zhou, C.; Wang, Y. Recent Progress in the Conversion of Biomass Wastes into Functional Materials for Value-Added Applications. *Sci Technol Adv Mater* **2020**, *21* (1), 787–804. https://doi.org/10.1080/14686996.2020.1848213.
(65) Balakshin, M. Y.; Capanema, E. A.; Sulaeva, I.; Schlee, P.; Huang, Z.; Feng, M.; Borghei, M.; Rojas, O. J.; Potthast, A.; Rosenau, T. New Opportunities in the Valorization of Technical Lignins. *ChemSusChem* **2021**, *14* (4), 1016–1036. https://doi.org/10.1002/cssc.202002553.
(66) Hu, Z.; Du, X.; Liu, J.; Chang, H.; Jameel, H. Structural Characterization of Pine Kraft Lignin: BioChoice Lignin vs Indulin AT. *Journal of Wood Chemistry and Technology* **2016**, *36* (6), 432–446. https://doi.org/10.1080/02773813.2016.1214732.
(67) Spieser, H.; Denneulin, A.; Deganello, D.; Gethin, D.; Koppolu, R.; Bras, J. Cellulose Nanofibrils and Silver Nanowires Active Coatings for the Development of Antibacterial Packaging Surfaces. *Carbohydrate Polymers* **2020**, *240*, 116305. https://doi.org/10.1016/j.carbpol.2020.116305.
(68) Valencia, L.; Kumar, S.; Nomena, E. M.; Salazar-Alvarez, G.; Mathew, A. P. In-Situ Growth of Metal Oxide Nanoparticles on Cellulose Nanofibrils for Dye Removal and Antimicrobial Applications. *ACS Appl. Nano Mater.* **2020**, *3* (7), 7172–7181. https://doi.org/10.1021/acsanm.0c01511.
(69) Hoeng, F.; Denneulin, A.; Bras, J. Use of Nanocellulose in Printed Electronics: A Review. *Nanoscale* **2016**, *8* (27), 13131–13154. https://doi.org/10.1039/C6NR03054H.

(70) Kargarzadeh, H.; Mariano, M.; Gopakumar, D.; Ahmad, I.; Thomas, S.; Dufresne, A.; Huang, J.; Lin, N. Advances in Cellulose Nanomaterials. *Cellulose* **2018**, *25* (4), 2151–2189. https://doi.org/10.1007/s10570-018-1723-5.
(71) Saito, T.; Isogai, A. Introduction of Aldehyde Groups on Surfaces of Native Cellulose Fibers by TEMPO-Mediated Oxidation. *Colloids and Surfaces A: Physicochemical and Engineering Aspects* **2006**, *289* (1), 219–225. https://doi.org/10.1016/j.colsurfa.2006.04.038.
(72) Rol, F.; Belgacem, M. N.; Gandini, A.; Bras, J. Recent Advances in Surface-Modified Cellulose Nanofibrils. *Progress in Polymer Science* **2019**, *88*, 241–264. https://doi.org/10.1016/j.progpolymsci.2018.09.002.
(73) Moon, R. J.; Martini, A.; Nairn, J.; Simonsen, J.; Youngblood, J. Cellulose Nanomaterials Review: Structure, Properties and Nanocomposites. *Chem. Soc. Rev.* **2011**, *40* (7), 3941–3994. https://doi.org/10.1039/C0CS00108B.
(74) Zhang, Y.; Naebe, M. Lignin: A Review on Structure, Properties, and Applications as a Light-Colored UV Absorber. *ACS Sustainable Chem. Eng.* **2021**, *9* (4), 1427–1442. https://doi.org/10.1021/acssuschemeng.0c06998.
(75) Cavallo, E.; He, X.; Luzi, F.; Dominici, F.; Cerrutti, P.; Bernal, C.; Foresti, M. L.; Torre, L.; Puglia, D. UV Protective, Antioxidant, Antibacterial and Compostable Polylactic Acid Composites Containing Pristine and Chemically Modified Lignin Nanoparticles. *Molecules* **2021**, *26* (1), 126. https://doi.org/10.3390/molecules26010126.
(76) Lavoine, N.; Desloges, I.; Dufresne, A.; Bras, J. Microfibrillated Cellulose – Its Barrier Properties and Applications in Cellulosic Materials: A Review. *Carbohydrate Polymers* **2012**, *90* (2), 735–764. https://doi.org/10.1016/j.carbpol.2012.05.026.
(77) Trovagunta, R.; Zou, T.; Österberg, M.; Kelley, S. S.; Lavoine, N. Design Strategies, Properties and Applications of Cellulose Nanomaterials-Enhanced Products with Residual, Technical or Nanoscale Lignin—A Review. *Carbohydrate Polymers* **2021**, *254*, 117480. https://doi.org/10.1016/j.carbpol.2020.117480.
(78) Bajwa, D. S.; Pourhashem, G.; Ullah, A. H.; Bajwa, S. G. A Concise Review of Current Lignin Production, Applications, Products and Their Environmental Impact. *Industrial Crops and Products* **2019**, *139*, 111526. https://doi.org/10.1016/j.indcrop.2019.111526.
(79) Yang, W.; Owczarek, J. S.; Fortunati, E.; Kozanecki, M.; Mazzaglia, A.; Balestra, G. M.; Kenny, J. M.; Torre, L.; Puglia, D. Antioxidant and Antibacterial Lignin Nanoparticles in Polyvinyl Alcohol/Chitosan Films for Active Packaging. *Industrial Crops and Products* **2016**, *94*, 800–811. https://doi.org/10.1016/j.indcrop.2016.09.061.
(80) Zhang, X.; Yang, M.; Yuan, Q.; Cheng, G. Controlled Preparation of Corncob Lignin Nanoparticles and Their Size-Dependent Antioxidant Properties: Toward High Value Utilization of Lignin. *ACS Sustainable Chem. Eng.* **2019**, *7* (20), 17166–17174. https://doi.org/10.1021/acssuschemeng.9b03535.
(81) Yang, W.; Weng, Y.; Puglia, D.; Qi, G.; Dong, W.; Kenny, J. M.; Ma, P. Poly(Lactic Acid)/Lignin Films with Enhanced Toughness and Anti-Oxidation Performance for Active Food Packaging. *International Journal of Biological Macromolecules* **2020**, *144*, 102–110. https://doi.org/10.1016/j.ijbiomac.2019.12.085.
(82) Schneider, W. D. H.; Dillon, A. J. P.; Camassola, M. Lignin Nanoparticles Enter the Scene: A Promising Versatile Green Tool for Multiple Applications. *Biotechnology Advances* **2021**, *47*, 107685. https://doi.org/10.1016/j.biotechadv.2020.107685.
(83) Österberg, M.; Sipponen, M. H.; Mattos, B. D.; Rojas, O. J. Spherical Lignin Particles: A Review on Their Sustainability and Applications. *Green Chem.* **2020**, *22* (9), 2712–2733. https://doi.org/10.1039/D0GC00096E.
(84) Ago, M.; Huan, S.; Borghei, M.; Raula, J.; Kauppinen, E. I.; Rojas, O. J. High-Throughput Synthesis of Lignin Particles (∼30 Nm to ∼2 Mm) via Aerosol Flow

Reactor: Size Fractionation and Utilization in Pickering Emulsions. *ACS Appl. Mater. Interfaces* **2016**, *8* (35), 23302–23310. https://doi.org/10.1021/acsami.6b07900.

(85) Abbati de Assis, C.; Greca, L. G.; Ago, M.; Balakshin, M. Yu.; Jameel, H.; Gonzalez, R.; Rojas, O. J. Techno-Economic Assessment, Scalability, and Applications of Aerosol Lignin Micro- and Nanoparticles. *ACS Sustainable Chem. Eng.* **2018**, *6* (9), 11853–11868. https://doi.org/10.1021/acssuschemeng.8b02151.

(86) Liu, Y. Strong and Flexible Nanocomposites of Carboxylated Cellulose Nanofibril Dispersed by Industrial Lignin. *ACS Sustainable Chem. Eng.* **2018**, *6* (4), 5524–5532. https://doi.org/10.1021/acssuschemeng.8b00402.

(87) Farooq, M.; Zou, T.; Riviere, G.; Sipponen, M. H.; Österberg, M. Strong, Ductile, and Waterproof Cellulose Nanofibril Composite Films with Colloidal Lignin Particles. *Biomacromolecules* **2019**, *20* (2), 693–704. https://doi.org/10.1021/acs.biomac.8b01364.

(88) Rivière, G. N.; Pion, F.; Farooq, M.; Sipponen, M. H.; Koivula, H.; Jayabalan, T.; Pandard, P.; Marlair, G.; Liao, X.; Baumberger, S.; Österberg, M. Toward Waste Valorization by Converting Bioethanol Production Residues into Nanoparticles and Nanocomposite Films. *Sustainable Materials and Technologies* **2021**, *28*, e00269. https://doi.org/10.1016/j.susmat.2021.e00269.

(89) Notley, S. M.; Norgren, M. Surface Energy and Wettability of Spin-Coated Thin Films of Lignin Isolated from Wood. *Langmuir* **2010**, *26* (8), 5484–5490. https://doi.org/10.1021/la1003337.

(90) Qian, Y.; Zhong, X.; Li, Y.; Qiu, X. Fabrication of Uniform Lignin Colloidal Spheres for Developing Natural Broad-Spectrum Sunscreens with High Sun Protection Factor. *Industrial Crops and Products* **2017**, *101*, 54–60. https://doi.org/10.1016/j.indcrop.2017.03.001.

(91) Richter, A. P.; Bharti, B.; Armstrong, H. B.; Brown, J. S.; Plemmons, D.; Paunov, V. N.; Stoyanov, S. D.; Velev, O. D. Synthesis and Characterization of Biodegradable Lignin Nanoparticles with Tunable Surface Properties. *Langmuir* **2016**, *32* (25), 6468–6477. https://doi.org/10.1021/acs.langmuir.6b01088.

(92) Adamcyk, J.; Beisl, S.; Amini, S.; Jung, T.; Zikeli, F.; Labidi, J.; Friedl, A. Production and Properties of Lignin Nanoparticles from Ethanol Organosolv Liquors—Influence of Origin and Pretreatment Conditions. *Polymers* **2021**, *13* (3), 384. https://doi.org/10.3390/polym13030384.

(93) Lourencon, T. V.; Greca, L. G.; Tarasov, D.; Borrega, M.; Tamminen, T.; Rojas, O. J.; Balakshin, M. Y. Lignin-First Integrated Hydrothermal Treatment (HTT) and Synthesis of Low-Cost Biorefinery Particles. *ACS Sustainable Chem. Eng.* **2020**, *8* (2), 1230–1239. https://doi.org/10.1021/acssuschemeng.9b06511.

(94) Cusola, O.; Kivistö, S.; Vierros, S.; Batys, P.; Ago, M.; Tardy, B. L.; Greca, L. G.; Roncero, M. B.; Sammalkorpi, M.; Rojas, O. J. Particulate Coatings via Evaporation-Induced Self-Assembly of Polydisperse Colloidal Lignin on Solid Interfaces. *Langmuir* **2018**, *34* (20), 5759–5771. https://doi.org/10.1021/acs.langmuir.8b00650.

(95) Cusola, O.; Rojas, O. J.; Roncero, M. B. Lignin Particles for Multifunctional Membranes, Antioxidative Microfiltration, Patterning, and 3D Structuring. *ACS Appl. Mater. Interfaces* **2019**, *11* (48), 45226–45236. https://doi.org/10.1021/acsami.9b16931.

Chapter III
New method for preparation of lignin particles

Table of content – Chapter III

Introduction to Chapter III 155

Chapter III. 1. Lignin particles size effect on cellulose nanofibers film structure and properties 157

INTRODUCTION 157

EXPERIMENTAL SECTION 159

Lignin particles preparation. 159

Characterization of the morphology of LP. 159

Preparation of CNF film containing lignin particles. 160

Characterization of the films. 160

RESULTS AND DISCUSSION 162

Characterization of LPtCNF 162

Comparison of structure of LP + tCNF and LPtCNF films. 164

Influence of LP size on UV barrier and antioxidant properties of the films. 166

Influence of lignin particle size on gas barrier properties. 170

CONCLUSION 171

Chapter III. 2. *In-situ* preparation of lignin particles with different nanofiber supports 173

INTRODUCTION 173

EXPERIMENTAL SECTION 175

Chitin nanofibers production. 176

In-situ preparation of lignin particles. 176

Characterization of the suspensions. 176

Film preparation. 178

Characterization of the films. 178

RESULTS AND DISCUSSION 179

In-situ growth of lignin nanoparticles. 179

Interfacial interactions between lignin and the nanofibers. 183

Preparation of films from nanofibers carrying LPs. 186

CONCLUSION 191

Conclusion to Chapter III 193

References 194

Introduction to Chapter III

Chapter II described the preparation of colloids; in **Chapter III** we look in more detail at the interactions between the biobased colloids in suspension and after film formation (**Figure III.1**). First, interactions between LP of different sizes and tCNF are studied and in the second part, we focus on the interactions between lignin nanoparticles and different nanofibers (CNF or ChNF).

As mentioned in the previous chapter, LP from an aerosol reactor are micrometric particles that when integrated into tCNF film can disrupt the nanofibers network and weaken the film. After comparison with the literature, we hypothesized that the size of the particles could be responsible for that network disruption. Therefore, in **Chapter III.1**, we prepare lignin nanoparticles and integrate them in tCNF film with different amounts. We then compare the films' structure depending on LP size. Functionalities relative to the presence of lignin particles and beneficial for food packaging applications are also studied depending on the LP size and content.

As lignin nanoparticles seem promising as active particles in the nanofiber films, further investigation of the preparation method is carried out in **Chapter III.2**. A modified solvent shifting method was used to prepare lignin nanoparticles in the presence of nanofibers. Hence, in this part, we study the influence of the surface charge of two different types of nanofibers: cellulose nanofibers and chitin nanofibers. Interactions between lignin particles and nanofibers in suspension are studied to investigate the particles formation process.

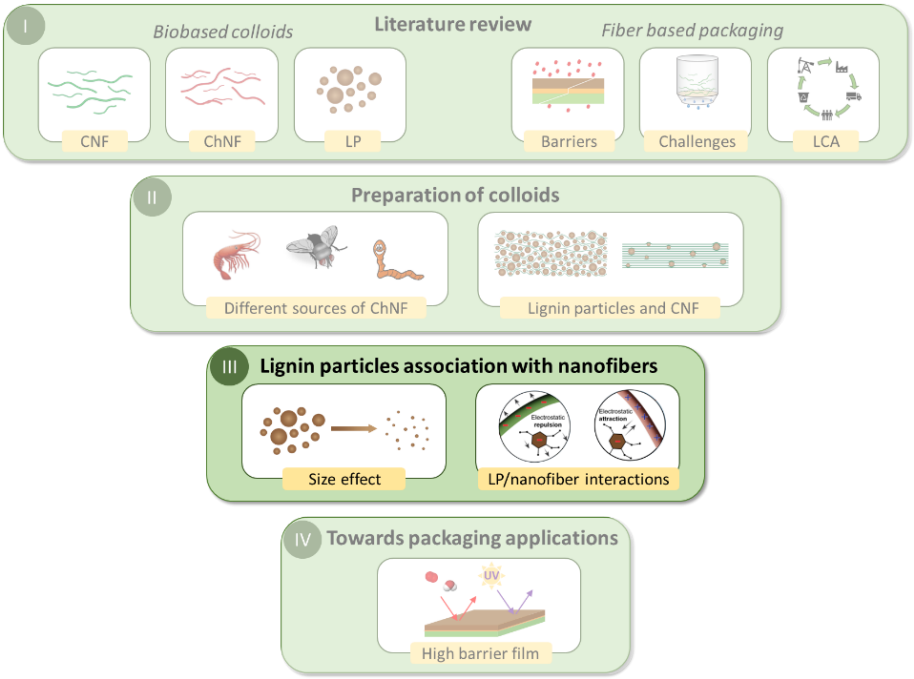

Figure III.1. Global scheme of the PhD project where Chapter III is highlighted.

Chapter III. 1. Effects of lignin particles size on cellulose nanofibers film structure and properties

Adapted from "Integration of lignin micro- and nano-particles in cellulose nanofiber films, size effect on film structure and properties", E. Pasquier, B. D. Mattos, N. Belgacem, O. J. Rojas, J. Bras, manuscript in preparation

INTRODUCTION

The research on nanoparticles has increased in the past decades due to the incredible performance and new properties that arise due to their reduced size and high specific surface area. Understanding the size-related impact of NPs on functions and properties has opened new opportunities in several fields of research with applications in electronics, biomedical, energy harvesting, catalysis, sensing.[1] For example, metallic and semi-conductive NPs present new electronic and optical properties at the nanoscale due to electron confinement and quantum effects.[2] For organic NPs, the main specificity is the high specific surface area that is present at the nanoscale. Even if the high specific surface raises concerns about the nontargeted activity and toxicity of such NPs,[3,4] it also allows high reactivity of the particles for chemical reactions in dispersed state, favor stable colloid suspensions and also leads to increased surface exchange for example to release active molecules.[5]

Biobased organic nanoparticles can be prepared following a top-down approach, for example the extraction of nanoparticles directly from nature, such as cellulose and chitin nanofibers or nanocrystals.[6] A bottom-up strategy is also possible and consists of buildup particles from molecular building blocks, which allows a better control on the NPs properties (size, shape, surface chemistry, among others) by monitoring the synthesis parameters.[7,8]

Bottom-up strategies for nano or microparticles formation were key to enable the application of lignin, a polyphenolic bioactive molecule extracted from wood,[9] in a large range of technologies. Lignin insolubility in water and structure complexity favored its utilization as particles instead of soluble molecules.[10,11] Despite the different synthesis pathways that allow controlling particle sizes,[12] most contributions investigated the influence of LP content and lignin type on a given functionality,[13–16] whereas only few analyzed the impact of particle sizes.[17] Zhang *et al*. recently studied the antioxidant activity of LP from corncob in suspension, and were among the first to show that the radical scavenging activity increased with decreasing particle size.[18] UV absorbance is also enhanced by decreasing the size of LP, which has been

shown in the context of sunscreen.[19] Moreover, comparison between lignin powder and lignin particles in a CNF matrix has recently been investigated;[20] however, there is a gap of knowledge on the effect of particle size of spherical LP embedded in such nanofibrous matrix on its active properties, as well as mechanical strength of the resulting material.

Inspired by previous efforts demonstrating significant improvements on functional properties when using lignin nanoparticles,[20–22] we investigated how the mechanical and functional properties of LP-containing nanocellulose films change when the LP sizes vary from the micrometer to the nanometer scale (**Figure III.2**). Therefore, properties important in the context of food packaging applications, like barrier or antioxidant properties, were studied with regard to LP size and content.

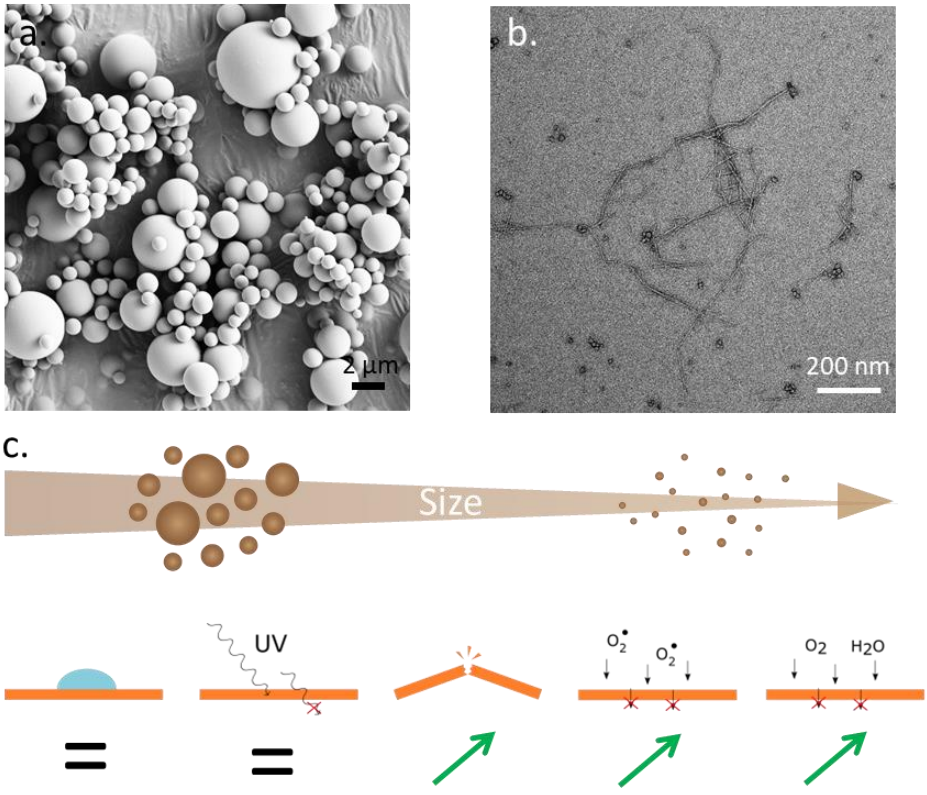

Figure III.2. Images of the micrometric (**a.**) and nanometric (**b.**) lignin particles associated with (**c.**) the effect of LP size on different film properties (water contact angle, UV shielding, mechanical performance, antioxidant activity and gas barrier properties).

EXPERIMENTAL SECTION

Materials. TEMPO-oxidized cellulose nanofibers (tCNF) from wood pulp were obtained from University of Maine, as a 1 wt% suspension. Technical Kraft lignin (Indulin AT) from softwood was purchased from MeadWestvaco (USA) and used for particle preparation. Ammonium hydroxide, anhydrous $CaCl_2$, $K_2S_2O_8$, and ABTS (2,2'-azino-bis(3-ethylbenzothiazoline-6-sulphonic acid)) were provided by Sigma-Aldrich and acetone >99.5% by Roth. All chemicals were used as received.

Lignin particles preparation.

(i) The micrometric LP were prepared with an aerosol reactor as described in **Chapter II.2**. Briefly, lignin was dissolved at 2% (w/v) in ammonium hydroxide solution (14% w/v). The solution was then nebulized, the droplets were dried at 150°C and converted into particles that were collected in a cyclone collector heated at 100°C. Particles are stored at ambient room temperature.

(ii) The nanometric LP were prepared by solvent precipitation.[12,19] The method was adapted by adding tCNF to the antisolvent medium before precipitation. For this purpose, a solution of lignin at 2 g/L in acetone:water (9:1) was prepared and agitated for 1 h with magnetic stirring. After filtration on filter paper, the solution was dropped into 100 mL of dispersed 0.5 % tCNF suspension. The final suspension contained 5 wt%, 9 wt% or 23 wt% of lignin, relative to the total dry mass of lignin and tCNF, depending on the amount of lignin solution added. The suspensions will be referred as LPtCNF X%, where X is the amount of LP relative to the total dry mass of lignin and nanocellulose.

Characterization of the morphology of LP.

The morphology of micrometric LP was obtained by using scanning electron microscopy (SEM), Zeiss Sigma VP, after sputtering 4 nm of Au/Pd on the dry powder. The morphology of the nanometric LP in LPtCNF suspensions was assessed by transmission electron microscopy (TEM) using a JEOL JEM 2100-Plus microscope operating at 200 kV. Suspensions of tCNF and LPtCNF were diluted and cast on copper grid, followed by addition of uranyl acetate to improve the image contrast. Particle size was measured on TEM image with ImageJ software. At least 100 measurements were obtained from multiple images and the size distribution is presented.

Preparation of CNF film containing lignin particles.

All films were prepared to obtain a final basis weight of 47 g/m^2. The film with micrometric LP was prepared by mixing tCNF and LP. Micrometric LP were dispersed in water using 10 min of bath ultrasonication followed by 2 min of tip ultrasonication (amplitude 50%), and then mixed with tCNF using high shear homogenization. The final LP content relative to the total dry mass was 9%. All the films were made by evaporation casting at 23°C and 50% RH until the final mass of the film was constant. Films of nanometric LP were prepared by weighting the correct amount of suspension followed by the same casting and drying method. A film of pure tCNF was also prepared as reference. The film with micrometric LP will be referred as LP + tCNF 9% and the films with nanometric LP prepared *in-situ* will be referred as LPtCNF X%, where X is the amount of LP within the CNF film.

Characterization of the films.

All films were stored in a room at 50% relative humidity and 23°C at least 24h before characterization. Film thicknesses were measured with at least ten repetitions in different places of the film using a micrometer thickness tester for paper.

Surface topography. Atomic Force Microscopy (AFM) was used to assess the surface topography with a Dimension Icon AFM (Bruker) operating in tapping mode. The tip was a silica-coated cantilever (OTESPA® 300 kHz-42 N/m). Films were tapped on smooth surfaces beforehand.

Mechanical strength. A dynamic mechanical analyzer device (DMA) (TA Instruments RSA 3) was used to measure the tensile strength of the films. The test speed was set to 0.1 mm/s and the gap between the clamps was 1.5 cm. The films were cut in 0.5 cm wide strips, with thicknesses being measured prior the tests. At least three repetitions were done.

Wettability. Water contact angle (WCA) was measured with a OCA20 device, using a 5 µL droplet volume. The contact angle was measured with CCD camera, after 2 minutes of deposition. The reported values were average of at least 5 measurements of the WCA in separate parts of the films.

Antioxidant activity. The radical scavenging activity (RSA) of the films was determined with the radical 2,2'-azino-bis(3-ethylbenzothiazoline-6-sulphonic acid) (ABTS) in water. A stock solution of radical ABTS was prepared by activating the radical with potassium persulfate overnight in the dark.[23] After activation, a solution with an absorbance of 0.8 at 734 nm was prepared by dilution, half of it was used a reference while 3 mg of film was added to the other half. The light absorbance at 734 nm was monitored as function of time and the RSA was calculated following Equation (III.1).

$$RSA\ (\%) = 100 - \frac{A_{ref} - A_{sample}}{A_{ref}} \times 100 \qquad \text{(III.1)}$$

Where *Aref* is the absorbance of the reference solution, and *Asample* the absorbance of the sample at a given time.

UV blocking. A UV-Vis spectrophotometer (UV-1800, Shimadzu) was utilized to measure the direct light transmission of the films between 200 and 800 nm. The measure was done in triplicate.

Gas barrier properties. Oxygen transmission rate (OTR) was measured with a Systech Illinois M8001 Oxygen Permeation Analyzer at 23°C and 0% RH in both oxygen and nitrogen chambers. Masks with specific surface area of 2.5 cm^2 were used. Experiments were conducted in duplicate.

Water vapor transmission rate (WVTR) was obtained following T448 om-09 TAPPI standard. Aluminum masks with exchange surface area of 2.5 cm^2 were placed as lid on cups containing $CaCl_2$ as desiccant. The cups were placed in a room with constant temperature and humidity set at 23°C and 50% RH and the humidity inside the cup was considered as 0% RH due to the presence of $CaCl_2$. The weight of the cups was monitored regularly until the increase in mass was constant over time. WVTR in g/(m^2.day) was calculated using the following equation:

$$WVTR = \frac{\Delta m}{A \times \Delta t} \qquad \text{(III.2)}$$

Where *Δm* represents the increase in mass during a given time (Δt) and A the exchange area of the films.

RESULTS AND DISCUSSION

To study the influence of particle size on tCNF film structure and properties, we first prepared lignin microparticles and lignin nanoparticles. Lignin microparticles were prepared with an aerosol reactor by spraying droplets of dissolved lignin and drying them at high temperature. Dry particles with average size of 1.4 ± 0.6 µm were obtained (**Figure III.3a**), more details on the preparation and characterization of such particles were given in the **Chapter II.2**. Preparation and characterization of the lignin nanoparticles will be the focus of the next part.

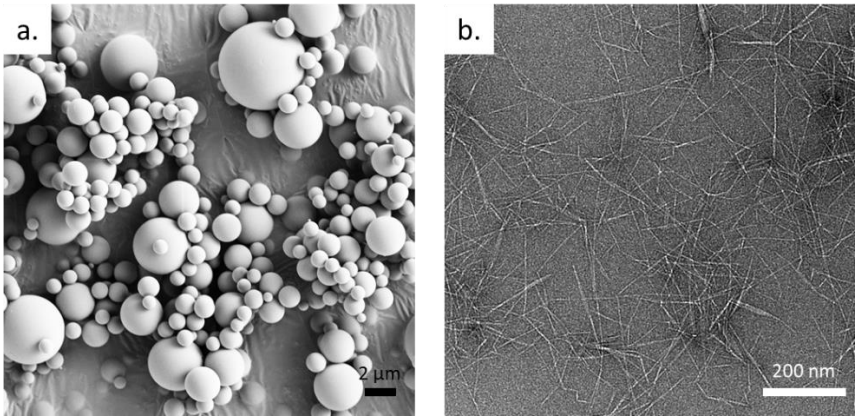

Figure III.3. a. SEM image of micrometric lignin particles prepared by aerosol reactor. **b.** TEM image of TEMPO oxidized nanofibers.

Characterization of LPtCNF

Nanosized LP were prepared by a modified solvent precipitation method, which typically comprises a step of lignin dissolution in a suitable solvent, and a second step of pouring the solution in an antisolvent (*e.g.* water) for lignin precipitation. In our method, lignin was dissolved in a mix of acetone:water (9:1) and the antisolvent, instead of water, was a diluted aqueous suspension of tCNF (**Figure III.4b**). This resulted in spherical single (or very small aggregates) LP in LPtCNF 9% with an average diameter of 18 ± 5 nm (**Figure III.4b**), smaller than the LPs obtained by the common approach directly in water without tCNF (*ca.* 100-500 nm). The size distribution was narrow and no particles above 50 nm were observed (**Figure III.4e**). The presence of nanofibers together with the LP prevented the use of conventional technics like DLS or zeta-potential to characterize the LPs. **Figure III.4a** and **c** show the TEM images of the suspension of LPtCNF 5% and LPtCNF 23% associated with their size distribution. The average diameter of LP in LPtCNF 5% was 18 nm with 90% of LP under 25 nm. The LP in LPtCNF 23% had an average size of 36 nm with 90% of LP under 75 nm.

Increase in lignin content led to an increase in LP size and size distribution, this is in accordance with literature as increase in final lignin concentration usually lead to larger particles size.[12]

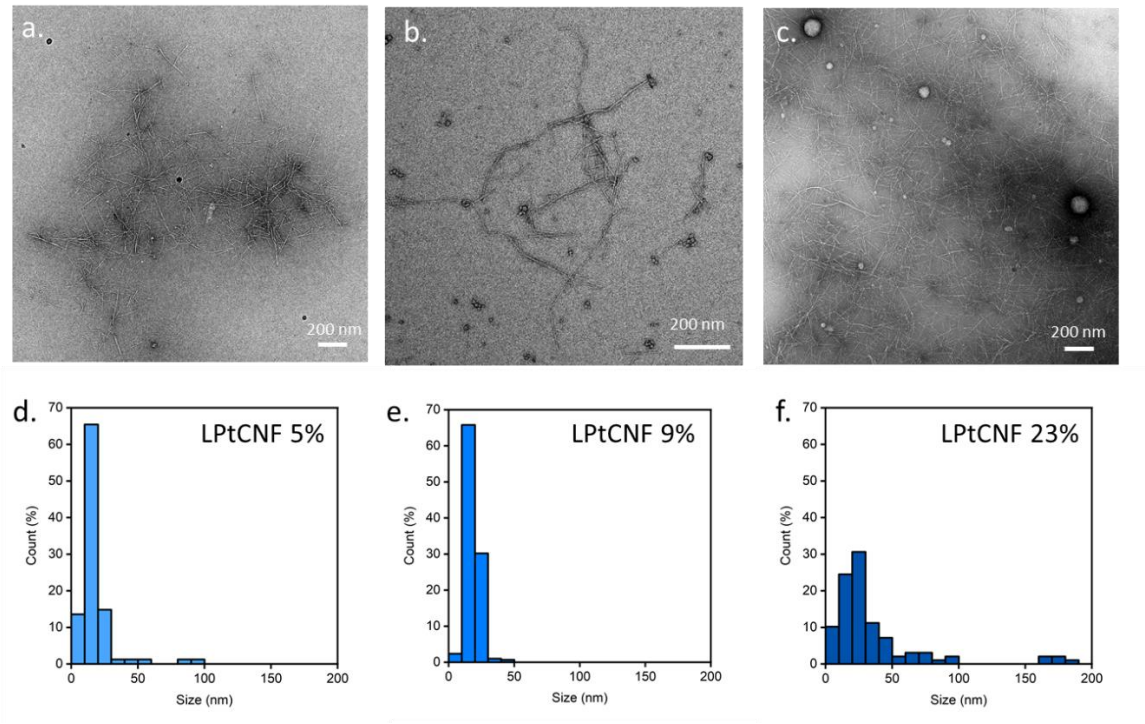

Figure III.4. TEM images of the LPtCNF with 5% (**a.**) 9% (**b.**) and 23% (**c.**) of LP prepared *in-situ* and their respective size distribution measured from the TEM images **(d-f)**.

The mechanism of formation of LP by solvent shifting has been thoroughly studied.[24,25] Particle formation starts with the nucleation step, by precipitation of the high molecular weight lignin moieties that are usually less soluble in water, followed by growth of the particles with low molecular weight and more hydrophilic lignin, thus concentrating more hydrophilic groups of lignin at the particle surface. The mechanism of LP formation with an aerosol reactor has been investigated to a smaller extend.[26,27] However, it was reported that particles first dry on the surface and then shrink isotropically when solvent evaporate from the inside leading to spherical particles with smooth surface.[26] Suzuki *et al*. studied the surface energy of LP from aerosol reactor compared to non-structured Kraft lignin.[27] They emphasized the polar nature of LP and reported higher hydrophilicity of the LPs when compared to powdered Kraft lignin, thus revealing the presence of functional groups such as phenolic and aliphatic hydroxyls or ether groups being dominant at the LPs surface.

Although the preparation method to obtain micrometric or nanometric particle was different, we used the same lignin precursor. Therefore, their surface chemistry should be similar due to

the presence of hydrophilic groups on the surface for both methods. The charged surface as well as presence of hydroxyl groups on the LP surface should play an important role in the interfacial interactions between LP and tCNF. Thus, the main difference between both types of particles is their size as they differ by a factor 100 (1.4 ± 0.6 µm for the aerosol reactor technology *vs* 18 ± 5 nm for the solvent shifting method), with size distribution also varying, nanoparticles being less polydisperse. The impact of particle size on their integration in tCNF matrices and functionalization of these matrices will be assessed in the next part.

Comparison of structure of LP + tCNF and LPtCNF films.

Films containing 9 wt% of LP were prepared, by casting and drying at 23°C, with the two different kind of particles. The films will be referred as LPtCNF 9% and LP + tCNF 9% for the film with nanoparticles prepared *in-situ* (in the nanofiber suspensions), and the film formed by mixing microparticles and tCNF *ex-situ*, respectively. **Figure III.5a-c** show the visual aspects of the dried films, which appeared homogeneous at the macroscale. The presence of LP added light brown color to the films which was more pronounced in the presence of microparticles. The film surface was imaged by AFM as displayed in **Figure III.5d-f**, the difference in particles size strongly influences the roughness of the films as shown by the height scale of the images.

The cross-sections of the films show the internal structure and repartition of the LP within the films. In the LPtCNF 9% film, single nanoparticles are not visible due to their small size and no large aggregates are present. The film kept the well-known lamellar structure of the tCNF film. On the other hand, the microparticles in LP + tCNF 9% film are clearly visible and homogenously distributed within the film. The lamellar structure of tCNF is still visible however, it is disrupted by the presence of lignin microparticles, and voids are visible around the LPs.

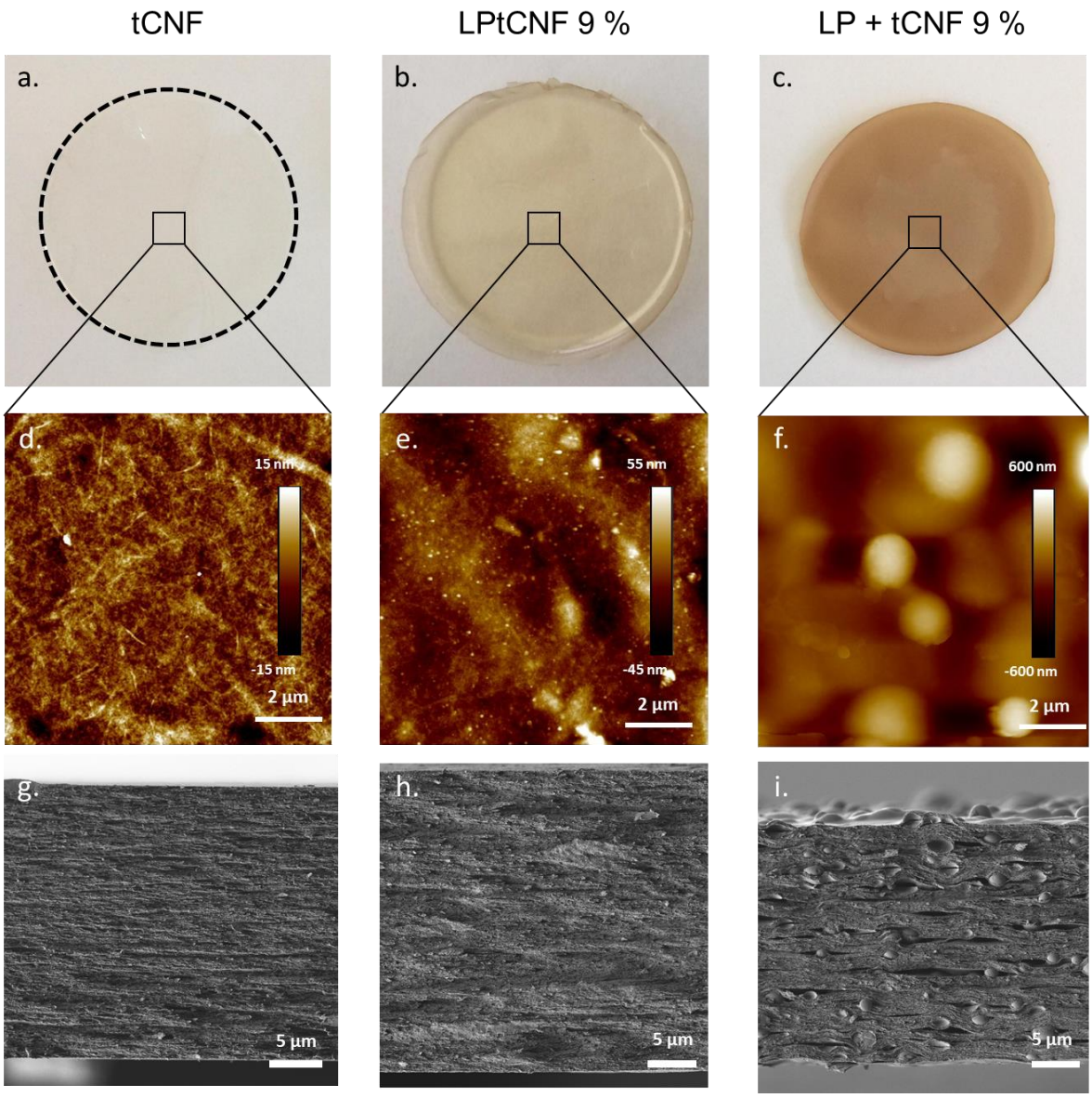

Figure III.5. Visual aspects of the films of tCNF (**a.**), LPtCNF (**b.**) and LP + tCNF (**c.**) containing 9% of lignin particles associated with the respective AFM images of their surface (**d-f**) and SEM images of their cross-section (**g-i**).

The influence of the LPs size on the mechanical performance of the films was investigated by tensile tests, displayed in **Figure III.6a**. Both the maximum stress and strain were impacted by the presence of LP; however, the decrease was more pronounced in the presence of microparticles. This is also true regarding the elastic modulus of the films, with tCNF film displaying a Young's modulus of 3.3 ± 0.3 GPa whereas LPtCNF 9% and LP + tCNF 9% showed 2.6 ± 0.4 GPa and 1.6 ± 0.1 GPa respectively. The larger size of the microparticles had more influence on the nanofiber network disruption which led to significant decrease in both elastic modulus and tensile strength.

The promising results observed in the LPtCNF films incentivized the preparation of films containing different amount of lignin nanoparticles to investigate the influence of LP amount on films properties. **Figure III.6b** shows similar mechanical properties of films containing 5% and 23% of LP made *in-situ* when compared to the LPtCNF 9%. This indicates that even 23% (mass fraction) of small lignin particles cannot disrupt further the fibrillar tCNF network, while already 9% of microparticles reduces remarkably the interfibrillar network.

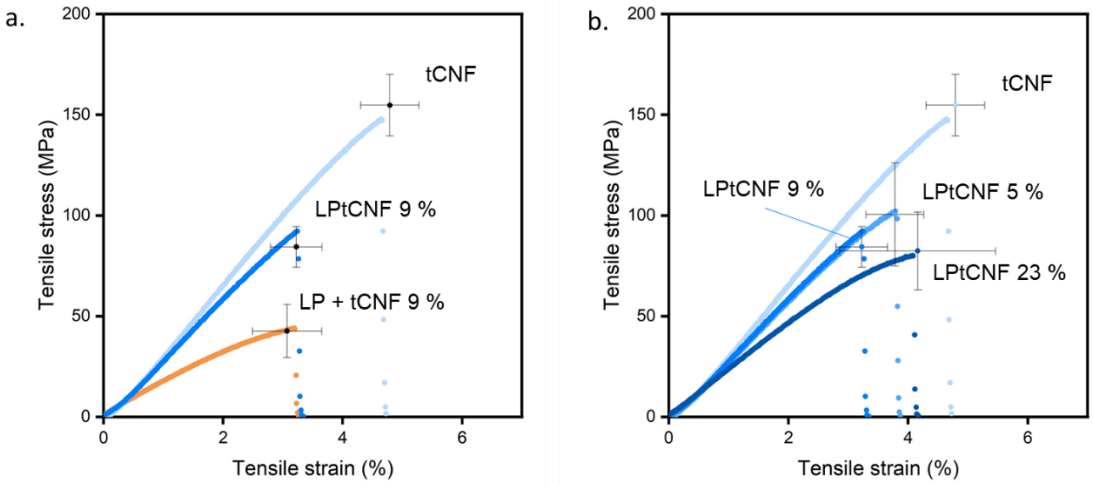

Figure III.6. Tensile mechanical properties of the films as function of the LP size (a.) and as a function of the LP content (b.)

Influence of LP size on UV barrier and antioxidant properties of the films.

Films of CNF containing lignin or lignin particles were shown to display relevant properties for packaging applications. In fact, lignin, due to its phenolic nature, is UV absorbent and has radical scavenging properties that could be interesting to increase food stability regarding light and oxygen.[28] Moreover, CNF films offer high barrier against oxygen as a result of its capability to form tight networks driven by hydrogen bonding and its semi-crystalline nature.[29] Hence, we measured properties relative to food packaging applications such as anti-oxidant behavior, transparency and surface hydrophilicity.

Lignin phenolic character is relevant for radical scavenging. Oxygen or light can interact with food and produce radicals that oxidize food which induce flavor loss and change of color and texture. In presence of antioxidant molecules, radicals can be stabilized and prevent food spoilage.[30] Phenolic molecules such as lignin can donate electrons to stabilize external radicals, and then create phenoxy radicals that are stabilized within lignin. Here the antioxidant activity of the films was measured using ABTS radical as it is soluble in water, considering that the

presence of an organic solvent (ethanol, methanol) would dissolve lignin and interfere with the measurements. **Figure III.7a** shows the antioxidant behavior of the films with the different LP sizes. The decrease in radical activity was significantly faster for the film containing nanoparticles (LPtCNF 9%), when compared with microparticles (LP + tCNF 9%). This can be correlated with the lignin particle surface available for reaction. Considering the particles as perfect non-porous spheres, we estimated the LP nanoparticles to have surface area 6000 times higher than the microparticles. Similar effect is observed while increasing the mass of LP in the film (see **Figure III.7b**). Due to their nanoscale, release of particles from the film during measurement is also possible and would positively impact the measurement. Lignin release has not been quantified here; however, it is assessed in the next subchapter (**Chapter III.2**).

Similar increase of antioxidant activity with decreasing LP size has been recently observed by Zhang *et al*. when measuring the antioxidant capacity of LP directly in suspension.[18] Moreover, Gerbin *et al*. compared the radical scavenging capacity of dissolved lignin and LP and found that LP had slightly lower antioxidant activity due to lower accessibility of phenolic groups that could be in the core of the particles.[31] In addition, when LP were incorporated in CNC film, the activity was also decreased compared to LP alone because of the limited access to the lignin particles inside the film. Besides, the antioxidant activity is directly linked to the phenolic hydroxyl content of lignin, the molecular weight of lignin and its polydispersity are also factors that could influence the antioxidant response.[32] Hence these results are directly linked to the type of lignin used, which opens possibilities to fine tune antioxidant capacity in LP enriched matrices.

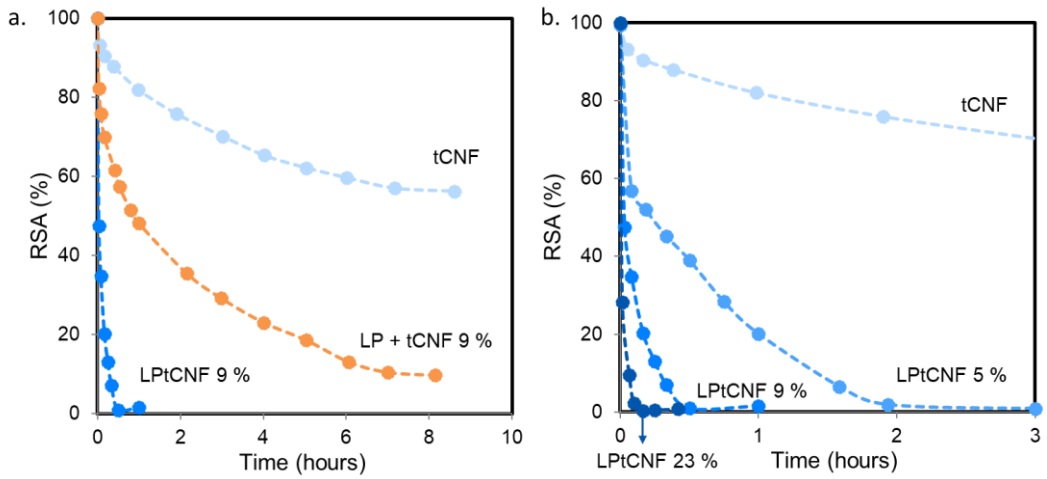

Figure III.7. Radical scavenging activity (RSA) as a function of time depending on the LP size (a.) and on the LP content (b.)

Transparency is also an important asset in packaging materials, especially for fresh food packaging. However, UV light is detrimental for food and can cause photo-oxidization and photo-degradation of fat and proteins for example.[33] UV light can also degrade the packaging itself which would alter its primary protective function. UV protection while keeping some transparency is a good compromise to satisfy both consumer and retailer. **Figure III.8** displays the light transmittance of the films in the UV-Vis range. tCNF film has high transparency, around 90% across the visible light range, which is explained by the high density of the film and homogeneous nanosize of the fibers.[34] The incorporation of small loads of LP reduced the transmittance in the UV range (200 – 350 nm) to near zero for all the films containing LP. Similarly, to the antioxidant behavior, UV blocking is related to the phenolic nature of lignin. However, in the visible range, the transmittance also decreased depending on the LP content and size. Increasing the LP content led to significant decrease in visible transmittance, with near zero transmittance over the whole UV-Vis range when using lignin microparticles.

In the case of nanoparticles, the particles are smaller than the wavelength of light then the light scattering follows the Rayleigh scattering rules where the intensity of the scattered light is proportional to particle diameter to the power six.[35] The higher the scattering the lower the transmittance,[34] hence, the particles size is of great importance for films transparency. This also explains the low transmittance of LPtCNF 23% as in this film the LP content increased as well as the LP size, two parameters that go towards reduction of transmittance. Porosity of the films and size distribution of the pores could also highly influence their transparency.[34] Therefore, a notable size effect of the LP on the film properties is observed. In comparison, it has been recently reported that incorporation of lignin powder to CNF film also resulted in near zero transmittance in the UV and visible range.[20]

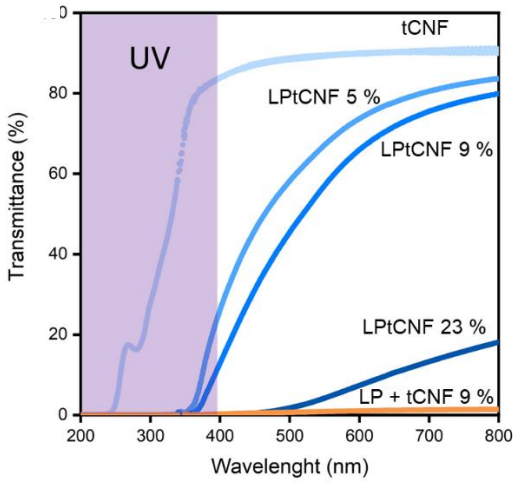

Figure III.8. Transmittance of the different films, the UV domain is highlighted between 200 and 400 nm.

Furthermore, to have an insight on surface water interactions, the water contact angle (WCA) was measured. No clear difference was observed between the films. LPtCNF 5% had the highest contact angle at 50 ± 5° while LPtCNF 9% had the lowest contact angle at 37 ± 9°. The reference tCNF film had a contact angle of 46 ± 1° (and LPtCNF 23%, 41 ± 2°, LP+tCNF, 49 ± 9°). Here the parameter that influenced the contact angles was any change in porosity of the films that would increase the water absorption and at the same time decrease the contact angle. Surprisingly, the film containing micrometric LP which appeared more porous from the cross-section images, had a WCA equivalent or higher than the other films. Moreover, due to high standard deviation, no clear trend was observed. The surface energy of cellulose and lignin colloids can be considered rather similar given the hydrophilic nature of their surface. Despite the presence of hydrophobic moieties in lignin, lignin particles formed by precipitation have lower surface energy than lignin due to the rearrangement of the molecules during precipitation. The hydrophobic groups are oriented towards the core of the particle away from water while the hydrophilic groups turn towards the surface of the particles.[24,25] It was reported that thin films of LP had contact angle of 26.8 ± 0.8° while thin film of dissolved lignin had contact angle of 62.8 ± 2.0°.[36]

Influence of lignin particle size on gas barrier properties.

Gas barrier is key for food packaging, with specific type and level of barrier needed depending on the foodstuff to be protected. Typically high barrier (i.e. low WVTR or OTR) are the most difficult to obtain.[37] CNF are already known to have high barrier against oxygen at low humidity[29] but low barrier against water vapor. Water vapor permeability of cellulosic based materials has been a limiting factor for the application of these materials in food packaging. Here, we aim to investigate the impact of LP on the gas barrier properties of tCNF films.

Figure III.9 displays the oxygen transmission rate (OTR) and water vapor transmission rate (WVTR) of the pure and composite films. First, the oxygen transmission rate (OTR) value for tCNF here is surprisingly higher than what can be found in literature (3 cm^3/m^2.day at 50% RH and 23°C).[38] OTR is influenced by the thickness, the film making process and the raw material itself. The high OTR value could be explained by the quite low thickness of the films (around 30 µm), the absence of a heat treatment or compression in the film preparation, and to a lesser extent to type of tCNF. In our case, fibers were short and homogeneous and it has been reported that the larger the aspect ratio, the lower the OTR due to high entanglement of the fibers and increase of tortuosity and diffusion pathway for molecules to pass through the films.[39] Moreover, heat treatment during drying increases the crystallinity of CNF which improves OTR.[38,40]

In comparison with tCNF, LPtCNF 5% had similar barrier properties but LPtCNF 9% and LPtCNF 23% had lower oxygen permeability. It should be noticed that LPtCNF 9% and 23% had an OTR below the detection limit of the device which is 1 cm^3/m^2.day. Improvement in OTR with increasing amount of LP could be due to pore filling and increase in diffusion pathway length.[41] While the presence of lignin nanoparticles decreased the OTR, the same amount of microparticles increased the OTR of tCNF from 47 cm^3/m^2.day to 110 cm^3/m^2.day. Particles with larger size were not able to fill the pores and increased the porosity of the films due to the size difference between the nanofibers and the particles, as seen on the SEM images of the cross-section. The presence of LP in the films had no negative impact on the WVTR of the samples. On contrary, there was a slightly improvement in WVTR in the film LPtCNF 23%, which arises from the formation of a packed particle-fiber network, with minimized interfibrillar spaces that are filled by very small LP.

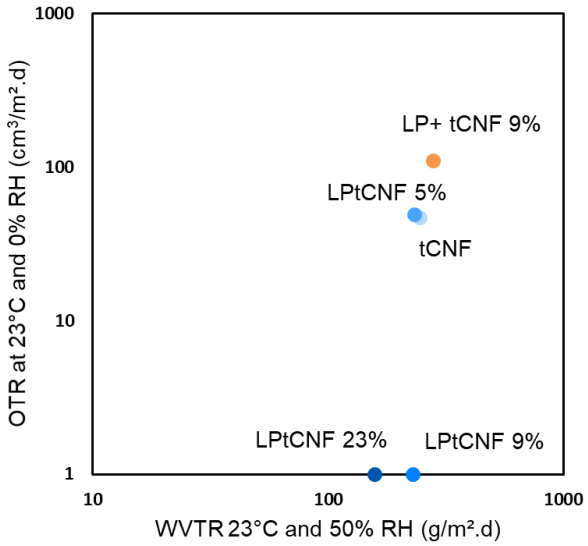

Figure III.9. Gas barrier properties including oxygen transmission rate (OTR) and water vapor transmission rate (WVTR) of the films.

In summary, LP had positive impact in several functional properties that are relevant for food packing. Particle size was significant for the reactivity of lignin towards radicals and the transparency of the films. Films containing lignin nanoparticles are promising for food packaging applications as they demonstrated antioxidant properties, high UV blocking capacity while maintaining transparency. Furthermore, even though the water sensitivity of tCNF and low barrier towards water vapor needs to be further improved, the films containing lignin nanoparticles had high barrier against oxygen at low humidity.

CONCLUSION

Lignin nanoparticles were prepared by adapting the solvent precipitation method, particles with diameter of 18 ± 5 nm were obtained with narrow size distribution. To compare the size effect of LP on tCNF film properties, LP with micron size from aerosol reactor were used. Film containing nanoparticles demonstrated higher tensile strength, transparency, antioxidant activity and oxygen barrier properties than the microparticles counterpart. The increased surface area of the nanoparticles was responsible for its increased reactivity towards free radicals. We demonstrated that particles size is an important factor that should be considered, additionally to particle content, in supporting matrices.

The lignin nanoparticles prepared by solvent shifting *in-situ* with the tCNF showed promising results, arising from the small LP size and narrow size distribution that are obtained more easily

by following our method for particle formation. This is a new method that needs further studies to determine the mechanism of particles formation in the presence of nanofibers. This will be the topic of the next chapter where *in-situ* precipitation of lignin particles in the presence of two different nanofibers (cellulose and chitin) will be further studied.

Chapter III. 2. *In-situ* preparation of lignin particles with different nanofiber supports

Adapted from "Lignin nanoparticle nucleation and growth on cellulose and chitin nanofibers", E. Pasquier, B. D. Mattos, N. Belgacem, J. Bras, O. J. Rojas, published in Biomacromolecules, 2020

INTRODUCTION

Materials assembled from polysaccharide nanofibrillar networks are known for their remarkable mechanical performance. Highly cohesive structures arise from the interconnectivity and entanglement of high-aspect ratio nanofibers, which leads to a high density of physical crosslinks.[42,43] Fibrillar biocolloids, such as cellulose (CNF) and chitin (ChNF) nanofibers, are amongst the most suitable building blocks for the development of materials. This is due to their high strength, flexibility and morphology that yield tight, interconnected nanonetworks upon drying from aqueous media.[44–46] Unlike covalent bonding, supramolecularly-driven colloidal interactions can readily reform after bond breaking under mechanical stress, leading to a cascade of short-range bond breaking/reforming events that yield materials that are both tough and strong.[47] Moreover, the biological and chemical inertness of CNF and ChNF make them ideal supports for selective incorporation of functionalities, such as hydrophobicity, flame retardancy or conductivity, among others.[48–50] Compositing with nanoparticles (so far mostly inorganic), represents a low-energy route to introduce functionalities in CNF or ChNF matrices,[51,52] avoiding the need for the otherwise typical non-sustainable, expensive and time-consuming protocols used for chemical modification.[53]

Here we demonstrate the introduction of functional nanoparticles within nanofibrillar matrices by simply mixing and *in-situ* nucleation. The latter provides better control over particle-fiber interactions and the associated morphologies of the resulting networks. Nucleation of metallic nanoparticles on biobased nanofibers have been shown to produce high formation yields and, simultaneously, leads to a good dispersion of narrow sized nanoparticles across the network.[54,55] Nucleation and growth take place from the adsorption of the metallic precursor on the nanofibrils surface followed by the reduction of the precursor with the addition of an external reagent. Interactions between given precursors and supporting nanofibers, their nature and strength, have been shown to be key factors to enable efficient functionalization. For instance, Olsson *et al*. successfully synthesized fully anchored cobalt ferrite ($CoFe_2O_4$)

nanoparticles using nanocellulose aerogel templates. In their work, the initial Fe/Co metal cations adsorbed on the nanocellulose surface interacted strongly with the formed complexes in the liquid phase, leading to the absence of free nanoparticles in the system.[56] Padalkar *et al*. used a cationic surfactant to monitor the interactions between cellulose nanocrystals and metallic ions (Ag, Au, Cu, Pt) for the formation of supported nanoparticles.[57] Using similar protocols, Errokh *et al.* used modified CNFs as templates for the synthesis of silver nanoparticles, aiming at anti-microbial composites with limited silver release.[58] Although related formation mechanisms are not fully understood, it is known that interfacial interactions play a determining role for the nucleation and *in-situ* growth of metallic nanoparticles on biobased nanofibers. Much less is known in relation to the formation of organic nanoparticles on biobased templates, which is a subject that deserves attention, especially given the prospective uses of such systems.

Here we investigated the use of biobased nanofibers – CNF and ChNF – as nucleating solid supports for the formation of organic lignin nanoparticles (LPs). The latter results in a fully bio-based material, which can potentially address concerns related to the generation of microplastics from synthetic polymers used in packaging materials. The polyphenolic nature of lignin leads to interesting photocatalytic effects, such as UV shielding and antioxidant activity, which are especially relevant for food packaging considering that light is very detrimental for food.[33] Lignin colloids have also been explored in sunscreens applications[59] and recent developments indicate a great promise for nanocellulose in cosmetics. Thus, lignin can bring great benefits if incorporated in fibrillar matrices, especially in the form of nanoparticles which could be exploited to impart improved mechanical performance.[20,21]

In this study, we propose a new method for creating tailorable particle-fibers nanonetworks with better control over their final morphology by exploring interfacial interactions during the heterogenous nucleation and growth of lignin nanoparticles. Our method is inspired by the solvent shifting method, which is scalable, low cost and leads to round-shaped particles.[60,61] We use chitin (positively charged) and cellulose (slightly negatively charged) nanofibers as templates to investigate the effects of such different nucleation sites for the *in-situ* formation of lignin constructs (**Figure III.10**). We discuss adsorption and interfacial phenomena in relation to the biocolloidal components to better understand the interactions involved during the formation process. Lastly, films were synthesized from our hybrid colloidal suspensions, aiming to combine the ability of the nanofibers to create strong materials with the lignin photocatalytic properties, offering a viable platform for application in films for food packaging.

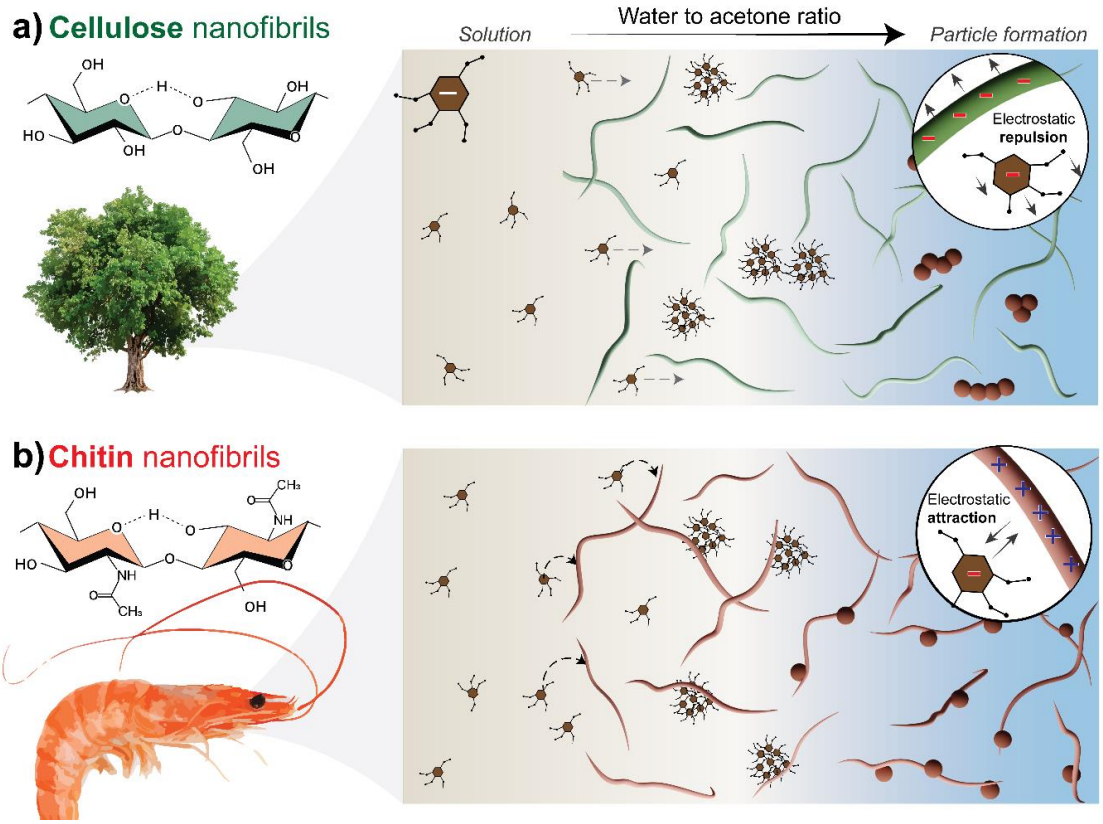

Figure III.10. Schematic illustration of the solvent exchange process that leads to the nucleation and growth of lignin nanoparticles in the presence of **a.** cellulose and **b.** chitin nanofibers, both of which acted as templating supports. From an increased water-to-acetone ratio, lignin nanoparticles (LPs) were formed with a morphology that is controlled by the surface chemistry of the nanofibers. As such, LPs are formed loosely in suspension with non-interacting cellulosic templates. Conversely, strongly anchored LPs were formed on the surface of the chitin nanofibers, *via* electrostatic effect.

EXPERIMENTAL SECTION

Materials. Technical Kraft lignin (Indulin AT) from softwood was obtained from MeadWestvaco (USA). Cellulose nanofibers (CNF) were provided by the Centre Technique du Papier (CTP, Grenoble, France). Cellulose was sourced from bleached birch pulp refined and enzymatically pre-treated before homogenization (3 passes at 1500 bars) with an Ariete homogenizer from GEA (Italy). Chitin flakes of shrimp shells, $K_2S_2O_8$, and ABTS were purchased from Sigma Aldrich and acetone >99.5%, KOH, NaOH, HCl from Roth, all chemicals were used as received.

Chitin nanofibers production.

Chitin nanofibers (ChNF) were produced from chitin flakes of shrimp shells; the purification of the fibers followed the procedure of Ifuku *et al*.[62] First, residual proteins were removed with KOH (5 wt%, 6 h, 100 °C). After washing to neutral pH, the fibers were soaked in HCl (5%, 48 h, 25 °C) to remove any minerals. Then, another deproteinization step was conducted with KOH (5 wt%, 48 h, 25 °C) followed by bleaching with sodium chlorite (2 h at 80 °C). Finally, the fibers were defibrillated with a grinder (Masuko) to obtain chitin nanofibers (ChNF). The acetylation degree of the ChNF suspension was 91 %, measured by conductimetric titration.

***In-situ* preparation of lignin particles.**

The *in-situ* preparation of lignin particles was adapted from the classic solvent shifting method[63] but in the presence of nanofibers in the anti-solvent medium (water). For this purpose, 50 mg of lignin were dissolved in acetone:water (9:1) at 2 g/L. After mixing for 1 h, the solution was filtrated and the filtrate was dropped into 100 mL of a suspension of dispersed cellulose (CNF) or chitin (ChNF) nanofibers at 0.5%, aiming at a final lignin content of 9%. As a reference, the same experiment was conducted in the absence of nanofibers. In addition, suspensions with 15% and 23% of lignin were also prepared with chitin nanofibers. The proportion of each component was always calculated on a dry mass basis.

Characterization of the suspensions.

Morphology. The colloidal suspensions were imaged with transmission electron microscopy (TEM) using a JEOL JEM 2100-Plus microscope operating at 200 kV. Samples were dropped on copper grids and uranyl acetate was used as negative staining. At least 10 images were obtained by samples and the most representative is used for the discussions. Lignin particle size was measured from TEM images using Image J software with at least 100 measurements using at least three different images.

Surface charge measurement. The zeta-potential of the nanofibers before and after lignin particles preparation was measured with a Zetasizer Nano ZS (Malvern Panalytical) with a folded capillary cell. The concentration of the suspensions was 0.1 wt.% and their conductivity was adjusted to 0.65 mS/cm. The average of three measurements was used in the discussion.

Hydrodynamic size measurement. The size of the lignin particles was evaluated by dynamic light scattering (DLS) in a VASCO device (Cordouan Technologies), using the Cumulant method. The suspension was diluted around 0.05 wt.% before measurements.

Lignin quantification by UV spectroscopy. To understand the interactions between lignin and the nanofibers, a separation by centrifugation was carried out and lignin was quantified in the sediment. After centrifugation at 10 000 rpm for 5 min, the supernatant containing the LP and the sediment containing the nanofibers were separated and the sediment was washed 2 times with water, to remove residual LP. Lee *et al.*[64] showed that it was possible to quantify the amount of dissolved lignin with UV-Vis spectroscopy after dissolution in NaOH. Following their method, dissolution of the lignin present in the sediment with NaOH 0.035 M was carried out; for this purpose, NaOH was added to the sediment and dissolved lignin was collected after centrifugation (10 000 rpm, 5 min). The dissolution was repeated two more times to extract the lignin. After bringing the supernatants together, the solutions were analyzed with UV spectroscopy (UV-1800, Shimadzu). Dilution was done when necessary. To quantify the lignin, a calibration curve with known amount of lignin dissolved in NaOH 0.035 M was performed beforehand (**Figure III.11**).

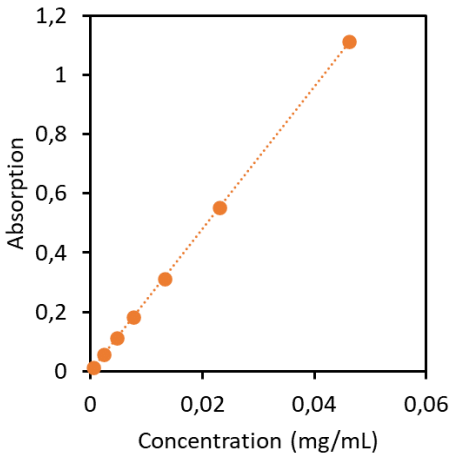

Figure III.11. UV-Vis absorbance calibration at 287 nm for lignin dissolved in NaOH 0.035 M. Linear regression: $Abs = 24.035\ C - 0.0007$ with coefficient of regression: $R^2 = 0.9999$

Lignin interactions with the nanofibers. Paper chromatography was used to study the interactions between dissolved lignin and the nanofibers. First, the stationary phase was prepared; for this purpose, chromatography paper was coated with 0.5% nanofibers suspension using a bar coater (K Control Coater, RK Print Coat Instruments Ltd.). A spirally wound bar with 0.25 mm wire diameter was used, leading to a wet coating thickness of 150 µm. The coatings were dried in an oven at 105°C. The mobile phase was composed of an acetone:water mixture (4:6 v:v); the ratio was optimized to obtain a suitable result. Lignin was dissolved in

acetone:water (9:1 v:v) and filtrated similarly to the lignin solution used for lignin particle preparation. A drop of 5 µL solution was deposited on the coated paper and the paper was placed in a beaker containing the mobile phase. Image analysis was performed with Python, after cropping the image; the full images were analyzed averaging the blue pixel values of each line. The image length was normalized for comparison purposes.

Film preparation.

Films were prepared for a grammage of 47 g/m^2. Therefore, a given suspension volume was cast on PTFE Petri dish and degassed, to avoid bubbles in the suspension. The suspensions were dried at 50% relative humidity (RH) and 25 °C. The films were acclimated at 50% RH and 25°C before analysis.

Characterization of the films.

All films were stored at least 24h in 50% RH and 25°C before characterization. *Mechanical strength.* Tensile tests were conducted with a dynamic mechanical analyzer device (DMA) (TA Instruments RSA 3), with a rate of 0.1 mm/s and a gap between the clamping jaws of 15 mm. Strips of 0.5 cm width were cut in the films, and their thickness and exact width were measured before analyses.

Scanning Electron Microscopy (SEM). The film morphology was studied with a SEM (FEI Quanta 200), films were broken in liquid nitrogen and the cross-section was imaged. Metallization with carbon was done before imaging.

Atomic Force Microscopy (AFM). The film's top surface was imaged with a Dimension Icon AFM (Bruker) operated in tapping mode. Samples of the films were attached to a support with double-sided tape. At least 3 images were obtained from the samples and the most representative ones were used for discussion.

Transparency. Transmittance of the films was measured with a UV-Vis spectrophotometer (Shimadzu) from 200 nm to 800 nm.

Wettability. Water contact angles were measured with an OCA20 device, equipped with a CCD camera, using a drop volume of 5 µL. Measurement were repeated at least 3 times and the angle was measured after 2 min of contact, using the SCA20 software.

Antioxidant activity. The radical scavenging capacity of the films was determined using 2,2'-azino-bis(3-ethylbenzothiazoline-6-sulphonic acid) (ABTS). First, a stock solution of radical was prepared mixing 18 mg of ABTS with and 3.3 mg of potassium persulfate as an oxidant to form the radical $ABTS^{+\bullet}$ in 5 mL of water.[23] After overnight reaction, the solution was diluted in order to have 20 mL solution with an absorbance of 0.8 at 734 nm. This solution was divided equally in two vials: the first one was the reference and 3 mg of films were added to the second one. The decrease in absorbance at 734 nm was measured as function of time as the film reacted with the radical. The radical scavenging activity was calculated following Equation (III.3).

$$RSA\ (\%) = 100 - \frac{A_{ref} - A_{sample}}{A_{ref}} \times 100 \qquad \text{(III.3)}$$

With A_{ref} the absorbance of the reference solution, and A_{sample} the absorbance of the sample at a given time. Tannic acid was used as a model molecule to compare the samples. For this purpose, the same experiment was realized but instead of a film, different quantities of tannic acid were added to the radical solution, and after calculation of the RSA, a calibration curve of the RSA as a function of the mass of tannic acid was plotted. The Tannic Acid Equivalent (TAE) was calculated by dividing the equivalent mass of tannic acid reaching the same RSA than the sample by the mass of the film. All the comparisons were made after one hour of reaction with the radical solution.

Particles release study. Release of lignin and lignin particles from the films was studied in the same conditions than the antioxidant properties of the films. For this purpose, films (3 mg) were placed in 10 mL water and the samples were agitated. After one hour, the samples were centrifuged, and the supernatant was analyzed by UV spectroscopy after adjusting the NaOH concentration to 0.035 M.

RESULTS AND DISCUSSION

In-situ growth of lignin nanoparticles.

CNF and ChNF were used as nucleating support for the formation of lignin nanoparticles (LPs) by solvent shifting. We enriched the water, used as antisolvent medium for the exchange process, with CNF and ChNF to which we poured an acetone solution of lignin. When the acetone fraction in the mixture reached values < 20%, the colloidal particles were formed due to the limited lignin solubility in water.[61] Remarkably, using an antisolvent with the presence of nanofibers, the morphology of the LNPs differ greatly form that observed in their absence (**Figure III.12**). Images from Transmission Electron Microscopy (TEM) of CNF and ChNF,

before and after LP formation, are shown in **Figures III.12a-b** and **III.12d-e**, respectively, along with the nanoparticle size distribution. For comparison, the morphology and size distribution (TEM and DLS) of lignin particles produced in the nanofiber-free antisolvent are displayed in **Figures III.12g-h**.

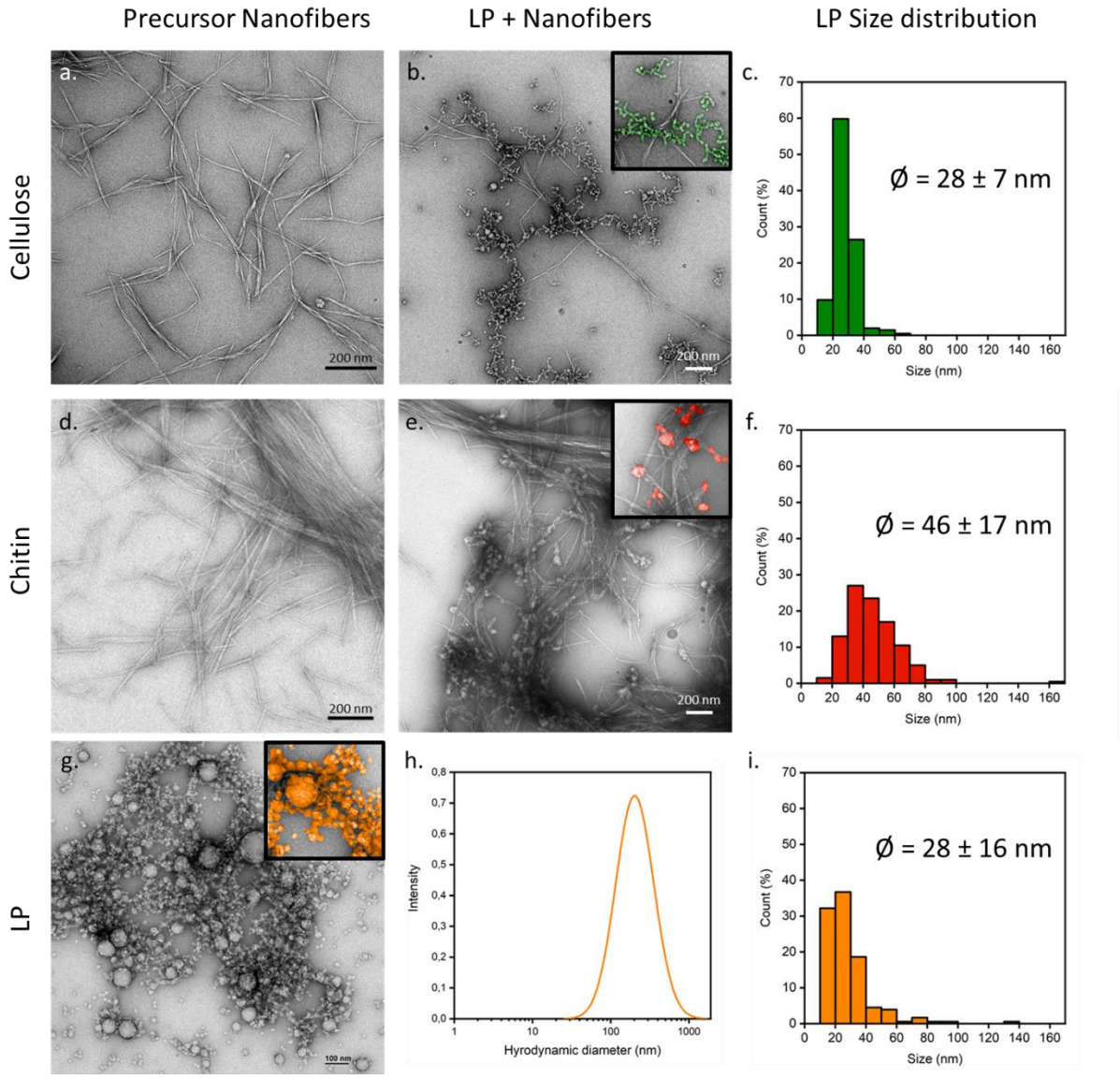

Figure III.12. TEM images of nanofibers (CNF, **a** and ChNF, **d**) and the respective system after formation of lignin particles (9%), LP_{CNF} (**b**) and LP_{ChNF} (**e**). The particle size distribution measured from TEM images is also included (LP_{CNF}, **c** and LP_{ChNF}**, f**) as well as lignin particles prepared in the absence of fibers (TEM, **g**) with their size distribution reported from DLS (**h**) and from TEM imaging (**i**).

The average diameter of lignin nanoparticles (LP) prepared in the presence of cellulose nanofibers (LP_{CNF}) had a lateral dimension equivalent to 28 ± 7 nm, with a relatively narrow size distribution (over 95% of the LP_{CNF} were between 10 and 40 nm). This average size is similar to the values observed for LPs obtained in the absence nanofibers (28 ± 16 nm). These values are fairly similar to those reported in the literature from similar process and conditions.[12] With the solvent exchange method, in the presence or absence of CNF, the LP were well defined and presented a spherical shaped. In both cases, single lignin particles were observed, but most of them were clustered. Such aggregation is likely the result of drying during sample preparation. The LP_{CNF} particles seemed not to interact with the nanofibers, pointing to the possibility that the cellulosic surface was non-interactive. Cellulose induced a narrow LP size distribution. Such phenomenon can be explained by a spatial restriction, where the fiber network kept the particles apart from each other and prevented coalescence during formation. Electrostatic repulsion between the negatively charged LPs (-52 ± 2 mV zeta potential) and the cellulose nanofibers (-17.0 ± 0.6 mV zeta potential) greatly improved the colloidal stability of the resulting system. In the absence of CNF, LPs displayed a greater tendency to aggregate, as shown by their average hydrodynamic diameter (187 ± 5 nm from DLS, **Figure III.12h**). Discrepancies in diameter accessed from DLS and TEM are likely a result of LP swelling.[25]

The lignin particles (LP_{ChNF}) produced in the presence of chitin nanofibers were observed to be attached to the nanofibers and their shape was less spherical compared to LP_{CNF}. The size and distribution, on average, was slightly larger, 46 ± 17 nm (**Figure III.12f**). Despite the similar morphology of CNF and ChNF, the observed differences in particle morphology are explained by the distinctive surface chemistry of such substrates. While CNF and ChNF are polysaccharide-based nanoparticles, chitin differs from cellulose by the substitution of one hydroxyl group by an acetyl amine group in the C2 position. When partially deacetylated, even to a small degree, the acetyl amine group in ChNF becomes a primary amine that can be protonated in mild acidic pH, yielding positively charged nanofibers. The latter, with a zeta potential of 27 ± 1 mV, interacts strongly with the deprotonated lignin molecules, leading to an instantaneous lignin adsorption, *via* electrostatic interactions. Thus, ChNF acts as a nuclei for subsequent growth of lignin molecules. Here, we prepared the particles at pH 4 to induce protonation of the ChNF and, at the same time, keep their colloidal stability. The zeta potential of lignin particles at such pH was measured to be -37.5 ± 0.6 mV. Hence, the observed reduction in zeta-potential, compared to that at neutral pH, relates to the effect of charge neutralization, which leads to destabilization of the system. Therefore, precipitation of lignin on the ChNF is promoted. By increasing the interfacial interactions between lignin and the

nanofibers, it is possible to endow a more uniform particle distribution within the nanofiber network, resulting in a more homogenous colloidal suspension. The ChNF charge prevailed in the suspension after LP_{ChNF} preparation at pH 4, resulting in an overall net charge of 24 ± 2 mV. Although the zeta potential remained positive, the absolute value was lower than that of the precursor ChNF, indicating that the lignin particles adsorbed on the surface. The presence of free positive charges is promising as far as the possibility of further increasing the lignin nanoparticle loading.

Based on our data, and the supporting literature, we speculate on the mechanism behind LP formation and their associated morphology, highly depending on the nature of the template. Lignin particle formation *via* controlled precipitation in an anti-solvent is a near instantaneous process that goes through a metastable stage.[10] When templated, the formation of anchored or free lignin nanoparticles occurs before a metastable stage. In the earliest stage of particle formation, adsorption occurs, depending on the nature of the surface. This step is analogous to the formation of templated metallic nanoparticles;[56,65] however, in the case of LPs there is no reduction step and growth solely occurs by the coalescence (cumulative adsorption) of non-soluble molecules, as the solvent fraction (acetone) decreases. Since the precipitation of lignin molecules is rapid, due to their limited water solubility, a very strong interfacial interaction is required for adsorption, before precipitation. This is achieved by using a template that favors electrostatic attraction with lignin, such as ChNF. H-bonding between lignin and CNF is not sufficient to promote adsorption before the onset of particle growth.

We studied the formation of LPs on chitin nanofibers from a homogeneous suspension *via* a one-step process that was influenced by mixing. The nucleation of lignin particles directly on the nanofibers allowed a homogeneous distribution of the LPs with sizes below 100 nm. A relevant observation is that of Ashok *et al*. who indicated the possibility of producing lignin particles at an industrial scale by solvent shifting,[60] which translates into a promise for our LP_{ChNF}. The process still needs to be further studied in relation of optimized processing conditions, such as the lignin addition rate and lower limits of initial lignin concentration, which have been shown to reduce the particles size.[12] In addition, considering our system, parameters such as nanofibers concentration i.e. the viscosity of the antisolvent system, lignin-to-nanofibers ratio or nanofibers charge content could influence the lignin particles size. By increasing the degree of deacetylation of the chitin nanofibers, it is possible to further increase the lignin content without flocculation, given the effects of charge hindrance. This might also increase the number of nucleation sites and hence decrease the particles size. The size of the nanoparticles is also important for further functionalization and composite formation. In fact,

smaller sizes tend to increase the compatibility of reinforcing elements. For example, Nair *et al*. demonstrated that smaller and more homogeneous lignin particle size facilitated their dispersion in polyvinyl alcohol.[66] The final properties, such as anti-oxidant activity, were found to be influenced by the particles size, as the activity increased with the surface area available for reaction.[18] Here we devised the initial concentration needed to achieve small particles while maintaining a reasonable final volume. In the presence of the nanofibers, we obtained LPs with sizes < 50 nm, smaller compared to those obtained in the absence of solid interfaces.[12,19] Hence, formation of LPs in the presence of CNF and ChNF, opens a unique opportunity for the efficient integration of the particles in matrices, for example, for material development.

Interfacial interactions between lignin and the nanofibers.

We investigated the interfacial interactions between lignin particles and the templating nanofibers, for instance, by promoting destabilization and segregation under centrifugal fields (10 000 rpm, 5 min). The formed lignin particles presented colloidal sizes that warrant better stability compared to mechanically fibrillated nanofibers, with lengths in the micrometer range. Upon centrifugation, the brownish color of lignin, which contrasts with that of CNF and ChNF, can be easily identified for visual observation, e.g., to conclude whether the particles are sedimented with the nanofibers or remained suspended, in the supernatant (**Figure III.13a-b.**). Photos of the supernatants and sediments of systems subjected to centrifugation are shown in **Figure III.13a-b**. In the LP_{CNF} system, a brown supernatant was observed, indicating the presence of lignin particles. In contrast, a whitish sediment indicated nearly pure CNF fully separated from the lignin particles. In the case of LP_{ChNF}, the sediment containing the ChNF was brown, and the supernatant was colorless, indicating that the LPs interacted strongly with ChNF. It was possible to quantify the lignin present in the sediment (UV-Vis analysis) after dissolving the lignin particles in NaOH[64] (see **Figure III.13c**). A lignin content of 4.5 ± 0.3% was measured in the sediment containing CNF, while the ChNF sediment contained 67.4 ± 0.6% of the total lignin, a result of the precipitated lignin together with the positively charged chitin nanofibers. Lignin particles above the colloidal size or aggregated could sediment along with the nanofibers, which could explain the presence of lignin with the sedimented cellulose nanofibers. The lignin present on the sediment of chitin nanofibers imply that electrostatic interactions are strong enough to favor adsorption of LP (mainly < 100 nm and thus colloidally stable). This supports our hypothesis derived from TEM imaging, which indicated that lignin has better affinity with chitin than with cellulose.

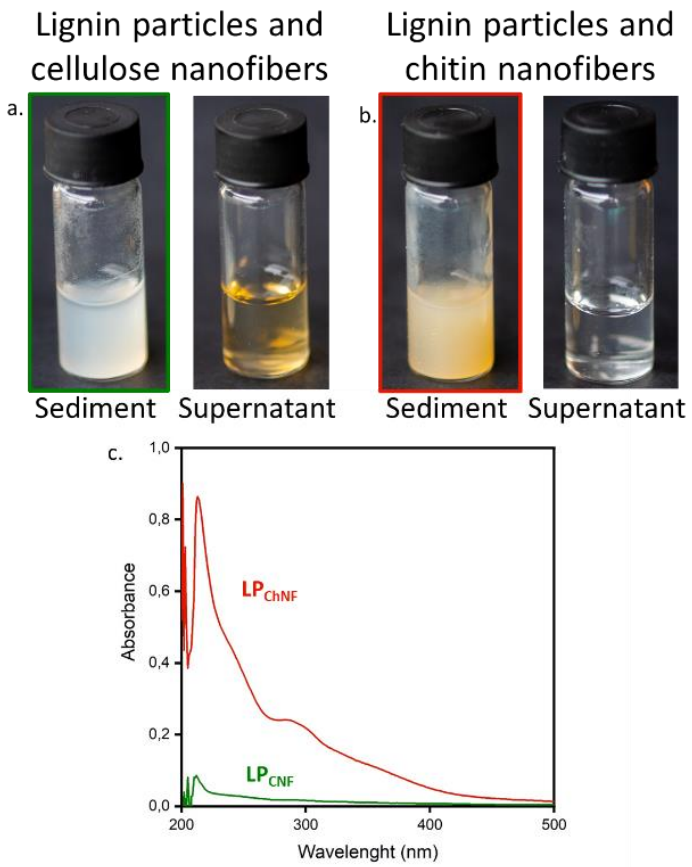

Figure III.13. Photos of LP mixed with a. cellulose and b. chitin nanofibers after centrifugation (10 min 10 000 rpm). c. The associated UV-Vis spectra of the dissolved lignin from the sediments.

To gain deeper insights on the interactions between lignin and the nanofibers, we used thin layer chromatography (TLC) in our system, e.g., to confirm a greater affinity of lignin with chitin compared to cellulosic surface (**Figure III.14c**). Here chromatographic paper was coated with the respective nanofiber suspension to produce CNF and ChNF surfaces that were later used as TLC stationary phases. The mobile phase (eluent) was a mixture of acetone:water (4:6), which was used to investigate solvent-surface-molecule competitive interactions. **Figure III.14b**, includes blue profiles of the images (acquired by image analysis software), taken after elution and under UV light to increase the contrast (**Figure III.14a**). On CNF-coated paper, lignin interacted poorly with CNF and moved far in the stationary phase with the eluent, mostly accumulating at the top of the TLC paper. For ChNF, we observed milder shades of blue along the elution direction, confirming that the lignin molecules spread along the TLC paper, a result from strong interactions with the stationary phase. Lignin molecules also spread on the CNF-coated paper; however, within a narrower region, showing that lignin also interacted partly

with cellulose. Such interactions are driven by weak, secondary interactions such as H-bonding; in contrast, stronger electrostatic interactions take place at the ChNF-lignin interface. Hydrophobic interactions between acetyl groups of chitin and aromatic moieties in lignin may also improve the affinity between the two components; however, they might be difficult to resolve due to overlapping by ionic pairing. With this, we demonstrated that the surface chemistry of the nanofibers is a key for the formation of LP *in-situ*. In consequence, additionally to the nature of the nanofibers, further chemical modification in the nanofibers would also influence their interfacial interactions with lignin. Thus, the method used for nanofibers preparation is of importance on the behavior of the system.

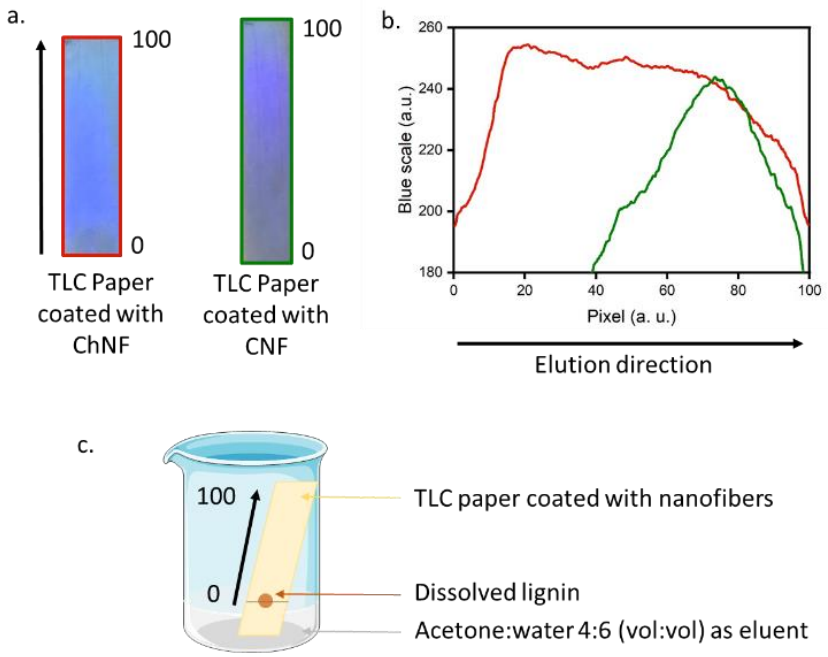

Figure III.14. Thin layer chromatography (TLC) using paper coated with CNF and ChNF and acetone:water as eluent: **a.** images taken under UV light for image analysis. **b.** average blue intensity value of each pixel lines normalized to 100 (0 represents the start line and 100 the solvent front). **c.** Scheme of the paper chromatography experimental set up.

We demonstrate that the electrostatic interactions between chitin and lignin can be harnessed to develop hybrid colloids enriched with strongly coupled nanoparticles. We investigated the effect of lignin content on particle formation by varying the amount of suspended lignin, from 9% to 15% and 23%. A high lignin concentration enhanced the properties of the obtained material, such as lignin's antioxidant activity. However, a compromise between functionality and stability of the network needs to be maintained. When forming the LP_{ChNF} from more

concentrated lignin solutions (accounting for 15 and 23 wt%.), the sizes (TEM) of the lignin particles attached on the nanofibers were 59 ± 19 nm and 61 ± 25 nm for 15% and 23% of lignin, respectively (**Figure III.15**). We observed that with an increased lignin content, the particles size increased (as well as the size distribution). This is a result of the reduced ratio between nucleation sites on the chitin nanofibers and the amount of lignin available for adsorption. The morphology of the network may be further tailored by controlling the addition rate during solvent exchange, since a faster addition is expected to increase the density of nucleation sites and therefore homogenize the size distribution.

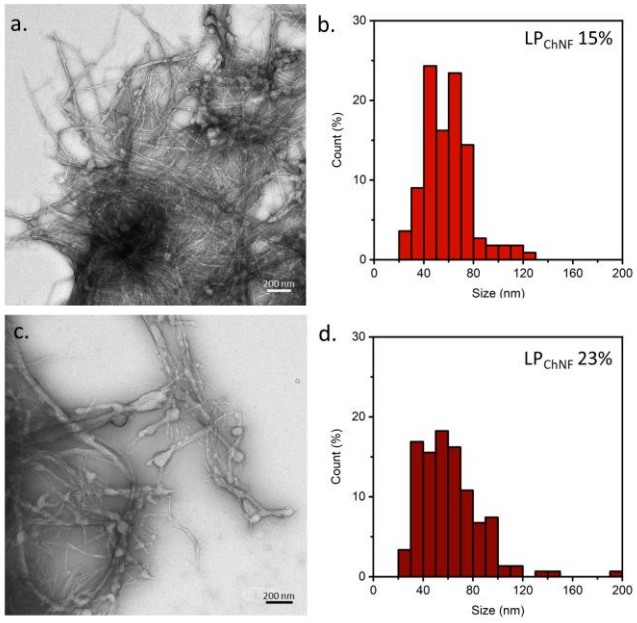

Figure III.15. TEM images (a. and c.) and size distribution (b. and d.) of ChNF with 15% and 23% LP respectively.

Preparation of films from nanofibers carrying LPs.

We discuss the effect of incorporation of lignin particles, from *in-situ* formation on CNF and ChNF, for films preparation. We evaluated the properties of the films considering their application for food packaging. The impact of the particles on films structuring and mechanical strength was studied (**Figure III.16**) followed by the UV-shielding and antioxidant activity (**Figure III.18**).

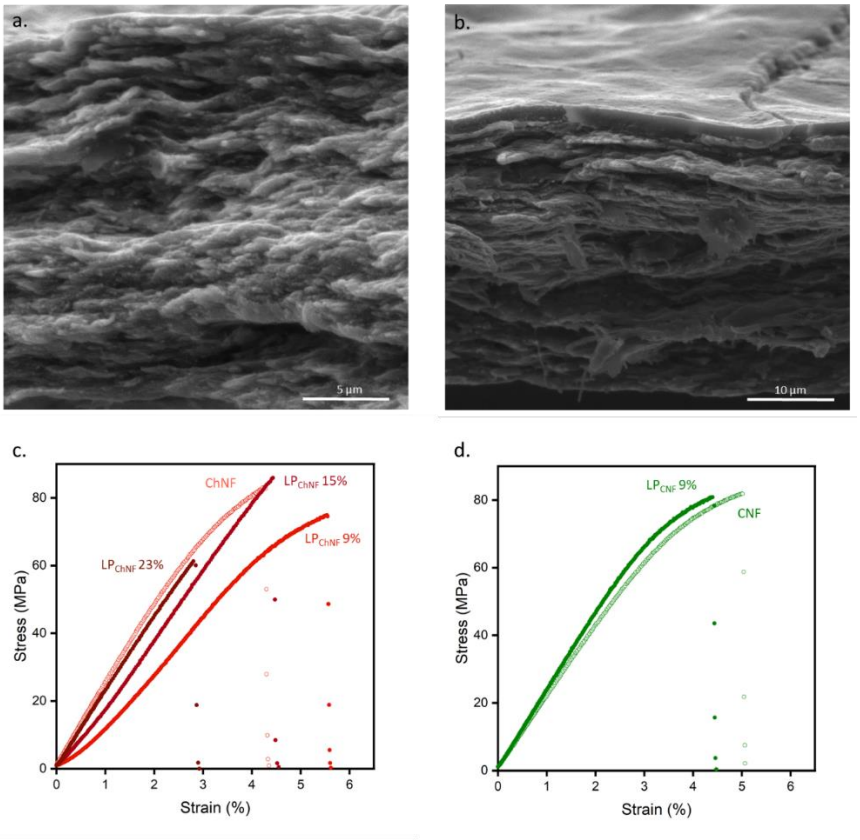

Figure III.16. Cross-section images (SEM) of the films: **a.** chitin and **b.** cellulose nanofibers containing 9% LP. Tensile stress *versus* strain profiles used to evaluate the mechanical strength of films made with **c.** chitin nanofibers with 0% (o), 9% (●), 15% (●) and 23% (●) LP and **d.** cellulose nanofibers with 0% (o) and 9% (●) LP, as indicated.

The CNF and ChNF films loaded with different LP content were produced by solvent casting on PTFE Petri dishes. **Figure III.16a-b** shows SEM cross-section images of the films containing 9% LP_{CNF} and LP_{ChNF}. In both cases, it is possible to identify a fibrillar network as well as the formation of a lamellar structures. The observations indicate that the incorporation of 9% LP did not interfere with film structuring. The reduced nanoparticles size was key to avoid the disruption of a strong fibrillar network. In the LP_{ChNF} film, the structure was homogeneous, and the LPs were shown to be incorporated homogeneously; however, the structure of LP_{CNF} film displayed two distinct components: a fibrillar web and an upper, lignin particle layer. AFM analysis of the surface of the LP_{CNF} film clearly suggested the presence of a dense LP layer on the surface, not observed in the LP_{ChNF} film (**Figure III.17**). In the case of CNF, the fibrils sedimented and the LPs, which are colloidally stable, remained suspended during water evaporation. This led to the accumulation of LPs on the surface of the formed film. In fact, the lack of interfacial interaction between LP and CNFs led to segregation, driven

by capillary pulling forces that developed during drying. The observations agree with results from separation, *via* centrifugation, that showed sedimentation of CNF with simultaneous accumulation of LPs particles in the suspended medium. Filtration is suggested as a method to obtain a better mixing between LPs and CNF, provided that particle drainage is avoided through the forming mesh.

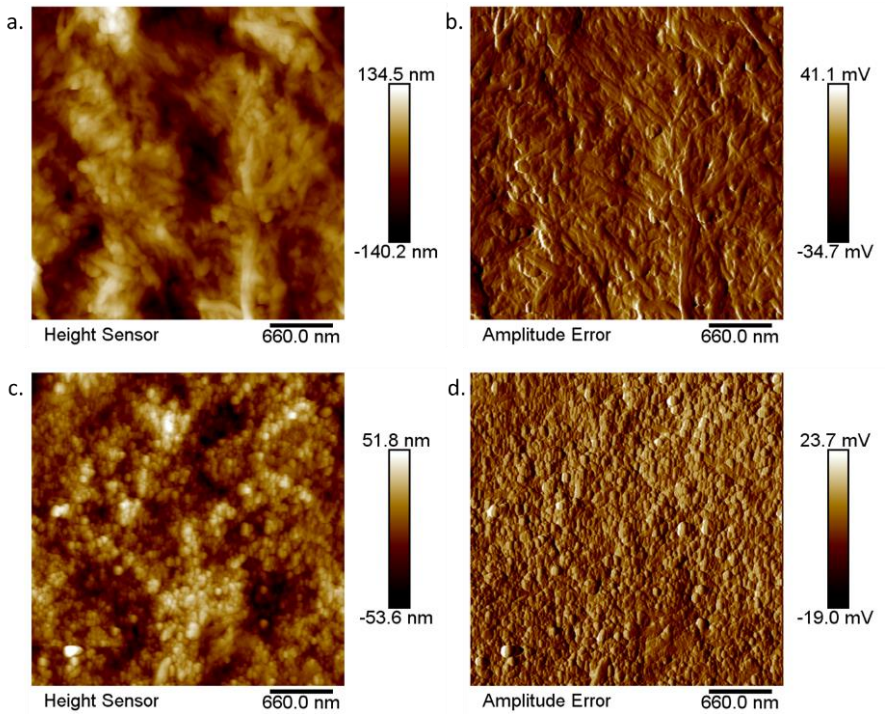

Figure III.17: AFM images of the top surface of LP_{ChNF} (a. height image, b. amplitude image) and LP_{CNF} (c. height image, d. amplitude image) films.

In the case of LP_{CNF} films, the mechanical properties were similar to those of neat CNF films, which is explained by the fact that LPs accumulated on the surface of LP_{CNF} films. This hinders the contribution of the particles with respect to fibrillar entanglement, which is a main factor explaining the development of film cohesion. The lignin content in LP_{ChNF} films, did not interfere the mechanical performance, up to 15% of LP loading. However, at 23% LP the stress-strain profiles followed a similar trend, but the rupture occurred at lower stresses and strains (*ca.* 3%) indicating a reduction in toughness. The stiffness of LP_{ChNF} films increased with LP content, from 9 to 23%; this could be explained by the loss of interfibrillar hydrogen bonding due to the presence of LPs that disturb the film structure, leading to brittle films.[20]

A low film wettability is desirable for packaging applications. To investigate such feature, we measured the contact angle of films with and without LPs (**Table III.1**). In general, the contact angle of the films, regardless their nature, increased with LP loading. For the neat CNF film,

the decrease in drop volume was relatively high (> 40%), meaning that high water absorption took place by the effect of the bulk film; however, in the presence of 9% LP the decrease in volume was limited to *ca*. 6%. This is explained by the presence of a dense LP layer on top of the film which reduced the absorption of water, also leading to a higher contact angle. For LP_{ChNF} films, water absorption also decreased with increasing LP content, which relates to LP filling of the pores.[21] Therefore, the contact angle follows the same trend. Water is a major challenge when considering polysaccharide building blocks for material development; therefore, our results for water-biocolloid interactions can open new opportunities.

Table III.1. Contact angles and final water drop volume measured after 2 min in contact with the films

LP %	LP_{ChNF}		LP_{CNF}	
	Contact Angle	Final Drop Volume (% of initial volume)	Contact Angle	Final Drop Volume (% of initial volume)
0	32 ± 6°	87 ± 11	22 ± 8°	62 ± 16
9	56 ± 2°	90 ± 5	55 ± 5°	94 ± 4
15	72 ± 5°	91 ± 1	-	-
23	63 ± 1°	94 ± 4	-	-

So far, we have shown that LP coupling with cellulose and chitin nanofibers does not deteriorate the mechanical performance of the respective films while increasing their water resistance. Moreover, the addition of lignin is expected to endow the films with photocatalytic activities. The polyphenolic lignin promotes UV absorption and free radical scavenging, thus making it a suitable component for food packaging. Additionally, the nanosized particles enhance the respective efficiency and, at the same time, their association with a network of chitin nanofibers prevents leakage.

The transmittance data for LP_{ChNF} films measured by UV-Vis spectroscopy are shown in **Figure III.18a** for 0 to 23% LP loading. All the lignin-containing films presented negligible transmittance below 400 nm, e.g., full UV shielding was achieved. A higher transparency in the visible range was observed for smaller fibers and particles.[67] The antioxidant activity of the films was measured using the ABTS radical in water, to avoid dissolution of lignin in the commonly used solvents applied in the DPPH test – ethanol or methanol. After bringing the films in contact with the radical solution, the decrease in radical activity was measured by UV-

Vis spectrometry, showing a remarkable reduction in radical activity. To draw film comparisons, the radical scavenging activity was calculated after 1 h contact and compared with a control based on tannic acid, which is a well-known natural antioxidant (high radical scavenging activity)[68]. In **Figure III.18b**, the tannic acid equivalent (TAE) for LP_{ChNF} films is shown as a function of LP content: an increased antioxidant activity was noticed with increased LP content. Films with smaller sizes but same LP content showed an enhanced antioxidant activity compared, for instance, with recent results.[20] In agreement with our observations, Zhang *et al*. showed that decreasing particles size led to an increased antioxidant activity, which was explained by a higher accessibility of phenolic groups.[18] Release experiments were performed, for systems under same conditions: < 5% lignin release (based on the total loading in each film) was measured, indicating that the radical scavenging activity is ascribed to the surface of the film .

By considering films with different lignin loading, 15% LP was found to be a suitable balance between mechanical strength, wettability and antioxidant activity. However, depending on the desired application for such LP_{ChNF} films, the lignin content can be further optimized. Whereas films with < 9% LP are likely to be effective for complete UV-shielding, higher antioxidant activity is obtained with higher lignin content. Complete UV shielding and high antioxidant activity are beneficial effects in food packaging applications. In fact, UV light penetration through the packaging material creates free radicals, increasing food degradation rate and reducing shell life.[33] The incorporation of LPs in chitin nanofiber networks and respective electrostatic interactions are expected to prevent particle leakage, which is key with regards to food safety. As the interactions between lignin and chitin prevent any LP leakage, this system could also be of interest for drug release applications. In fact, it has been demonstrated that dissolved drugs could be encapsulated in LP during solvent shifting preparation[25] therefore the *in-situ* preparation of LP on nanofibers could be a one step process for drug encapsulation and LP anchoring on a matrix. Our system could also be of interest in applications such as sunscreen[69] where the UV blocking ability of LP combined with the nanofibers rheological properties could be exploited. Active membranes for filtration could be another potential application as nanofibers have the ability to form 3D network that could be functionalized with LP,[52] the interactions between LP and the matrix would prevent any particles leakage.

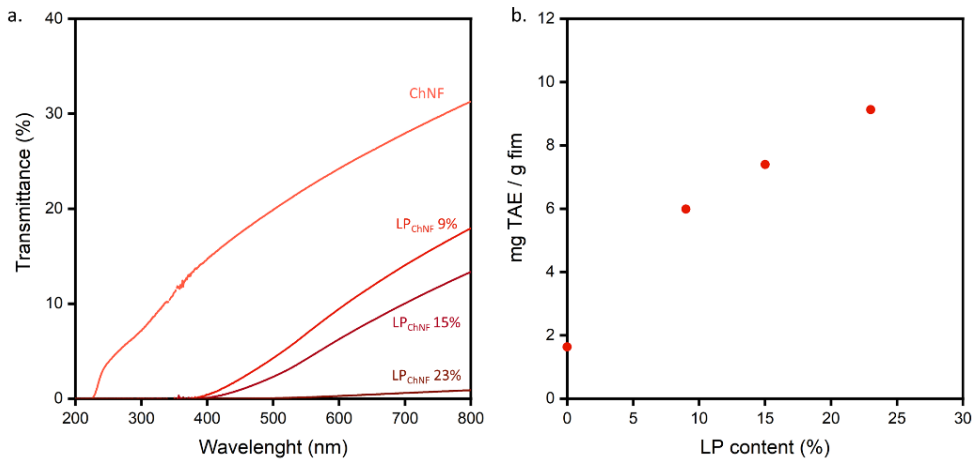

Figure III.18. Functional properties of LP_{ChNF} films: **a.** UV-Visible transmittance of the LP_{ChNF} films containing given fractions of LP. **b.** Antioxidant activity of films measured by the tannic acid equivalent (TAE) as function of LP loading in ChNF films.

CONCLUSION

We developed a new process to produce lignin nanoparticles in the presence of bio-based nanofibers *via* solvent shifting. Lignin nanoparticles of sizes < 100 nm were synthesized in the presence of cellulose and chitin nanofibers. The positive charges in chitin enabled electrostatic interactions with lignin, leading to a strong and homogeneous distribution of LP on the chitin nanofiber network. Suspensions with high lignin content were successfully prepared leading to increased LP sizes. Investigation of relevant parameters such as lignin type, fibers size and concentration as well as morphology should be considered to optimize the process and properties of the hybrid nanofibers.

LPs with a narrow size distribution were formed in the presence of cellulose nanofibers, but displayed electrostatic repulsion, which resulted in phase separation during film formation and non-homogeneous repartition of LPs in the film. In contrasts, the films prepared with chitin nanofibers showed well-dispersed LPs, which resulted in a high film mechanical strength, similar to that of the neat nanofiber film. Complete UV shielding was achieved for all the films containing LPs, with an antioxidant activity that tracked LP loading. The results offer great promise in applications such as food packaging.

Conclusion to Chapter III

Chapter III aimed at studying the interactions between LP and nanofibers. In the first part, the influence of LP-size was studied while in the second part the role of the nanofiber chemistry in the LP preparation was assessed.

Chapter III.1 described the preparation of tCNF films containing lignin microparticles and nanoparticles. Nanoparticles with an average diameter of 18 ± 5 nm were obtained by preparing LP in the presence of nanofibers by solvent precipitation. Films containing lignin nano- and microparticles were prepared, and structural properties were studied. Functional properties such as UV shielding and antioxidant activity were achieved for films containing lignin, however, the degree of antioxidant activity was size-dependent and increased exponentially with the decrease in particle size due to surface activity. Moreover, due to their small size lignin nanoparticles only blocked the light in the UV range and had a limited impact on the films' transparency. It would be interesting to see if this size phenomenon is valid for other kinds of particles in nanofiber matrices and to which extend.

Due to the interesting results brought by the lignin nanoparticles, we had a closer look at the preparation methods used for nano LP synthesis. **Chapter III.2** aimed at understanding the formation of the particles in the presence of two different types of nanofibers. Both LP and CNF are negatively charged which led to repulsion during the precipitation of lignin and non-homogeneous dispersion of the LP in the CNF film formed. On the other hand, the positive surface charge of ChNF induced attractive electrostatic forces between LP and ChNF. Homogeneous ChNF films were produced from suspensions containing different amounts of LP. Antioxidant activity and UV shielding properties were reported as expected from Chapter III.1 results.

For further studies, synthesis parameters relative to the nanofibers such as their size, concentration, or morphology could be investigated. The influence of the lignin type on the interactions and particles morphology would also bring information on the preparation mechanism and tune the functional properties of lignin.

References

(1) Heiligtag, F. J.; Niederberger, M. The Fascinating World of Nanoparticle Research. *Materials Today* **2013**, *16* (7), 262–271. https://doi.org/10.1016/j.mattod.2013.07.004.

(2) Dadfar, S. M.; Camozzi, D.; Darguzyte, M.; Roemhild, K.; Varvarà, P.; Metselaar, J.; Banala, S.; Straub, M.; Güvener, N.; Engelmann, U.; Slabu, I.; Buhl, M.; van Leusen, J.; Kögerler, P.; Hermanns-Sachweh, B.; Schulz, V.; Kiessling, F.; Lammers, T. Size-Isolation of Superparamagnetic Iron Oxide Nanoparticles Improves MRI, MPI and Hyperthermia Performance. *Journal of Nanobiotechnology* **2020**, *18* (1), 22. https://doi.org/10.1186/s12951-020-0580-1.

(3) Kulkarni, S. K. Nanotechnology and Environment. In *Nanotechnology: Principles and Practices*; Springer International Publishing: Cham, 2015; pp 349–354. https://doi.org/10.1007/978-3-319-09171-6_13.

(4) McClements, D. J.; Xiao, H. Is Nano Safe in Foods? Establishing the Factors Impacting the Gastrointestinal Fate and Toxicity of Organic and Inorganic Food-Grade Nanoparticles. *npj Sci Food* **2017**, *1* (1), 6. https://doi.org/10.1038/s41538-017-0005-1.

(5) Yang, Y.-N.; Lu, K.-Y.; Wang, P.; Ho, Y.-C.; Tsai, M.-L.; Mi, F.-L. Development of Bacterial Cellulose/Chitin Multi-Nanofibers Based Smart Films Containing Natural Active Microspheres and Nanoparticles Formed in Situ. *Carbohydrate Polymers* **2020**, *228*, 115370. https://doi.org/10.1016/j.carbpol.2019.115370.

(6) Tardy, B. L.; Mattos, B. D.; Otoni, C. G.; Beaumont, M.; Majoinen, J.; Kämäräinen, T.; Rojas, O. J. Deconstruction and Reassembly of Renewable Polymers and Biocolloids into Next Generation Structured Materials. *Chem. Rev.* **2021**, *121* (22), 14088–14188. https://doi.org/10.1021/acs.chemrev.0c01333.

(7) Kämäräinen, T.; Ago, M.; Greca, L. G.; Tardy, B. L.; Müllner, M.; Johansson, L.-S.; Rojas, O. J. Morphology-Controlled Synthesis of Colloidal Polyphenol Particles from Aqueous Solutions of Tannic Acid. *ACS Sustainable Chem. Eng.* **2019**, *7* (20), 16985–16990. https://doi.org/10.1021/acssuschemeng.9b02378.

(8) Lee, C.-M.; Lim, S.; Kim, G.-Y.; Kim, D.; Kim, D.-W.; Lee, H.-C.; Lee, K.-Y. Rosin Microparticles as Drug Carriers: Influence of Various Solvents on the Formation of Particles and Sustained-Release of Indomethacin. *Biotechnol. Bioprocess Eng.* **2004**, *9* (6), 476–481. https://doi.org/10.1007/BF02933489.

(9) Tao, J.; Li, S.; Ye, F.; Zhou, Y.; Lei, L.; Zhao, G. Lignin – An Underutilized, Renewable and Valuable Material for Food Industry. *Critical Reviews in Food Science and Nutrition* **2020**, *60* (12), 2011–2033. https://doi.org/10.1080/10408398.2019.1625025.

(10) Österberg, M.; Sipponen, M. H.; Mattos, B. D.; Rojas, O. J. Spherical Lignin Particles: A Review on Their Sustainability and Applications. *Green Chem.* **2020**, *22* (9), 2712–2733. https://doi.org/10.1039/D0GC00096E.

(11) Ago, M.; Tardy, B. L.; Wang, L.; Guo, J.; Khakalo, A.; Rojas, O. J. Supramolecular Assemblies of Lignin into Nano- and Microparticles. *MRS Bulletin* **2017**, *42* (5), 371–378. https://doi.org/10.1557/mrs.2017.88.

(12) Richter, A. P.; Bharti, B.; Armstrong, H. B.; Brown, J. S.; Plemmons, D.; Paunov, V. N.; Stoyanov, S. D.; Velev, O. D. Synthesis and Characterization of Biodegradable Lignin Nanoparticles with Tunable Surface Properties. *Langmuir* **2016**, *32* (25), 6468–6477. https://doi.org/10.1021/acs.langmuir.6b01088.

(13) Cavallo, E.; He, X.; Luzi, F.; Dominici, F.; Cerrutti, P.; Bernal, C.; Foresti, M. L.; Torre, L.; Puglia, D. UV Protective, Antioxidant, Antibacterial and Compostable Polylactic Acid Composites Containing Pristine and Chemically Modified Lignin Nanoparticles. *Molecules* **2021**, *26* (1), 126. https://doi.org/10.3390/molecules26010126.

(14) Posoknistakul, P.; Tangkrakul, C.; Chaosuanphae, P.; Deepentham, S.; Techasawong, W.; Phonphirunrot, N.; Bairak, S.; Sakdaronnarong, C.; Laosiripojana, N. Fabrication and

Characterization of Lignin Particles and Their Ultraviolet Protection Ability in PVA Composite Film. *ACS Omega* **2020**, *5* (33), 20976–20982. https://doi.org/10.1021/acsomega.0c02443.

(15) Tian, D.; Hu, J.; Bao, J.; Chandra, R. P.; Saddler, J. N.; Lu, C. Lignin Valorization: Lignin Nanoparticles as High-Value Bio-Additive for Multifunctional Nanocomposites. *Biotechnology for Biofuels* **2017**, *10* (1), 192. https://doi.org/10.1186/s13068-017-0876-z.

(16) Lee, S. C.; Yoo, E.; Lee, S. H.; Won, K. Preparation and Application of Light-Colored Lignin Nanoparticles for Broad-Spectrum Sunscreens. *Polymers* **2020**, *12* (3), 699. https://doi.org/10.3390/polym12030699.

(17) Freitas, F. M. C.; Cerqueira, M. A.; Gonçalves, C.; Azinheiro, S.; Garrido-Maestu, A.; Vicente, A. A.; Pastrana, L. M.; Teixeira, J. A.; Michelin, M. Green Synthesis of Lignin Nano- and Micro-Particles: Physicochemical Characterization, Bioactive Properties and Cytotoxicity Assessment. *International Journal of Biological Macromolecules* **2020**, *163*, 1798–1809. https://doi.org/10.1016/j.ijbiomac.2020.09.110.

(18) Zhang, X.; Yang, M.; Yuan, Q.; Cheng, G. Controlled Preparation of Corncob Lignin Nanoparticles and Their Size-Dependent Antioxidant Properties: Toward High Value Utilization of Lignin. *ACS Sustainable Chem. Eng.* **2019**, *7* (20), 17166–17174. https://doi.org/10.1021/acssuschemeng.9b03535.

(19) Qian, Y.; Zhong, X.; Li, Y.; Qiu, X. Fabrication of Uniform Lignin Colloidal Spheres for Developing Natural Broad-Spectrum Sunscreens with High Sun Protection Factor. *Industrial Crops and Products* **2017**, *101*, 54–60. https://doi.org/10.1016/j.indcrop.2017.03.001.

(20) Farooq, M.; Zou, T.; Riviere, G.; Sipponen, M. H.; Österberg, M. Strong, Ductile, and Waterproof Cellulose Nanofibril Composite Films with Colloidal Lignin Particles. *Biomacromolecules* **2019**, *20* (2), 693–704. https://doi.org/10.1021/acs.biomac.8b01364.

(21) Liu, Y. Strong and Flexible Nanocomposites of Carboxylated Cellulose Nanofibril Dispersed by Industrial Lignin. *ACS Sustainable Chem. Eng.* **2018**, *6* (4), 5524–5532. https://doi.org/10.1021/acssuschemeng.8b00402.

(22) Yang, W.; Weng, Y.; Puglia, D.; Qi, G.; Dong, W.; Kenny, J. M.; Ma, P. Poly(Lactic Acid)/Lignin Films with Enhanced Toughness and Anti-Oxidation Performance for Active Food Packaging. *International Journal of Biological Macromolecules* **2020**, *144*, 102–110. https://doi.org/10.1016/j.ijbiomac.2019.12.085.

(23) Re, R.; Pellegrini, N.; Proteggente, A.; Pannala, A.; Yang, M.; Rice-Evans, C. Antioxidant Activity Applying an Improved ABTS Radical Cation Decolorization Assay. *Free Radical Biology and Medicine* **1999**, *26* (9), 1231–1237. https://doi.org/10.1016/S0891-5849(98)00315-3.

(24) Zwilling, J. D.; Jiang, X.; Zambrano, F.; Venditti, R. A.; Jameel, H.; Velev, O. D.; Rojas, O. J.; Gonzalez, R. Understanding Lignin Micro- and Nanoparticle Nucleation and Growth in Aqueous Suspensions by Solvent Fractionation. *Green Chem.* **2021**, *23* (2), 1001–1012. https://doi.org/10.1039/D0GC03632C.

(25) Sipponen, M. H.; Lange, H.; Ago, M.; Crestini, C. Understanding Lignin Aggregation Processes. A Case Study: Budesonide Entrapment and Stimuli Controlled Release from Lignin Nanoparticles. *ACS Sustainable Chem. Eng.* **2018**, *6* (7), 9342–9351. https://doi.org/10.1021/acssuschemeng.8b01652.

(26) Ago, M.; Huan, S.; Borghei, M.; Raula, J.; Kauppinen, E. I.; Rojas, O. J. High-Throughput Synthesis of Lignin Particles (∼30 Nm to ∼2 Mm) via Aerosol Flow Reactor: Size Fractionation and Utilization in Pickering Emulsions. *ACS Appl. Mater. Interfaces* **2016**, *8* (35), 23302–23310. https://doi.org/10.1021/acsami.6b07900.

(27) Suzuki, M.; Kondor, A.; Sakuraba, Y.; Rojas, O.; Ago, M. Electromagnetic Transparency of Composites of Unsaturated Polyester and Nanolignin: Morphological and Surface Energy Considerations. **2021**. https://doi.org/10.21203/rs.3.rs-556483/v1.
(28) Schneider, W. D. H.; Dillon, A. J. P.; Camassola, M. Lignin Nanoparticles Enter the Scene: A Promising Versatile Green Tool for Multiple Applications. *Biotechnology Advances* **2021**, *47*, 107685. https://doi.org/10.1016/j.biotechadv.2020.107685.
(29) Lavoine, N.; Desloges, I.; Dufresne, A.; Bras, J. Microfibrillated Cellulose – Its Barrier Properties and Applications in Cellulosic Materials: A Review. *Carbohydrate Polymers* **2012**, *90* (2), 735–764. https://doi.org/10.1016/j.carbpol.2012.05.026.
(30) Ahankari, S. S.; Subhedar, A. R.; Bhadauria, S. S.; Dufresne, A. Nanocellulose in Food Packaging: A Review. *Carbohydrate Polymers* **2021**, *255*, 117479. https://doi.org/10.1016/j.carbpol.2020.117479.
(31) Gerbin, E.; Rivière, G. N.; Foulon, L.; Frapart, Y. M.; Cottyn, B.; Pernes, M.; Marcuello, C.; Godon, B.; Gainvors-Claisse, A.; Crônier, D.; Majira, A.; Österberg, M.; Kurek, B.; Baumberger, S.; Aguié-Béghin, V. Tuning the Functional Properties of Lignocellulosic Films by Controlling the Molecular and Supramolecular Structure of Lignin. *International Journal of Biological Macromolecules* **2021**, *181*, 136–149. https://doi.org/10.1016/j.ijbiomac.2021.03.081.
(32) García, A.; Toledano, A.; Andrés, M. Á.; Labidi, J. Study of the Antioxidant Capacity of Miscanthus Sinensis Lignins. *Process Biochemistry* **2010**, *45* (6), 935–940. https://doi.org/10.1016/j.procbio.2010.02.015.
(33) Kwon, S.; Orsuwan, A.; Bumbudsanpharoke, N.; Yoon, C.; Choi, J.; Ko, S. A Short Review of Light Barrier Materials for Food and Beverage Packaging. *KOREAN JOURNAL OF PACKAGING SCIENCE & TECHNOLOGY* **2018**, *24* (3), 141–148. https://doi.org/10.20909/kopast.2018.24.3.141.
(34) Toivonen, M. S.; Onelli, O. D.; Jacucci, G.; Lovikka, V.; Rojas, O. J.; Ikkala, O.; Vignolini, S. Anomalous-Diffusion-Assisted Brightness in White Cellulose Nanofibril Membranes. *Advanced Materials* **2018**, *30* (16), 1704050. https://doi.org/10.1002/adma.201704050.
(35) Brar, S. K.; Verma, M. Measurement of Nanoparticles by Light-Scattering Techniques. *TrAC Trends in Analytical Chemistry* **2011**, *30* (1), 4–17. https://doi.org/10.1016/j.trac.2010.08.008.
(36) Farooq, M.; Tao, Z.; Valle-Delgado, J. J.; Sipponen, M. H.; Morits, M.; Österberg, M. Well-Defined Lignin Model Films from Colloidal Lignin Particles. *Langmuir* **2020**, *36* (51), 15592–15602. https://doi.org/10.1021/acs.langmuir.0c02970.
(37) Lindström, T.; Österberg, F. Evolution of Biobased and Nanotechnology Packaging – a Review. *Nordic Pulp & Paper Research Journal* **2020**, *35* (4), 491–515. https://doi.org/10.1515/npprj-2020-0042.
(38) Bardet, R.; Reverdy, C.; Belgacem, N.; Leirset, I.; Syverud, K.; Bardet, M.; Bras, J. Substitution of Nanoclay in High Gas Barrier Films of Cellulose Nanofibrils with Cellulose Nanocrystals and Thermal Treatment. *Cellulose* **2015**, *22* (2), 1227–1241. https://doi.org/10.1007/s10570-015-0547-9.
(39) Helanto, K.; Matikainen, L.; Talja, R.; Rojas, O. J. Bio-Based Polymers for Sustainable Packaging and Biobarriers: A Critical Review. *BioRes* **2019**, *14* (2), 4902–4951.
(40) Xia, J.; Zhang, Z.; Liu, W.; Li, V. C. F.; Cao, Y.; Zhang, W.; Deng, Y. Highly Transparent 100% Cellulose Nanofibril Films with Extremely High Oxygen Barriers in High Relative Humidity. *Cellulose* **2018**, *25* (7), 4057–4066. https://doi.org/10.1007/s10570-018-1843-y.
(41) Arora, A.; Padua, G. W. Review: Nanocomposites in Food Packaging. *Journal of Food Science* **2010**, *75* (1), R43–R49. https://doi.org/10.1111/j.1750-3841.2009.01456.x.

(42) Zhu, J.; Yang, M.; Emre, A.; Bahng, J. H.; Xu, L.; Yeom, J.; Yeom, B.; Kim, Y.; Johnson, K.; Green, P.; Kotov, N. A. Branched Aramid Nanofibers. *Angewandte Chemie International Edition* **2017**, *56* (39), 11744–11748. https://doi.org/10.1002/anie.201703766.

(43) Mittal, N.; Ansari, F.; Gowda.V, K.; Brouzet, C.; Chen, P.; Larsson, P. T.; Roth, S. V.; Lundell, F.; Wågberg, L.; Kotov, N. A.; Söderberg, L. D. Multiscale Control of Nanocellulose Assembly: Transferring Remarkable Nanoscale Fibril Mechanics to Macroscale Fibers. *ACS Nano* **2018**, *12* (7), 6378–6388. https://doi.org/10.1021/acsnano.8b01084.

(44) Ling, S.; Kaplan, D. L.; Buehler, M. J. Nanofibrils in Nature and Materials Engineering. *Nat Rev Mater* **2018**, *3* (4), 1–15. https://doi.org/10.1038/natrevmats.2018.16.

(45) Ifuku, S.; Saimoto, H. Chitin Nanofibers: Preparations, Modifications, and Applications. *Nanoscale* **2012**, *4* (11), 3308–3318. https://doi.org/10.1039/C2NR30383C.

(46) Kontturi, E.; Laaksonen, P.; Linder, M. B.; Nonappa; Gröschel, A. H.; Rojas, O. J.; Ikkala, O. Advanced Materials through Assembly of Nanocelluloses. *Advanced Materials* **2018**, *30* (24), 1703779. https://doi.org/10.1002/adma.201703779.

(47) Zhu, H.; Zhu, S.; Jia, Z.; Parvinian, S.; Li, Y.; Vaaland, O.; Hu, L.; Li, T. Anomalous Scaling Law of Strength and Toughness of Cellulose Nanopaper. *PNAS* **2015**, *112* (29), 8971–8976. https://doi.org/10.1073/pnas.1502870112.

(48) Reverdy, C.; Belgacem, N.; Moghaddam, M. S.; Sundin, M.; Swerin, A.; Bras, J. One-Step Superhydrophobic Coating Using Hydrophobized Cellulose Nanofibrils. *Colloids and Surfaces A: Physicochemical and Engineering Aspects* **2018**, *544*, 152–158. https://doi.org/10.1016/j.colsurfa.2017.12.059.

(49) Ghanadpour, M.; Carosio, F.; Larsson, P. T.; Wågberg, L. Phosphorylated Cellulose Nanofibrils: A Renewable Nanomaterial for the Preparation of Intrinsically Flame-Retardant Materials. *Biomacromolecules* **2015**, *16* (10), 3399–3410. https://doi.org/10.1021/acs.biomac.5b01117.

(50) Sasso, C.; Zeno, E.; Petit-Conil, M.; Chaussy, D.; Belgacem, M. N.; Tapin-Lingua, S.; Beneventi, D. Highly Conducting Polypyrrole/Cellulose Nanocomposite Films with Enhanced Mechanical Properties. *Macromolecular Materials and Engineering* **2010**, *295* (10), 934–941. https://doi.org/10.1002/mame.201000148.

(51) Mattos, B. D.; Tardy, B. L.; Greca, L. G.; Kämäräinen, T.; Xiang, W.; Cusola, O.; Magalhães, W. L. E.; Rojas, O. J. Nanofibrillar Networks Enable Universal Assembly of Superstructured Particle Constructs. *Science Advances* **2020**, *6* (19), eaaz7328. https://doi.org/10.1126/sciadv.aaz7328.

(52) Cusola, O.; Rojas, O. J.; Roncero, M. B. Lignin Particles for Multifunctional Membranes, Antioxidative Microfiltration, Patterning, and 3D Structuring. *ACS Appl. Mater. Interfaces* **2019**, *11* (48), 45226–45236. https://doi.org/10.1021/acsami.9b16931.

(53) Rol, F.; Belgacem, M. N.; Gandini, A.; Bras, J. Recent Advances in Surface-Modified Cellulose Nanofibrils. *Progress in Polymer Science* **2019**, *88*, 241–264. https://doi.org/10.1016/j.progpolymsci.2018.09.002.

(54) Lokanathan, A. R.; Uddin, K. M. A.; Rojas, O. J.; Laine, J. Cellulose Nanocrystal-Mediated Synthesis of Silver Nanoparticles: Role of Sulfate Groups in Nucleation Phenomena. *Biomacromolecules* **2014**, *15* (1), 373–379. https://doi.org/10.1021/bm401613h.

(55) Hoeng, F.; Denneulin, A.; Neuman, C.; Bras, J. Charge Density Modification of Carboxylated Cellulose Nanocrystals for Stable Silver Nanoparticles Suspension Preparation. *J Nanopart Res* **2015**, *17* (6), 244. https://doi.org/10.1007/s11051-015-3044-z.

(56) Olsson, R. T.; Samir, M. A. S. A.; Salazar-Alvarez, G.; Belova, L.; Ström, V.; Berglund, L. A.; Ikkala, O.; Nogués, J.; Gedde, U. W. Making Flexible Magnetic Aerogels and Stiff Magnetic Nanopaper Using Cellulose Nanofibrils as Templates. *Nature Nanotech* **2010**, *5* (8), 584–588. https://doi.org/10.1038/nnano.2010.155.
(57) Padalkar, S.; Capadona, J. R.; Rowan, S. J.; Weder, C.; Won, Y.-H.; Stanciu, L. A.; Moon, R. J. Natural Biopolymers: Novel Templates for the Synthesis of Nanostructures. *Langmuir* **2010**, *26* (11), 8497–8502. https://doi.org/10.1021/la904439p.
(58) Errokh, A.; Magnin, A.; Putaux, J.-L.; Boufi, S. Hybrid Nanocellulose Decorated with Silver Nanoparticles as Reinforcing Filler with Antibacterial Properties. *Materials Science and Engineering: C* **2019**, *105*, 110044. https://doi.org/10.1016/j.msec.2019.110044.
(59) Wang, B.; Sun, D.; Wang, H.-M.; Yuan, T.-Q.; Sun, R.-C. Green and Facile Preparation of Regular Lignin Nanoparticles with High Yield and Their Natural Broad-Spectrum Sunscreens. *ACS Sustainable Chem. Eng.* **2019**, *7* (2), 2658–2666. https://doi.org/10.1021/acssuschemeng.8b05735.
(60) Ashok, R. P. B.; Oinas, P.; Lintinen, K.; Sarwar, G.; Kostiainen, M. A.; Österberg, M. Techno-Economic Assessment for the Large-Scale Production of Colloidal Lignin Particles. *Green Chem.* **2018**, *20* (21), 4911–4919. https://doi.org/10.1039/C8GC02805B.
(61) Leskinen, T.; Smyth, M.; Xiao, Y.; Lintinen, K.; Mattinen, M. L.; Kostiainen, M. A.; Oinas, P.; Österberg, M. Scaling up Production of Colloidal Lignin Particles. *Nord Pulp Pap. Res. J.* **2017**, *32* (4), 586–596. https://doi.org/10.3183/NPPRJ-2017-32-04-p586-596.
(62) Ifuku, S.; Nogi, M.; Abe, K.; Yoshioka, M.; Morimoto, M.; Saimoto, H.; Yano, H. Preparation of Chitin Nanofibers with a Uniform Width as α-Chitin from Crab Shells. *Biomacromolecules* **2009**, *10* (6), 1584–1588. https://doi.org/10.1021/bm900163d.
(63) Yearla, S. R.; Padmasree, K. Preparation and Characterisation of Lignin Nanoparticles: Evaluation of Their Potential as Antioxidants and UV Protectants. *Journal of Experimental Nanoscience* **2016**, *11* (4), 289–302. https://doi.org/10.1080/17458080.2015.1055842.
(64) Lee, R. A.; Bédard, C.; Berberi, V.; Beauchet, R.; Lavoie, J.-M. UV–Vis as Quantification Tool for Solubilized Lignin Following a Single-Shot Steam Process. *Bioresource Technology* **2013**, *144*, 658–663. https://doi.org/10.1016/j.biortech.2013.06.045.
(65) Valencia, L.; Kumar, S.; Nomena, E. M.; Salazar-Alvarez, G.; Mathew, A. P. In-Situ Growth of Metal Oxide Nanoparticles on Cellulose Nanofibrils for Dye Removal and Antimicrobial Applications. *ACS Appl. Nano Mater.* **2020**, *3* (7), 7172–7181. https://doi.org/10.1021/acsanm.0c01511.
(66) Nair, S. S.; Sharma, S.; Pu, Y.; Sun, Q.; Pan, S.; Zhu, J. Y.; Deng, Y.; Ragauskas, A. J. High Shear Homogenization of Lignin to Nanolignin and Thermal Stability of Nanolignin-Polyvinyl Alcohol Blends. *ChemSusChem* **2014**, *7* (12), 3513–3520. https://doi.org/10.1002/cssc.201402314.
(67) Chinga-Carrasco, G. Optical Methods for the Quantification of the Fibrillation Degree of Bleached MFC Materials. *Micron* **2013**, *48*, 42–48. https://doi.org/10.1016/j.micron.2013.02.005.
(68) Vilchez, A.; Acevedo, F.; Cea, M.; Seeger, M.; Navia, R. Applications of Electrospun Nanofibers with Antioxidant Properties: A Review. *Nanomaterials* **2020**, *10* (1), 175. https://doi.org/10.3390/nano10010175.
(69) Qian, Y.; Qiu, X.; Zhu, S. Lignin: A Nature-Inspired Sun Blocker for Broad-Spectrum Sunscreens. *Green Chem.* **2014**, *17* (1), 320–324. https://doi.org/10.1039/C4GC01333F.

Chapter IV
Towards packaging applications

Table of content – Chapter IV

Introduction to chapter IV 203

Chapter IV. Multilayered film with high barrier properties 205

INTRODUCTION 205
EXPERIMENTAL SECTION 207
Wax particle suspension preparation. 208
Characterization of the wax nanoparticle suspensions. 208
Preparation of CNF film containing wax. 209
Characterization of the films. 210
RESULTS AND DISCUSSION 213
Formation of stable wax nanoparticles suspension. 213
Optimization of the wax and CNF layers design to reduce water vapor permeability. . 214
Influence of the wax and CNF designs onto films mechanical properties. 219
Final Multilayer film with high barrier properties. 222
Final Multilayer film possible applications in food packaging 228
CONCLUSION 231

Conclusion to Chapter IV 233

References 234

Introduction to Chapter IV

In the previous chapters, we looked at the transformation of biobased precursors into colloids (**Chapter II**) and the interactions between the different colloids in suspension as well as when integrated into nanofiber matrices (**Chapter III**). In **Chapter IV**, optimization of films towards high barrier properties for food packaging application is studied (**Figure IV.1**).

In the first part of this Chapter, wax from carnauba trees is processed into CNF films to obtain high water vapor barrier properties. Different films are designed and their water vapor permeabilities are measured. Moreover, mechanical properties provide insights on wax-CNF interactions.

In the second half of the chapter, the film with the highest water vapor barrier is used to prepare a multilayer film composed of cellulose nanofibers / wax / chitin nanofibers containing lignin particles. Different barrier properties of the multilayer film are studied including oxygen, water vapor, grease, and UV light. Finally, an accelerated storage test on dry food products is done as a proof of concept.

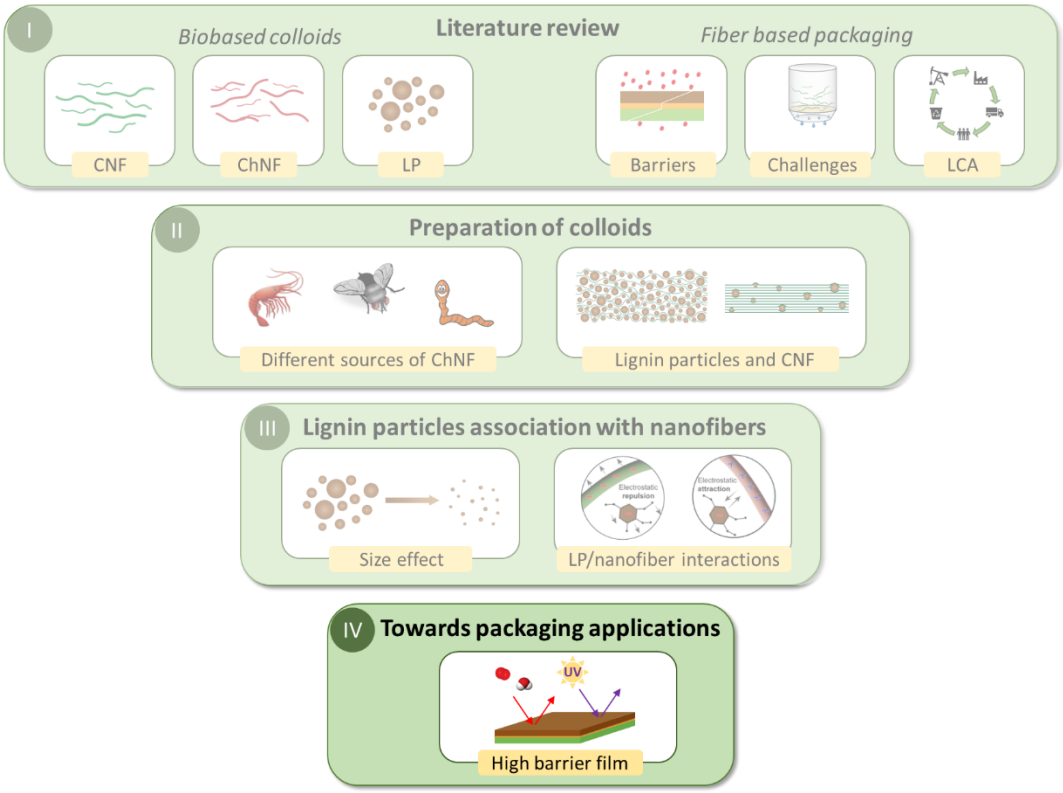

Figure IV.1. Global scheme of the PhD project where Chapter IV is highlighted.

Chapter IV. Multilayered films with high barrier properties

Adapted from "High barrier multilayered film fabricated from bio-based polymers", E. Pasquier, B. D. Mattos, H. Koivula, A. Khakalo, M. N. Belgacem, J. Bras, O. J. Rojas, manuscript in preparation.

INTRODUCTION

Replacement policies for petroleum-based plastics, as well as the current regulations on single-use plastics, are incentivizing the development of biobased materials for packaging.[1] Biobased plastics include a wide range of materials, such as polymers obtained from biobased monomers and biosynthesized polymers (biopolymers) that can be extracted from nature.[2] Biopolymers extracted from nature offer a better end-of-life due to their biodegradable features, which is not the case of other biobased plastics like bio-polyethylene, bio-polypropylene or bio-PET. Natural biopolymer-based packaging can degrade in natural environments within short time when not chemically modified.[3] Cellulose fibers, one of the best film-forming biopolymer, can be extracted from plant biomass which offers advantages in terms of geographic availability.[4] However, up to now, natural fiber-based materials have limited applications in food packaging because of their high gas permeability.[5]

Cellulose nanofibers (CNF) are cellulose colloids that can lead to materials with high oxygen and grease barrier properties.[6,7] They are obtained by mechanical fibrillation of cellulose fibers and lead to nanofibers that are a few micrometers long and only tenth of nanometers wide.[8] CNF can be assembled into self-standing films or coated on different substrates such as paper board or plastic (PLA, PET).[9–12] Upon drying, the entanglement of the high aspect ratio nanofibers leads to high internal cohesion within the CNF network. This cohesive film form a packed structure that has high air, oxygen and grease barrier properties.[7,9] However, cellulose is hydrophilic and very sensitive to water, which increases exponentially the oxygen transmission rate (OTR) of CNF films at 50-80% relative humidity because of the swollen effect on the nanofibrillar network.[13,14] CNF typical water vapor transmission rate (WVTR) ranges between 100 and 500 g/m^2.day at 50% RH which is too high for most commercial applications.[15]

Many parameters can influence water vapor permeability (WVP) of cellulose films including density, pore structure of the film, surface chemistry, crystallinity, and the parameters chosen

for films drying.[2,15] Sharma *et al*. have shown that heat-treatment (3 h at 175 °C) of CNF films decreased WVP by a factor of two,[16] which was explained by the decrease in porosity of the film that slowed down gas diffusion and an increase in cellulose crystallinity that limited water vapor solubility in the CNF. However, heat treatments induced brittleness in CNF films. WVTR of CNF films has been also reduced by applying hydrophobic coatings. CNF film when dipped in melted paraffin displayed decrease of WVTR from 600 to 40 g/m^2.day as wax formed a continuous hydrophobic layer on both sides of the film.[17] Multilayer systems were also proposed by coating paper with CNF and shellac wax to decrease the gas permeability of paper.[18] WVTR was decrease from 50-70 g/m^2.day to 6-8 g/m^2.day with the presence of 10 µm of shellac coating. Among the different waxes, carnauba wax is a vegetal wax with low water vapor permeability and despite its lipidic nature it also contains hydrophilic groups such as esters and hydroxyls which could improve interactions with CNF.[19]

Inspired by currently commercialized multilayered packaging materials, a completely renewable multilayered material with high barrier properties was fabricated by engineering carnauba wax and cellulose nanofibers into layers that display specific and complementary functions. Moreover, aiming at introducing an additional barrier against UV light and antioxidant properties, we introduced a layer of immobilized UV-absorbing lignin nanoparticles.[20] Therefore, we produced a multilayer film with three layers designed especially to impose barrier against oxygen, water vapor and UV light. Multilayer films are widely used in the food packaging industry because no single material can provide all the requirements needed for protecting foods, with required features varying from mechanical properties to high barrier, printability and sealability for example. The major drawback of current multilayer materials is their end-of-life, as each additional layer impacts recyclability or biodegradability of the whole packaging.[21] Herein we use unmodified biopolymers that when combined together can display multiple barrier features while maintaining their biodegradable characters. Multilayer of CNF, wax and chitin nanofibers containing lignin nanoparticles (LPChNF) were prepared (**Figure IV.2 a-c**). Each layer having a specific barrier: oxygen by CNF, water vapor by wax and UV light by LPChNF. The precursors were combined in wet state with layer-by-layer filtration and dried as one film (**Figure IV.2d**). In this Chapter, the wax layer was optimized using different processes to incorporate wax into a CNF film to decrease its water vapor permeability. Then, multilayer films were prepared, and their morphology was assessed as well as their oxygen, water vapor, grease, and UV barrier.

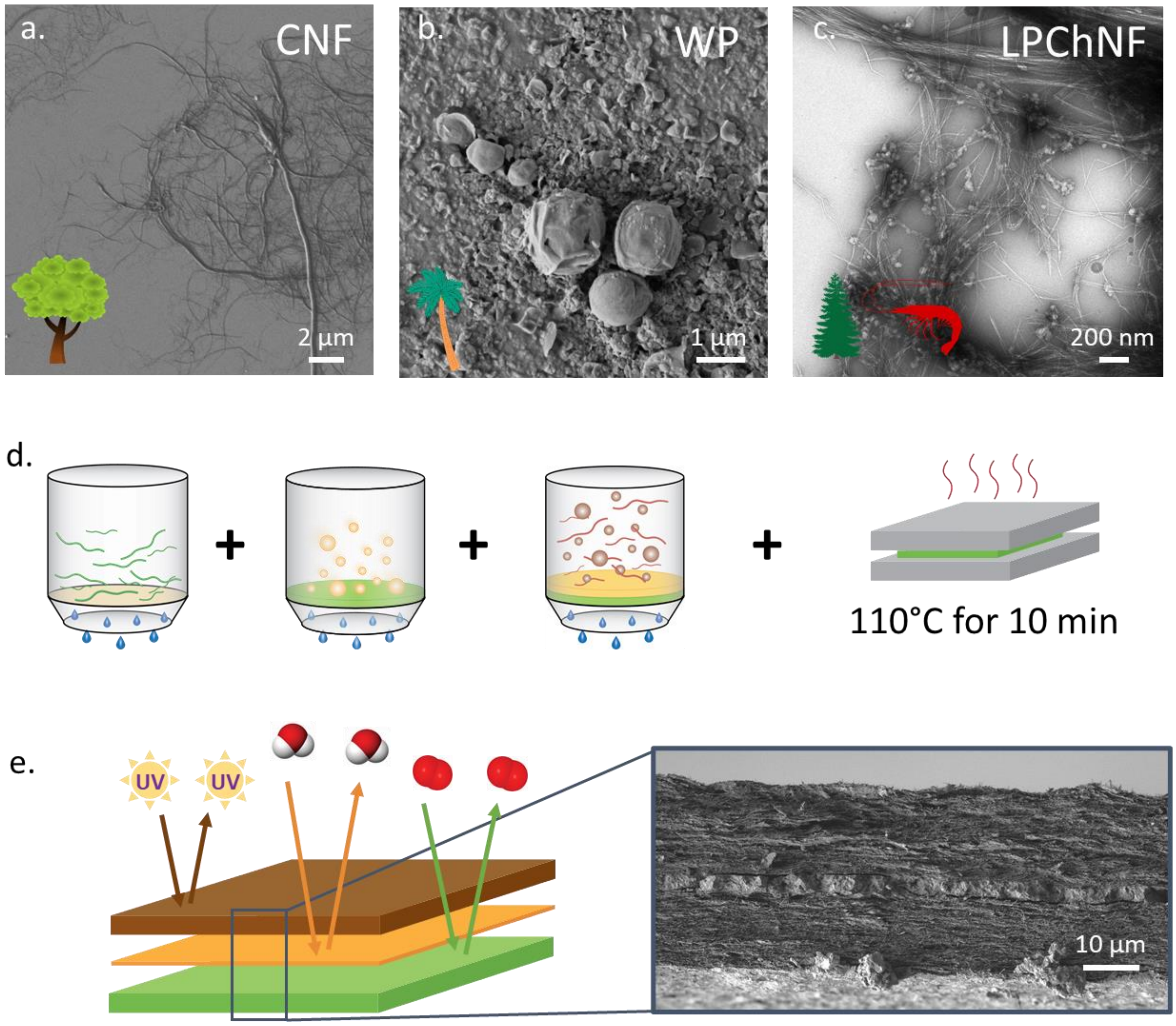

Figure IV.2. SEM image of different colloids used in the multilayer film: **a.** cellulose nanofibers (CNF), **b.** wax particles (WP) and **c.** lignin particles with chitin nanofibers (LPChNF). Filtration and drying steps used to produce the multilayer film (**d.**) and scheme of the produced multilayer with UV light, water vapor and oxygen barrier properties associated with an SEM image of the cross-section (**e.**).

EXPERIMENTAL SECTION

Materials. Technical Kraft lignin (Indulin AT) from softwood was purchased from MeadWestvaco (USA). Cellulose nanofibers (CNF) were prepared by microfluidization (M-110P, Microfluidics, Inc., USA) of never dried bleached Kraft hardwood pulp with 6 passes at 2000 bar with 200 - 100 µm chambers. Chitin nanofibers (ChNF) were prepared from dried shrimp chitin flakes purchased from Sigma-Aldrich. First, purification of the chitin was carried out following the method in **Chapter II.1.** Briefly, demineralization (0.25 M HCl, 2h, room temperature), deproteinization (1M NaOH, 4h, 50°C) and chlorite bleaching (80°C, 2h) were

done with washing steps in between. The fiber suspension was then acidified to obtain a final acetic acid concentration of 0.1% and mechanically fibrillated. High shear homogenizer was used as a pre-treatment for 10 min followed by microfluidization (M-110P, Microfluidics, Inc., USA) with 1 pass at 1500 bar with 400 and 200 µm chambers and 6 passes at 2000 bar with 200 and 100 µm chambers.

Lignin particles were prepared *in-situ* with ChNF following the procedure described in **Chapter III.2**. For this purpose, a solution of lignin was prepared at 2 g/L in acetone/water (9:1). The solution was then filtrated on paper filter and the purified solution was dropped in a 0.5% suspension of ChNF. The final lignin content was 9% of the total dry mass (ChNF + lignin). The suspension was dialyzed against distilled water to remove residual acetone.

Carnauba wax, acetic acid, calcium chloride ($CaCl_2$), HCl, NaOH, $NaClO_2$, "Oil Red O" (1-[2,5-dimethyl-4-(2,5-dimethylphenylazo)phenylazo]-2-naphthol or Solvent Red 27) were purchased from Sigma-Aldrich. Crackers were supplied from the local supermarket.

Wax particle suspension preparation.

Wax particles were prepared following Lozhechnikova *et al.*[22] method. Briefly, wax was melted at 100°C in distilled water at 1 g/L. When the wax was completely melted, the solution was sonicated at 50% amplitude (45 W) for 5 min, the emulsion was then rapidly cooled in an ice bath under stirring. Suspension was filtrated on a 90 µm nylon mesh before use.

Characterization of the wax nanoparticle suspensions.

Morphology of nanoparticles. Wax suspension was dropped on silica and dried overnight. Au/Pd coating of 4 nm was sputtered on the sample before observation with Zeiss Sigma VP scanning electron microscope (SEM). Several images were taken and the most representative one is shown.

Hydrodynamic size measurement. Dynamic light scattering device (Malvern Zetasizer Nano) was used to measure the wax particles size. Time stability was assessed by measuring the particles size at different time: the day of preparation, one week, two weeks, one month, two months, three months, and six months after the preparation. The measurement was done in duplicate.

Surface charge measurement. Zeta-potential of the WP was measured with a Malvern Zetasizer Nano using a dip cell. Suspension was diluted to 0.05% and conductivity was adjusted to 0.13 mS/cm with diluted NaCl. The measurement was done in triplicate.

Preparation of CNF film containing wax.

CNF suspension was diluted to 0.2% and homogenized for 2 min with a high shear homogenizer (Ultra-Turax) at room temperature (RT) prior to filtration. The CNF content was kept constant between the different films to obtain a film with a grammage of 40 g/m^2 and a wax content of 9 wt% of the total mass for all the films, see **Table IV.1** for exact masses. Films were prepared with a vacuum filtration unit and PVDF membranes with pore size of 0.45 µm were used as filters. All suspensions were bath sonicated for 2 min prior to filtration. **Figure IV.3** shows the 6 different films produced in this Chapter. The reference film contains only CNF and will be called "CNF". After filtration, a second PVDF membrane was placed on top of the film before drying. All the films were dried in two steps, the first one consisted of pressing at 100 bar and heating at 100°C for 10 min followed by 35 min cooling to RT under similar pressure. The films were then left to dry overnight at RT under a 5 kg weight.

The second film was a mix of CNF and WP. Both suspensions were mixed before filtration and filtered together, it will be later referred as "Mix".

The third films, called "Top layer" was produced by filtering first the CNF suspension and, when no visible water remained, WP suspension was poured over and filtered. For the drying of the Top layer film, a Teflon plate was placed on top of the film to avoid leakage of the wax while melting.

The fourth film was composed of a WP layer positioned in between two CNF layers, following the same method as used in the Top layer assembly, but the film was produced by filtration of first half the CNF then the WP suspension and finally the second half of the CNF. This film will be referred as "Sandwich".

Another Sandwich film with small amount of CNF-WP mix (9% CNF relative to WP weight) was prepared, it is called "Sandwich WP_{CNF}".

Final multilayer film preparation.

The final multilayer film was prepared using the same method utilized to make the Sandwich film but replacing the top CNF suspension by LPChNF suspension to add the UV barrier feature. The amount of nanofiber was kept constant within the films (**Table IV.1**). The chitin

nanofibers containing lignin particles suspension (LPChNF) was diluted to 0.2% with diluted acetic acid. Before filtration, the suspension was bath sonicated for 5 min to remove bubbles. A film containing only LPChNF was also prepared as reference for testing the mechanical properties.

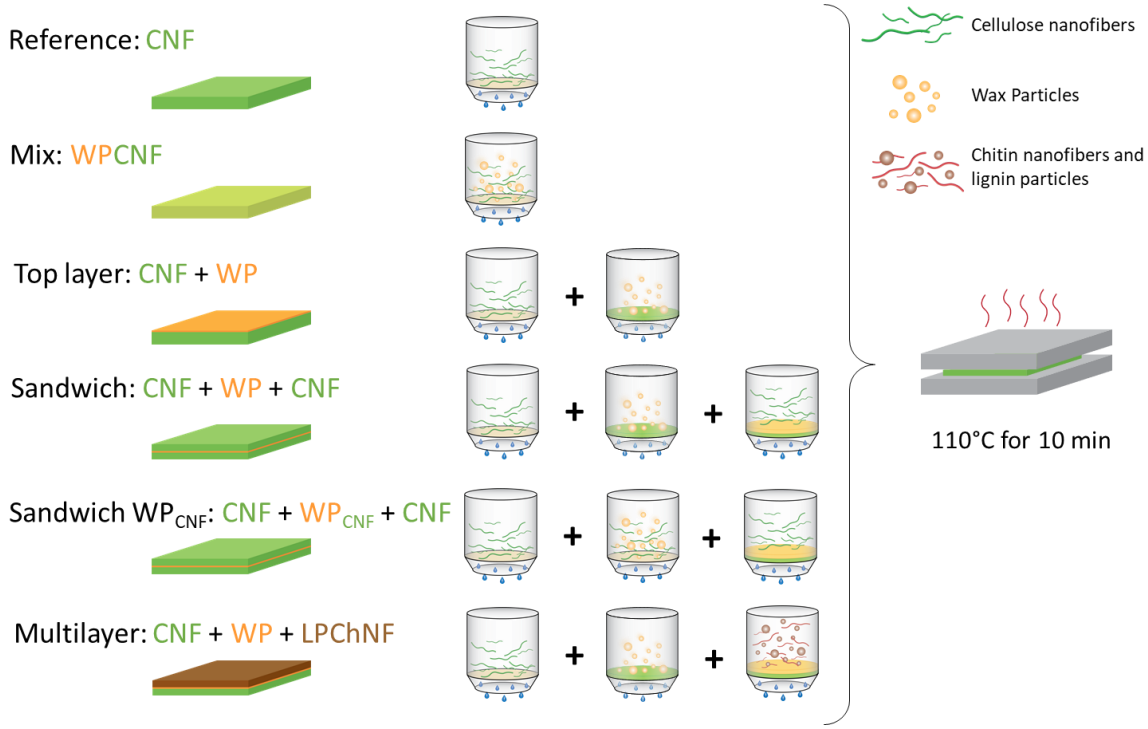

Figure IV.3. Different films prepared and their filtration steps.

Characterization of the films.

All films were conditioned at 50% relative humidity (RH) and 23 °C for at least 24h before any characterization.

Apparent density. Films were weighted at 23 °C and 50% relative humidity and their thickness was measured with a thickness tester for paper and board (Lorentzen & Wettre). Due to the pressing during the drying process, the films had a smooth surface hence thickness could be measured with a thickness tester or paper. Films were circular and their diameter was measured with a regular ruler. Density was calculated according to the following equation:

$$d = \frac{m}{thickness \times area} \quad \text{(IV.1)}$$

Where *m* represents the mass of the film in g and *thickness* and *area* are measured in cm and cm^2 respectively.

Mechanical properties. Tensile tests were performed with an Instron 5944 with a 100 N load cell at a strain rate of 1 mm/min. The initial gap between the clamps was set at 30 mm and the samples were cut as strips with dimensions of 50 x 5 mm. The width of samples was precisely measured with a caliper before each test. The strips were glued in a paper frame to avoid fracture at the clamp edge. Triplicates (or more) were performed for each sample.

Surface analysis of the delaminated films. During mechanical tests, some of the Sandwich films delaminated. To better understand which layers delaminated and why, FTIR analysis of the delaminated surfaces was performed. PerkinElmer spectrometer, operated in ATR mode, was used to acquire spectra with a resolution of 2 cm^{-1} and accumulation of at least 10 scans on minimum of 3 different zones on delaminated surface. The most representative spectra were used for the discussion.

Morphology of the films. Cross-sections of the films after tensile test were imaged by Scanning Electron Microscopy (SEM). A conductive 4 nm-thick coating of Au/Pd was sputtered on the samples, prior their imaging with a Zeiss Sigma VP SEM. At least 10 images were taken for each sample and the most representative was selected.

Water vapor transmission rate (WVTR). Water vapor properties of the films were measured at 23°C, 50% RH and 23°C, 80% RH. For that purpose, 10 g of dried $CaCl_2$ were placed in a 100 mL glass vial which was closed by a cap with a hole. An aluminum mask with an exchange surface area of 4.9 cm^2 surrounded the film that was placed on top of the glass vial to close it tightly with the holed screw cap. Vials were placed in a controlled humidity chamber and their mass was monitored until the increase in mass was constant. Three films were measured for each sample. WVTR was calculated using the following equation:

$$WVTR = \frac{\Delta m}{\mathrm{A} \times \Delta t} \quad \text{(IV.2)}$$

Where Δm represents the increase in mass during a given time (Δt) and A the exposed area of the films. Experiments were conducted in triplicate. Water vapor permeability (WVP) was calculated using the thickness of the film in µm and the saturation pressure of water vapor outside the vial (P_{sat}) depending on the relative humidity (Δ% RH).

$$WVP = \frac{WVTR \times thickness}{P_{sat} \times \Delta\%RH} \quad \text{(IV.3)}$$

Water surface interaction. Water contact angle (WCA) was measured with a Theta Flex optical tensiometer (Biolin Scientific) using 5-µL water drops. Contact angles were recorded for 120 s after drop contact with the surface, three measurements were performed for each sample.

Grease barrier properties. Resistance to grease penetration was measured following a method described elsewhere.[23] Briefly, a samples (25 mm diameter) were placed between two blotting papers on top of a transparent glass plate. Then 200 µL of "Oil Red O"-dyed olive oil was added to the upper blotting paper and a 50 g weight was placed on top. Both upper blotting paper and weight had a diameter of 30 mm. Grease permeation was monitored by taking images of the lower blotting paper through the glass plate with an image scanner (300 dpi, 24-bit color). The whole system was placed in a chamber at 40°C and periodic images were taken for 170 h. Three parallel measurements were done for each sample.

Optical properties. Transmittance of the films was measured between 200 and 800 nm with a UV-Vis spectrophotometer (Shimadzu, UV-2550). Measurements were performed in triplicate.

Oxygen transmission rate (OTR). Oxygen barrier properties were measured in a Systech Illinois M8001 Oxygen Permeation Analyzer. Measurements were done at 23°C and 50% RH or 80% RH, with the same humidity on both side of the films. A 5 cm^2 mask was used to reduce the exchange surface. OTR was given by the device in cm^3/m^2.day and the oxygen permeability (OP) was then calculated using the thickness of the film and atmospheric pressure (P_{atm}). Duplicates or triplicates were measured.

$$OP = OTR \times \frac{thickness}{P_{atm}} \quad \text{(IV.4)}$$

Food test. Equal mass of commercial crackers (between 2.2 and 2.3 g) was placed in glass bottles just after opening the food packaging. The glass bottles were closed with the holed screw cap, which was covered with the different films. The Sandwich and Multilayer films were tested, and CNF was used as reference. The packaging of the crackers was used as positive reference. The bottles were placed in a humidity chamber for one week at 23°C and 80% RH. Uniaxial compression tests were done after one week in order to evaluate the texture of the crackers, given the humidity changes in the container. A texture analyzer (TA XT plus, Stable Micro Systems) was equipped with a cylindrical probe with diameter smaller than the crackers so that the area of compression was constant at 126.68 mm^2. The test was performed at constant

speed of 1 mm/s and measurement stopped when 70% strain was reached. Dry mass of the crackers was measured after the test by drying them overnight at 105°C. Triplicate were performed.

RESULTS AND DISCUSSION

Herein we prepare a multilayer film that is composed by layered biomolecules or colloids, each of them having a specific barrier property: cellulose nanofibers are used for oxygen barrier, wax for water vapor barrier and chitin nanofibers containing lignin particles for UV shielding. The CNF and chitin/lignin layers have already been optimized in previous Chapters.

The first part of this Chapter consists of the optimization of the wax layer aiming at high water vapor barrier properties and the second part combines the different layers in one multilayer film that is thoroughly characterized. The pathway chosen for the incorporation of wax in the film has been designed to facilitate its handling, in aqueous medium and at room temperature. Wax particles are integrated in four different ways to a CNF film and only the film with the best performance was used to assemble the final multilayer film that also includes the chitin nanofibers and lignin particles.

Formation of stable wax nanoparticles suspension.

Wax particles (WP) were produced by emulsification of melted wax (without surfactant) followed by fast cooling (**Figure IV.4a**) using a previously reported method.[22] Non spherical particles with diameter of 367 ± 21 nm were obtained (**Figure IV.4b,c**). These results agreed with previous studies on preparation of WP where particles with the same order of magnitude (261 ± 4 nm) were obtained with similar wax concentration.[22] The formation of stable WP suspension was explained by the presence of hydrophilic groups (-OH, -COOH, -CHO) in carnauba wax that rearrange on the surface of the particles during their formation, which is confirmed by a negative surface charge of - 43 ± 2 mV when measuring the zeta potential. The particle yield was *ca.* 75%, with bigger wax residues being retained in the filter after the cooling stage; the residual wax could potentially be melted again and reintroduced in subsequent particle manufacturing. The WP suspension was stable over 6 months, with average particle size being constant within the standard error and no extensive particle aggregation was noted in the DLS measurement (**Figure IV.4c**).

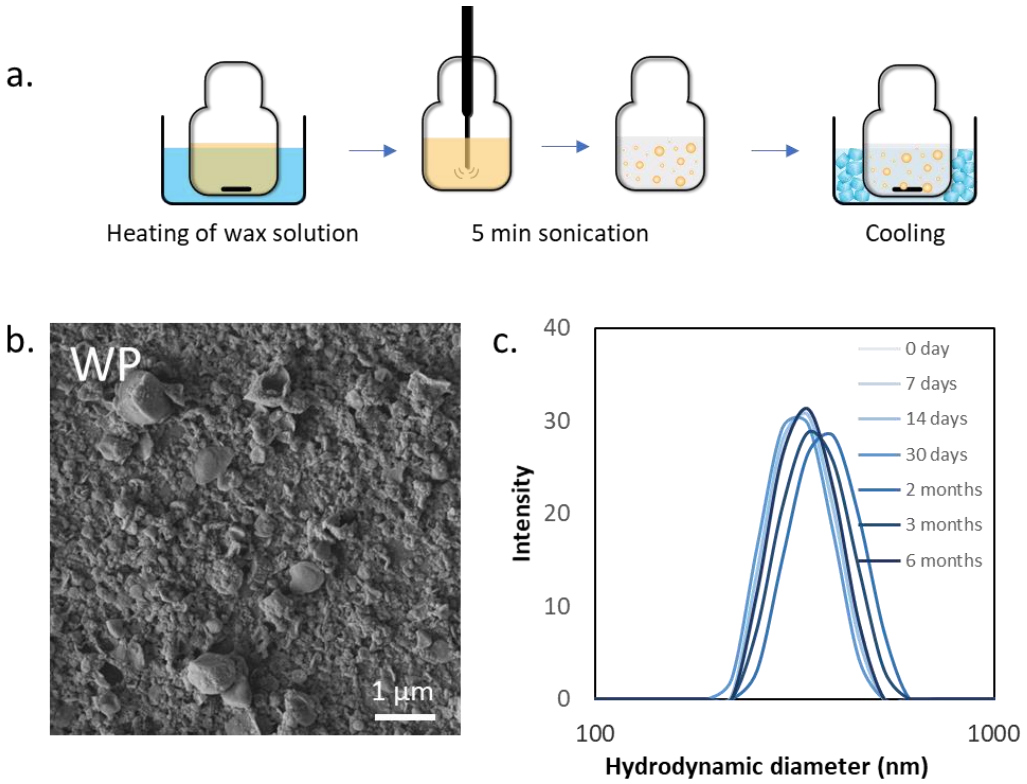

Figure IV.4. a. Wax particles preparation consisting of wax melting in boiling water followed by 5 min of sonication and fast cooling of the resulting emulsion. **b.** SEM image of the wax particles associated with the **c.** evolution of their size distribution over time.

Optimization of the wax and CNF layers design to reduce water vapor permeability.

All films were made by filtration and drying using the same method (hot pressing for 10 min followed by cooling and drying under pressure). However, suspensions were filtrated with three different procedures (**Figure IV.3**). The first film was prepared by mixing CNF and wax particles suspensions before filtration ("Mix"), whereas the second was obtained by filtering the CNF suspension first followed by filtration of the WP suspension on top and drying of the two layers together ("Top layer"). The last film was prepared by successive and intercalated filtrations of the CNF-WP-CNF suspensions ("Sandwich") – CNF total content was divided equally in each layer (first and last). A similar film to the Sandwich but with small amount of CNF present in the WP suspension (9% relative to the WP mass) was also prepared to boost the adhesion and the mechanical properties of the layered assembly, which will be referred as "Sandwich WP_{CNF}". A CNF film without wax was prepared as a reference ("CNF"). Both the Top layer film and the Sandwich were designed to obtain a continuous layer of wax upon drying of the film at high temperature ($T > T_{melting}$ wax) to partially melt the wax particles.

Table IV.1 displays the composition of the films; constant amount of wax and CNF was used and only the process used to make the films differs. The films thicknesses and apparent densities are also reported in **Table IV.1**. Thicknesses of the films varied with the total mass, the high thickness and low density of the Top layer was caused by the formation of an uneven surface of the film as shown by the higher standard deviation of the thickness compared to the other films. The other wax containing films had an apparent density similar to that of the CNF film. Slight differences in apparent density could be explained by the lower density of wax (0.99 g/cm^3) compared to cellulose (1.5 g/cm^3).

Table IV.1. Composition, thickness, and apparent densities of the resulting films.

	CNF	Wax	ChNF	LP	Thickness	Density
	mg	mg	mg	mg	µm	
CNF	54				32 ± 2	1.35 ± 0.07
Mix	54	5.3			37 ± 3	1.26 ± 0.11
Top layer	54	5.3			47 ± 5	1.03 ± 0.15
Sandwich	54	5.3			37 ± 2	1.33 ± 0.04
Sandwich WP_{CNF}	54.5	5.3			38 ± 3	1.31 ± 0.08
Multilayer	27	5.3	27	2.7	45 ± 4	1.20 ± 0.05

The overall morphology of the films was investigated by SEM imaging of their cross-sections (**Figure IV.5**). The microstructure of "Mix" film is homogeneous and comparable to the structure of the reference film which comprises packed CNF layers. No macropores or aggregation of wax was visible which demonstrates a homogenous mixture during melting, and good compatibility between wax and CNF. The wax layer can be well-identified in the Top layer and both Sandwich designs, as a dense and uniform layer.

The thicknesses of the wax layer measured from the SEM images were 0.9 ± 0.4 µm, 3.3 ± 0.5 µm and 4.6 ± 0.7 µm for the Top layer, the Sandwich, and the Sandwich WP_{CNF} designs respectively. However, the wax layer was not continuously spread on the surface of the Top layer film. The interface at the wax layer differed during drying of the Top layer and Sandwich

films. While in the Sandwich design the wax was surrounded by two layers of CNF, in the Top layer the wax was in between one layer of CNF and a Teflon plate. The presence of smooth Teflon could have encouraged the coalescence of wax droplets during the melting step and adhesion between the Teflon plate and the wax during drying could led to partial removal of the wax layer when the plate was separated from the film. In the Sandwich WP_{CNF} design, the presence of CNF in the wax layer increased the thickness of the intercalated layer from 3.3 ± 0.5 µm to 4.6 ± 0.7 µm. However, the film density did not change, which shows a good packing and compatibility between CNF and wax.

Moreover, the control of the temperature as well as the time of heating during pressing are key parameters for the formation of a continuous layer of wax. Preliminary experiments showed that lower temperatures and/or shorter times did not give enough time for the wax to melt and form a dense layer while higher temperatures and/or longer times completely melted the wax and formed non-continuous, coalesced patches of wax across the film. Presence of water during drying as well as CNF in the WP layer could also influence the melting of the wax.

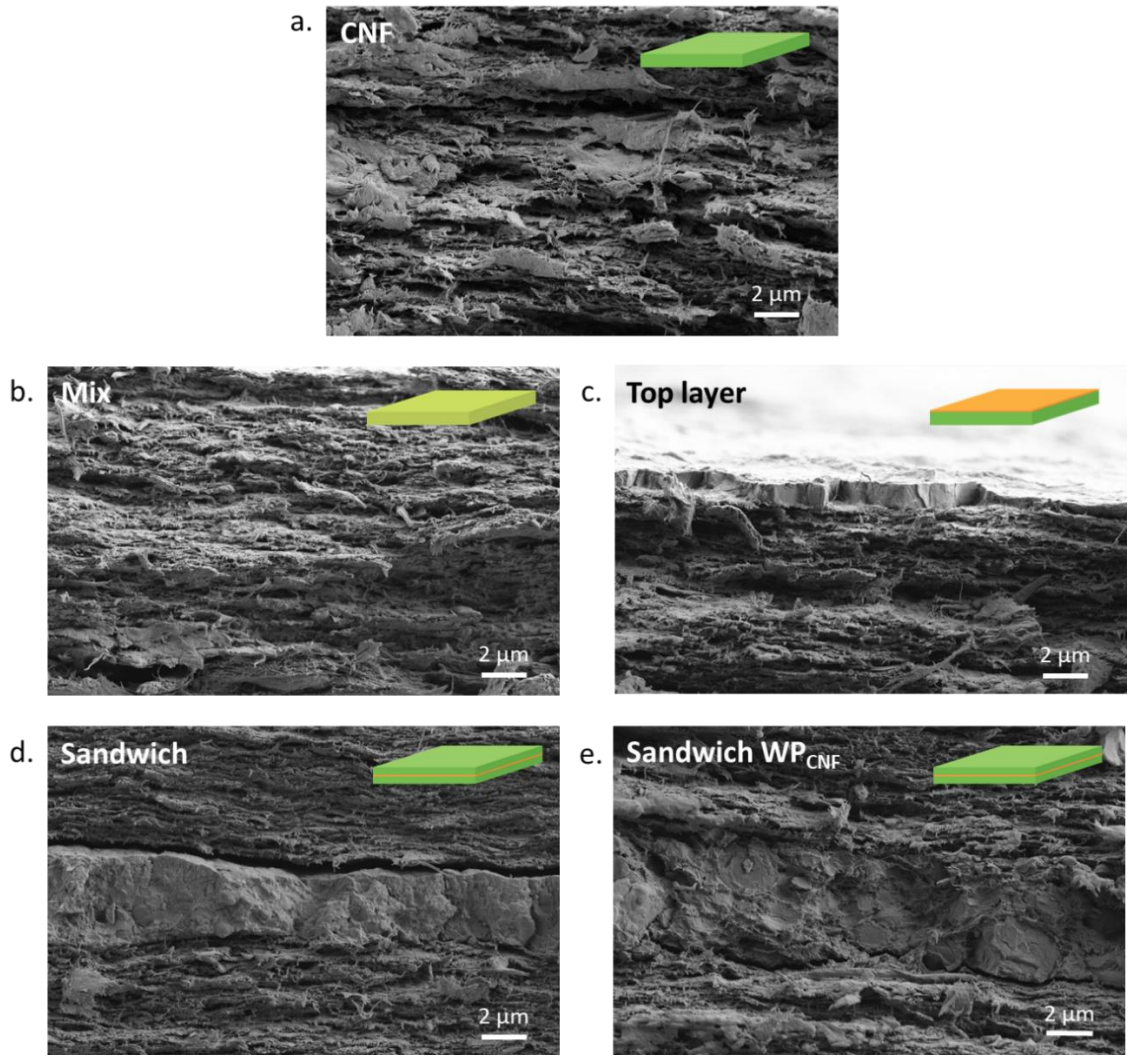

Figure IV.5. SEM images of the cross-sections of the films containing wax. **a.** CNF alone, **b.** Mix of wax and CNF, **c.** layer of wax on top of a CNF film, **d.** wax layer in between two CNF layers and **e.** wax layer containing CNF in between two CNF layers.

Wax layer was added to the multilayer design to decrease its water vapor transmission rate (WVTR); therefore, we analyzed the WVTR of the different films at two different humidity (**Figure IV.6a**). At 50% RH, the Mix design had high WVTR of 107 ± 14 g/m^2.day which is close to pure CNF films, while the Top layer and Sandwich had significantly lower WVTR of 11 ± 5 g/m^2.day and 5 ± 1 g/m^2.day respectively. This shows that the presence of wax in the film is not enough to decrease WVTR but that a continuous layer of wax is necessary to effectively act as a barrier for water vapor. These results are very promising as only a thin layer of wax can decrease the WVTR by 20 times. This is in accordance with Lange and Wyser who stated that laminar structure decreases the permeability exponentially while particulate system

leads to a linear decrease of permeability with the volume of additives.[24] Moreover, Spence *et al.* showed that the diffusion of water vapor through a microfibrillated cellulose film occurs mainly through the pores of the film following Fick's law.[25] Diffusion of water vapor is then controlled by the pore network (size of the pores, distribution within the film) but when a wax layer was present on the film it became the limiting factor for controlling the water vapor permeability.[25] In fact, water vapor permeability (WVP) of carnauba wax was reported to be 29 µm.g/m^2.day.kPa[26] due to the low solubility of water vapor in the wax matrix because of its apolar character. On the other hand, we calculated the WVP of CNF to be 4700 ± 500 µm.g/m^2.day.kPa. This explained that the WVTR of the film is controlled by the wax layer; in this case, the thickness of the wax layer becomes the key parameter to control the WVTR.

Compared to 50% RH, the WVTR at 80% RH increased for all the films partly due to the higher difference in water vapor pressure between outside and inside the measurement setup but also due to the swelling of the (hydrophilic) nanofiber network that favored the diffusion of water vapor through its newly expanded pores. The increase was limited for the Sandwich film, which remained at 14 ± 2 g/m^2.day. However, even if the Sandwich WP_{CNF} design (containing small amount of CNF in the wax layer) showed WVTR of 13 ± 1 g/m^2.day at 50% RH, at high humidity it increased to over 100 g/m^2.day. The CNF dispersed in the wax layer could swell at high humidity which creates discontinuities (or even cracks) and a porous path through the wax layer for water vapor to diffuse. The Top layer design had a WVTR of 49 ± 36 g/m^2.day at 80% RH, the inhomogeneity and low thickness of the wax layer was exacerbated at high humidity as shown by the standard deviation.

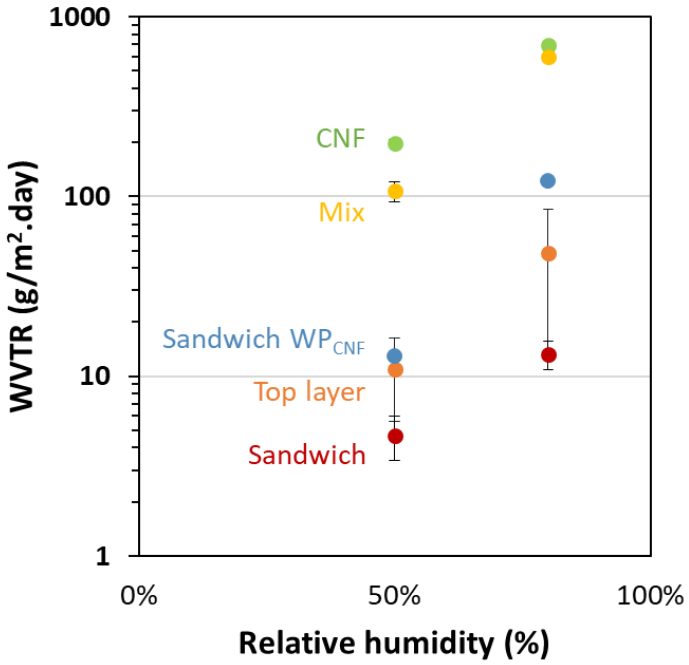

Figure IV.6. WVTR of the different films at 50% and 80% RH.

Influence of the wax and CNF designs onto films mechanical properties.

We then evaluated the mechanical properties (**Figure IV.7**) of the various designs to assess the effect of the wax layer configuration on the robustness of the CNF film. **Figure IV.7a** shows the tensile profiles of the films. The Mix configuration had similar mechanical properties (strength, strain, and Young's Modulus) as the reference CNF film while the Sandwich and Top layer films presented similar maximum strain but lower strength and Young's Modulus. The lower modulus and strength of the Sandwich and Top layer materials could be explained by the presence of the wax layer that increases the total thickness of the film but do not contribute to the cohesion of the supporting network. In fact, when looking at the tensile profile of the *force vs displacement* (**Figure IV.7b**), we observed similar Young's Modulus and force at break for all the films which indicated that the mechanical properties are driven by the cellulose nanofibers layer(s), as expected.

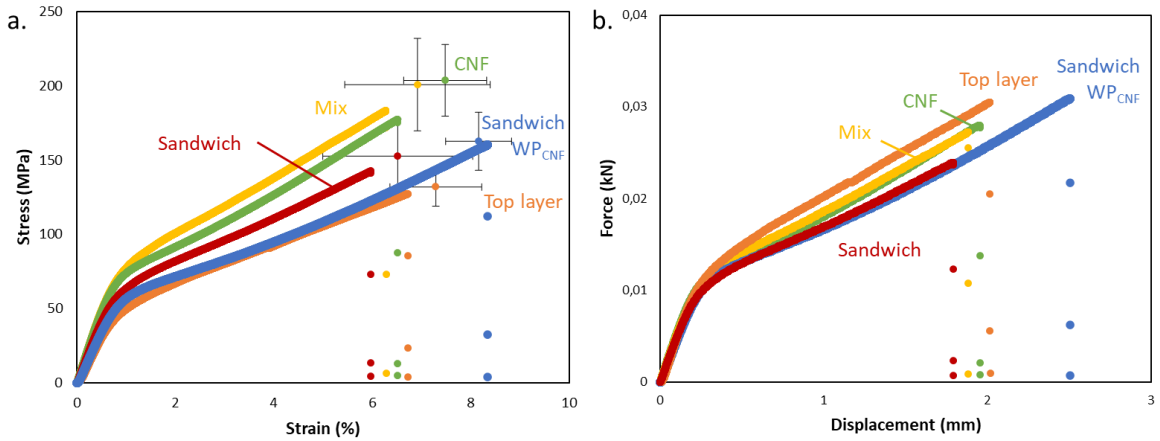

Figure IV.7. a. Tensile stress *vs* strain profile of the different films, as well as their average stress and strain. **b.** Force *vs* displacement of the same films during tensile tests.

Furthermore, during the testing of the Sandwich design, double fracture occurred in a significant number (~40%) of samples **(Figure IV.8a)**. This behavior points at the materials breaking in two stages, first, one of the CNF layers fails followed by the second one inducing delamination of the construct.

To better understand the internal fracture and to determine if the double fracture is due to a lack of cohesion of the wax layer or a lack of adhesion between the different layers, we performed FTIR analysis of the inside surface of the delaminated films. **Figure IV.8b** includes the FTIR spectra of both inside surfaces as well as the spectra of wax and CNF alone. The inside surface of the top part had more wax on the surface as shown by the peaks at 2916 cm^{-1} and 2847 cm^{-1} characteristic of the CH_2 stretching of the wax while the cellulose signature between 1150 cm^{-1} and 890 cm^{-1} was not visible. On the other hand, the bottom part contained significantly more cellulose than wax. Hence, the wax layer was present mostly on one side which lead to the conclusion that the adhesion between the CNF and wax layer should be further optimized. This was confirmed by the SEM image of the cross-section of the Sandwich (**Figure IV.5**) that indicates a lack of adhesion between the wax layer and the CNF layer. Nevertheless, even with non-interacting surfaces we reached cumulated strength values close to those of pure CNF films. Babaei-Ghazvini *et al.* also obtained double fracture while measuring the tensile properties of starch/chitosan double layered film.[27] While wet lamination of cellulosic materials and drying together lead to strong adhesion between layers due to the formation of strong hydrogen bonds upon drying between the layers,[28] the hydrogen bonds between wax and CNF was limited because of the lipidic nature of the wax. Improvement in

adhesion between the layers is the next step to be optimized, it could be achieved for example by adding a tie layer that has both affinity towards CNF and wax.[29]

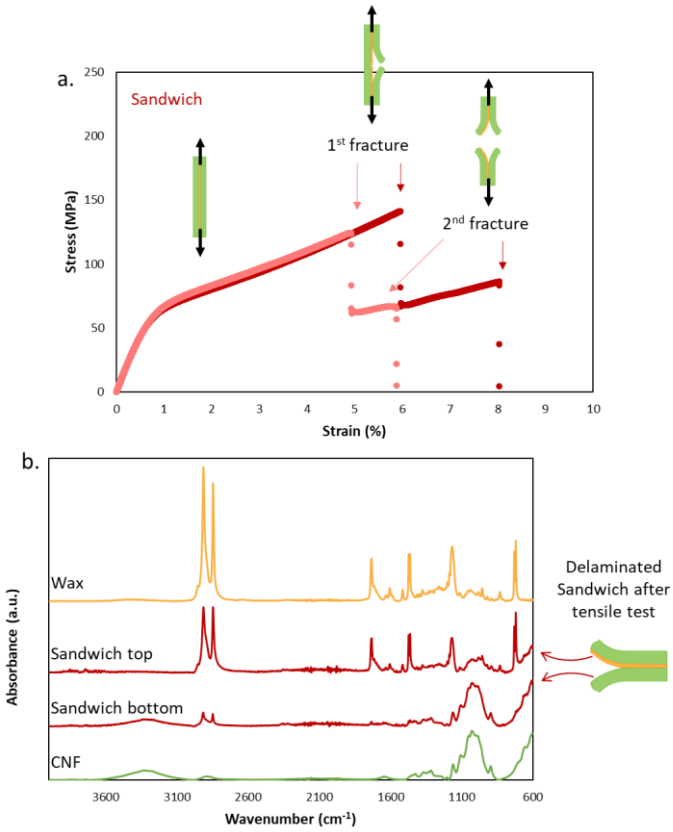

Figure IV.8. a. Behavior of some of the Sandwich films during tensile tests, arrows point at the different fracture. **b.** FTIR spectra of the inside surface of the films after delamination during the tensile tests associated with the spectra of wax and CNF alone.

As demonstrated here and in the literature,[29,30] blends tend to have higher mechanical properties than layered materials whereas layered materials have higher barrier properties. We showed that the presence of continuous wax layer was necessary to obtain high water vapor barrier properties. Among the two films that had continuous layer of wax, the Sandwich design comprised a more homogeneous wax distribution which was emphasized by the stable, and low WVTR. Moreover, humidity had limited impact on the WVTR as it was driven by the wax layer, the latter being inert to humidity. Even though delamination occurred during tensile testing, the final strength values are comparable to those of CNF, but we recognize that mechanical properties can be improved with further studies. In conclusion, we found the Sandwich film to be a good compromise between higher water vapor barrier and mechanical strength.

Final Multilayer film with high barrier properties.

Herein we emphasize the versatility of layered constructs and how these designs can be used to include multiple functionalities within the same film. In this context, we decided to functionalize our Sandwich film with lignin nanoparticles. Due to the phenolic nature of lignin, the addition of lignin particles to a nanofiber film brings UV shielding property. In **Chapter III.2**, we demonstrated the strong interfacial interaction between chitin nanofibers and lignin particles which would allow high retention of the particles during filtration. Film of chitin nanofibers containing 9% of lignin particles (LPChNF) displayed complete UV shielding and antioxidant property at the surface of the film. To include UV-light barrier properties to our high gas barrier material, we designed a multilayer assembly by replacing one of the CNF layers in the Sandwich by LPChNF. **Table IV.1** shows the amount of each materials used, with the wax and total nanofiber amount being kept constant between the Sandwich and Multilayer materials. The same filtration and drying methods as the Sandwich design were used to produce the Multilayer film.

Figure IV.9a shows the SEM image of the cross-section of the Multilayer film. Similar morphology as the Sandwich was observed as a dense wax layer was intercalated by two lamellar fibrous layers. Lignin particles were not visible in the top layer due to their nanometric size; however, due to the electrostatic attraction between lignin particles and chitin nanofibers we expect the lignin particles to be present only in the ChNF layer. The wax layer thickness was 3.3 ± 0.6 µm equivalent to that of the Sandwich film. The mechanical properties of the Multilayer are presented in **Figure IV.9b**. During the tensile tests, every sample of the Multilayer design ruptured in two steps. We noted that the LPChNF layer was always the first one to break, which is explained by the lower strength of LPChNF compared to CNF (**Figure IV.9b**). The ultimate strength of the whole layered material was limited by its weakest part which is a common thing among composite materials. The Multilayer film during tensile testing could be compared to two single layers competing, the CNF film, having double strength and 20% higher strain than LPChNF film, is expected to be more resistant.

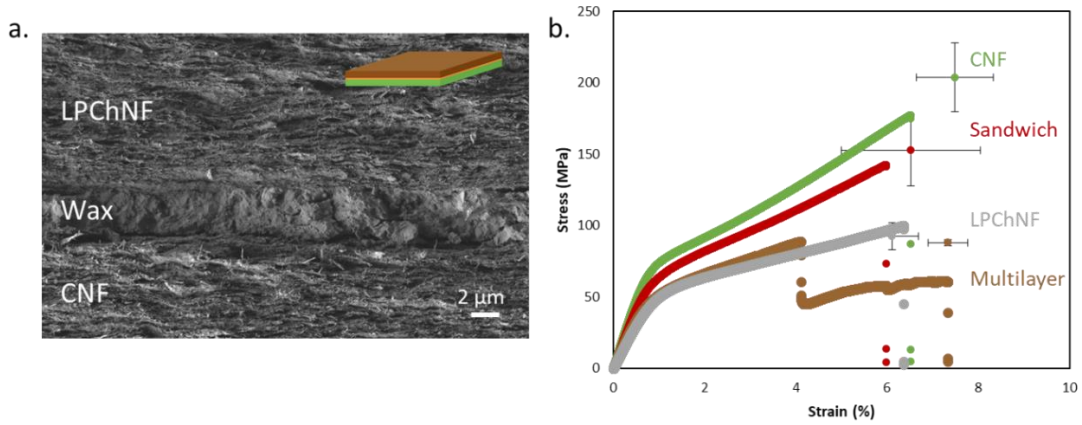

Figure IV.9. a. SEM picture of the cross-section of the multilayer film associated with the mechanical properties of the films (**b.**).

Surface properties and interactions with liquid are important for packaging applications especially for biobased materials that are sensitive to water, hence we measured the surface water interactions and grease penetration of the films. **Figure IV.10** shows the water contact angle (WCA) of the different films and its evolution with time. The WCA of the Top layer film was 114 ± 1°, it approximates the WCA of the wax alone as the surface of Top layer film is mainly made of melted wax. This observation is in line with the well-known hydrophobic nature of the wax. CNF film had the lowest WCA of 43 ± 1° followed by the Sandwich film, 55 ± 2°. The presence of wax in the film prevented water absorption and the decrease of contact angle with time. The Multilayer had a WCA of 70 ± 1°, it is higher than the Sandwich film because LPChNF was present on the surface. WCA of LPChNF was considerably higher than the one of CNF. Both chitin and lignin have hydrophobic functional groups that decrease the hydrophilicity of the polymers, in addition, strong ionic interactions between negatively charged LP and positively charged ChNF also reduce the potential interactions with water.

Grease penetration is also an essential property when packing a certain type of food. CNF have been reported to have barrier properties against liquid grease.[13,31] To confirm the grease barrier properties of the films, we tested the penetration of dyed olive oil through the CNF, Sandwich, and Multilayer films. After one week of contact at 40 °C, none of the tested films showed traces of oil penetration. This is in accordance with the literature where grease resistance properties were reported for CNF coated paper with coating weight as low as 11 g/m^2 measured with the Kit Test method.[9]

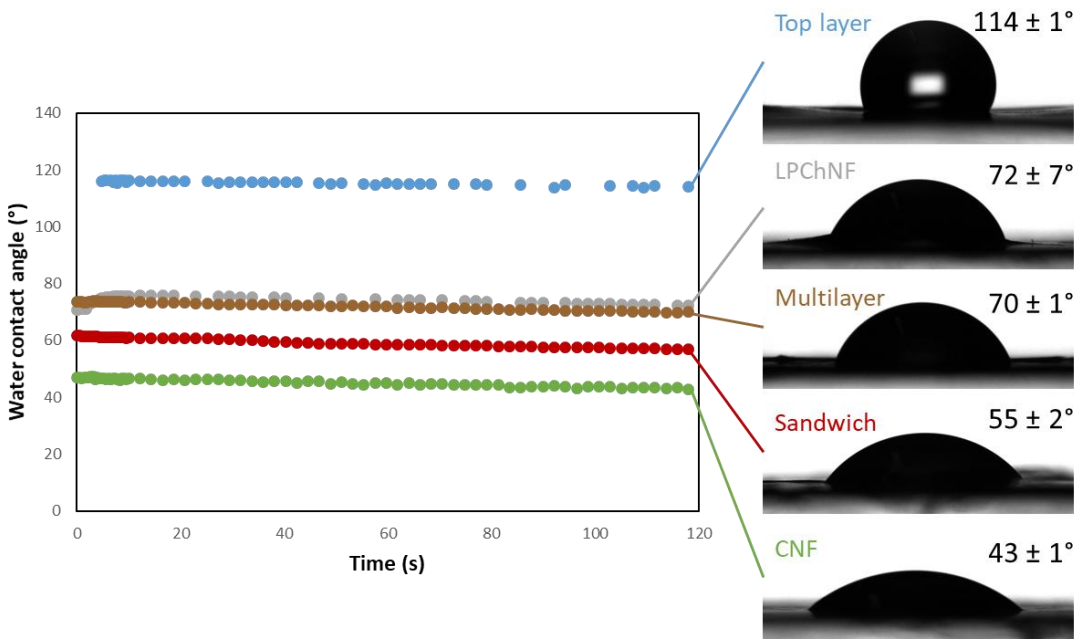

Figure IV.10. Water contact angle as function of time and images of the water droplets after 2 minutes of contact with the films.

The UV-barrier imposed by the presence of lignin in the Multilayer design was assessed by UV-Vis spectrophotometry (**Figure IV.11**). The films were visually homogeneous and transparent when in contact with a background. However, CNF had only a transmittance between 20% and 40% in the visible range which shows the translucent property of the films in general. The addition of wax in the Sandwich film reduced remarkably the UV transmittance between 200-240 nm and 290-320 nm, but it did not induce complete UV-blockage. After adding the lignin-containing layer, the transmittance in the visible range remained similar while the transmittance in the UV range (from 200 to 350 nm) decreased to 0%. The Multilayer film contained only 4% of lignin and this was enough to provide complete UV shielding while keeping translucent properties. Similar phenomena occurred when lignin particles were added to poly(vinylalcohol) (PVA) matrices.[32,33] Posoknistakul *et al.* showed that 3% of lignin particles in PVA was needed to reach complete UV absorbance. The presence of lignin particles in the system can also improve the mechanical resistance of the film when exposed to UV light (unpublished data). In fact, UV rays are preferentially absorbed by LP which prevents the oxidation of cellulose and the increase its brittleness.[34]

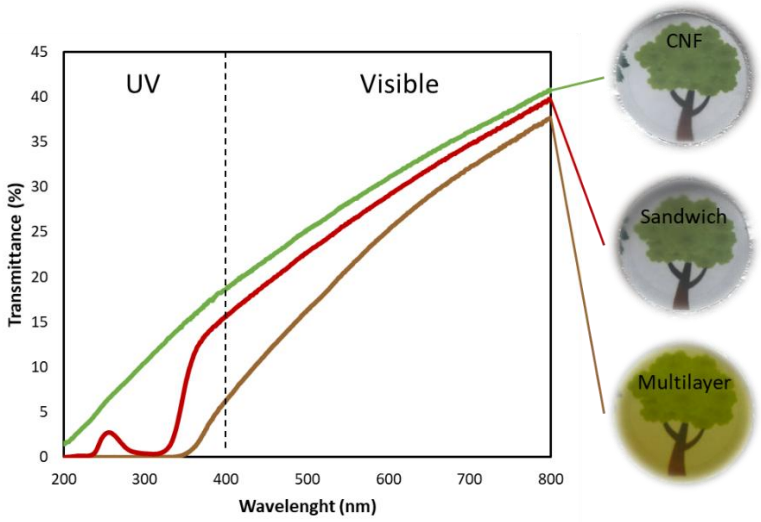

Figure IV.11. Films transmittance towards UV and visible light for the CNF, Sandwich and final Multilayer films and their respective images.

After optimizing water vapor, UV, and grease barrier we investigated the effects of the layered combination on the oxygen transmission rate (OTR), which is an important feature in packaging as oxygen has detrimental effects on foodstuff and can reduce their shelf-life.[2] CNF have high barrier properties against oxygen as they form packed layers bond together by inter and intra fibrils hydrogen bonds.[7] **Table IV.2** presents the OTR and WVTR of our final designs and reference materials measured at 50% RH and 23°C. It can be noticed that the presence of the wax layer did not influence the OTR of the films, and it even slightly decreased it due to an increase in the thickness. Chitin nanofibers are also known to have high oxygen barrier properties due to the high aspect ratio of the nanofibers and their entanglement,[35] which explains the similar OTR values between the final Multilayer and the Sandwich films. The WVTR of the Multilayer is similar to the Sandwich film as the amount of wax and the layer thickness were the same.

Table IV.2. Oxygen and water vapor transmission rates measured at 50% RH and 23°C associated with their permeabilities calculated using their thicknesses. Wax permeabilities extracted from[26]

50% RH	OTR	OP	WVTR	WVP	Thickness
	$cm^3/m^2.day$	$\mu m.cm^3/m^2.day.kPa$	$g/m^2.day$	$\mu m.g/m^2.day.kPa$	µm
CNF	5 ± 3	1.4 ± 1.1	197 ± 3	4734 ± 511	32 ± 2
Sandwich	4 ± 1	1.5 ± 0.6	5 ± 1	121 ± 35	37 ± 2
Multilayer	3 ± 1	1.5 ± 0.4	6 ± 1	174 ± 21	45 ± 4
Wax		157		28	

The permeabilities of the films were also calculated as they do not take into consideration the thickness of the films. However, for Multilayer design it considers the full thickness of the film while some layers do not contribute as a barrier, possibly resulting in permeabilities that differ from the single components. The oxygen permeability (OP) of the CNF is two orders of magnitude lower than the permeability of carnauba wax (**Table IV.2**), hence the oxygen diffusion is driven by the nanofiber layers (cellulose and chitin). Their thickness, density, and crystallinity will influence the OTR of the Multilayer. On the other hand, the water vapor permeability (WVP) of the CNF is two orders of magnitude higher than the WVP of carnauba wax (**Table IV.2**), so we expect the wax layer to be the controller of the transport of water vapor through the film. The difference in WVP between the Multilayer and the wax is explained by the main contribution of the nanofibers to the thickness of the film. Moreover, if one calculates the WVTR of a 3.3 µm thick wax layer one would obtain a value of 12 $g/m^2.day$, meaning that the nanofiber layers also participated in decreasing the WVTR by creating a porous network around the wax layer that slows down the diffusion of water molecules.[25] **Figure IV.12** summarized by a schematic of the multilayer film, the layers driving the different gas barrier properties.

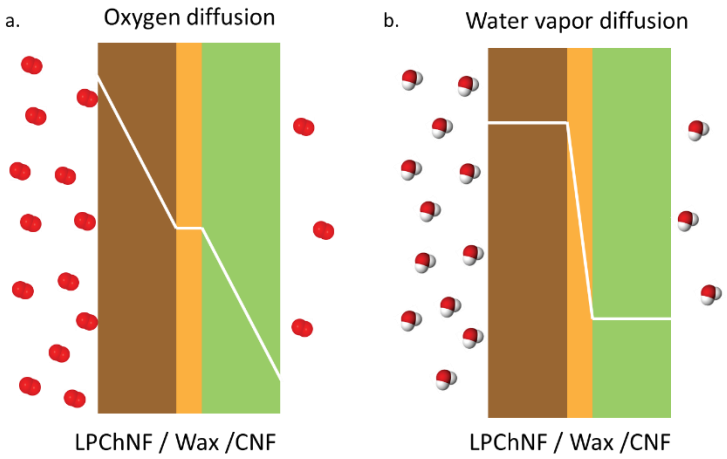

Figure IV.12. Schematic of the diffusion of oxygen (**a.**) and water vapor (**b.**) throughout the Multilayer film.

To evaluate the impact of humidity on the barrier properties of the films, OTR and WVTR were also measured at 80% RH and 23°C (**Table IV.3**). The OTR of all the films increased by one order of magnitude with humidity while the WVTR increased to a smaller extend. As shown in literature, the sensitivity to water of both cellulose and chitin nanofibers explains the increase in OTR. At high humidity, the film swells due to the presence of water that penetrates and weakens the film cohesion by competing with the hydrogen bonds between nanofibers.[15] Unlike cellulose and chitin, carnauba wax has a lipidic nature and does not interact with water. Yet, despite its hydrophobic nature carnauba wax contains polar groups and its sensitivity to water is directly linked to their amount.[26] Moreover, the increase in OTR at high humidity was smaller for the Sandwich and Multilayer materials than for the CNF reference showing that even with its high OP, the presence of wax had an influence on the OTR at high humidity.

Table IV.3. Oxygen and water vapor transmission rates measured at 80% RH and 23°C associated with their permeabilities calculated using their thicknesses.

80% RH	OTR	OP	WVTR	WVP	Thickness
	$cm^3/m^2.day$	$\mu m.cm^3/m^2.day.kPa$	$g/m^2.day$	$\mu m.g/m^2.day.kPa$	µm
CNF	61 ± 7	19 ± 3	695 ± 6	10501 ± 7779	32 ± 2
Sandwich	39 ± 3	15 ± 1	14 ± 2	236 ± 34	37 ± 2
Multilayer	55 ± 2	27 ± 1	16 ± 2	304 ± 39	45 ± 4

Final Multilayer film possible applications in food packaging

To compare with the literature, we plotted the OTR *vs* WVTR graph and positioned our films on it at different humidity conditions (**Figure IV.13a**) and with respect to common polymers and food specificities (**Figure IV.13b**). Common polymers used for food packaging such as polyethylene (PE) and polypropylene (PP) have low WVTR but high OTR, so they are usually used in multilayers.[36] This graph shows that no single material can reach high barrier properties for both oxygen and water vapor, which is the main reason why multilayer assemblies are driving the packaging market for long time. We can see that CNF films/layers have already sufficient oxygen barrier properties to pack several kinds of food but their WVTR is too low for any application. Adding a wax layer and reducing the WVTR by almost two orders of magnitude allows us to consider biobased packaging materials for food types such as milk, nuts, and snacks.[29] Moreover, tuning the thickness of the wax layer would allow to meet the requirements for meat and modified atmosphere packaging (MAP).

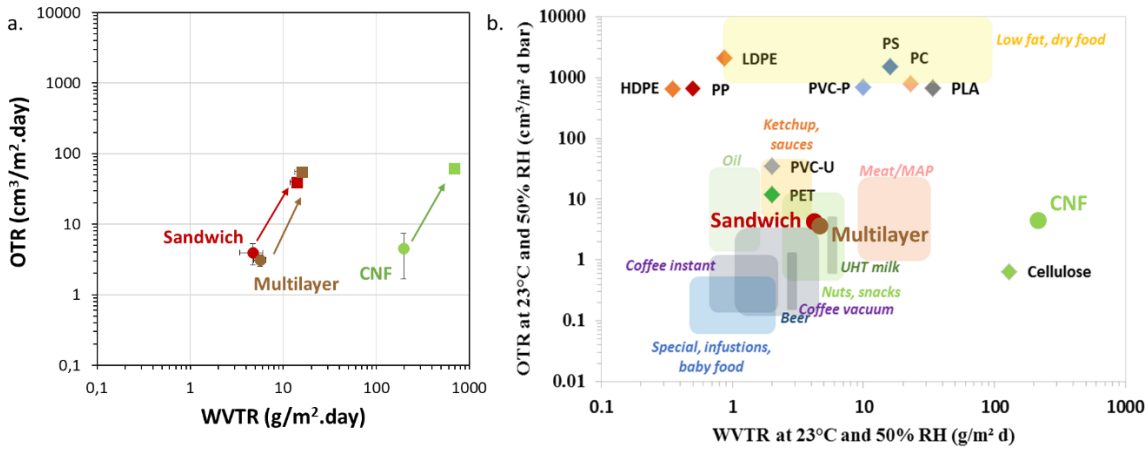

Figure IV.13. a. Barrier properties of the films at 50% (●) and 80% (■) relative humidity and comparison with some food requirements and existing polymers (**b.**). Image adapted from[37]

As our material is composed of several layers, it is more appropriate to compare it with similar multilayered materials. **Table IV.4** presents the barrier properties of biobased multilayers from literature associated with the thickness of different layers. Most contributions added PLA as water vapor barrier layer as it is considered biodegradable depending on the degradation conditions and it has higher water vapor barrier than cellulose; however, this resulted in medium water vapor barrier properties around 30-40 g/m^2.day as it is limited by the WVP of PLA. Coating of HDPE with CNF resulted in high barrier properties towards both oxygen and water vapor; however, at 80% RH the OTR of the same film was 310 ± 40 cm^3/m^2.day due to

the very low thickness of the CNF layer.[38] Moreover, similar film than our Sandwich design was prepared by dipping CNF film in paraffin wax solution, which resulted in a wax/CNF/wax multilayer with low OTR and WVTR.

Table IV.4. OTR and WVTR measured at 50% RH for biobased multilayer films in literature.

	OTR	WVTR	Thickness	Reference
	$cm^3/m^2.day$	$g/m^2.day$	µm	
CNF/wax/CNF	4 ± 1	5 ± 1	16/4/16	our work
CNF/wax/LPChNF	3 ± 1	6 ± 1	16/4/27	our work
Paperboard/MFC/PLA	10.5	43 ± 0.4	270/8/19	Koppolu *et al.* 2019[10]
Paperboard/CNC/PLA	6	28 ± 0.2	270/8/19	Koppolu *et al.* 2019[10]
PLA/$(CNC/ChNF)_2$	70	65	25/4	Satam *et al.* 2018[35]
HDPE/CNF	0.5 ± 0.1*	2.2 ± 0.3[#]	48/1	Vähä-Nissi *et al.* 2017[38]
PLA/CNF/PLA	30*	50	25/30/25	Le Gars *et al.* 2020[37]
Paper/CNF/Shellac wax	4466 ± 103	6.54 ± 1.12	63/3/11	Hult *et al.* 2010[18]
Paraffin wax/CNF/wax	0.1	40	70	Österberg *et al.* 2013[17]

*OTR measured at 0% RH [#]WVTR measured at 75% RH, MFC = microfibrilated cellulose, PLA = polylactic acid, CNC = cellulose nanocrystals, HDPE = high density polyethylene,

We have shown that the Sandwich and Multilayer films display suitable barrier for packaging of dry food. Hence, we set up an experiment to test their effectiveness in keeping the texture of commercial crackers. The selected crackers are sensitive to humidity, becoming soft even with little content of humidity. The crackers were placed in glass bottles that are sealed by our films and the respective controls (**Figure IV.14a**). After one week at 80% RH, we performed compression tests on the crackers to evaluate changes in texture (**Figure IV.14b**). Cracking texture was only observed when the crackers were protected by a high water vapor barrier film *i.e.* our Sandwich and final Multilayer, which performed similarly to the synthetic, original package. Crackers unprotected or protected by CNF showed soft texture due to the presence of humidity. Stress and strain profile of the compression tests are displayed in **Figure IV.14d**, the

cracking during the tests is indicated by arrows. In fact, cracking in the crackers correspond to an instantaneous release of stress which is shown by a peak in the stress-strain curve. The presence of multiple cracks during the compression test points that the crackers were well preserved and that their main textural property was maintained. Crackers protected by the CNF film displayed smooth compression profile with no peak, with similar results obtained when no film were used.

The efficiency of our films is also highlighted by the final moisture content of the crackers after one week being conditioned at 80% RH (**Figure IV.14c**). Crackers protected by the Sandwich and Multilayer designs had a similar moisture content than crackers protected by the original package while the one protected by the CNF film had double moisture content.

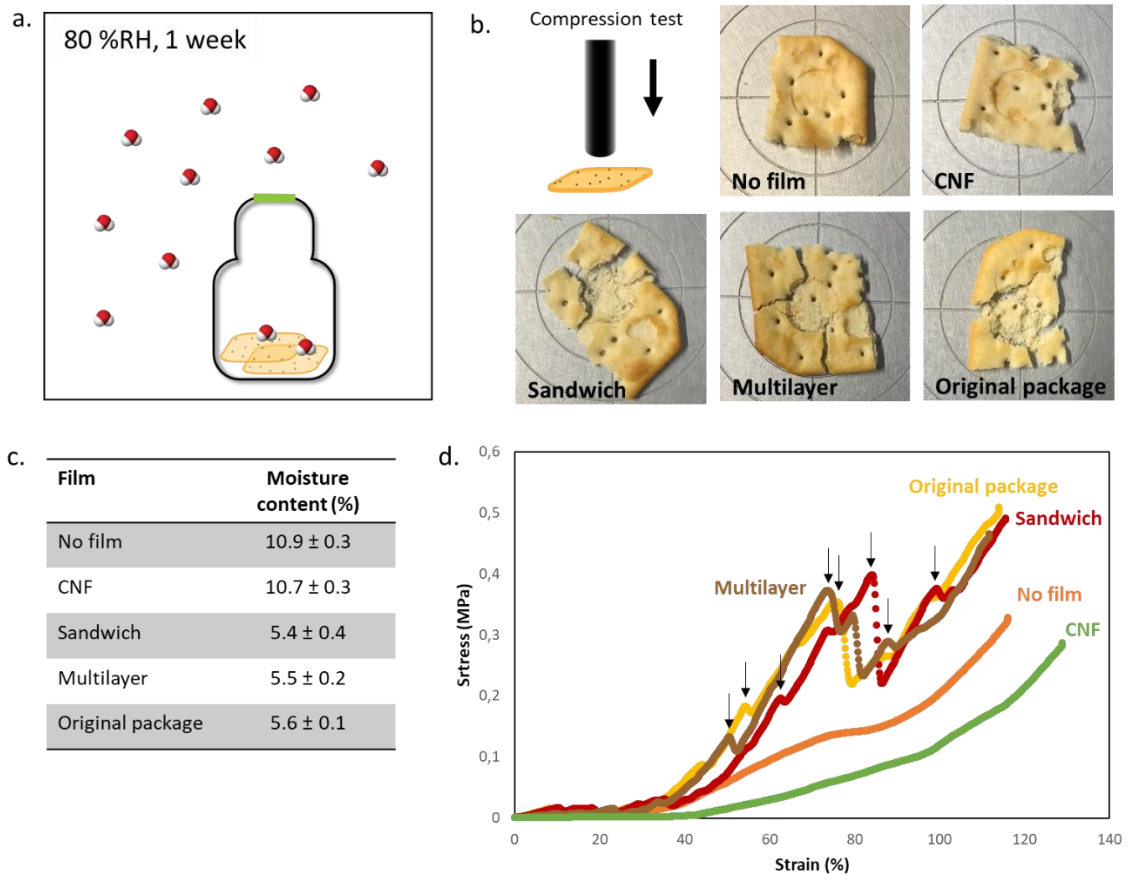

Film	Moisture content (%)
No film	10.9 ± 0.3
CNF	10.7 ± 0.3
Sandwich	5.4 ± 0.4
Multilayer	5.5 ± 0.2
Original package	5.6 ± 0.1

Figure IV.14. a. Set up of the packaging test on crackers, green line represents the tested film **b**. Images of the crackers after compression tests **c.** Moisture content of the crackers at the end of the packaging test. **d.** Compression profiles of the crackers packed with the different films, arrows point at cracks during the compression tests.

We demonstrated that our Sandwich (CNF/wax/CNF) film can be further functionalized by including anchored nanoparticles. We exemplify with UV-blocking lignin particles, but other active molecules or nanoparticles could also be incorporated. The gas barrier properties (oxygen and water vapor) were not influenced by the presence of the functional layer. Comparison with literature showed that as a fully biobased multilayer, our films stand out for its high barrier properties. Moreover, packaging test on crackers was done to demonstrate the low water vapor permeability of our film and its real impact on the maintaining the texture of dry food, showing a practical case to replace food packaging by bio-based and biodegradable high-performance solutions.

CONCLUSION

By tuning the process to incorporate carnauba wax to cellulose nanofiber films, we optimized films towards high water vapor barrier properties. WVTR as low as 5 ± 1 g/m^2.day was obtained when a wax layer of 3.3 µm was introduced in between two CNF layers. The high barrier properties of CNF towards oxygen were also maintained at 4 ± 1 cm^3/m^2.day at 50% RH. Moreover, we demonstrated the possibility to add lignin nanoparticles to one of the nanofiber layers to provide UV shielding properties to the multilayer film while keeping translucent properties. The high gas barrier properties of the film were not impacted by the presence of functional nanoparticles. An example with dry food application demonstrated all the potential of this innovative multilayer biobased solution. Moreover, we foresee that functionalization with other kind of active particles or molecules is possible using the same method.

Problems of adhesion between the wax layer and the cellulose or chitin layers was pointed out by delamination during the tensile testing of the films, but we point out that even with delamination the ultimate strength of our materials was comparable to the CNF reference. Moreover, the addition of a tie layer to improve compatibility between the layers should be further studied. Considering the high barrier properties of the obtained films, further study on upscaling of the process is a viable next step to be done. We consider a cellulosic substrate as support with coating or wet lamination of the different suspensions (CNF, wax) the most promising idea on a short-term basis.

Conclusion to Chapter IV

In this last Chapter, knowledge from the previous chapters on colloids preparation, as well as interactions was combined to form one multilayer film with several barrier properties. For this purpose, stable wax nanoparticles suspension was prepared by high energy emulsification of the wax at high temperature. Stability of the suspension in water allowed to process the wax in different ways by mixing it with CNF or filtering it on top of a CNF layer without disrupting the CNF network. The CNF films containing wax were tested for their water vapor barrier properties. Low permeabilities were obtained when the wax was present as a continuous layer. Mechanical tests of the different designs highlighted problems of adhesion between CNF and wax layers. Improvement of the adhesion by process optimization or addition of compatibilizer would be the next step to continue this study.

Following the same successive filtration process, a functional multilayer film containing CNF, wax and LPChNF was produced. After structural characterization, its barrier properties were tested. Due to the presence of lignin particles, the film presented a high barrier against UV light while staying translucent. It was also effective against oil penetration. The gas barriers were measured at different humidity. The oxygen permeability was controlled by the presence of cellulose and chitin nanofibers while the water vapor diffusion through the film was ruled by the wax layer. As oxygen permeability was controlled by the CNF layer, sensitivity to humidity was reported and optimization of OTR at high humidity is still needed.

A preservation test on dry food was realized and the films seemed promising. Further study on scale-up of the fabrication process would be interesting. Coating of the different layers on a paper substrate seems the most promising approach on a short-term basis.

References

(1) Kumar, P. Reduce, Reuse, Recycle. Plastic and Packaging Waste in the European Green Deal and Circular Economy Action Plan. *IASS Discussion Paper* **2020**. https://doi.org/10.2312/iass.2020.014.

(2) Helanto, K.; Matikainen, L.; Talja, R.; Rojas, O. J. Bio-Based Polymers for Sustainable Packaging and Biobarriers: A Critical Review. *BioRes* **2019**, *14* (2), 4902–4951.

(3) Leppänen, I.; Vikman, M.; Harlin, A.; Orelma, H. Enzymatic Degradation and Pilot-Scale Composting of Cellulose-Based Films with Different Chemical Structures. *J Polym Environ* **2020**, *28* (2), 458–470. https://doi.org/10.1007/s10924-019-01621-w.

(4) García, A.; Gandini, A.; Labidi, J.; Belgacem, N.; Bras, J. Industrial and Crop Wastes: A New Source for Nanocellulose Biorefinery. *Industrial Crops and Products* **2016**, *93*, 26–38. https://doi.org/10.1016/j.indcrop.2016.06.004.

(5) Schenker, U.; Chardot, J.; Missoum, K.; Vishtal, A.; Bras, J. Short Communication on the Role of Cellulosic Fiber-Based Packaging in Reduction of Climate Change Impacts. *Carbohydrate Polymers* **2021**, *254*, 117248. https://doi.org/10.1016/j.carbpol.2020.117248.

(6) Hubbe, M. A.; Ferrer, A.; Tyagi, P.; Yin, Y.; Salas, C.; Pal, L.; Rojas, O. J. Nanocellulose in Thin Films, Coatings, and Plies for Packaging Applications: A Review. *BioResources* **2017**, *12* (1), 2143–2233. https://doi.org/10.15376/biores.12.1.2143-2233.

(7) Lavoine, N.; Desloges, I.; Dufresne, A.; Bras, J. Microfibrillated Cellulose – Its Barrier Properties and Applications in Cellulosic Materials: A Review. *Carbohydrate Polymers* **2012**, *90* (2), 735–764. https://doi.org/10.1016/j.carbpol.2012.05.026.

(8) Foster, E. J.; Moon, R. J.; Agarwal, U. P.; Bortner, M. J.; Bras, J.; Camarero-Espinosa, S.; Chan, K. J.; Clift, M. J. D.; Cranston, E. D.; Eichhorn, S. J.; Fox, D. M.; Hamad, W. Y.; Heux, L.; Jean, B.; Korey, M.; Nieh, W.; Ong, K. J.; Reid, M. S.; Renneckar, S.; Roberts, R.; Shatkin, J. A.; Simonsen, J.; Stinson-Bagby, K.; Wanasekara, N.; Youngblood, J. Current Characterization Methods for Cellulose Nanomaterials. *Chem. Soc. Rev.* **2018**, *47* (8), 2609–2679. https://doi.org/10.1039/C6CS00895J.

(9) Kumar, V.; Elfving, A.; Koivula, H.; Bousfield, D.; Toivakka, M. Roll-to-Roll Processed Cellulose Nanofiber Coatings. *Ind. Eng. Chem. Res.* **2016**, *55* (12), 3603–3613. https://doi.org/10.1021/acs.iecr.6b00417.

(10) Koppolu, R.; Lahti, J.; Abitbol, T.; Swerin, A.; Kuusipalo, J.; Toivakka, M. Continuous Processing of Nanocellulose and Polylactic Acid into Multilayer Barrier Coatings. *ACS Appl. Mater. Interfaces* **2019**, *11* (12), 11920–11927. https://doi.org/10.1021/acsami.9b00922.

(11) Spieser, H.; Denneulin, A.; Deganello, D.; Gethin, D.; Koppolu, R.; Bras, J. Cellulose Nanofibrils and Silver Nanowires Active Coatings for the Development of Antibacterial Packaging Surfaces. *Carbohydrate Polymers* **2020**, *240*, 116305. https://doi.org/10.1016/j.carbpol.2020.116305.

(12) Aulin, C.; Karabulut, E.; Tran, A.; Wågberg, L.; Lindström, T. Transparent Nanocellulosic Multilayer Thin Films on Polylactic Acid with Tunable Gas Barrier Properties. *ACS Appl. Mater. Interfaces* **2013**, *5* (15), 7352–7359. https://doi.org/10.1021/am401700n.

(13) H. Tayeb, A.; Tajvidi, M.; Bousfield, D. Paper-Based Oil Barrier Packaging Using Lignin-Containing Cellulose Nanofibrils. *Molecules* **2020**, *25* (6), 1344. https://doi.org/10.3390/molecules25061344.

(14) Bardet, R.; Reverdy, C.; Belgacem, N.; Leirset, I.; Syverud, K.; Bardet, M.; Bras, J. Substitution of Nanoclay in High Gas Barrier Films of Cellulose Nanofibrils with

Cellulose Nanocrystals and Thermal Treatment. *Cellulose* **2015**, *22* (2), 1227–1241. https://doi.org/10.1007/s10570-015-0547-9.

(15) Ahankari, S. S.; Subhedar, A. R.; Bhadauria, S. S.; Dufresne, A. Nanocellulose in Food Packaging: A Review. *Carbohydrate Polymers* **2021**, *255*, 117479. https://doi.org/10.1016/j.carbpol.2020.117479.

(16) Sharma, S.; Zhang, X.; Nair, S. S.; Ragauskas, A.; Zhu, J.; Deng, Y. Thermally Enhanced High Performance Cellulose Nano Fibril Barrier Membranes. *RSC Adv.* **2014**, *4* (85), 45136–45142. https://doi.org/10.1039/C4RA07469F.

(17) Österberg, M.; Vartiainen, J.; Lucenius, J.; Hippi, U.; Seppälä, J.; Serimaa, R.; Laine, J. A Fast Method to Produce Strong NFC Films as a Platform for Barrier and Functional Materials. *ACS Appl. Mater. Interfaces* **2013**, *5* (11), 4640–4647. https://doi.org/10.1021/am401046x.

(18) Hult, E.-L.; Iotti, M.; Lenes, M. Efficient Approach to High Barrier Packaging Using Microfibrillar Cellulose and Shellac. *Cellulose* **2010**, *17* (3), 575–586. https://doi.org/10.1007/s10570-010-9408-8.

(19) Chick, J.; Hernandez, R. J. Physical, Thermal, and Barrier Characterization of Casein-Wax-Based Edible Films. *Journal of Food Science* **2002**, *67* (3), 1073–1079. https://doi.org/10.1111/j.1365-2621.2002.tb09455.x.

(20) Sadeghifar, H.; Ragauskas, A. Lignin as a UV Light Blocker—A Review. *Polymers* **2020**, *12* (5), 1134. https://doi.org/10.3390/polym12051134.

(21) Anukiruthika, T.; Sethupathy, P.; Wilson, A.; Kashampur, K.; Moses, J. A.; Anandharamakrishnan, C. Multilayer Packaging: Advances in Preparation Techniques and Emerging Food Applications. *Comprehensive Reviews in Food Science and Food Safety* **2020**, *19* (3), 1156–1186. https://doi.org/10.1111/1541-4337.12556.

(22) Lozhechnikova, A.; Bellanger, H.; Michen, B.; Burgert, I.; Österberg, M. Surfactant-Free Carnauba Wax Dispersion and Its Use for Layer-by-Layer Assembled Protective Surface Coatings on Wood. *Applied Surface Science* **2017**, *396*, 1273–1281. https://doi.org/10.1016/j.apsusc.2016.11.132.

(23) Khakalo, A.; Tanaka, A.; Korpela, A.; Orelma, H. Delignification and Ionic Liquid Treatment of Wood toward Multifunctional High-Performance Structural Materials. *ACS Appl. Mater. Interfaces* **2020**, *12* (20), 23532–23542. https://doi.org/10.1021/acsami.0c02221.

(24) Lange, J.; Wyser, Y. Recent Innovations in Barrier Technologies for Plastic Packaging—a Review. *Packaging Technology and Science* **2003**, *16* (4), 149–158. https://doi.org/10.1002/pts.621.

(25) Spence, K. L.; Venditti, R. A.; Rojas, O. J.; Pawlak, J. J.; Hubbe, M. A. Water Vapor Barrier Properties of Coated and Filled Microfibrillated Cellulose Composite Films. *BioResources* **2011**, *6* (4), 4370–4388. https://doi.org/10.15376/biores.6.4.4370-4388.

(26) Donhowe, G.; Fennema, O. Water Vapor and Oxygen Permeability of Wax Films. *Journal of the American Oil Chemists' Society* **1993**, *70* (9), 867–873. https://doi.org/10.1007/BF02545345.

(27) Babaei-Ghazvini, A.; Acharya, B.; Korber, D. R. Multilayer Photonic Films Based on Interlocked Chiral-Nematic Cellulose Nanocrystals in Starch/Chitosan. *Carbohydrate Polymers* **2022**, *275*, 118709. https://doi.org/10.1016/j.carbpol.2021.118709.

(28) Roig-Sanchez, S.; Jungstedt, E.; Anton-Sales, I.; Malaspina, D. C.; Faraudo, J.; Berglund, L. A.; Laromaine, A.; Roig, A. Nanocellulose Films with Multiple Functional Nanoparticles in Confined Spatial Distribution. *Nanoscale Horiz.* **2019**, *4* (3), 634–641. https://doi.org/10.1039/C8NH00310F.

(29) Wang, J.; Gardner, D. J.; Stark, N. M.; Bousfield, D. W.; Tajvidi, M.; Cai, Z. Moisture and Oxygen Barrier Properties of Cellulose Nanomaterial-Based Films. *ACS Sustainable Chem. Eng.* **2018**, *6* (1), 49–70. https://doi.org/10.1021/acssuschemeng.7b03523.
(30) Zhao, K.; Wang, W.; Teng, A.; Zhang, K.; Ma, Y.; Duan, S.; Li, S.; Guo, Y. Using Cellulose Nanofibers to Reinforce Polysaccharide Films: Blending vs Layer-by-Layer Casting. *Carbohydrate Polymers* **2020**, *227*, 115264. https://doi.org/10.1016/j.carbpol.2019.115264.
(31) Al-Gharrawi, M.; Ollier, R.; Wang, J.; Bousfield, D. W. The Influence of Barrier Pigments in Waterborne Barrier Coatings on Cellulose Nanofiber Layers. *J Coat Technol Res* **2021**. https://doi.org/10.1007/s11998-021-00482-0.
(32) Tian, D.; Hu, J.; Bao, J.; Chandra, R. P.; Saddler, J. N.; Lu, C. Lignin Valorization: Lignin Nanoparticles as High-Value Bio-Additive for Multifunctional Nanocomposites. *Biotechnology for Biofuels* **2017**, *10* (1), 192. https://doi.org/10.1186/s13068-017-0876-z.
(33) Posoknistakul, P.; Tangkrakul, C.; Chaosuanphae, P.; Deepentham, S.; Techasawong, W.; Phonphirunrot, N.; Bairak, S.; Sakdaronnarong, C.; Laosiripojana, N. Fabrication and Characterization of Lignin Particles and Their Ultraviolet Protection Ability in PVA Composite Film. *ACS Omega* **2020**, *5* (33), 20976–20982. https://doi.org/10.1021/acsomega.0c02443.
(34) Ahn, K.; Zaccaron, S.; Zwirchmayr, N. S.; Hettegger, H.; Hofinger, A.; Bacher, M.; Henniges, U.; Hosoya, T.; Potthast, A.; Rosenau, T. Yellowing and Brightness Reversion of Celluloses: CO or COOH, Who Is the Culprit? *Cellulose* **2019**, *26* (1), 429–444. https://doi.org/10.1007/s10570-018-2200-x.
(35) Satam, C. C.; Irvin, C. W.; Lang, A. W.; Jallorina, J. C. R.; Shofner, M. L.; Reynolds, J. R.; Meredith, J. C. Spray-Coated Multilayer Cellulose Nanocrystal—Chitin Nanofiber Films for Barrier Applications. *ACS Sustainable Chem. Eng.* **2018**, *6* (8), 10637–10644. https://doi.org/10.1021/acssuschemeng.8b01536.
(36) Tyagi, P.; Salem, K. S.; Hubbe, M. A.; Pal, L. Advances in Barrier Coatings and Film Technologies for Achieving Sustainable Packaging of Food Products – A Review. *Trends in Food Science & Technology* **2021**, *115*, 461–485. https://doi.org/10.1016/j.tifs.2021.06.036.
(37) Le Gars, M.; Dhuiège, B.; Delvart, A.; Belgacem, M. N.; Missoum, K.; Bras, J. High-Barrier and Antioxidant Poly(Lactic Acid)/Nanocellulose Multilayered Materials for Packaging. *ACS Omega* **2020**, *5* (36), 22816–22826. https://doi.org/10.1021/acsomega.0c01955.
(38) Vähä-Nissi, M.; Koivula, H. M.; Räisänen, H. M.; Vartiainen, J.; Ragni, P.; Kenttä, E.; Kaljunen, T.; Malm, T.; Minkkinen, H.; Harlin, A. Cellulose Nanofibrils in Biobased Multilayer Films for Food Packaging. *Journal of Applied Polymer Science* **2017**, *134* (19). https://doi.org/10.1002/app.44830.

General conclusion and perspectives

General conclusion and perspectives

The main objective of this PhD project was to study the interactions between cellulose nanofibers (CNF), chitin nanofibers (ChNF), and lignin particles (LP). These three biobased colloids present interesting properties for the preparation of food packaging materials, hence properties relevant for packaging application were more specifically studied. Different steps were studied, from biopolymer extraction to film assembly. The thesis results were divided into three parts (**Table 1**). The first part related to the preparation of the different colloids and the influence of the source on ChNF preparation, with a focus on products valorization from insect farming. The second part dealt with a new method to prepare lignin nanoparticles and studied the interactions between nanofibers and LP. Finally, the last part, described a new process to make continuous wax layer impermeable to water vapor and its integration in a high barrier multilayer film, suitable for food packaging applications.

In **Chapter I**, the recent literature on the biocolloids preparation and properties as well as their use in packaging applications was reviewed. It was shown that various sources exist for the preparation of each colloid, including waste or by-products from different industries. The nanofiber preparation method was found to be diverse and their optimization towards low energy consumption has been the focus of research during the last decade. The production of lignin particles has been reported more recently and new preparation methods are still under investigation. Chapter I shows that cellulose and chitin nanofibers can form film matrices with interesting barrier properties, for instance, for food packaging application. Meanwhile, lignin particles could be incorporated in the matrices for further functionalization.

The properties of the nanofiber matrices relative to mechanical stress and gas or liquid penetration were reviewed. Their limitations were discussed. Processes to incorporate the colloids with existing fiber-based packaging were reported and insights on the end-of-life and life cycle assessment of biobased polymers were given. We demonstrated that biobased colloids are promising for food packaging applications; however, we also showed some of the identified limitations, especially related to water interactions, including high viscosity at low concentration and sensitivity to water when dried.

Table 1. Main results and perspectives discussed in the different chapters of this PhD thesis.

Chapter	*Section*	*Key results*	*Perspectives*
II. Preparation of colloids and first assembly into films	1. Production of chitin nanofibers and films from insect	✓ ChNF production from insect is possible. ✓ ChNF from fly have higher fibrillation degree than ChNF from shrimp. ✓ Fibrillation of ChNF/CNF together showed interesting film properties.	➢ Optimization towards greener extraction processes. ➢ Partial removal of proteins and influence on the ChNF properties. ➢ Further study of ChNF/CNF mix.
	2. Preparation of lignin microparticles and their incorporation in CNF films	✓ Preparation of LP with an aerosol reactor. ✓ Influence of particle content on film structure.	➢ Preparation of nanoparticles with an aerosol flow reactor.
III. New method for integration of lignin particles	1. Lignin particles size effect on cellulose nanofibers film structure and properties	✓ Effect of particles size on fibrous matrices. ✓ Nanoparticles are more active and have less negative influence on film structure and properties than microparticles.	➢ Generalization to other type of particles organic and inorganic.
	2. *In-situ* preparation of lignin particles with different nanofiber supports	✓ Preparation of lignin nanoparticles with narrow size distribution using nanofibers as templating agent ✓ Influence of nanofiber charge on LP morphology and distribution.	➢ Study different preparation parameters such as: fiber size and concentration, lignin chemistry and their impact on LP size, shape, and size distribution.
IV. Towards packaging applications	1. Multilayered film with high barrier properties	✓ Preparation of water vapor barrier wax layer using wax nanoparticles. ✓ Processing of functional biobased multilayer film with high oxygen, water vapor, grease, and UV light barrier properties.	➢ Improvement of the layer adhesion. ➢ Scale-up of the process by coating on cellulosic substrate. ➢ Study the end of life of the film (recyclability, biodegradability).

The goal of **Chapter II** was to study the preparation of the colloids and more specifically the influence of the source of chitin for ChNF preparation. Two different insect farming sources were used as well as a conventional source. ChNF from insects had similar properties as that from shrimp shells, with an even higher fibrillation degree. A mix of CNF and ChNF was obtained and showed interesting mechanical properties, with toughness twice higher than

ChNF alone. The interactions between CNF and ChNF can be further studied to identify possible synergies that could develop from simultaneous fibrillation processes. The process of purification and extraction of ChNF was not optimized and should be further studied to reduce energy and chemicals consumption and hence the environmental footprint. Partial purification has shown promising results in the literature and could also be a route for the preparation of ChNF.

In the same chapter, lignin particles preparation and the first approach to mix them with CNF were reported. The particles produced with an aerosol reactor were dry, round-shaped, and polydisperse in size (with an average size of 1.4 ± 0.6 µm). They were mixed with TEMPO-oxidized CNF (tCNF) at different mass ratio to form films *via* casting evaporation. The tCNF film structure was significantly influenced by the presence of LP. Films with smaller particles sizes would be less impacted and hence the preparation of lignin nanoparticles could be considered.

In **Chapter III**, we developed a method to prepare LP with diameters < 100 nm. Films of tCNF with different sizes of LP were prepared and as hypothesized, smaller particles had less influence on the structure of tCNF films and resulted in improved mechanical properties. The nanoparticles were also more active as radical stabilizers compared to the microparticles, due to their high active surface area. These results are promising, and it would be interesting to investigate further if the same size effect in nanofiber matrices applies to different kinds of particles, both organic and inorganic.

The method used to prepare nanosized particles was then studied in more detail. The influence of the nature of the nanofiber in the process of LP formation was studied. We identified links between the electrostatic surface charge of the nanofibers and LP morphology and distribution in the suspension. The LP properties (size, size distribution, and morphology) could be further tuned by changing the synthesis parameters, in particular nanofiber concentration and morphology.

The repulsion between LP and CNF resulted in the formation of non-homogeneous films while attractive forces between ChNF and LP allowed a uniform distribution of the LP within the films. The presence of LP added radical scavenging activity and UV absorption property to the films. The activity of lignin was influenced by its chemistry and the use of different types of lignin could further tune these properties.

Chapter IV reported the fabrication of a multilayer film with high barrier properties, relevant to food packaging materials. First, water vapor barriers of CNF films were optimized by integrating wax following different processes. We concluded that a continuous layer of wax was needed to obtain a high-water vapor barrier at low and high humidity. Problems of adhesion between the layers were highlighted during the mechanical tests and further work on layers compatibilization could be a perspective.

A multilayer film was then engineered using the optimized ChNF suspension containing LP. The final material demonstrated remarkable barrier properties against oxygen, water vapor, UV light, and grease. The only flaw was the increase of oxygen transmission rate with humidity, which could be improved. Considering the promising properties, preservation tests on dry food were conducted and we showed that the films behaved the same as the original package, for instance in terms of water vapor permeability. The results are encouraging, and the next step would be the scaling up of the process for example by designing such multilayer onto a fiber-based substrate like a paper or cardboard.

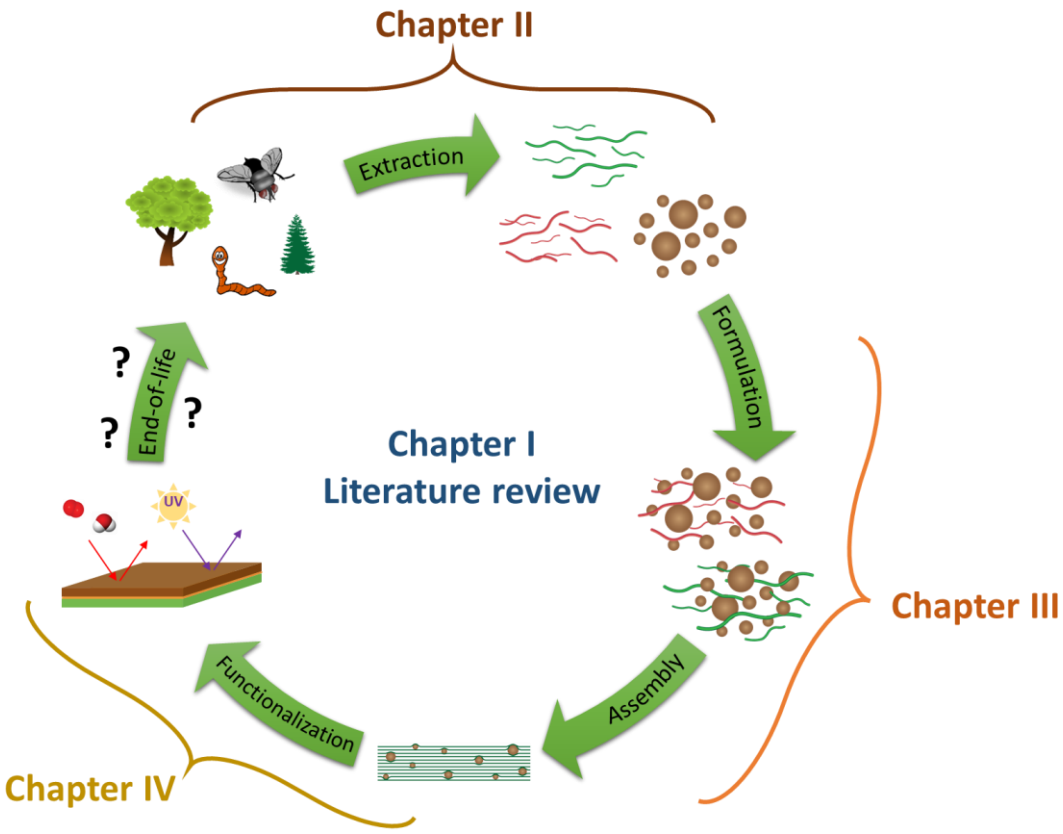

Figure 1. Life cycle of biobased colloids associated with the PhD thesis, divided in chapters.

To conclude, this PhD project brought knowledge on three important biobased polymers that can form colloids: cellulose, lignin, and chitin. Different aspects of their life cycle were studied, from their extraction to their interactions and assembly (**Figure 1**). It was shown that chitin nanofibers could be produced from different sources, including by-products from insect farming. A new method to prepare lignin nanoparticles was developed and the interactions between lignin particles and cellulose or chitin nanofibers were studied. Finally, a multilayer film with promising barrier properties was engineered and tested for dry food preservation. To go further, the end-of-life of the materials formed from the different colloids, their biodegradability and recyclability, could be considered in further studies, given that these topics are most relevant to packaging materials.

Poster

Aalto University
School of Chemical Engineering

LGP2

In-situ preparation of lignin nanoparticles on different types of cellulose and chitin nano-fibers

Pasquier Eva[1,2], Bras Julien[1], Naceur Belgacem[1], Orlando Rojas[2]
1 Univ. Grenoble Alpes, CNRS, Grenoble INP, LGP2, F-38000 Grenoble, France
2 Bio-based Colloids and Materials (BioMat) group, Dep of Bioproducts and Biosystems, Aalto University, Espoo, Finland

Abstract

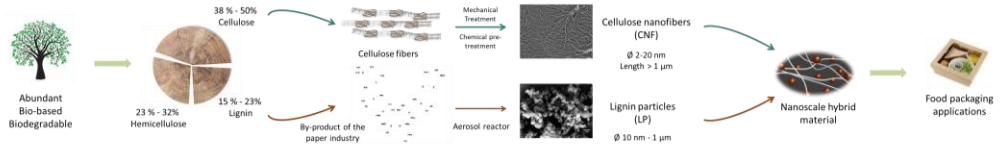

Introduction

The food packaging market is growing and as the climate changes, it is more and more important to shift from fossil based to **bio-based and biodegradable packaging**. Therefore polymers coming from biomass and food waste are an interesting alternative.

Cellulose nanofibers is a new promising material, as they have a **high aspect ratio**. When dried as a film they arrange as a dense network with **good barrier properties against oxygen**.

Chitin is also a biopolymer mainly originating from **crustacean shell**. It is interesting to consider replacing cellulose nanofibers by chitin nanofibers as they have a different **surface charge**.

Finally, lignin is also a bio-based and biodegradable polymer but with a more complex structure. Its chemistry makes it interesting for the packaging industry as it has **anti-oxidant properties** due to the high amount of phenolic groups. It is also possible to make nanoparticles from lignin to increase the specific surface area.

Materials & Methods

In-situ synthesis

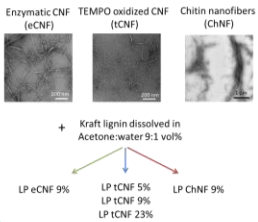

Characterisation methods

- Oxygen permeability/Water vapor transmission rate (WVTR)
- Contact angle
- Transparency
- TEM images
- Mechanical properties are measured with a DMA. Parameters are
  - speed: 0.1 mm/s
  - gap: 15 mm
- Anti-oxidant tests are conducted with ABTS

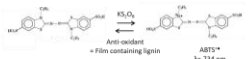

UV-Vis analysis of the decrease in absorbance at 734 nm

Results & discussion

Suspensions

TEM images of the suspensions:

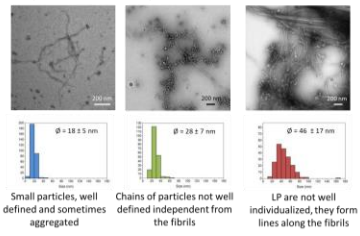

Small particles, well defined and sometimes aggregated

Chains of particles not well defined independent from the fibrils

LP are not well individualized, they form lines along the fibrils

- The surface charge of the nanofibers has an influence on the LP size, organization and interaction with the fibers

Films characterizations

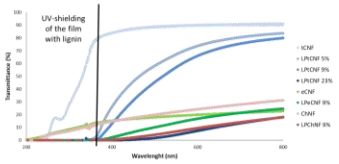

UV-Vis transmittance of the different films

The presence of lignin leads to complete absorption of the UV rays.

The addition of lignin particles decreases the Young's modulus for the TEMPO-CNF and ChNF films. The water contact angle increases with the addition of lignin except for films with high lignin content. This might be due to structural changes (increase of porosity). The increase is more significant for ChNF and eCNF because the fibers are coarser.

Sample	Young's modulus (Gpa)	Contact angle (°)	A. A. (mg tannic acid / g film)
tCNF	3.3 ± 0.3	46 ± 1	0.2
LP tCNF 5%	2.5 ± 0.4	50 ± 5	1.3
LP tCNF 9%	2.6 ± 0.4	51 ± 6	> 1.6
LP tCNF 23%	2.4 ± 0.2	41 ± 2	> 1.6
eCNF	2.02 ± 0.08	24 ± 9	0
LP eCNF 9%	2.2 ± 0.2	55 ± 5	1.2
ChNF	2.3 ± 0.2	32 ± 6	0.1
LP ChNF 9%	1.8 ± 0.3	56 ± 2	1.4
LP + tCNF 9%	1.6 ± 0.1	49 ± 8	0.8

Comparison of the Young's modulus, contact angles and anti-oxidant activities (AA) of the films with and without lignin particles

The addition of micrometric particles *ex-situ* (LP + tCNF 9%) leads to worse mechanical properties (half the Young's modulus). The anti-oxidant activity is decreased by at least a factor 2 compared to tCNF films.

- Good UV-shielding of all the films containing lignin. The contact angles increase but a deterioration of the mechanical properties is observed.

Anti-oxidant properties

The radical scavenging activity of the films decreases with time. It is possible to compare the activity with tannic acid, which is a well known anti-oxidant (see table above).

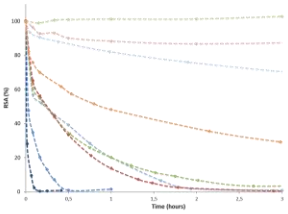

Radical scavenging activity (RSA) as a function of time for films with and without LP

- Higher lignin content and smaller particles gives better anti-oxidant effect.

Barrier properties against O_2 and water vapor

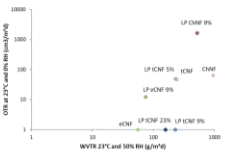

Oxygen transmission rate (OTR) and water vapor transmission rate (WVTR) of the different films

- Oxygen permeability is decreased for tCNF and it is increased for eCNF and ChNF without consequences on WVTR.

Conclusions & Perspectives

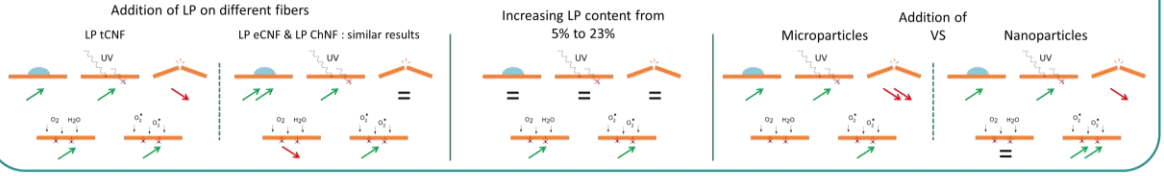

Acknowledgment: The project leading to this publication has received funding from Grenoble INP (Bourse Présidence) and Aalto University. We acknowledge support from the European Research Council (ERC) under the European Union's Horizon 2020 research and innovation program (ERC Advanced Grant agreement No 788489, "BioElCell")

References: R. Re et al., *Free Radic. Biol. Med.*, **1999**, 26, 123
M. Ago et al., *Appl. Mater. Interfaces*, **2016**, 8, 23302

LGP2, 461 rue de la papeterie, CS10065, 38402 Saint-Martin-d'Hères
LGP2
Eva.pasquier@grenoble-inp.fr
Oralndo.rojas@aalto.fi

Synthesis of zero valent iron nanoparticles on cellulose nanofibers for active food packaging applications

Pasquier Eva[1,2], Charlet Laurent[2], Bras Julien[1]
1 Univ. Grenoble Alpes, CNRS, Grenoble INP, LGP2, F-38000 Grenoble, France
2 Univ. Grenoble Alpes, CNRS, IRD, IFSTTAR, Institut des Sciences de la Terre (ISTerre), 38000 Grenoble, France

Abstract

This study presents the synthesis of zero valent iron nanoparticles (NPs) on cellulose nanofibers (CNF) with the aim of preparing films for **food packaging** applications. It is known that cellulose nanofibers films have good **barrier properties** against oxygen therefore they are suitable for food packaging. The goal here is to improve these films by adding iron zero as **oxygen absorber**. For that purpose, cellulose nanofibers with three different pre-treatments were analyzed as the support material. Bare **iron zero NPs** were also synthesized and characterized. The iron NPs are polydisperse in size and aggregated in solution. They are not stable in air as they can be oxidized to magnetite and hematite under certain conditions. Mixing iron NPs with the different cellulose nanofibers leads to micrometer size aggregates on the nanofibers as well as single iron NPs. Whereas the synthesis of iron NPs directly on the nanofibers suspensions produced **dispersed iron NPs adsorbed on the fibers**. X-ray diffraction (XRD) measurements show that the iron always stays zero under dry conditions when it is in a nanocellulose film. Therefore, the cellulose nanofibers allow **stabilizing the iron NPs** while preventing their aggregation.

Introduction

Oxygen is the main factor responsible for the food degradation, controlling its quantity inside food packaging is a problem of a great concern. For this reason, we decided to create a new material containing cellulose nanofibers and iron nanoparticles.

- Nanocellulose films are known for their good barrier properties against oxygen.
- Iron powder is the most commonly use oxygen scavenger in the food industry.

Designing a film with both materials would us allow to combine their properties against oxygen to increase food shelf life.

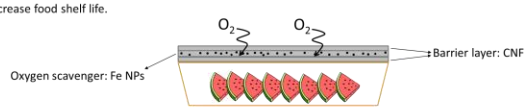

Materials & Methods

Ex-situ mixing

Iron NPs freshly prepared — Nano-cellulose suspension 0.125%

Shake for 3 days

Vacuum filtration
Or film casting

In-situ synthesis

Nano-cellulose suspension 0.125%

+ $NaBH_4$, 10 min, RT, under N_2

Characterisation methods

- Transmission Electron Microscopy (TEM)
- Scanning Electron Microscopy (SEM)
- Atomic Force Microscopy (AFM)
- Fourier Transform Infrared Spectroscopy (FTIR)
- X-Ray diffraction (XRD)
- X-Ray nanotomography

Glove box used to keep iron free from oxygen

Results & discussion

Raw materials

Three different types of cellulose nanofibers were used.

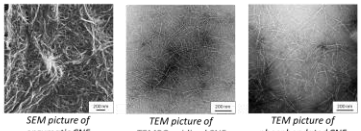

SEM picture of enzymatic CNF Ø 30 ± 10 nm — *TEM picture of TEMPO oxidized CNF Ø 13 ± 7 nm* — *TEM picture of phosphorylated CNF Ø 7 ± 5 nm*

Nano-cellulose (charge)		Iron amount	Fe NPs mean diameter	Comments
Enzymatic (0.06 mmol/g)	In-situ Synthesis	9 $\%_{wt}$	16 ± 5 nm	A few iron NPs aggregates are present
	In-situ Synthesis	50 $\%_{wt}$	30 ± 12 nm	Iron NPs aggregates, some iron NPs are not on the fiber
	Ex-situ Mixing	9 $\%_{wt}$	N.A	Large iron NPs aggregates, films are not homogeneous
TEMPO oxidized (1.6 mmol/g)	In-situ Synthesis	9 $\%_{wt}$	10 ± 6 nm	Iron NPs aggregates are present
	In-situ Synthesis	50 $\%_{wt}$	12 ± 6 nm	Iron NPs aggregates, some iron NPs are not on the fiber
	Ex-situ Mixing	9 $\%_{wt}$	N.A.	Large iron NPs aggregates, films are not homogeneous
Phosphorylated (2.8 mmol/g)	In-situ Synthesis	9 $\%_{wt}$	14 ± 11 nm	Iron NPs aggregates are present
	Ex-situ Mixing	9 $\%_{wt}$	N.A.	Iron NPs aggregates, films are not homogeneous

Summary of the different experiments with sizes measured on TEM images

Ex-situ mixing of CNF and iron NPs

The different CNF didn't allow to separate the iron NPs which were already aggregated before mixing. Aggregation of the particles decreases the active surface available for oxygen reaction. Single iron NPs are also present.

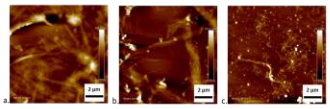

AFM pictures of the suspension of iron nanoparticles mixed with a. Enzymatic CNF b. TEMPO oxidized CNF c. Phosphorylated CNF

- Ex-situ mixing leads to aggregation of iron NPs, this strategy was not kept for further experiments.

In-situ synthesis of iron NPs on CNF

Small individual particles are formed (10 to 16 nm) with this method. Iron NPs on enzymatic CNF are well dispersed, that is the most promising result. To increase the scavenging effect, the iron content is increased but it creates large iron aggregates in the suspension.

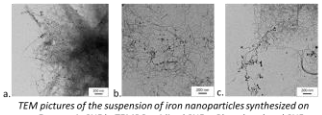

TEM pictures of the suspension of iron nanoparticles synthesized on a. Enzymatic CNF b. TEMPO oxidized CNF c. Phosphorylated CNF

Infrared spectra of the three different CNF before and after reaction show that the cellulose did not degrade during the reaction.

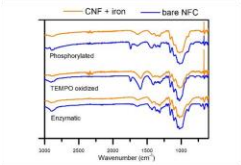

- In-situ method shows promising results for the formation of well dispersed small iron nanoparticles.

Oxidation degree of iron

XRD of a TEMPO CNF film with iron NPs was done, it shows the cellulose peaks as well as the iron zero peaks. The measurement was done under argon and after contact with air, the iron stays zero valent even after contact with air, which is not the case with the iron NPs powder without nanocellulose. At high relative humidity, iron start to oxidize and peaks of different oxides are observed.

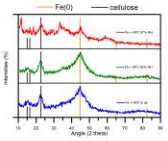

$$Fe^0 + O_2 + 2\,H_2O \leftrightarrow 2\,Fe(OH)_{2\,(s)}$$

$$6\,Fe(OH)_{2\,(s)} + O_2 \leftrightarrow 2\,Fe_3O_{4\,(s)}$$

Diffractograms of a TEMPO oxidized nanofibers film containing iron NPs at different relative humidity. Theoretical spectra are from JCPDS files: Iron zero PDF#006-0696, cellulose PDF#050-2241. Oxidation reactions of iron.

- CNF film stabilizes the oxidation degree of iron but iron oxidizes at high relative humidity.

Conclusions & Perspectives

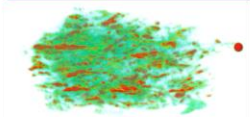

Nano-tomography of a film of synthesised iron NPs on enzymatic CNF (1:10)

- Iron nanoparticles aggregation explains the **limited success of mixing** the cellulose nanofibers and the iron NPs. In fact, AFM pictures showed in this case many iron aggregates and the aggregation can be observed to the naked eyes on the final films.
- The **synthesis of iron NPs** grafted directly on the nanocellulose gave better results. FTIR spectra show no cellulose degradation during the reaction. The Fe/Enzymatic NFC 1:10 mass ratio showed promising results as the iron NPs were smaller than the bare iron NPs and **well dispersed** on the fibers. Furthermore, the oxidation state of iron stayed zero when the films are kept in air in dry conditions.
- Next steps, would be to measure the **oxygen permeability** with different relative humidity. Furthermore, doing a multilayer film including a plastic support would be great to better compare with real industrial packaging.

References: He, F. & Zhao, D. *Environ. Sci. Technol.* **39,** 3314–3320 (2005)
Bossa, N., Carpenter, A. W., Kumar, N., Lannoy, C.-F. de & Wiesner, M. *Environ. Sci. Nano* **4,** 1294–1303 (2017)

Acknowledgment: The project leading to this publication has received funding from Excellence Initiative of Aix-Marseille University - A*MIDEX, a French "Investissements d'Avenir" program, through its associated Labex SERENADE project.
A special thanks to D. Borschneck and V. Vidal from Cerege for the nano-tomography

LGP2, 461 rue de la papeterie, CS10065, 38402 Saint-Martin-d'Hères
http://pagora.grenoble-inp.fr/recherche/
Eva.pasquie@grenoble-inp.fr
Julien.bras@grenoble-inp.fr

Extended French abstract

Entre 1950 et 2015, 8300 millions de tonnes de plastique ont été produites dans le monde. Il a été estimé que parmi les déchets produits, 9% ont été recyclés, 12% incinérés et 79% enfouis ou mis en décharge (**Figure 1**). En Europe en 2018, 33% du plastique collecté a été recyclé et 43% utilisé comme source d'énergie, ce qui montre que les taux de recyclage sont en augmentation, notamment dans les pays développés.[1] Cependant, ces chiffres prennent uniquement en compte le plastique collecté et aucune statistique sur la quantité totale de plastique utilisé n'a été trouvée.[2] Les emballages alimentaires représentent la plus grande part de la demande en plastique en Europe, cela correspond à 40% du marché final et à environ 20 millions de tonnes chaque année.[2] Le polyéthylène basse densité et haute densité, le polypropylène et le polyéthylène téréphtalate sont les plus utilisés pour les emballages alimentaires. Ils sont recyclables dans une certaine mesure, mais aucun d'entre eux n'est biodégradable.

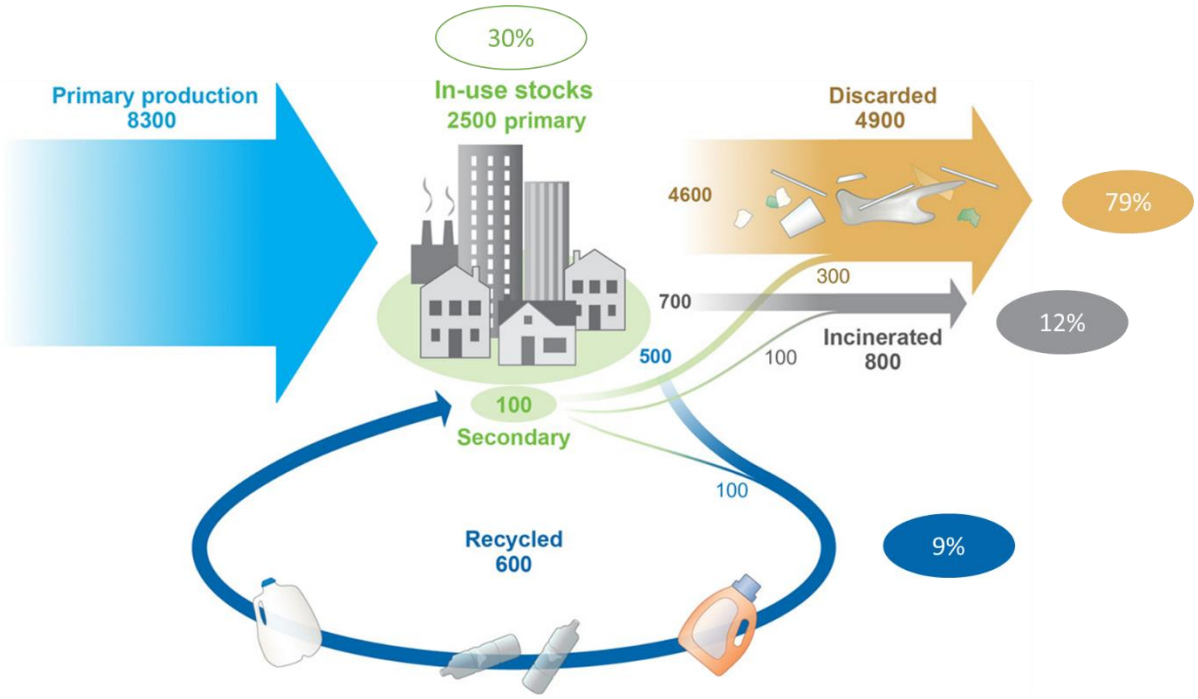

Figure 1. Production, stockage et fin de vie du plastique produit mondialement en million de tonnes entre 1950 et 2015. Extrait de[1]

Même si de nouvelles solutions de recyclage sont en cours de développement et d'amélioration, les taux de recyclage du plastique sont encore très bas. De plus, plusieurs pays et institutions commencent à introduire de nouvelles lois concernant la limitation de l'utilisation du plastique,

par exemple, la directive sur les plastiques à usage unique de l'Union Européenne qui interdit l'usage de plastique pour les 10 produits en plastique les plus trouvés sur les plages.

C'est pourquoi, des solutions sont nécessaires. La réduction de la quantité totale d'emballages, peu importe sa composition, devrait être la première étape. Cependant, les emballages alimentaires sont primordiaux pour la bonne conservation des aliments et pour éviter le gaspillage de nourriture. En effet, l'empreinte environnementale de la production de nourriture est élevée (occupation des sols, consommation d'eau, d'engrais, empreinte carbone lors de la distribution…), il est donc important de ne pas jeter cette nourriture.[3] Par conséquent, il est important de se focaliser sur la recherche d'emballages alternatifs ayant des propriétés équivalentes ou supérieurs au plastique.

Dû aux diverses sources et fin de vie possibles, les fibres biosourcées tel que la cellulose et la chitine sont des matériaux prometteurs pour remplacer le plastique dans les emballages. De plus, l'utilisation de déchets ou de sous-produits de l'agriculture et de l'industrie comme matière première peut réduire leur empreinte environnementale. En effet, la cellulose peut être extraite de plusieurs sous-produits de l'agriculture, comme la paille, la bagasse, les cosses ou coques de plusieurs cultures (riz, maïs, canne à sucre…).[4] Par ailleurs, la chitine est déjà extraite de sous-produits de l'industrie des crustacés et pourrait bientôt être extraite de sous-produits de l'élevage d'insectes.[5] La diversification des sources de fibres est amenée à jouer un rôle déterminant afin de répondre à la demande en matériaux biosourcés. Il faut aussi compter sur l'utilisation de déchets et l'augmentation des taux de recyclages des fibres.[6]

De plus, il a été démontré pendant la dernière décennie que la cellulose et la chitine peuvent former des suspensions stables de nanofibres présentant des performances intéressantes pour les emballages alimentaires. Les nanofibres de cellulose (CNF) et de chitine (ChNF) sont préparées par fibrillation mécanique de leurs fibres respectives et forment des gels à basse concentration (**Figure 2a** et **2c**).[7] Ces nanofibres ont un rapport diamètre/longueur, une cristallinité et une surface spécifique élevés et peuvent former des films résistants, translucides et barrières aux graisses et à l'oxygène.[8–10]

D'autre part, la lignine provient de sources semblables à la cellulose et est déjà disponible en quantités industrielles. De nature aromatique, elle est antioxydante, barrière aux UV et antimicrobienne, propriétés pertinentes pour les emballages alimentaires. Comme rapporté dans différentes revues de littérature,[11–15] il existe différents procédés humides ou secs pour fabriquer des particules de lignine (**Figure 2b**). Lorsque la lignine est sous forme particulaire,

elle peut être facilement manipulable en solution aqueuse. De plus, cela réduit sa complexité à la chimie de surface des particules. En plus d'apporter des propriétés actives aux matrices de nanofibres, les particules peuvent augmenter la stabilité des suspensions de CNF.[16]

CNF, ChNF et LP sont trois colloïdes biosourcés qui sont disponibles en grandes quantités et qui ont des propriétés prometteuses pour les emballages alimentaires. Ils ont tous été plus ou moins étudiés individuellement lors des vingt dernières années, cependant leurs interactions ont été jusqu'à maintenant négligées. Ici nous utilisons les propriétés individuelles de chaque colloïde ainsi que leurs interactions pour former des matériaux complexes et fonctionnels.

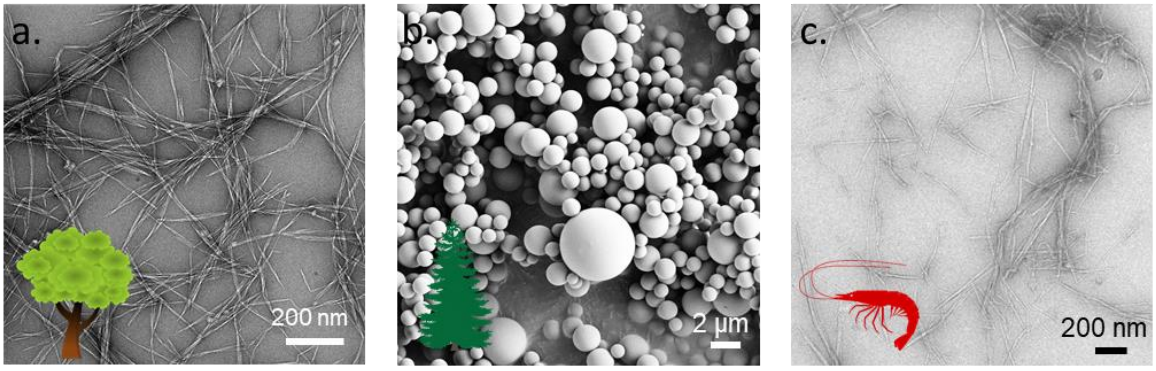

Figure 2. Images des trois colloïdes biosourcés étudiés dans le cadre de cette thèse associés à un exemple de leurs sources. **a.** Nanofibres de cellulose, **b.** particules de lignine et **c.** nanofibres de chitine.

Cette thèse a commencé fin 2018 d'un partenariat entre le laboratoire de génie des procédés papetiers (LGP2) de l'université de Grenoble Alpes et le groupe de Colloïdes et Matériaux Biosourcés de l'université d'Aalto en Finlande. Le projet a été financé par la bourse Présidence de Grenoble INP ainsi que le projet « BioElCell » financé par le Conseil Européen de la recherche. Le temps passé dans chaque laboratoire a été divisé équitablement et des réunions de projet ont eu lieu régulièrement afin de combiner les expertises des deux équipes. Le projet se concentre sur la préparation de colloïdes biosourcés ainsi que leurs interactions. Etant donné les propriétés pertinentes de chaque colloïde pour les emballages alimentaires, une attention particulière est donnée à la formation de films pour des applications d'emballages. La thèse est divisée en quatre chapitres (voir **Figure 3**). Le premier décrit la littérature associée avec les trois colloïdes et leurs utilisations dans les emballages. Les chapitres suivants sont les expériences et résultats obtenus durant la thèse, présentés sous forme de publications.

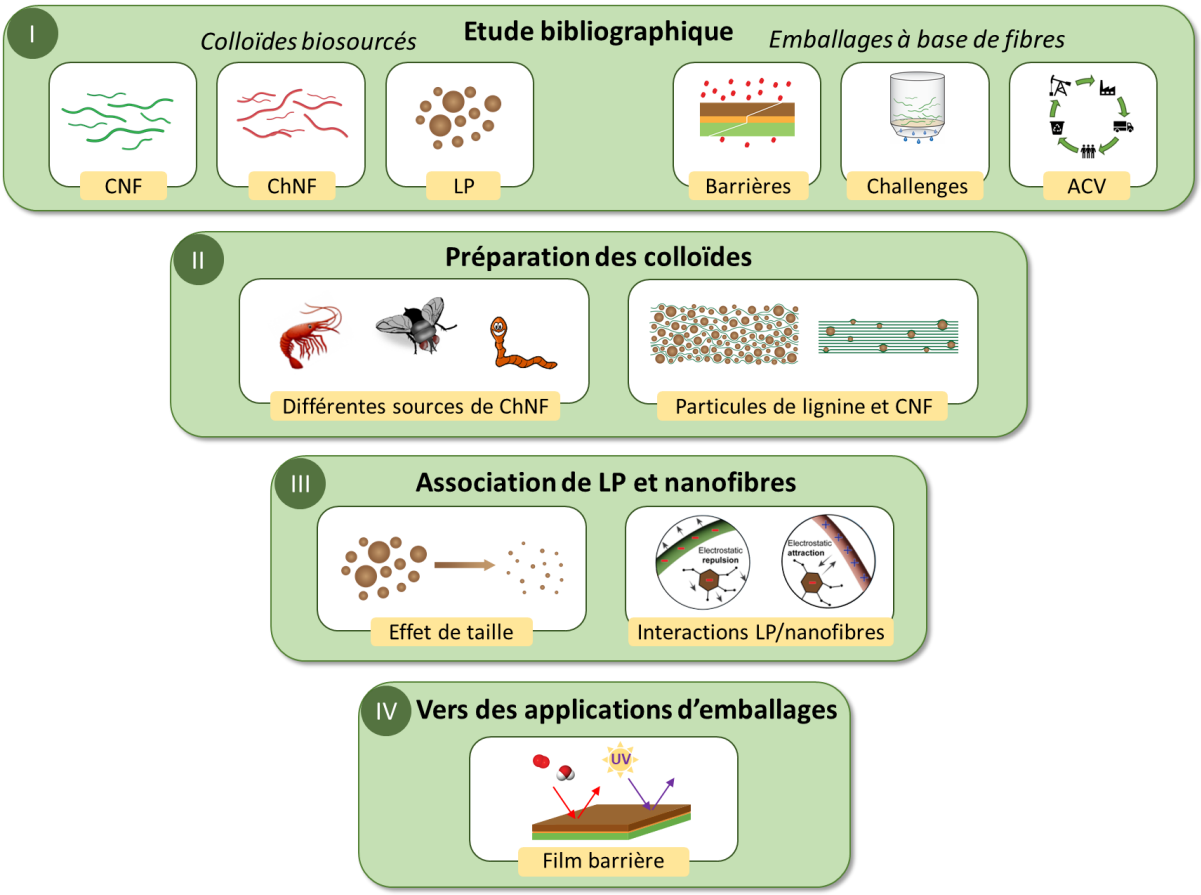

Figure 3. Schéma global de l'organisation de la thèse

Le **Chapitre I** de la thèse présente sous la forme d'une revue de littérature les avancées qui ont été faites en lien avec les trois colloïdes étudiés dans cette thèse. La première partie parle de la préparation des colloïdes (nanofibres de cellulose, nanofibres de chitine et particules de lignine). Les sources à partir desquelles ils sont extraits, les techniques d'extraction ainsi que de préparation y sont détaillés. De plus, les propriétés des colloïdes notamment en suspension y sont présentées.

Dans un second temps, les propriétés des colloïdes en lien avec les emballages alimentaires sont rapportées. Les nanofibres peuvent former des films lorsqu'elles sont séchées et ces films sont barrières à l'oxygène et aux graisses à basse humidité. Ce sont également des matrices idéales pour accueillir des particules fonctionnelles tel que les particules de lignine qui ont des propriétés antioxydantes et barrière aux rayons UV. Cependant, ces films ont aussi des limitations notamment concernant leur sensibilité à l'eau et nous proposons également des solutions pour répondre à ces limitations. De plus, nous présentons les procédés de formation des films ainsi que leur fin de vie et l'analyse de cycle de vie de ces matériaux.

Le **Chapitre II** de la thèse se concentre sur la préparation des colloïdes. Une première partie développe la préparation de nanofibres de chitine (ChNF) à partir de différentes sources d'insectes (**Figure 4**). Dans la deuxième partie, des particules de lignine (LP) sont préparées et des premiers films de nanofibres de cellulose (CNF) contenant des LP sont formés. Trois sources différentes ont été choisies pour la préparation de ChNF. La première est issue de chitine de larve de mouches extraite par un procédé industriel. La deuxième source est un sous-produit de l'élevage de vers de farine constitué de mue des verres ainsi que de résidus cellulosiques provenant de leur alimentation. La troisième source est de la chitine extraite de carapaces de crevettes et sert de référence. Après purification des différentes chitines, les fibres sont fibrillées afin d'obtenir des suspensions de ChNF. Les ChNF de mouches présentent un degré de fibrillation supérieur aux ChNF de crevettes. De plus, les ChNF de vers sont composées à moitié de CNF issues des résidus cellulosiques et à moitié de ChNF issues des mues de vers. Les différentes suspensions ont ensuite été filtrées et pressées afin de former des films. Il a été conclu que le procédé utilisé lors de la préparation des films avait une plus grande influence que la source de chitine sur les propriétés finales des films. Les films contenant un mix de CNF et ChNF présentent des propriétés mécaniques intéressantes notamment en termes d'élongation. Une étude plus approfondie du procédé de fibrillation des deux types de fibres ensemble pourrait être intéressante pour la suite.

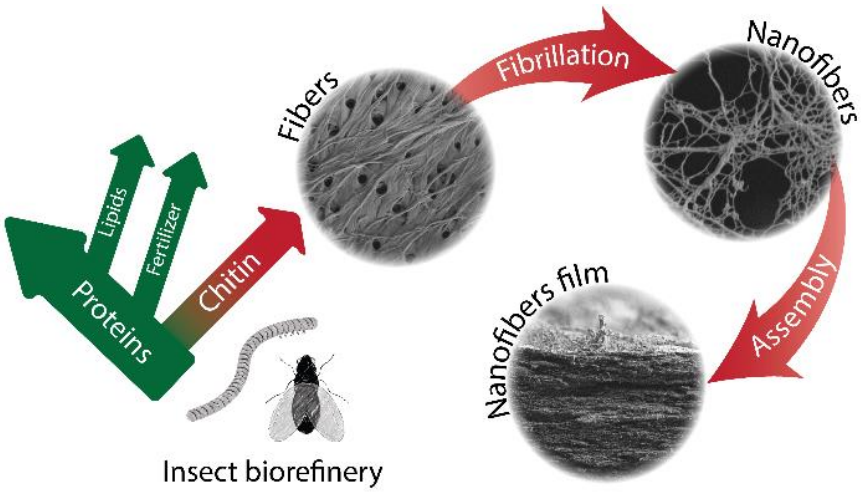

Figure 4. Stratégie de préparation des films de nanofibres de chitine extraite d'insectes.

Dans la seconde partie du Chapitre II, des particules de lignine ont été préparées avec un réacteur à aérosols. Les particules obtenues sous forme sèche avaient un diamètre moyen de 1.4 ± 0.6 µm. Les premiers mélanges entre LP et CNF ont été fait avec différentes quantités de LP. La structure des films est dépendante de la quantité de LP. Nous avons déterminé qu'en

dessous de 33% de LP, les films avaient une structure lamellaire proche des films purs de CNF alors qu'au-dessus de 33% la structure des films était contrôlée par les particules de lignine. Les propriétés mécaniques de ces films n'étant pas satisfaisantes, nous avons choisi de préparer un deuxième type de particules de lignine avec un diamètre plus petit.

Le **Chapitre III** se compose également de deux parties, la première rapporte la fabrication de nanoparticules de lignine et l'effet de la taille des LP sur les films de CNF. Dans un second temps, nous étudions plus en détail le mécanisme de préparation de nanoparticules de lignine et notamment l'influence de la chimie de surface des fibres. Dans le premier sous-chapitre, nous avons adapté la méthode de précipitation par échange de solvant en ajoutant des nanofibres de cellulose lors de la précipitation. Des nanoparticules avec une taille moyenne de 18 ± 5 nm ont été obtenues en solution avec les CNF. Afin de déterminer l'influence de la taille des particules sur les propriétés et structure des films, nous avons préparé des films de CNF contenant la même quantité de LP. La présence de nanoparticules de lignine dans une matrice de CNF a moins d'influence sur la structure des films que la présence de microparticules. De plus, grâce à l'augmentation de la surface spécifique des nanoparticules, les films obtenus présentent une plus grande activité antioxydante. Les interactions avec la lumière visible sont aussi moindres du fait de la taille nanométrique des particules. Les films présentent une plus grande transparence en présence de nanoparticules comparé aux microparticules. Ces résultats prometteurs pour les nanoparticules de lignine nous ont poussé à étudier plus en détail le mécanisme de préparation de LP.

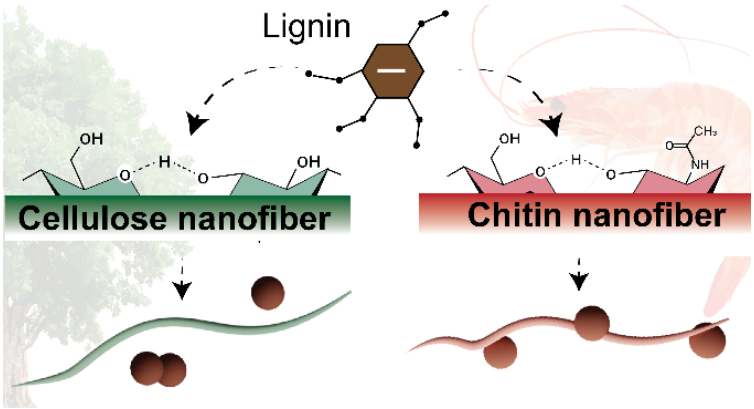

Figure 5. Résultat de la formation de particules de lignine en présence de nanofibres de cellulose ou nanofibres de chitine.

Le deuxième sous-chapitre étudie le mécanisme de préparation de nanoparticules de lignine. La méthode utilisée est adaptée de la synthèse par précipitation par échange de solvant qui consiste à dissoudre la lignine dans un bon solvant puis à la faire précipiter dans un mauvais solvant qui est généralement de l'eau. Dans notre méthode de préparation, des nanofibres de cellulose ou de chitine sont ajoutées dans l'eau avant la précipitation. Les nanofibres peuvent donc servir de point d'ancrage pour la nucléation des particules de lignine. De plus, les CNF sont chargées négativement en surface alors que les ChNF sont chargées positivement, cela entraîne une différence dans les interactions de surface avec les LP chargées négativement. Lorsque les ChNF sont présentes dans l'eau la lignine va s'adsorber en surface des nanofibres puis les particules vont croître à partir de ces points d'ancrage. D'autre part, lorsque les CNF sont présentes dans l'eau, la lignine et les CNF vont se repousser ce qui va limiter le grossissement des particules et contrôler la taille finale des LP (**Figure 5**). L'adsorption des LP sur les ChNF permet de former des films de ChNF avec une répartition homogène de LP avec des taux de 9%, 15% et 23%. Due à la présence de LP, les films démontrent des propriétés antioxydantes et barrières aux UV. L'augmentation de la quantité de lignine lors de la synthèse a influencé la taille des particules mais d'autres paramètres, tel que la concentration en nanofibres ou le type de lignine, pourraient être étudié afin de mieux comprendre l'influence des paramètres de synthèse sur la taille et morphologie des particules.

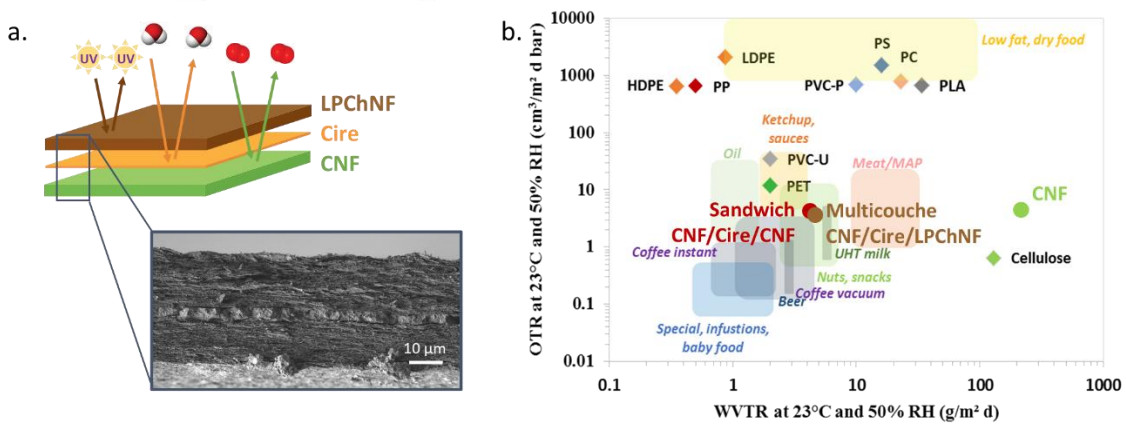

Figure 6. a. Film multicouche composé d'une couche de nanofibres de cellulose (CNF), d'une couche de cire et d'une couche de nanofibres de chitine contenant des particules de lignine (LPChNF) associé avec une image MEB d'une coupe du film. b. Vitesse de transmission de l'oxygène (OTR) et de la vapeur d'eau (WVTR) à travers différents films associés avec des exemples de spécificités de certains aliments.

L'objectif du **Chapitre IV** est de préparer un film multicouche avec plusieurs propriétés barrières, chaque couche ayant une fonction spécifique (**Figure 6a**). La première couche est composée de CNF qui ont des propriétés barrières à l'oxygène. Ensuite, une couche de cire de carnauba sert de barrière à la vapeur d'eau. La troisième couche se compose de ChNF contenant 9% de LP. Grâce à la nature phénolique de la lignine, cette couche est barrière aux rayons UV et a potentiellement des propriétés antioxydantes. Dans un premier temps, l'intégration de la couche de cire a été optimisée pour obtenir un minimum de transmission de la vapeur d'eau en utilisant plusieurs façons d'intégrer la cire dans le film de CNF. Le film « Sandwich » composé d'une couche de cire entre deux couches de CNF montre les meilleurs résultats avec une vitesse de transmission de la vapeur d'eau de 5 ± 1 g/m^2.jour. Il a donc été choisi comme modèle pour le film multicouche où la couche de cire se situe au milieu d'une couche de CNF et ChNF contenant des LP. Le film multicouche démontre des propriétés barrières à la vapeur d'eau équivalentes au film Sandwich et des propriétés barrières à l'oxygène équivalentes à un film de CNF seul (**Figure 6b**). De plus, il a été démontré que le film est barrière à la graisse et barrière aux rayons UV tout en restant translucide. A haute humidité, la perméabilité à l'oxygène augmente légèrement, il serait donc nécessaire de limiter cette augmentation. De plus, l'adhésion entre les couches de nanofibres de cire est faible ce qui entraîne une délamination lors des tests de traction. Un travail supplémentaire serait donc d'améliorer l'adhésion des couches. Un test de conservation du côté craquant de biscuits secs a été réalisé et a démontré des résultats comparables aux emballages du commerce pour une durée de test d'une semaine à 80% d'humidité relative.

Tableau 1. Principaux résultats clés de la thèse associés aux perspectives, organisé par chapitres.

Chapitre	*Section*	*Résultats clés*	*Perspectives*
II. Préparation de colloïdes et premiers assemblages de films	1. Production de nanofibres de chitine (ChNF) à partir d'insectes	✓ Production de ChNF à partir d'insectes. ✓ Obtention de ChNF de larve de mouches avec un degré de fibrillation supérieur aux ChNF de carapace de crevettes. ✓ Fibrillation de ChNF/CNF ensemble et formation de films avec des élongations supérieures.	➢ Optimisation de l'extraction avec des procédés verts. ➢ Purification partielle des protéines et influence sur les propriétés des ChNF. ➢ Etude approfondie du mélange CNF/ChNF.
	2. Préparation de microparticules de lignine et leur incorporation dans les films de CNF	✓ Préparation de LP avec un réacteur à aérosol. ✓ Influence du taux de particules sur la structure des films.	➢ Préparation de nanoparticules avec un réacteur à aérosol.
III. Nouvelle méthode pour la préparation de particules de lignine	1. Effet de la taille des particules de lignine sur la structure et les propriétés des films de nanofibres de cellulose (CNF).	✓ Effet de la taille des particules dans une matrice fibreuse. ✓ Réactivité des nanoparticules comparé aux microparticules de lignine.	➢ Généralisation à d'autres types de particules organiques et inorganiques.
	2. Préparation *in-situ* des particules de lignine avec plusieurs nanofibres comme support.	✓ Préparation de nanoparticules de lignine avec une distribution de taille réduite en utilisant les nanofibres comme agent de nucléation. ✓ Influence de la charge des nanofibres sur la morphologie et distribution de taille des LP.	➢ Etude des différents paramètres de préparation comme la taille et la concentration des nanofibres, la chimie de la lignine et leurs impacts sur la taille des LP, leur morphologie et leur distribution de tailles.
IV. Vers des applications d' emballages	1. Film multicouche avec des propriétés barrières élevées	✓ Préparation d'une couche de cire à haute barrière contre la vapeur d'eau grâce à des nanoparticules de cire. ✓ Fabrication d'un film biosourcé multicouche barrière à l'oxygène, la vapeur d'eau, les rayons UV et les graisses.	➢ Amélioration de l'adhésion entre les couches. ➢ Changement d'échelle du procédé par couchage sur un substrat cellulosique. ➢ Etude de la fin de vie du des films (recyclabilité et biodégradabilité).

Pour conclure, cette thèse a apporté des connaissances sur trois colloïdes biosourcés (nanofibres de cellulose, nanofibres de chitine et particules de lignine) et notamment sur leurs interactions. Plusieurs étapes de leur cycle de vie ont été abordées, de l'extraction à l'assemblage et la formation d'un film fonctionnel (**Figure 7**). Il a été démontré que les insectes et leurs sous-produits d'élevage pouvaient être utilisé comme source de nanofibres de chitine. Une nouvelle méthode de préparation de LP a été développée, elle a permis de préparer des LP inférieurs à 50 nm en présence de CNF ou ChNF et par la même occasion d'étudier les interactions entre LP et nanofibres. Enfin, un film multicouche présentant de nombreuses propriétés barrières nécessaires aux emballages alimentaires a été produit et testé sur des biscuits secs. Pour aller plus loin, la fin de vie des matériaux préparés, que ce soit la biodégradabilité ou la recyclabilité, pourrait être étudiée, cela représentant une étape majeure dans le cycle de vie des emballages alimentaires.

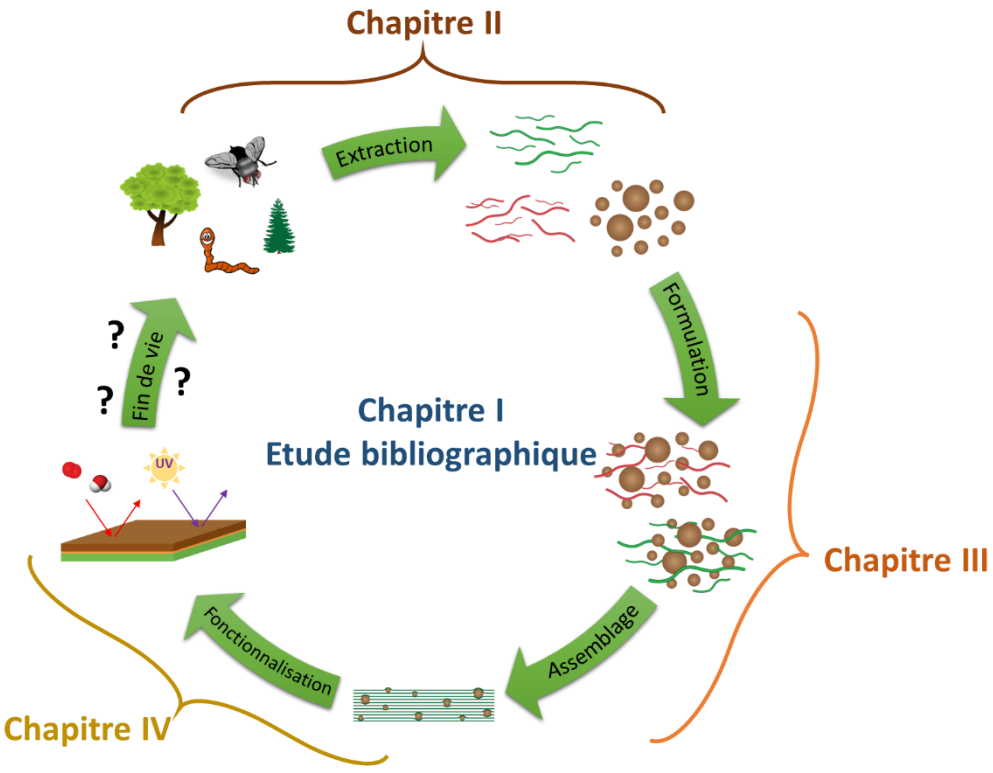

Figure 7. Cycle de vie des colloïdes biosourcés avec les parties étudiées dans la thèse.

REFERENCES

(1) Geyer, R.; Jambeck, J. R.; Law, K. L. Production, Use, and Fate of All Plastics Ever Made. *Science Advances* **2017**, *3* (7), e1700782. https://doi.org/10.1126/sciadv.1700782.

(2) Market data :: PlasticsEurope https://www.plasticseurope.org/en/resources/market-data (accessed 2021 -05 -20).

(3) Otoni, C. G.; Azeredo, H. M. C.; Mattos, B. D.; Beaumont, M.; Correa, D. S.; Rojas, O. J. The Food–Materials Nexus: Next Generation Bioplastics and Advanced Materials from Agri-Food Residues. *Advanced Materials* **2021**, 2102520. https://doi.org/10.1002/adma.202102520.

(4) García, A.; Gandini, A.; Labidi, J.; Belgacem, N.; Bras, J. Industrial and Crop Wastes: A New Source for Nanocellulose Biorefinery. *Industrial Crops and Products* **2016**, *93*, 26–38. https://doi.org/10.1016/j.indcrop.2016.06.004.

(5) Hahn, T.; Tafi, E.; Paul, A.; Salvia, R.; Falabella, P.; Zibek, S. Current State of Chitin Purification and Chitosan Production from Insects. *Journal of Chemical Technology & Biotechnology* **2020**, *95* (11), 2775–2795. https://doi.org/10.1002/jctb.6533.

(6) Josset, S.; Orsolini, P.; Siqueira, G.; Tejado, A.; Tingaut, P.; Zimmermann, T. Energy Consumption of the Nanofibrillation of Bleached Pulp, Wheat Straw and Recycled Newspaper through a Grinding Process. *Nordic Pulp & Paper Research Journal* **2014**, *29* (1), 167–175. https://doi.org/10.3183/npprj-2014-29-01-p167-175.

(7) Rol, F.; Belgacem, M. N.; Gandini, A.; Bras, J. Recent Advances in Surface-Modified Cellulose Nanofibrils. *Progress in Polymer Science* **2019**, *88*, 241–264. https://doi.org/10.1016/j.progpolymsci.2018.09.002.

(8) Ahankari, S. S.; Subhedar, A. R.; Bhadauria, S. S.; Dufresne, A. Nanocellulose in Food Packaging: A Review. *Carbohydrate Polymers* **2021**, *255*, 117479. https://doi.org/10.1016/j.carbpol.2020.117479.

(9) Ling, S.; Kaplan, D. L.; Buehler, M. J. Nanofibrils in Nature and Materials Engineering. *Nat Rev Mater* **2018**, *3* (4), 1–15. https://doi.org/10.1038/natrevmats.2018.16.

(10) Salaberria, A. M.; Labidi, J.; Fernandes, S. C. M. Different Routes to Turn Chitin into Stunning Nano-Objects. *European Polymer Journal* **2015**, *68*, 503–515. https://doi.org/10.1016/j.eurpolymj.2015.03.005.

(11) Österberg, M.; Sipponen, M. H.; Mattos, B. D.; Rojas, O. J. Spherical Lignin Particles: A Review on Their Sustainability and Applications. *Green Chem.* **2020**, *22* (9), 2712–2733. https://doi.org/10.1039/D0GC00096E.

(12) Schneider, W. D. H.; Dillon, A. J. P.; Camassola, M. Lignin Nanoparticles Enter the Scene: A Promising Versatile Green Tool for Multiple Applications. *Biotechnology Advances* **2021**, *47*, 107685. https://doi.org/10.1016/j.biotechadv.2020.107685.

(13) Ago, M.; Tardy, B. L.; Wang, L.; Guo, J.; Khakalo, A.; Rojas, O. J. Supramolecular Assemblies of Lignin into Nano- and Microparticles. *MRS Bulletin* **2017**, *42* (5), 371–378. https://doi.org/10.1557/mrs.2017.88.

(14) Beisl, S.; Miltner, A.; Friedl, A.; Beisl, S.; Miltner, A.; Friedl, A. Lignin from Micro- to Nanosize: Production Methods. *International Journal of Molecular Sciences* **2017**, *18* (6), 1244. https://doi.org/10.3390/ijms18061244.

(15) Gao, W.; Fatehi, P. Lignin for Polymer and Nanoparticle Production: Current Status and Challenges. *The Canadian Journal of Chemical Engineering* **2019**, *97* (11), 2827–2842. https://doi.org/10.1002/cjce.23620.

(16) Liu, Y. Strong and Flexible Nanocomposites of Carboxylated Cellulose Nanofibril Dispersed by Industrial Lignin. *ACS Sustainable Chem. Eng.* **2018**, *6* (4), 5524–5532. https://doi.org/10.1021/acssuschemeng.8b00402.

English abstract

The goal of this project is to better understand the interactions between three different biobased colloids. The three most abundant polymers that can be extracted from nature are cellulose, chitin, and lignin. Cellulose and chitin fibers can be mechanically fibrillated into colloidally stable nanofibers while lignin particles (LP) can be prepared from dissolved lignin. These colloids have been studied individually however the interactions between each other have been so far overlooked. To create fully biobased materials, it is important to understand the colloids' behavior but also their interactions. Moreover, these colloids are promising for food packaging applications. Cellulose and chitin nanofibers can act as matrices to make strong films with high oxygen barrier properties while lignin can form active particles that have antioxidant and UV absorbing properties. The first part of the project focuses on the preparation of the colloids, in particular, chitin nanofibers (ChNF) from shrimp, fly or mealworm sources. Promising mechanical properties were obtained from films made from chitin and cellulose fibrillated together. Then, a new method to prepare LP in the presence of cellulose or chitin nanofibers was studied. Electrostatic attraction between ChNF and LP led to homogeneous repartition of LP into ChNF films. Finally, we took advantage of the different colloids interactions to prepare multilayer films with promising high barrier properties including oxygen, water vapor, UV, and grease barriers. This thesis brings some understandings on biobased colloids interactions and how to use these interactions to create fully biobased functional films towards food packaging applications.
Key words: cellulose nanofibers, chitin nanofibers, lignin particles, food packaging, biobased colloids

Résumé français

Le but de ce projet est de mieux comprendre les interactions entre plusieurs colloïdes biosourcés. Les trois polymères les plus abondants qui peuvent être extraits de la nature sont la cellulose, la chitine et la lignine. Or les fibres de cellulose et de chitine peuvent être fibrillées mécaniquement pour former des nanofibres stables en suspension et des particules de lignine peuvent être préparées à partir de solution de lignine. Ces différents colloïdes ont été étudiés séparément mais l'étude de leurs interactions est encore méconnue. Afin de préparer dans l'avenir des matériaux complétement biosourcés, il est important de comprendre le comportement des colloïdes mais également leurs interactions. De plus, ils présentent chacun un intérêt pour la fabrication d'emballages alimentaire. Les nanofibres de cellulose et de chitine forment des films résistants qui ont des propriétés barrières à l'oxygène alors que les particules de lignine ont des propriétés antioxydantes et absorbent les rayons UV. La première partie du projet se concentre sur la fabrication des colloïdes, notamment de nanofibres de chitine provenant de déchets de crevettes ou insectes. Des propriétés mécaniques prometteuses ont été obtenues à partir de films de nanofibres de cellulose et chitine fibrillées ensemble et extraites de déchets de l'élevage de vers de farine. Ensuite, une nouvelle méthode de préparation de particules de lignine en présence de nanofibres de cellulose et de chitine a été étudiée. Grâce à l'attraction électrostatique entre les nanofibres de chitine et les particules de lignine, des films avec une répartition homogène des particules ont été obtenus. Finalement, nous nous sommes servis des différentes interactions entre les colloïdes pour préparer des films multicouches présentant plusieurs propriétés barrières notamment à l'oxygène, la vapeur d'eau, la graisse et les rayons UV. Cette thèse apporte des connaissances sur les interactions de trois colloïdes biosourcés et comment utiliser ces interactions pour fabriquer des films fonctionnels complétement biosourcés pour des applications d'emballage alimentaire.
Mots clés : nanofibres de cellulose, nanofibres de chitine, particules de lignine, emballage alimentaire, colloïdes biosourcés